

This file is part of the following work:

Jayasinghe, Nandana Chana (2012) *The distribution of wind loads and vulnerability of metal clad roofing structures in contemporary Australian houses.*
PhD Thesis, James Cook University.

Access to this file is available from:

<https://doi.org/10.25903/qdx8%2Dmm38>

Copyright © 2012 Nandana Chana Jayasinghe

The author has certified to JCU that they have made a reasonable effort to gain permission and acknowledge the owners of any third party copyright material included in this document. If you believe that this is not the case, please email

researchonline@jcu.edu.au

ResearchOnline@JCU

This file is part of the following reference:

Jayasinghe, Nandana Chana (2012) *The distribution of wind loads and vulnerability of metal clad roofing structures in contemporary Australian houses*. PhD thesis, James Cook University.

Access to this file is available from:

<http://researchonline.jcu.edu.au/39226/>

The author has certified to JCU that they have made a reasonable effort to gain permission and acknowledge the owner of any third party copyright material included in this document. If you believe that this is not the case, please contact

ResearchOnline@jcu.edu.au and quote <http://researchonline.jcu.edu.au/39226/>

The Distribution of Wind Loads and Vulnerability of Metal Clad Roofing
Structures in Contemporary Australian Houses

Thesis submitted by

Nandana Chana JAYASINGHE BSc (Hons)

in January 2012

For the degree of Doctor of Philosophy

in School of Engineering and Physical Sciences

James Cook University

Townsville

Statement of access

I, the undersigned, the author of this thesis, understand that James Cook University will make it available for use within the University Library and via the Australian Digital thesis network for use elsewhere.

I understand that as an unpublished work a thesis has significant protection under the Copyright act and I do not wish to place restriction on access to this work.

.....

.....

Nandana Chana Jayasinghe

Date

Statement of sources

I declare that this thesis is my work and has not been submitted for another degree or diploma at any university or other institution of tertiary education. Information derived from published or unpublished work of others has been acknowledged in the text and a list of references is given.

.....

Nandana Chana Jayasinghe

.....

Date

Statement on the contribution of others

Grants: This research was mainly supported by Cyclone Testing Station (CTS) at James Cook University, Townsville and additional funding was received from the School of Engineering and Physical Sciences, James Cook University (JCU), Townsville.

Supervision: A/Prof. J.D Ginger (JCU) principal supervisor for this research. Other supervision was provided by Dr. D.J Henderson (JCU) and Prof. G.R Walker (JCU).

Editorial Assistance: The editorial assistance for this thesis was provided by A/Prof. J.D Ginger, Dr. D.J Henderson and Prof. G.R Walker from James Cook University, Townsville.

Software: Mr. Martin Wehner from Geosciences Australia provided the software, VAWS and did additional coding whenever necessary to incorporate output results from this study.

Acknowledgements

First and foremost, I would like to express my sincere gratitude to my Principal supervisor A/Prof. John Ginger for his excellent guidance, technical expertise and continuous support throughout this research. I also thank my Co-Supervisors Dr. David Henderson and Prof. George Walker for their guidance and valuable inputs to this work. I am grateful to these supervisors for the education, direction, encouragement and examples they have provided.

The research was supported by Cyclone Testing Station (JCU) and School of Engineering and Physical Sciences (JCU). This support is gratefully acknowledged.

I also would like to thank staff and the technicians of Cyclone Testing Station for their support, assistance and advice. Specially, I would like to thank Mr. Stu Peterson for his support for setting up and assisting with conducting the structural tests.

I gratefully acknowledge the engineering workshop technician, Mr. Curt Arrowsmith for his support on constructing the wind tunnel model and Mr. Peter Kim for assisting me on doing the wind tunnel experiments.

Finally, I would like to thank my friends and family for their steady support and encouragement. I'm especially grateful to my wife, Susanthi, for helping me and keeping my life in proper perspective and balance.

Abstract

Windstorms cause most of the damage to houses, worldwide. The roof is subjected to the largest wind loads and is usually the most vulnerable part of the house. However, data on the transfer of wind loads within the roof structure is scarce. Such data is required for the application of structural reliability analysis and for development of building codes. The fluctuating nature and variable distribution of wind loads, combined with the change from linear to non-linear structural behaviour as the loads increase, can pose challenges for calculating structural response. This is also required for developing the performance based design of structures and for understanding wind load transfer within the roof structure and the effect of progressive failure on the sharing and redistribution of loads. Most vulnerability models do not accurately incorporate the structural behaviour of the houses during windstorms, which may produce unreliable estimates of damage. These vulnerability models have mainly focused on the wind loads acting on the connection tributary area and the strength of the connections.

This research study analysed the transmission of wind loads within a commonly used roof structural system of contemporary houses obtained from a survey in the cyclonic region of Australia. The distribution of wind pressure on the roof of such a typical house was determined using a wind tunnel model. The wind loads on selected roof fixings were further analysed to obtain the wind load data in terms of probabilistic parameters. The strength capacities of the roofing connection were also determined in terms of probabilistic parameters using available test data. The structural response of a roof was studied by testing sub-assemblies of the roof applying point and line loads and measuring the reactions at batten-to-truss connections and the deflections at selected locations in a range of conditions and damage states to simulated loads. The results were also compared with analytical solutions. The variation of reactions with increasing load was discussed in terms of a reaction coefficient. The coefficients were assessed for loads in the linear and non-linear states of roofing components/connections. The study integrated the wind loading and structural information on transfer of wind load effects through the structure to determine the loads and vulnerability of batten-to-truss connections. These

outputs were compared with the results obtained from conventional methods for calculating load on connections and vulnerability assessments.

The study found that loads on the batten-to-truss connection of these contemporary houses are influenced by the flexibility of the battens and cladding, and the directional stiffness characteristics of the cladding, as is the redistribution of batten-to-truss connection loads following failure of the cladding fastener and batten-to-truss connections. As a result estimates based on application of pressures to connection tributary area, which is the normal design practice, can lead to underestimation of the connection loads. The study shows that a larger tributary area should be considered to obtain the batten-to-truss connection loads on these structural systems. Furthermore, the study shows that estimates of the vulnerability of a batten-to-truss connection based on the incorporation of load distribution effects in the reliability analysis are greater than those obtained from the methods used in current practice. Hence, the study suggests that load sharing effects must be incorporated when determining the vulnerability of connections. The vulnerability estimates on cladding fixings and truss-to-wall connections were also determined and the results show that the cladding fixings are the most vulnerable and then batten-to-truss connections and truss-to-wall connections respectively.

A main outcome of the thesis is the establishment of an improved procedure for analysing the variation of the connection loads with time taking account of the spatial and temporal variation in wind pressures and the structural response characteristics of the roof system, which is a necessary first step in the assessment of their vulnerability. These outcomes make a significant contribution to understanding the wind loading distribution and developing vulnerability functions for houses to windstorms. The results can also be used to assess the system reliability for a well defined limit state and hence can contribute significantly to performance based evaluation of masonry block houses in cyclonic regions. The results could also be used as a basis to study adaptation measures and for the development of software models for assessing building vulnerability to windstorms.

TABLE OF CONTENTS

1	INTRODUCTION	14
1.1	Background	14
1.2	Objectives.....	19
1.3	Thesis outline	19
2	LITERATURE REVIEW	21
2.1	International studies on residential construction subjected to windstorms	21
2.2	Damage to Australian houses from windstorms	21
2.2.1	Structural Reliability	23
2.3	Wind loads on houses.....	24
2.4	Strength capacity of connections	28
2.5	Wind related full scale housing and sub assembly testing	30
2.6	Vulnerability studies based on engineering approach outside Australia	34
2.6.1	Damage prediction models.....	36
2.7	Vulnerability studies in Australia.....	39
2.8	Summary and Discussion	43
3	ROOF STRUCTURE OF A CONTEMPORARY HOUSE AND ANALYSIS METHODS	46
3.1	Masonry Block House.....	46
3.2	Roofing connections.....	48
3.2.1	Connection Strengths	49
3.3	Design of houses	51
3.3.1	Design approach for wind loads	51
3.4	Reliability theory.....	53
3.4.1	Dead load	54
3.5	Wind load probabilistic model	54
3.6	Summary and Discussion	55
4	WIND LOADING	57
4.1	Experimental setup.....	57
4.2	Experimental results.....	61
4.2.1	Pressure distribution-cladding.....	61
4.2.2	Pressure distribution-Battens.....	64
4.3	Probability distributions	66
4.4	Structural Load effects on Trusses	68
4.5	Summary and Discussion	71
5	STRUCTURAL TESTING AND RESPONSE.....	73
5.1	Load sharing and progressive failure	73
5.2	Experimental set up # 1.....	74

5.2.1	Test procedure.....	76
5.2.2	Elastic range tests.....	77
5.2.3	Loading until failure.....	79
5.2.4	Analytical model.....	80
5.2.5	Results and Discussion.....	80
5.3	Experimental test set up # 2.....	94
5.3.1	Results and Discussions for Test Set up #2.....	96
5.4	Summary and Discussion.....	114
6	VULNERABILITY OF THE ROOF SYSTEM.....	116
6.1	Load distribution on Roof system.....	116
6.2	The effect of cladding fastener failure.....	126
6.3	The effect of batten-to-truss connection failure.....	127
6.4	Reliability Analysis.....	128
6.5	Summary and Discussion.....	138
7	CONCLUSIONS AND RECOMMENDATIONS.....	140
7.1	Conclusions.....	140
7.2	Recommendations.....	144
8	REFERENCES.....	147
	APPENDIX A.....	154
	APPENDIX B- Test Matrix.....	158
	APPENDIX C.....	187
	APPENDIX D- Vulnerability and Adaptation to Wind Simulation (VAWS).....	195

LIST OF FIGURES

Figure 1.1: Damaged house from Brisbane thunderstorm (Leitch <i>et al.</i> (2010)).....	14
Figure 1.2: Building damage in Cyclone Larry (Henderson <i>et al.</i> (2006)).....	14
Figure 1.3: Completed Masonry Block house.....	16
Figure 1.4: Schematic diagram of a Masonry Block House	17
Figure 2.1: Change in Lateral response with addition of elements	31
Figure 2.2: Test house at UWO (Morrison and Kopp (2009)).....	33
Figure 2.3: 1/3 scale model building (Mensah <i>et al.</i> (2011)).....	34
Figure 2.4: Roof panel fragility of two typical houses (Exposure B(ASCE 7-05))	36
Figure 2.5: Vulnerability curves for masonry buildings in central Florida (Pinelli <i>et al.</i> (2008))	38
Figure 2.6: Components of the vulnerability for a masonry medium strength structure (Pinelli <i>et al.</i> (2008)).....	38
Figure 2.7: Reference curves for heuristic ranking process by expert group engaged through workshop activity, N and C classification according to AS 4055(2006) (Geoscience Australia (2007)).....	41
Figure 2.8: Estimated probability of failure of components in the modelled houses (Henderson and Ginger (2007))	42
Figure 3.1: Masonry Block house under construction (Hip roof shape)	47
Figure 3.2: Battens and trusses in Masonry block house	48
Figure 3.3: Truss-to-wall connection	49
Figure 3.4: Batten-to-truss connection.....	49
Figure 3.5: Roof cladding-to-batten connections.....	49
Figure 4.1: Mean velocity profile.....	57
Figure 4.2: Turbulence intensity profile.....	58
Figure 4.3: Pressure tap layout.....	59
Figure 4.4: 10m x 19.8m x 2.7m gable end low rise house with 22.5°roof pitch	60
Figure 4.5: 1/50 scale model of the 10m x 19.8m x 2.7m house in the wind tunnel.....	60
Figure 4.6: Pressure coefficients vs wind direction – P (cladding).....	63
Figure 4.7: Pressure coefficients vs wind direction - Q (cladding).....	63
Figure 4.8: Pressure coefficients vs wind direction - T (cladding)	64
Figure 4.9: Pressure coefficients (Cp) vs wind direction – Batten-to-truss connection B2	65
Figure 4.10: Pressure coefficients (Cp) vs wind direction – Batten-to-truss connection B7	65
Figure 4.11: Pressure coefficients (Cp) vs wind direction – Batten-to-truss connection F5.....	66
Figure 4.12: Schematic diagram of roof truss showing batten to truss connection patches and truss to wall reaction forces	68

Figure 4.13: C_{V1} and C_{V2} vs wind approach angles -Truss B	70
Figure 4.14: C_{V1} and C_{V2} vs wind approach angles -Truss F.....	70
Figure 4.15: C_{V1} and C_{V2} vs wind approach angles -Truss L	71
Figure 5.1: Schematic diagram of the test set up #1 (all dimensions are in mm)	75
Figure 5.2: Test set up #1 before fixing the cladding.....	75
Figure 5.3: Batten-to-truss connection with load cell	76
Figure 5.4: Dummy load cell	76
Figure 5.5: Test set up with cladding fixed.....	76
Figure 5.6: Load application to the bottom surface of cladding with a foam mould and jack....	77
Figure 5.7: Load application to batten and deflection measurement	78
Figure 5.8: Line loads applied along a line over spacing between trusses.....	79
Figure 5.9: SPACEGASS 3D model of the test setup #1.....	80
Figure 5.10: Reaction coefficient at b2, R1($C_{b2, R1}$) for point load on batten b2.....	82
Figure 5.11: Deflection of batten b2 for load at (b2, 2)	82
Figure 5.12: Reaction coefficient, $C_{b2, R1}$, for point load on batten b2	83
Figure 5.13: The effect of cladding on reaction coefficient, $C_{b2, R1}$	84
Figure 5.14: Reaction coefficient, $C_{b2, R2}$ with point loads along W, X and Y	86
Figure 5.15: $C_{b2, R2}$ for point load on X on Panels P6 and P10.....	87
Figure 5.16: Reaction coefficients for loading at centre of Panel 6 until failure of fasteners.....	89
Figure 5.17: Application of point load showing a cladding fastener failure (pulling out of batten)	90
Figure 5.18: Plastic deformation of cladding around fasteners.....	91
Figure 5.19: Deflections at selected positions with the applied load along line X of P10.....	91
Figure 5.20: Reaction coefficient for a line load on P13 along line X.....	92
Figure 5.21: Line load on P13, X until failure of cladding fasteners	93
Figure 5.22: Deflection with the applied load on P13 along line X.....	94
Figure 5.23: Schematic diagram of the Test Set up #2	95
Figure 5.24: Schematic diagram of the connections studied.....	100
Figure 5.25: Reaction coefficients of adjacent connections when b2, R2 Failed	102
Figure 5.26: Reaction coefficients on connections for equal loads applied on P1, P2, P4 and P5	102
Figure 5.27: Reaction coefficients on connections when b2, R2 failed for equal loads applied on P1, P2, P4 and P5.....	103
Figure 5.28: Batten-to-Truss connection with one screw connection removed	104
Figure 5.29: Reaction coefficients for a partial failure of the connection b2, R2 for equal loads applied on P1, P2, P4 and P5	105
Figure 5.30: A connection with loose screws	106

Figure 5.31: Applied load on batten-to-truss connection.....	108
Figure 5.32: Reaction coefficients for total applied load on (b2, R2).....	109
Figure 5.33: Deflection measurement	110
Figure 5.34: The applied load vs deflection at (b2, R2).....	110
Figure 5.35: Plastic deformation of a batten-to-truss connection	111
Figure 5.36: Applied load vs Deflection on connection (b2, R2)	111
Figure 5.37: Failure of the connection (b2, R2).....	112
Figure 5.38: Variation of reaction coefficients with the applied load.....	113
Figure 5.39: Variation of deflections with the applied load.....	113
Figure 6.1: Schematic Diagram of connections considered	117
Figure 6.2: Conventional method #1-Tributary area for connection B7	118
Figure 6.3: Conventional method #2-Tributary area for connection B7	119
Figure 6.4: Proposed method - Tributary area for connection B7.....	119
Figure 6.5: Variation of CXb at B7 with the wind approach direction	122
Figure 6.6: CXb for undamaged system for $\theta = 150^\circ$	123
Figure 6.7: Pressure distribution around B7-Proposed method	124
Figure 6.8: Pressure distribution around B7-Conventional Method #1	124
Figure 6.9: Pressure distribution around B7-Conventional Method #2	124
Figure 6.10: CXb for undamaged system for $\theta = 90^\circ$	125
Figure 6.11: Failure of a cladding fastener	126
Figure 6.12: Load distribution-Undamaged system.....	128
Figure 6.13: Load distribution-B7 failed	128
Figure 6.14: Vulnerability of batten connections for $\theta = 150^\circ$ in TC 2.5	130
Figure 6.15: Vulnerability of batten truss connections for $\theta = 150^\circ$ in TC 2.5.....	130
Figure 6.16: Vulnerability of batten connections for $\theta = 150^\circ$ in TC 2.5	132
Figure 6.17: Vulnerability of batten truss connections for $\theta = 150^\circ$ in TC 2.5.....	132
Figure 6.18: Probability of batten-to-truss connection failure vs wind speed following the failure of B7 in TC 2.5- internal pressure coefficient- 0	133
Figure 6.19: The effect of factors in Eqn 3.14 on batten-to-truss connection vulnerability for $\theta = 150^\circ$ in TC 2.5- internal pressure coefficient- +0.7.....	135
Figure 6.20: Typical contemporary house (i.e. Figure 4.4).....	136
Figure 6.21: Probability of failure vs Basic Wind speed- Cladding connections for house in TC 2.5- internal pressure coefficient- +0.7.....	137
Figure 6.22: Probability of failure vs Basic Wind speed-Truss-to-wall connections for house in TC 2.5- internal pressure coefficient- +0.7.....	137

LIST OF TABLES

Table 3.1: Characteristics of Masonry block Houses.....	47
Table 3.2: Connection Capacity Statistics	50
Table 4.1: The probabilistic distribution of peak pressure (C_p/C_{pN}) on cladding fixings at P, Q and T regions	67
Table 5.1: Comparison of reaction coefficients from line loads with point loads	88
Table 5.2: Reaction coefficients of selected connections for load applied at P1 to P9.....	96
Table 5.3: Deflection at selected panels for line load application on panels	97
Table 5.4: Comparison of reaction coefficients for line loads applied in test set up #1 and #2..	98
Table 5.5: Comparison of deflections in Test set up #1 and #2	99
Table 5.6: Reaction coefficients for removing both screws in selected connections.....	100
Table 5.7: Reaction coefficients for removing screw 'I' of selected connections	105
Table 5.8: Reaction coefficients for loosening both screws on selected connections.....	107
Table 6.1: CXb for $\theta = 150^\circ$ - Undamaged roof using load distribution effects	121
Table 6.2: CXb for $\theta = 150^\circ$ - Undamaged roof using conventional method #1.....	122
Table 6.3: CXb for $\theta = 150^\circ$ - Undamaged roof using conventional method #2.....	122
Table 6.4: CXb for $\theta = 150^\circ$ - Cladding fastener failure (between B7 and C7).....	127
Table 6.5: CXb for $\theta = 150^\circ$ - Batten-to-truss connection B7 failed.....	128
Table 6.6: Statistical parameters for normalized values	134

1 INTRODUCTION

1.1 Background

Residential housing is the largest single asset for many people, and overall forms a very large proportion of the social investment in the community. These houses need to be protected against hazards with the potential to cause large scale disasters. Windstorms are generally recognized as the natural hazard that causes most of the damage to buildings in Australia. Windstorms can broadly be classified according to their meteorological parameters as, tropical cyclones, thunderstorms, tornados and gales. Thunderstorms and tornados are short-lived local events with their influence affecting distances of tens of kilometres. Cyclones generally impact coastal regions in the tropics, and can extend hundreds of kilometres, therefore having the potential to cause widespread damage. Windstorms such as Cyclone Tracy (Walker (1975)), Cyclone Winifred (Reardon *et al.* (1986)), Cyclone Larry (Henderson *et al.* (2006)), Cyclone Yasi (Boughton *et al.* (2011)) and Brisbane Thunderstorm (Leitch *et al.* (2010)) have caused significant damage to the structures in Australia. Figures 1.1 and 1.2 show damaged houses from such events. There has been a significant reduction in the level of damage to houses in recent times due to the improvements in design and construction of domestic/residential houses (Boughton *et al.* (2011)).



Figure 1.1: Damaged house from Brisbane thunderstorm (Leitch *et al.* (2010))



Figure 1.2: Building damage in Cyclone Larry (Henderson *et al.* (2006))

However, increasing concentration of population and the potential effects of climate change on the frequency and magnitude of windstorms may result in an increased risk to housing. If the nature of the disaster risks is to be fully understood and cost effective measures taken to mitigate them, it is important to have a better understanding of the structural response of houses to wind loading.

Full scale and wind tunnel model studies on houses reveal that the roof is subjected to large wind loads and post-damage surveys show that the roofing components are the most vulnerable part of a house to windstorms. Damage surveys (Walker (1975)) and full scale test data from the Cyclone Testing Station (Boughton and Reardon (1982, 1983, 1984)) have shown that the typical modes of roofing failure of houses to wind loading are associated with the strength capacity of the joints between components being exceeded. There are a range of house types in Australia with differences in size, shape, potential openings in envelope, cladding, roof shape and pitch, method of construction, structural system and age. The resistance of a house structure to wind loading depends on the effect of these features on the wind loads experienced and the strength of its components and connections. The roof of these houses consists of roof cladding, battens and roof trusses/rafters. The roof cladding is usually metal sheeting or roof tiles that are fixed to timber or metal “top hat” battens. The trusses or rafters are usually timber in residential construction.

The assessment of the vulnerability of these houses to windstorms requires knowledge of the loads and component strength and uncertainties associated with load actions and building response. The vulnerability in this research is defined as the susceptibility of structural failure to wind loads, and failure is defined as the state where the structure is unable to resist the applied load. These uncertainties are due to the variability of factors that are inherent to wind loads and component resistance, and inadequate knowledge resulting in incorrect assumptions and analysis methods. These uncertainties can be accounted for, when analysing a structural system by specifying the load action and building response in probabilistic terms. An important

component of this process is to obtain an accurate representation of the wind load transmitted through the structure of a house.

Contemporary houses in cyclonic regions of Australia are typically built on a concrete slab on ground with masonry block walls, timber roof trusses, metal top hat battens and corrugated metal roof claddings. These houses have predominantly either gable or hip roofs or a combination of these. Figure 1.3 shows a masonry block house with a metal clad gable end roof and Figure 1.4 shows a schematic diagram of a typical masonry block house.

The approach wind flow generates spatially and temporally varying pressure on the roof. These loads depend on the approach wind direction and also the terrain and topographic features. There have been many studies of wind pressures on roofs covering a large range of roof types, of which the studies by Holmes (1981), Reardon and Holmes (1981) and Meecham *et al.* (1991) are typical examples. The design wind loads on the roof given in Standards (AS/NZS 1170.2 (2011), ASCE 7-10 (2010)) are generally based on a conservative interpretation of results from such studies and are dependent on the geometry of the building. The spatial and temporal variation of wind load and the transfer of these loads to the roof structure must be determined in order to assess their vulnerability.



Figure 1.3: Completed Masonry Block house

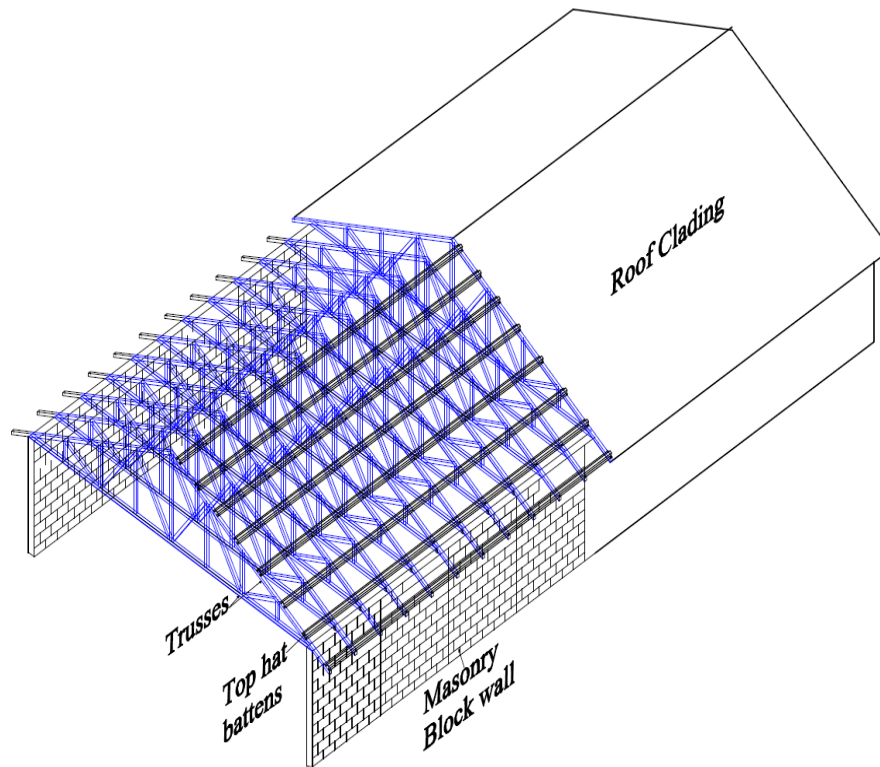


Figure 1.4: Schematic diagram of a Masonry Block House

Wind loads acting on the roof cladding are transferred via the supporting structure and the walls to the foundation. The roof cladding-to-batten connection, batten-to-truss connection, and truss-to-wall connection, are the critical parts of the load transfer path in these houses. The vulnerability assessment of these houses depends on the strength of these connections. Houses are complex structures with many load sharing components, making it difficult to quantify the resistance of each component especially as the availability of full scale data is limited. The loads applied to a house are shared by the structural and non-structural elements in a complex manner. Increasing wind speeds will result in progressive failures and possible changes to the load sharing and reactions in connections. Full scale testing provides a means of assessing the loading response and also determining the coefficients or factors for the load effects of interest. Full scale tests on complete houses, such as those by Boughton and Reardon (1982, 1983, 1984) provide quantitative data on the load sharing and interdependency between components and connections with increasing load. However, such studies have focused on the cumulative

performance of the structure and did not measure the reactions/loads of individual connections which are needed to determine the load redistribution and progressive failure. Therefore, more detailed descriptions of structural components and connections including their behaviour with increasing wind loads and quantitative analysis of load distributions are required in order to predict the overall response of roofing components during wind events. This is also required for developing performance based design of structures.

The vulnerability of houses to wind loads can be studied using the reliability method that is incorporated in design standards for structural design (Walker (2011)). Henderson and Ginger (2007) studied the vulnerability of high-set 1960's house with low pitch gable roof built in Northern Australia to wind speeds experienced in tropical cyclones by using reliability concepts. Studies by Rosowsky and Ellingwood (2002), Ellingwood *et al.* (2004), Pinelli *et al.* (2004), Lee and Rosowsky (2005), and Li and Ellingwood (2006) have assessed the vulnerability of residential construction in the US to wind loading using reliability methods and probability techniques. Engineering vulnerability models estimate the damage caused by wind loads of varying intensity by applying structural engineering techniques and statistical methods. The reliability theories incorporating probability theories and Monte Carlo simulation techniques are incorporated in these engineering models to assess the vulnerability.

However, most of the vulnerability models do not accurately incorporate the structural response of the house during windstorms, and hence may produce unreliable estimates of the damage. Typically these studies have focused on the wind load acting on the local tributary area and the strength of the connections. The determination of the vulnerability of roofs to wind loads requires a combination of the distribution of wind loads on a common roof structure, the connection strengths and the response of the actual roof structure to loads including load sharing and redistribution that results from progressive failure under wind loads. Such data inputs to the engineering models form an important part in determining the building vulnerability.

1.2 Objectives

The main objective of this thesis is to determine the transmission of wind loads through roofing components, including the effect of local failures, and the impact on the overall structural performance of the roof system. Specifically, the distribution of applied loads and associated structural response of a batten-to-truss connection from contemporary houses built in cyclonic region of Australia is investigated.

These objectives are met by;

- I. Determining a common roof system and the structural components used in contemporary houses built in cyclonic region of Australia and their strengths.
- II. Deriving the spatial and temporal variation of wind loads acting on the roof of a common contemporary house as a function of wind direction.
- III. Studying the effect of load sharing and interdependency between components and progressive failure by conducting a series of tests on selected subassemblies of the roof system, and using structural analysis.
- IV. Determining the load distribution on selected connections using measured wind loading distributions and structural response, and then comparing the results with conventional methods of analysis.
- V. Using reliability methods to estimate failure of roofing components under wind loads and assessing the vulnerability of components on various regions of the roof.

1.3 Thesis outline

Chapter 2 reviews work carried out around the world in this research area and identifies the methods for gaining required information. The damage to houses from windstorms, wind load

on low rise houses and studies on vulnerability of houses to windstorms are discussed. The damage prediction models currently being used and developed and full scale house /sub assembly tests associated with low rise construction are also described.

Chapter 3 describes the structural system including roofing components and connections of a common masonry block house based on a survey, and presents the capacities of the roof connections in terms of probabilistic parameters. The current design practices associated with the design of residential construction to wind loads and the theories used in this study to assess the vulnerability of roofing connections to windstorms are also discussed.

Chapter 4 presents the wind loads over the roof of the common masonry block house obtained from a wind tunnel model study. The distribution of the wind loads and variability of these loads in probabilistic terms over selected part of the roof with the wind approach direction, are also presented.

Chapter 5 presents a series of tests on full scale roof subassembly systems subjected to a range of loads and comparisons with analytical results. The progressive failure, load sharing and interdependency between components with increasing load are also studied.

Chapter 6 combines the wind load measured on the wind tunnel model and the full scale roof structure response to determine the distribution of load in the roof system of contemporary houses. Vulnerability curves are derived for roofing connections on selected parts using the reliability method and probability theories. The load-response results are also incorporated in the analysis.

Chapter 7 summarizes the main findings and conclusions. It also contains the discussion on results, their significance, limitations, possible ways of generating the results for more widespread application, and suggestions for future research.

2 LITERATURE REVIEW

Windstorms are responsible for most of the damage to houses from natural hazards, in many parts of the world. However, studies on the transmission of wind load within the roof required for quantifying the damage have been limited. Such studies provide a means of quantifying the performance of a type of house, linking it to reliability methods applied in building codes and standards. This Chapter reviews the research carried out around the world in this area and identifies methods for gaining required information.

2.1 International studies on residential construction subjected to windstorms

Windstorms such as Hurricane Hugo, Andrew, Iniki and Opal caused damages to the residential houses constructed in the US resulting in significant insurance payouts. Pielke and Pielke (1997) described that the vulnerability of society to windstorm is assessed as a combination of incidence (intensity and frequency of events) and societal exposure (people, preparedness and properties). Improving building resilience to these events reduces society's vulnerability. Empirical and engineering based vulnerability models have been developed in the US to assess the damage to the buildings and to improve the construction of residential houses. As described by Walker (2011), engineering based models require a large amount of detailed statistical information on the structural behaviour of buildings at component, sub-system, and whole of building level. There have been major advances in this area during last decade. The studies by Unanwa *et al.* (2000), Pinelli *et al.* (2004), Vickery *et al.* (2006b), Ellingwood *et al.* (2004), and Li and Ellingwood (2006) are some of these studies and the details are discussed later in this Chapter. The outcomes and methodologies used in these studies are important for developing vulnerability models for Australian housing.

2.2 Damage to Australian houses from windstorms

The report by Geoscience Australia (2007) provides an overview of the damage sustained by residential structures from natural hazards in Australia. The report indicates that windstorms

cause most of the damage. These events can result in major disruptions to communities, significant insurance payouts and loss of lives. Tropical cyclones Althea and Tracy impacted the Northern Australian towns of Townsville in 1971 and Darwin in 1974, respectively. Tropical Cyclone Tracy caused significant damage to domestic housing as detailed by Walker (1975) and Leicester and Reardon (1976). A major factor in the wide-spread damage was the loss of roofing materials which led to a significant loss of strength in many houses, leading to collapse and the production of a large amount of wind borne debris, causing further damage to the buildings. The roof cladding fixings in these houses proved to be inadequate with fatigue under fluctuating wind loads causing a reduction in strength. A major consequence of these events was the implementation of a nationwide requirement for housing to be structurally designed to the same codes and standards as larger buildings. The zoning of cyclone regions, fatigue failure of cladding fastener systems and increased internal pressure for housing design were the most radical impacts from cyclone Tracy on building regulations, as described by Walker (2010). This was a revolutionary change as the previous improvements in design had been based on correcting the observed weaknesses of components/connections.

Evidence of the resulting improvements to housing design standards and codes in Australia is found from the comparatively better performance of newer construction in recent windstorms, such as Cyclone Larry (Henderson *et al.* (2006)), Cyclone Ului (Henderson *et al.* (2010)), Cyclone Yasi (Boughton *et al.* (2011)) and Brisbane Thunderstorm (Leitch *et al.* (2010)). These reports show that most of the damage occurred to houses built before the new standards were introduced (pre-1980's houses). Contemporary housing performed considerably better than older housing, reflecting marked improvement of construction detailing and better structural condition, and satisfactory performance of relevant standards (AS/NZS 1170.2 (2011) and AS 4055 (2006)). In some cases, houses that did not have appropriate fixings to account for higher wind speed caused by topography on or near hill-tops had significant damage. Overall, contemporary houses performed well by resisting the wind loads (for wind speeds that were less than the regions' design wind speed). Generally, these new buildings had damages mainly to

roller doors and attachments such as guttering and fascias which have not been designed to meet requirements given in the codes. Where structural failures were observed on contemporary houses, they were associated with poor construction practice or application of incorrect site classification (i.e. low design wind speed). Breaches in the building envelope (from failed doors or windows, or debris impact) exacerbated the potential for failure from the resulting high internal pressure. Corrosion or rot of connections and framing elements initiated failures.

2.2.1 Structural Reliability

Structural reliability forms the basis of many current design codes and standards (AS/NZS 1170.0 (2002), AS/NZS 1170.1 (2002), AS/NZS 1170.2 (2011) and ASCE 7-10 (2010)). As described by many researchers such as Thoft-Christensen and Baker (1982), Melchers (1987) and others, structural reliability theory is concerned with the rational treatment of uncertainties in structural engineering and methods for assessing the safety and serviceability of structures. Uncertainties that exist in most areas of civil and structural engineering should be taken into account so that rational decisions can be made. These methods are applied to determine the reliability against extreme events such as collapse or fracture and also the breaching of any structural engineering requirement which the structure is expected to satisfy. The basic reliability theory used is discussed in Chapter 3, where the loads and the capacities of structural components in contemporary houses are given in probabilistic terms.

Current structural design codes and standards are based on concepts of limit state design, with safety checks based on structural reliability theory. These reliability concepts were applied by Galambos *et al.* (1982), Ellingwood *et al.* (1982), Leicester *et al.* (1985), Holmes (1985), and Pham (1985) for developing structural design standards to a limit state format (AS/NZS 1170.0 (2002), AS/NZS 1170.1 (2002), AS/NZS 1170.2 (2011) and ASCE 7-10 (2010)). The concept of a reliability index (or safety index) was used in the assessment of structural design codes. These studies defined the reliability index as a measure of evaluating uncertainty, performance and reliability of a building system subjected to loads. The studies also showed that the basic

framework for probability based design is provided by reliability theory and the probability of failure and the reliability index can be evaluated when the probability distribution of the loads and resistances are known. Melchers (1985) and Tang and Melchers (1985) discussed the applicability of reliability theory and Monte Carlo simulation techniques for obtaining the reliability of large structural systems. Pham *et al.* (1983) and Holmes (1985) described a probabilistic model for wind loads to enable reliability indices to be computed for structural design. These approaches and the concepts have been used by others to assess the vulnerability of residential constructions to wind events.

2.3 Wind loads on houses

Low rise structures fall within the layer of aerodynamic roughness on the earth's surface. Here, turbulence intensities are high and the highest loading on the surface of a low rise building are generally the suctions on the roof, where many structural failures initiate. In the early 1970's, the Building Research Establishment of the United Kingdom carried out full scale measurements of wind pressures and forces on two storey houses at Aylesbury. Eaton and Mayne (1975) described an extensive full scale experiment on several two storied houses. The principal contribution to wind engineering came from this project where extensive pressure measurements were made from an isolated experimental building with a variable pitch roof. Subsequently, comparative wind tunnel experiments were conducted in many laboratories (i.e. Holmes and Best (1977), Holmes (1983), Sill *et al.* (1989) and Sill *et al.* (1992)) on 1:50 and 1:100 scale models of the Aylesbury house. Holmes (1983) found some good agreements in the full scale and model scale results, but also identified deficiencies in the full scale experiments. These comparisons also found variations in pressure coefficients measured across the laboratories.

Following the Aylesbury study, full scale experiments have been conducted at Silsoe in the UK (Richardson *et al.* (1990)) and the Texas Tech in the US (Levitan *et al.* (1991)). Richardson and Surry (1991, 1992, 1994), Richardson and Blackmore (1995) and Richards and Hoxey

(2008) compared the results of full scale measurements of the Silsoe Building with wind tunnel model results and presented conclusions similar to those from the Aylesbury tests. They also found that areas of high negative pressure tended to be underestimated in wind tunnel measurements, as in the previous studies. A significant amount of data on the Texas Tech building has also been obtained and a range of analysis has been carried out by Levitan *et al.* (1991), Mehta *et al.* (1992), and Letchford *et al.* (1993). Wind tunnel simulations on this building have also been carried at many laboratories worldwide by Surry (1991), Cochran and Cermak (1992), Tieleman *et al.* (1996), Xu and Reardon (1996) and Ho *et al.* (2005). These studies also found that most pressure coefficients measured on the models were in close agreement with full scale pressure coefficients, but the largest negative peak coefficients at the roof edge and roof corners were under-estimated by the wind tunnel tests, as in the Aylesbury study. These studies have contributed to improvements in the wind tunnel simulation techniques, and data specified in revised codes and standards.

Wind pressures acting on the roofs of houses are dependent on their geometry and the approach wind direction. The wind pressure acting on the range of roofs given in the standards are based on many of wind tunnel model studies carried out on low rise building with hip and gable roofs having a range of slopes (Holmes (1981), Reardon and Holmes (1981), Meecham *et al.* (1991), Xu and Reardon (1998) and Ginger and Holmes (2005)). Meecham *et al.* (1991) showed that the hip roof house experiences smaller peak cladding loads compared to a gable roof of similar dimensions. Damage investigations also confirmed that hip roofs perform better than gable roofs. However, the wind resistance of roofs should be analysed based on the relationship between the pressure distribution and the underlying structural framing, implying that roof shape alone is not responsible for the performance (Meecham *et al.* (1991)). In addition, the spatial distribution of the pressures relative to the structural framing should be taken in to account. There is a large spatial and temporal variability of pressures, especially near windward roof corners, where the most severe wind loading and damage normally occurs. These large suction pressures are generated by the formation of conical vortices (Holmes (2007)). Several

studies have been carried out to assess the variation of wind loads on roof corners (Mehta *et al.* (1992) and Lin and Surry (1998)) and the influence of roof eaves (over hang) on the characteristics of pressures (Robertson (1991)).

Ho *et al.* (1990, 1991, 1992) investigated the effect of surrounding buildings on the wind loads on a low rise building and found that the results are considerably different from those predicted from isolated building tests and the coefficient of variation of the larger loads were 0.6 to 0.7. Furthermore, they suggested that the wind load specifications should be determined based on a reliability approach considering such a variation in wind loads. Case and Isyumov (1998) showed that a suburban exposure generates lower wind loads than those experienced in the open country exposure as suggested by others (Holmes and Best (1979) and Ho *et al.* (1992)). This reduction was most apparent on wall loads and roof suctions, with the reductions in local suctions may be up to 30%. Vickery *et al.* (2011) also conducted a range of wind tunnel experiments for hip and gable end roof buildings covering a wide range of roof slopes in open and suburban terrain conditions and compared the results with the pressure coefficient values given wind loading standard in the US, ASCE 7-10 (2010). They showed the changes in pressure coefficients in different areas of the roofs from open terrain to suburban terrain, and found that ASCE-7-10 generally underestimates the magnitude of the negative roof pressures acting on components and cladding.

Codes and standards such as AS/NZS 1170.2 (2011) give the design wind loads on parts of a building as a nominal peak design pressure based on a quasi-static pressure coefficient. The variability of the peak pressure should be taken into account, when assessing the vulnerability of components. Previous studies by Pham *et al.* (1983) and Holmes (1985) have investigated the probability distribution of wind pressure on buildings. They obtained the probabilistic descriptions of the normalized wind loading parameters through assumptions and wind tunnel studies. The wind loading parameters were treated as random variables with probability distributions and the product of these parameters was assumed to have a lognormal distribution.

Li *et al.* (1999) also found that a Lognormal distribution compared favourably against Gumbel and Weibull. Sadek and Simiu (2002) showed that the distribution of peaks can be represented by the Extreme Value Type I (Gumbel) distribution. Holmes and Cochran (2003) used several thousand extreme pressure coefficients from repeated time history samples from a wall tap and a roof tap on a model of the Texas Tech University Test Building to determine the appropriate probability distributions for the data. They found that the Generalized Extreme Value (GEV) distribution with a small positive shape factor fits the data well. The GEV distribution is described as Type I, Type II or Type III distribution depending on the value of the shape factor (i.e. shape factor = 0, Type I, shape factor > 0, Type II and shape factor < 0, Type III). Cope *et al.* (2005) also fitted several probability distribution functions for different regions on the roof under different wind directions and found that the negatively skewed Type I distribution is the best fit for most of the cases considered. Li *et al.* (2009) studied a similar type of full scale building and found that the Type III Extreme Value Distribution matched the data measured on a roof corner. Kasperski and Hoxey (2008) also found that Type III distribution can be fitted to the full scale test data on walls of 6m × 6m × 6m cube Silsoe building. Ben Ayed *et al.* (2011) carried out a probabilistic approach to analyse pressure and wind load distribution on the roof of full scale house. It was shown that the pressure coefficient time series follows a three parameter Gamma distribution while the peak pressure follows a two parameter Gumbel distribution.

Structural wind load effects can be determined by incorporating influence coefficients with the wind loads on the tributary area of interest, as shown by Henderson (2010) and Jayasinghe and Ginger (2011). Holmes and Best (1981) described a method for estimating overall structural loads which takes into account the correlation of pressures on a building using a covariance matrix method. The covariance data was used to calculate structural loads such as total uplift, drag and overturning moment. Ginger *et al.* (2000) also used the covariance integration method to calculate structural load effects on roofing components of a gable end house. The design (or peak) load effects of interest (i.e. roof hold down force) can also be statistically analysed for a reliability assessment. Furthermore, wind loads are applied on a tributary area with the

corresponding influence effect to determine the design load effects (uplift on cladding fastener, batten-truss connection, and truss to wall connection). Kasperski and Niemann (1992) also described a methodology called LRC (Load-Response-Correlation) to estimate the wind load distribution in linear and non-linear structural behaviour.

Damage investigations such as those by Walker (1975), Henderson *et al.* (2006), Boughton *et al.* (2011) and Leitch *et al.* (2010) have shown that large internal pressures arising from dominant openings contributes to large load effects and damage to houses. Several studies have been carried out on this subject to determine the internal pressure characteristics on the buildings with differences in volumes, sizes of the dominant openings etc (Liu and Saathoff (1981), Vickery (1986), Holmes (1979), Ginger *et al.* (1997), Ginger *et al.* (2008) and Ginger *et al.* (2010)). Design internal pressure data given in standards such as AS/NZS 1170.2 (2011) are based on results from similar studies.

2.4 Strength capacity of connections

In addition to the wind loads on the roof, dead loads (i.e. self weight) and the strength (i.e. capacity) of connections need to be determined for a full reliability analysis. The dead loads are usually based on material weights. Typically, the mean to nominal dead load ratio of 1.05 with a COV of 0.10 based on the assumed weight of the roof system and other roofing materials has been specified by Ellingwood *et al.* (1982), Galambos *et al.* (1982), Holmes (1985), Pham (1985) and Rosowsky and Cheng (1999a,b). The assumed probability distribution function in US studies (Ellingwood *et al.* (1982), Galambos *et al.* (1982) and Rosowsky and Cheng (1999a,b)) was Normal while Lognormal distributions were assumed in the Australian studies (Holmes (1985), Pham (1985) and Leicester *et al.* (1985)).

As described by Rosowsky and Cheng (1999a, b) the capacities of connections in light-frame wood construction in the US were found from engineering approaches such as individual nail capacity tests as well as non-engineering approaches (damage investigations and experience).

These statistics on connection capacities have been used by Rosowsky and Cheng (1999a,b), Ellingwood *et al.* (2004), Lee and Rosowsky (2005), and Li and Ellingwood (2006) for fragility assessment of light-frame wood construction. They used the Normal probability distribution for roofing component strength characteristics. Vickery *et al.* (2006b) used the Lognormal distribution for sheathing panel behaviour and the Normal distribution for strap and toe nail uplift resistance in truss-to-wall connections in their study. Shanmugam *et al.* (2009) derived probabilistic descriptions of the capacity of connections for light-frame wood construction in the US. They derived uplift capacities for roof-to-wall connection and sheathing units from field and laboratory tests and found that the Lognormal distribution is the best fit from statistical analysis to model uplift capacities of the nail connection types considered. Lognormal distributions were used by Holmes (2007) and Henderson and Ginger (2007) in Australian studies to describe the probabilistic characteristics of the connection strengths in older houses.

The capacities of a range of components and connections of contemporary houses in Australia have been tested by Cyclone Testing Station (CTS). The CTS data-base contains the capacity of connections for new and old types of constructions subjected to static and cyclic tests based on several test regimes. The major component damage during Cyclone Tracy was caused by low cycle fatigue cracking of the cladding under the fixings which resulted in extensive loss of light gauge roof cladding (Walker (1975)). Consequently, research by Mahendran (1989, 1995), Jancauskas *et al.* (1994), Xu (1995a,b) and Henderson (2010) have demonstrated through extensive test programs that the interaction of the cladding and fixing is a crucial part of the cladding's fatigue response to the applied loading. These studies have shown that the fatigue strength of cladding connections is less than the static capacities. Similarly, the fatigue strength of the top hat battens is also less than the static capacities as shown by Fowler (2003). The strength capacity of truss-to-wall connections on contemporary houses has also been studied by Cummins (2002).

2.5 Wind related full scale housing and sub assembly testing

The assessment of vulnerability (i.e. structural failure of connections/components) of a house type to wind loads requires an understanding of the load sharing and structural interdependency between components. The Cyclone Testing Station at James Cook University, Townsville has carried out studies on a range of full scale house types and tests on sub-assemblies of houses. Boughton and Reardon (1982) tested a forty year old house by applying simulated wind load in both uplift and horizontal directions in a total of 8 tests and measuring approximately 200 deflection readings. They were able to draw conclusions from this work on both the feasibility of testing full scale houses, and the mechanisms they used to resist wind loads. Those tests were valuable for evaluating analysis methods and were also used as a reference point for checking test results. However, the small amount of data collected limited the conclusions that could be drawn from those tests.

In order to rectify that problem, an instrumentation system was built to enable direct recording of response data on a digital computer. Boughton and Reardon (1983, 1984) showed the importance of testing a complete house to simulated winds by testing a new high set house designed for 42m/s, built according to the standard. Their analysis identified the load transfer and load sharing between elements, and pinpointed the areas of weakness or excessive strength. They applied uplift loads on the roof and determined the capacities and failure modes of the connections subjected to progressively increasing static and cyclic loading. These studies and many other studies such as those by Reardon (1986, 1990) and Reardon and Mahendran (1988) have pointed out the importance of the interactions between subassemblies of houses, the effect of boundary conditions, contribution of the non-structural components, and load-sharing mechanisms. Reardon and Henderson (1996) and Reardon (1996) have also demonstrated the strengths and weaknesses in conventional house construction in respect of wind forces and found that non-structural lining materials provide significant racking strength and stiffness as shown in Figure 2.1. The strength of the house was determined from combined racking and uplift loading and it was shown that the strength and stiffness of the house was increased with

the addition of various structural and non-structural components as shown in Figure 2.1. The behaviour of the individual components in the whole structure was highlighted in these studies. These studies have also shown that the behaviour and the failure modes of the components in the whole structure are different from isolated testing of the components. Thus, the studies indicated that the isolated component test results and their interpretations should be validated with full scale tests.

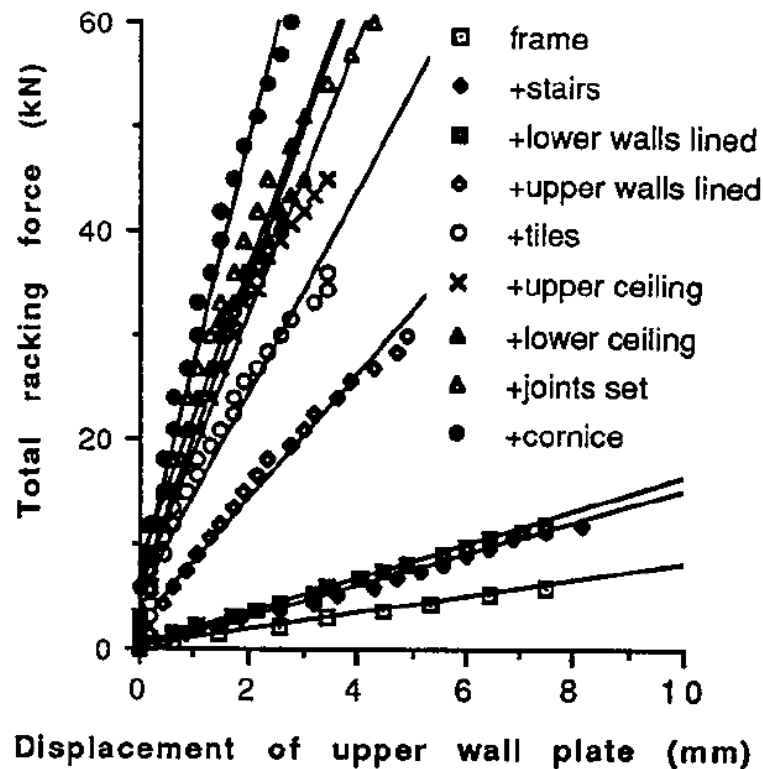


Figure 2.1: Change in Lateral response with addition of elements (Reardon and Henderson (1996))

Henderson (2010) carried out roofing subassembly tests to determine Australian metal clad roofing response to wind loading. The study found that the peak pressure measurement on a single pressure tap satisfactorily represents the load on a roof cladding fixing. It was also confirmed that the cladding fixing load is equal to the pressure on the tap multiplied by the tributary area of the fixing. Further, the study conducted tests for several cyclic and static tests and found that the cladding fastener response follows the applied load spectrum with minor

change to stiffness until failure, and then the load is transferred to adjoining fixings. These tests showed that static tests satisfactorily represent loading on fasteners from the wind load fluctuations. Furthermore, the spatial variations of wind loads can be captured by conducting a series of point load tests (i.e. application of point load on the pressure tap locations).

Realistic structural testing of building and building components can be conducted using Pressure Load Actuators (PLAs) developed at the University of Western Ontario. The roof of a full scale two story house built (as shown in Figure 2.2) to the Ontario building code was tested using 58 PLAs to examine the performance of the toe nailed roof-to-wall connection (Morrison and Kopp (2009)). Toe nail connection is the most common type of primary roof-to-wall connection of residential houses in the US and Canada. The loadings for the test were obtained from a wind tunnel study conducted on a 1:50 scale model of the test house. Furthermore, the toe nail connections were found to fail on the leeward side of the roof first. Hill *et al.* (2009) described the structural behaviour of wood roof sheathing panels subjected to realistic wind loading in order to determine whether dynamically tested panels respond in a similar manner to statically tested panels. It was found that dynamic loading of wood roof sheathing panels causes a reduction in capacity. Henderson (2010) studied the performance of roof cladding fastener connections used in Australian housing using similar real time pressure loading system and found similar results. Morrison and Kopp (2011) also obtained the uplift capacity of toe-nailed connection under realistic wind induced pressures. Morrison *et al.* (2011), Henderson *et al.* (2011) and Kopp *et al.* (2011) described the response of truss-to-wall toe nail connections in hip and gable roofs subjected to realistic wind loading. They determined the influence functions of toe nail connections from the application of patch loads (i.e area loads). These studies also have shown that the load is transferred to the adjacent connections with the progressively increasing failure of truss-to-wall connections.



Figure 2.2: Test house at UWO (Morrison and Kopp (2009))

Datin and Prevatt (2007) experimentally determined the load transfer functions for a scaled wood frame gable roof residential structure with wind tunnel derived pressure coefficients to determine uplift reactions at roof to wall connections. A roof section was constructed at one third scale trusses with load cells at roof-to-wall connection. The roof sheathing was modelled with oak strips scaled to the appropriate flexural stiffness to provide scaled load transfer between trusses. Eighteen loading points per truss were used to develop the influence surface. Time histories of the wind pressure coefficients obtained from a wind tunnel were converted to wind pressures and combined with the influence functions developed to generate wind load time histories for the truss-to-wall connections. Mensah *et al.* (2011) and Datin *et al.* (2011) derived influence functions normal to the roof on a 1/3 scale light frame wood structure shown in Figure 2.3, which was then subjected to a wind flow, while the surface pressures and structural reactions at roof-to-wall and wall-to-foundation connections were simultaneously recorded. They investigated the applicability of the database assisted design methodology which utilizes influence functions and wind load time histories to predict structural reactions of light framed wood structures subjected to fluctuating wind pressures. However, the scaled model used for these studies cannot be used to predict the non-linear behaviour and the progressive failure modes of the structural components.



Figure 2.3: 1/3 scale model building (Mensah *et al.* (2011))

2.6 Vulnerability studies based on engineering approach outside Australia

The engineering based vulnerability assessment to windstorms requires a good understanding of approach wind speed, the actual forces imposed on buildings by the wind and the structural behaviour of buildings under the wind loads up to failure. This requires the response of individual members in the elastic region, the post-elastic yielding, failure of individual elements, and the redistribution of loads through the structure as a result of local failures including time dependent effects such as fatigue. In practice there is usually insufficient information to develop a comprehensive engineering based vulnerability model and the most advanced models are from a combination of engineering science and expert opinion (Walker (2011)).

The majority of residential construction in the US is light-frame wood construction. The roofs of these houses consist of roof sheathing panels and rafters/trusses. The roof panels are connected to the rafters/trusses with nails. The rafters/trusses are connected to the wall/top plate with nails or Hurricane clips. The vulnerability defined in this study is also described as fragility in the US studies. The fragility of light-frame construction in the US to wind loads has been assessed using reliability and probability theories such as those described by Galambos *et al.* (1982), Ellingwood *et al.* (1982) and Ang and Tang (2007). Rosowsky and Cheng (1999a,b)

studied the reliability of roof system components of these houses subjected to high wind uplift loads. They selected three base-line structures and wind load statistics were determined using the historical wind speed records of three coastal regions. The statistics for other parameters in the wind load equation were obtained from a Delphi investigation by Ellingwood and Tekie (1999). A Lognormal distribution was assumed for wind loads in their reliability analysis. The statistical descriptions of strength were obtained from a combination of experimental and analytical investigations conducted previously. The results of the study identified a relatively small number of connections that dominate the modes of failure of these house types. It was determined that the critical sheathing panels were located at the edges of the roof, and critical roof-to-wall connections were located near the gable end.

Rosowsky and Ellingwood (2002) described an overview of the concepts of performance based design applied to residential construction and efforts taken to develop usable fragility (i.e. vulnerability) models and system reliability tools for assessing probable response in light-frame housing. A major driving force for this has been a move towards the development of performance based design of structures. Lee and Rosowsky (2005) presented a fragility assessment for roof sheathing in light-frame constructions built in high wind regions. The fragility curves show the probability of failure of a particular component or system with increasing wind speed. They developed a fragility model for individual and complete roof sheathing uplift using available fastener strength data, wind load statistics, and a code based approach for evaluating pressures. In this approach, they investigated five simple base-line structures with different wind directionality profiles, geographic locations, nail types and enclosure conditions using reliability concepts and probability theories. Ellingwood *et al.* (2004) also developed fragility curves for sheathing and truss-to-wall connections in light-frame wood construction subjected to wind hazards using similar theories. Li and Ellingwood (2006) proposed a probabilistic framework to evaluate reliability of low rise houses to wind hazards. Similar to previous studies, the fragility models were developed for the housing components. Figure 2.4 shows the fragility curves obtained for roof sheathing panels for different nails in

single story residential construction, and it shows the variability in curves with the nail type and roof overhang. It was assumed that damage results from breach of envelope, and roof panel and truss damage were due to wind uplift or higher wind pressure due to dominant openings. The study assessed the applicability of Lognormal cumulative distribution function in risk assessment of light-frame wood construction. The impact of uncertainties on structural reliability due to the use of different wind speed models expressed in probabilistic parameters (Weibull distribution with different parameters by others were used) was also studied and showed that the choice of different wind speed model for risk assessment purposes has a significant impact on structural reliability and on engineering decision analysis.

Many of these studies have focused on the behaviour of individual components. However, increasingly these studies also integrated this information to model the fragility of sub systems such as roof system and the whole house (Li and Ellingwood (2009) and Lindt and Dao (2009)).

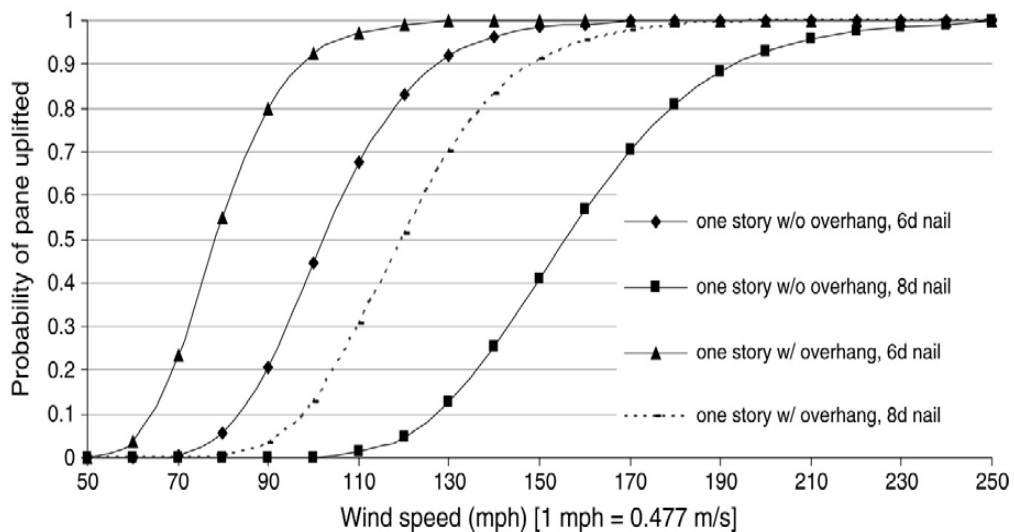


Figure 2.4: Roof panel fragility of two typical houses (Exposure B (ASCE 7-05)) (Li and Ellingwood (2006))

2.6.1 Damage prediction models

Unanwa *et al.* (2000) recognized the inherently probabilistic nature in the development of engineering vulnerability models. They presented a more detailed account of the process including modelling consequence of the failure of one component on the probabilities of failure

of other components. They outlined in considerable detail a framework for establishing a fully probabilistic engineering based vulnerability model for a building using fault trees to link all the possible modes of failure and interaction with each other, which they then applied to different classes of the buildings to obtain the damage to each class as a function of wind speed. This study incorporated a relatively large amount of expert engineering judgment especially in relation to the consequent failure of one component on the probabilities of failure of other components.

Pinelli *et al.* (2004) described a probabilistic framework for developing a practical probabilistic model for estimating damage from hurricane winds for residential structures in Florida, USA. Their study essentially followed the basic approach outlined by Unanwa *et al.* (2000) but describing it differently in terms of intersecting Venn diagrams to explain the interaction between the different modes of failure utilizing information on statistical characteristic of wind loads and structural behaviour. Their framework assured that all significant and possible types of wind damage scenarios were accounted and interaction between various types of damages were included in the calculations. They also described that the probabilistic input data should be based on laboratory studies, post damage surveys, insurance claims data, engineering analyses, and Monte Carlo simulation methods. The prediction model focused on various types of residential construction most common in Florida. The model also incorporated the uncertainties in loss calculations, based on uncertainties in the estimation of probability matrices, hurricane wind speeds, structural behaviour, component properties and costs, and building population. Later, the model was expanded to several commercial, residential and medium-rise buildings (Pita *et al.* (2009)). As described by Pinelli *et al.* (2008), the loss prediction model considered exterior damage (such as openings, roof cover, roof sheathing, walls and roof to wall connections), interior and utility damage and contents damage. The assessment of hurricane induced internal damage to low-rise buildings was also discussed by Pita *et al.* (2011). The combined results of external, internal and contents damages produced a set of probabilities of various level of overall damage ratio (expressed as a % of replacement cost) for a series of

prescribed peak 3s gust wind speeds. Figure 2.5 shows a set of vulnerability curves for weak, medium, and strong populations of masonry homes in central Florida and Figure 2.6 shows the contribution of different components of building damage to its vulnerability. Figure 2.6 shows that the interior and utility damages are also large contributors to the building vulnerability. The loss prediction model was validated and calibrated against the insurance claim data. A summary of the main components of the Florida public hurricane loss evaluation model is described by Hamid *et al.* (2010).

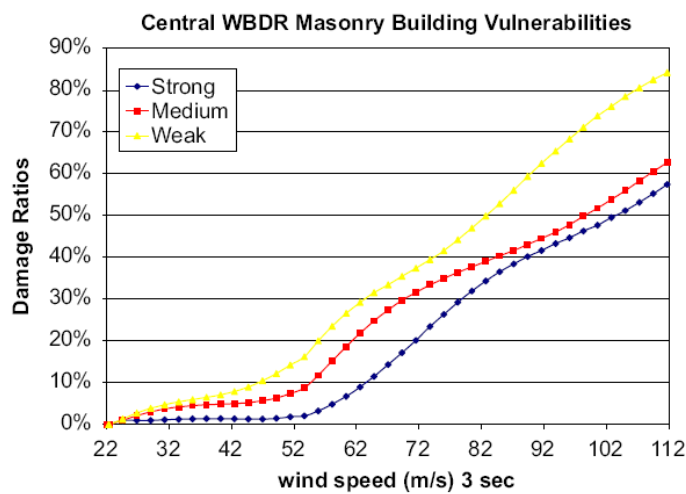


Figure 2.5: Vulnerability curves for masonry buildings in central Florida (Pinelli *et al.* (2008))

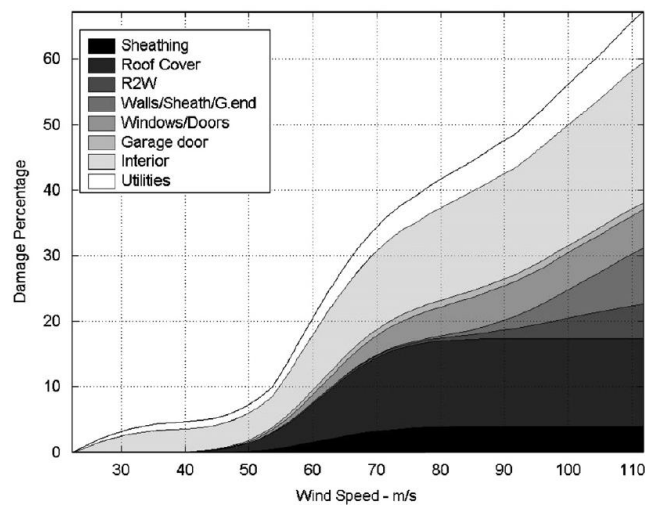


Figure 2.6: Components of the vulnerability for a masonry medium strength structure (Pinelli *et al.* (2008))

Vickery *et al.* (2006a) developed the HAZUS-MH hurricane model using wind engineering principles to enable detailed estimates of possible damage and loss to buildings and their contents due to windstorms. This hurricane hazard model was an improved version of the model developed by Vickery *et al.* (2000), and had undergone further validation studies. The wind hazard model provides the necessary inputs to estimate wind induced damage and loss, as described by Vickery *et al.* (2006b). Their model embodies most of the relationships described in previous studies. The damage to residential buildings was defined in four stages: minor, moderate, severe and destruction, and the failure probabilities were discussed with the increasing wind speed. The loss model estimates the costs associated with repairing the damaged building, replacing damaged contents, and estimating the costs associated with inability to occupy and use the damaged building. The vulnerability curves were developed in terms of variation of loss ratio (building and content loss divided by building and content value) with increasing wind speed. Their model has been validated through comparisons of modelled and actual insurance losses associated with hurricanes.

2.7 Vulnerability studies in Australia

A review of the current state of vulnerability modelling by Walker (2011), describes the evolution of techniques since the 1970's and the present state of capabilities. Most of the models used in the insurance industry are empirical models, based on fitting curves to data on damage, in the form of damage loss ratio versus the wind speed. The most common way of expressing the damage, damage loss ratio, is defined as the ratio of the damage repair cost to the replacement cost of the property. The most extensive development of empirical vulnerability models has been in the US by utilizing relatively large amount of data from losses from windstorms. However, the direct application of models developed in the US to other countries is unreliable due to the lack of data on local losses, the use of different forms of construction and different regulatory conditions. In general, buildings are classified according to classes which may include age, type of building, the form of structure and type of material, with separate

models for each. This approach was used by Walker (1995) to produce empirical damage curves that are used for estimating the damage and loss for pre-1980 and post-1980 houses built in cyclone regions of Australia. For a chosen wind speed, these models simulate the pattern of wind damage, in terms of the cost of repairing or replacing the damaged building. Empirical models are modified based as much on expert opinion as statistical analysis to accommodate significant changes that are made to house construction standards or when data is not available. A typical approach is to assume the shape of vulnerability curves for buildings of similar types, and validate these using available loss data or engineering judgment. As damage data at the higher wind speeds is often unavailable, considerable amount of expert opinion is needed to generate these curves. Henderson and Harper (2003) and Stewart (2003) produced vulnerability curves for a range of house types in cyclone regions of Queensland using similar methods and empirical approaches.

Following a series of discussions, Geoscience Australia (2007) produced vulnerability curves for a range of house types in Australia. They facilitated a series of wind vulnerability expert workshops to consolidate available information. The Australian residential building stock was categorized based on the wind region, the building age, and the building envelope materials. An expert group was engaged in a relative ranking exercise using the reference vulnerability curves in Figure 2.7. The overall ranking of vulnerability was expressed as a relative positioning to the curves in Figure 2.7. In order to be used reliably, these models based on expert opinion need to be validated with reliable data.

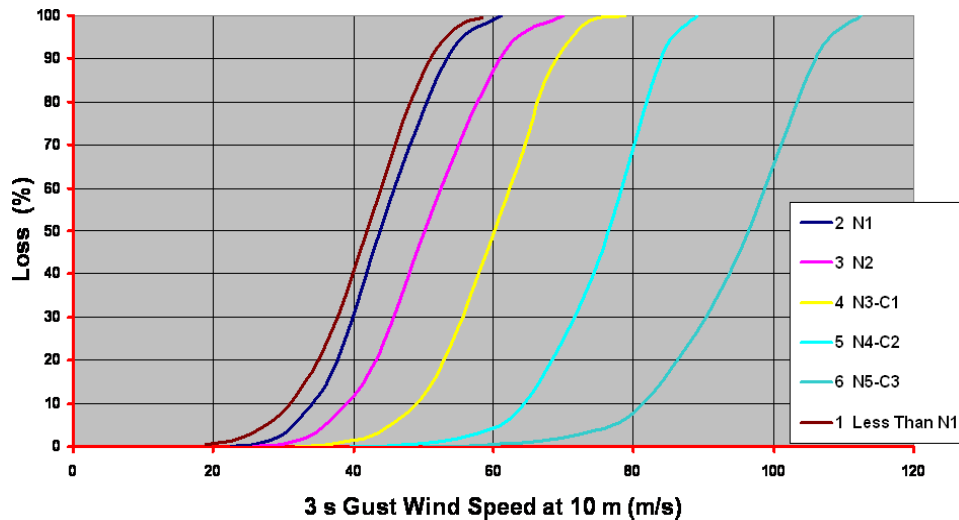


Figure 2.7: Reference curves for heuristic ranking process by expert group engaged through workshop activity, N and C classification according to AS 4055(2006) (Geoscience Australia (2007))

Compared to studies done in the US, limited work has been carried out on housing vulnerability in Australia using the engineering approach. Thus, only a few studies have been carried out using statistical descriptions of capacity of roofing components (based on test data) and wind loads considering the load transfer and interdependency between structural and non-structural components for Australian conditions. Henderson and Ginger (2007) studied the vulnerability of a high-set 1960's house with low pitch gable roof built in the northern part of Australia to wind speeds experienced in tropical cyclones by using reliability concepts. They assessed a common house which is of rectangular plan, timber-framed, elevated on piers about 2m high. The roofing is metal sheeting on a low or flat pitch roof. The metal cladding is screw fixed to the timber battens which are connected to the timber rafters with nails. The rafters are connected to the wall plate with skew nails. In these houses threaded steel rods tied down the top plate to the base of the houses at about 3m spacing around the perimeter. The vulnerability of each connection type was determined by using reliability methods incorporating probability theory and reliability concepts described by Holmes (1985), Leicester *et al.* (1985), Pham (1985), Pham *et al.* (1983), Melchers (1985), and Tang and Melchers (1985). The study estimated the likely failure mode and percentage of failure for a representative proportion of houses with increasing wind speed. The wind load and the component connection strengths were treated as random variables with Lognormal distributions. It considered the

interdependency between the structural components in the house, when estimating the types and percentages of the overall failures in the population of these houses. The load sharing between components were based on very limited testing and damage investigation results. The progressively increasing percentage of houses being subjected to high internal pressures resulting from damage to the envelope was considered. Figure 2.8 shows the typical vulnerability curves obtained from their study for different parts of the house with increasing wind speed. Results from their study also compared favourably with levels of damage and related modes of failure for high set houses observed in post cyclone damage surveys.

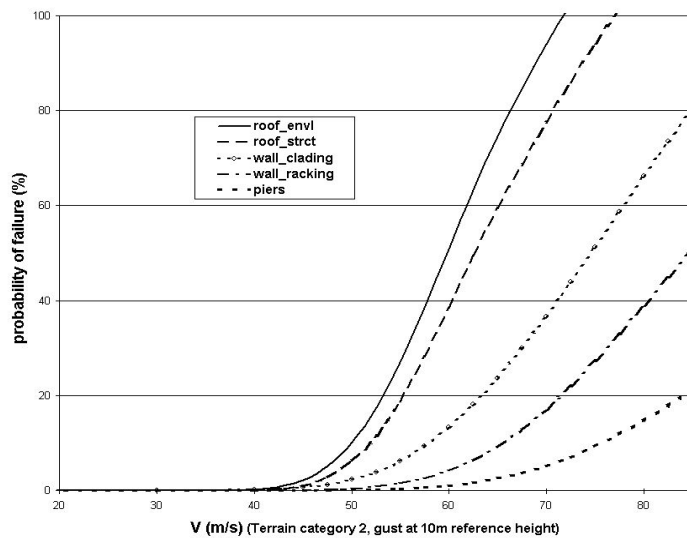


Figure 2.8: Estimated probability of failure of components in the modelled houses (Henderson and Ginger (2007))

Geoscience Australia in collaboration with Cyclone Testing Station and JDH Consulting, have commenced developing a software tool, called VAWS, to quantitatively model vulnerability of residential buildings to severe wind in Australia. Wehner *et al.* (2010b) described the software package and presented typical results. The software package is used to specify a type of house with values for component/connection strengths, external and internal pressure coefficients, shielding coefficients, wind speed profile, building orientation, debris damage parameters, and component weights sampled from pre-determined probability distributions. Then, for successive gust wind speed increments, it calculates the forces in all nominated connections and identifies

the connections that have failed and translates it into a damage scenario which is cost to calculate a damage index (expressed as the total repair cost) for that wind speed. The software package has been developed to model the damage to roof sheeting, roof battens, roof structure, wall cladding, damage from windborne debris and damage from water ingress. The model has been validated for a single house type: a timber frame high-set, fibro clad house type in residential building structures in the 1960's and early 1970's cyclone regions of Queensland to Darwin, as analysed by Henderson and Ginger (2007). It was implied that future work involved extending the scope of the tool to include damage to wall structure as well as calibrating results against damage observed during post-storm surveys.

2.8 Summary and Discussion

Recent damage investigations have shown that the structural system of contemporary houses generally performs satisfactorily in windstorms approaching the design wind speed. However, shortcomings in some aspects of design and construction mean that there is still an increased risk to contemporary housing from windstorms. The increasing population in cyclonic areas and the uncertainty regarding the potential effects of climate change on the frequency and magnitude of windstorm has increased this risk.

If the nature of the disaster risks is to be fully understood and cost effective measures taken to mitigate them, a better understanding of the structural response of contemporary houses to windstorm is required. Studying the response of the roof structure (i.e. the most vulnerable part of the house) to wind loading will provide data for assessing house performance in a windstorm. The response of the roof is dependent on the transfer of load from cladding to batten to truss to wall, the redistribution of load with progressive failure and the interdependency of structural elements, with increasing wind speed.

Most studies on reliability were primarily focused on individual component behaviours and consequence of their failure. The overall vulnerability of a house type is concerned with the

behaviour of whole house structural system including progressive damage with increasing loads. It is about the integration of the response of many components acting together as a structural system. The assessment of reliability for a complex structural system (such as the roof of a house) has to consider the interaction of all the structural components and members of the system. Furthermore, the number of possible failure modes can be quite large. These issues should be addressed by studying the load sharing and interdependency between components.

In order to develop vulnerability models for contemporary houses, it is essential to have knowledge of the variability and uncertainties of load actions and building response. The statistical parameters of connection strengths can account for the uncertainty and variability associated with loads. The structural system and the connections in the contemporary houses in Australia are different from previous studies on older Australian houses and other overseas studies. Most of those studies have used Normal and Lognormal distributions to describe the strength data. The probabilistic descriptions of connection strengths based on cyclic and static test data of are required to accurately assess the performance of houses of a selected type. Furthermore, accurate representation of load transfer among these connections is also significant.

Full scale and wind tunnel studies of low rise buildings have shown that the approach wind flow generates spatially and temporally varying pressure on roofs, and these loads are dependent on the approach wind direction and also the terrain and topographic features. A boundary layer wind tunnel test is the most effective means of obtaining appropriate pressure or force coefficients for use in wind loading standards. Standards such as AS/NZS 1170.2 (2011) provide a nominal design wind load on a structure and the direct use of such values in vulnerability assessment is a conservative interpretation. Several previous studies have determined the wind load acting on a range of house types, but studies on the area averaged pressure acting on individual components/connections over different areas of the roofs in probabilistic terms are scarce. Therefore, it is necessary to obtain the probabilistic descriptions of the wind pressure acting on connections in different areas of the roof in order to determine

vulnerability of its components and connections. The structural components of the buildings should be clearly identified and the wind loads acting on these elements needs to be determined. A dedicated wind tunnel model test on this type of house is carried out to provide an accurate representation of the wind loads.

Research on the structural response to wind loading has been focused on improving design procedures and design codes. Full scale and sub-assembly tests conducted by the Australian and international researchers have produced data on the overall response of houses to wind loads. However, there is limited test data available to describe the load sharing, progressive failure and resulting interdependency between components in contemporary Australian houses. A series of tests on a specimen roofing sub-assembly is carried out covering a range of scenarios to produce data that can be used in structural vulnerability models. The results from experiments can be used in combination with analytical results obtained from structural analysis models for assessing the structural response to a range of loads. Linear and non-linear behaviour of structural components are studied in order to predict the behaviour of housing components subjected to windstorms.

The vulnerability assessment of houses in Australia to windstorms has mostly been based on empirical approach and expert opinion. Only limited studies have been carried out on actual probabilistic nature of the damage to the housing from wind which is needed if a reliability performance based approach to design is to be developed. Some of the vulnerability models described use the codified values which may be conservative interpretations, for determining the load actions of the buildings. The use of these values can provide unreliable vulnerability estimates of houses or housing components. Furthermore, current vulnerability models do not satisfactorily account for load sharing, load distribution and progressive failure in house components. Physical tests carried out on a structural system provide data required for calibrating and validating the vulnerability models. Statistical descriptions of wind loading and component strength can be combined with sub-assembly test data to improve vulnerability models.

3 ROOF STRUCTURE OF A CONTEMPORARY HOUSE AND ANALYSIS METHODS

This chapter presents the structural system, roofing components and connections of a common masonry block house, based on a survey of housing in a cyclonic region of Australia. Furthermore, the capacities of roofing connections are presented in terms of probabilistic parameters. This chapter also describes theories and methods used in this thesis to calculate nominal design wind loads and to assess vulnerability of roofing connections.

3.1 Masonry Block House

A survey was carried out by a team from CTS including the author in cyclonic region of North Queensland in Australia, to obtain the structural characteristics of contemporary houses under construction. The features such as size, shape, cladding, roof shape and pitch, method of construction, type of connections and structural system were surveyed on approximately 100 houses. In addition, certified drawings of houses submitted to the local authorities were also reviewed. More than 90% of the houses surveyed were of masonry block type. A typical house of this type is constructed on a concrete slab on ground with masonry block walls filled with concrete and continuous reinforcement at regular intervals from the bond beam at the top of the wall to the slab. These houses have either gable or hip roof shape or a combination of these. This study focuses on the gable shape roof, as they experience larger wind loads and post disaster surveys reveal that they are more vulnerable to damage in windstorms.

Figure 3.1 shows a masonry block house under construction (i.e. a house with a hip roof shape) and Table 3.1 provides a summary of the survey data in statistical terms. Based on the survey data, a single story gable end $10\text{m} \times 19.8\text{m} \times 2.7\text{m}$ low rise house with 0.6m roof overhang and 22.5° pitch represents a common contemporary house.



Figure 3.1: Masonry Block house under construction (Hip roof shape)

Table 3.1: Characteristics of Masonry block Houses

Feature	Mean	Coefficient of variation
Length	19.7m	0.10
Width	11m	0.26
Roof Pitch	22.5°	0.14
Roof overhang	613mm	0.13
Wall Height	2.67m	0.18
Batten spacing	886mm	0.10
Truss spacing	915mm	0.07
Cladding fastener spacing	Every crest or every 2 nd corrugation (152mm)	N/A

3.2 Roofing connections

The roof structure of masonry block house consists of timber trusses and top hat battens clad with metal roof sheeting. The trusses and battens are spaced nominally 900mm apart with an overhang of 600mm to fit the house dimensions. Figure 3.2 shows a schematic of the trusses and battens in a masonry block house. The timber trusses are manufactured from machine grade pine (MGP12) 90mm × 35mm components joined with toothed truss connector metal plates and connected to the bond beam at the top of the wall with a metal cleat bolted to the truss, as shown in Figure 3.3. In some cases, straps or angle brackets are also used to connect the truss to the wall instead of cleats. Top hat battens, (40mm × 40mm), manufactured from G550 steel with a base metal thickness (BMT) of 0.75mm are fixed to the top chord of these trusses with two Type-17 screws (No14-10 × 25mm), as shown in Figure 3.4. The metal roof cladding is usually corrugated profile with a base metal thickness of 0.42mm and is attached to the battens using Type-17 cladding fasteners (No14-10 × 50mm) without cyclone washers, as shown in Figure 3.5. The spacing of the cladding fasteners is every second crest of the corrugations (152mm) but sometimes different spacings are used in the edges and middle of the roof. Ceiling sheeting (usually plasterboard) is fixed directly to the trusses or to metal ceiling battens connected to the bottom chord of trusses.

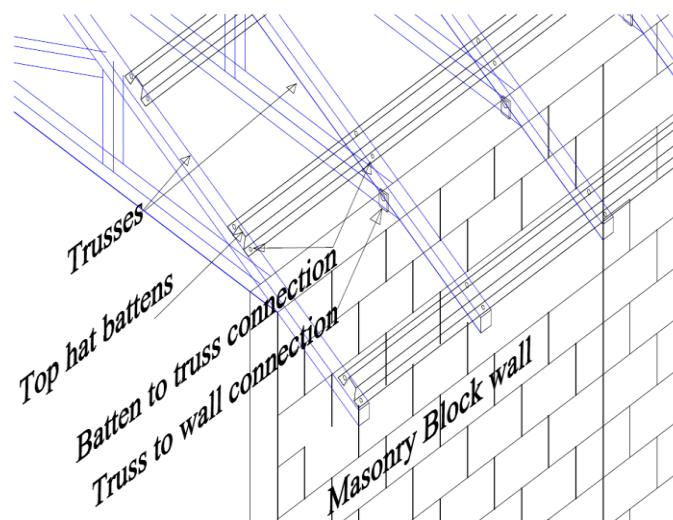


Figure 3.2: Battens and trusses in Masonry block house



Figure 3.3: Truss-to-wall connection

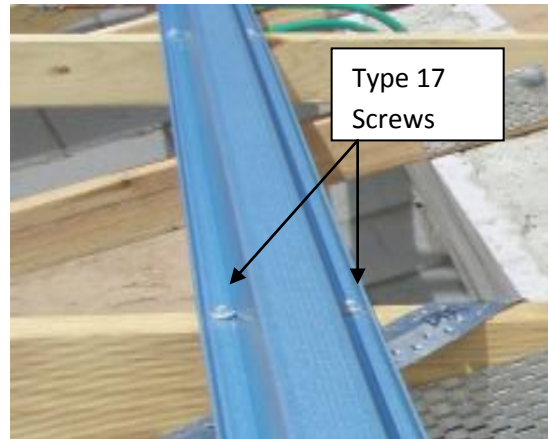


Figure 3.4: Batten-to-truss connection

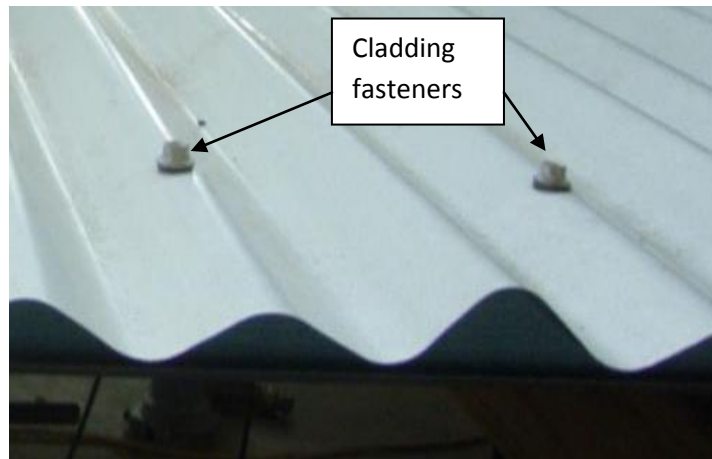


Figure 3.5: Roof cladding-to-batten connections

3.2.1 Connection Strengths

The variability of strength of components and connections in houses are associated with differences in design, materials, construction practices and workmanship. This variability that exists even in connections that are designed to the same specifications and other uncertainties are represented in the probabilistic models. This study analyses the responses and failure of

- Roof cladding fastener
- Batten-to-truss connection
- Truss-to-wall/bond beam connection

The Cyclone Testing Station (CTS) has compiled a database of strength capacities for a range of connection types, based on experiments, structural analysis and damage investigations. The capacities of these connections are derived from static and a range of cyclic test regimes by considering the full scale behaviour of roof systems. This database was used to obtain the statistical properties for the capacity of each connection. The particular probability distribution function (PDF) for each connection type was defined from fitting the available data with various distribution types (i.e. Normal, Lognormal, Rayleigh, Gamma and Weibull) and using the Anderson-Darling (A-D) goodness-of-fit test. The A-D test is particularly useful when the tails of a distribution is important (Ang and Tang (2007)). The values of the capacities are normalized by the design value of each connection, ϕR_N . Where ϕ is the capacity reduction factor ($\phi=0.8$ was used in this study) and R_N is the nominal capacity of the connection. The design values were obtained from codes and product manuals. Table 3.2 shows the statistical descriptions of the capacity for each connection.

Table 3.2: Connection Capacity Statistics

Connection	Mean($R/\phi R_N$)	COV	PDF
Roof cladding-to-batten connection	1.22	0.15	Lognormal
Batten-to-truss Connection	1.30	0.30	Lognormal
Truss-to-wall connection	1.40	0.30	Lognormal

The Lognormal distribution was found to be the best fit for all three connection strengths. It satisfied all the considered levels of significance (1%, 2%, 5%, 10% and 20%) for the cladding-to-batten connection (p-value 0.55). The batten-to-truss connection was most strongly a Lognormal distribution with p-value 0.995 (the higher the p-value the stronger the assumed distribution becomes) and truss-to-wall connection gave a p-value of 0.58 with satisfying all the confidence levels.

3.3 Design of houses

Structural design of houses is required in order to protect building occupants against injury or loss of life. Therefore, the main objective of current codes (BCA (2011)) and standards is to prevent building failures, leading to loss of life during extreme events. Over the past years, performance based design has been acknowledged as a rational approach in the design of structures, and is gradually becoming accepted around the world. In Australia, AS/NZS 1170.0 (2002), AS/NZS 1170.1 (2002), AS/NZS 1170.2 (2011) and AS 4055 (2006) are mainly used for deriving dead, live and wind load actions. AS/NZS 1170.0 (2002) stipulates combinations of loads including wind actions to be applied on structural system components that are checked against their design strength. Failure occurs when the combined load exceeds the component's strength. The limit state design takes a more rational approach to structural safety by defining partial load factors for each type of loading and separate resistance factor for the resistance.

The typical design relationship is given by

$$\phi R \geq S^* \quad (3.1)$$

Where S^* - Factored structural load effect given by the adverse combination of loads, R - Structural resistance, and ϕ - Capacity reduction factor

The ultimate design relationship for the wind load effects on roofing connections is given by Equation 3.2.

$$\phi R \geq \gamma_d D + \gamma_w W \quad (3.2)$$

Where D - Dead load, W - Wind load, γ_d - Dead load factor, γ_w -Wind load factor

3.3.1 Design approach for wind loads

The wind load standard AS/NZS 1170.0 (2002) used in Australia is based on the limit state design approach introduced in the 1980's. AS/NZS 1170.2 (2011) provides data for calculating the design wind speeds related to the return period, for the class of structure specified in BCA,

for cyclonic and non-cyclonic regions. The wind loads for housing standard AS 4055 (2006) is based on AS/NZS 1170.2 and uses a 500yr return period wind speed for ultimate limit state design. The 10 m height gust wind speed (V_R) as defined in AS/NZS 1170.2 (2011), for a 1:500yr probability in cyclonic region C and D is 69m/s and 88m/s, respectively. These wind speeds have a specified nominal probability of exceedance of about 10% in 50 yrs. In most cyclone and non-cyclone regions, the determination of wind loads for housing is carried out using the standard on wind loading for residential housing, AS 4055 (2006).

Wind loads for the design of cladding fixings on buildings can be calculated from pressures derived from nominal shape factors or pressure coefficients, provided in Standards such as AS/NZS 1170.2 (2011). The design pressures are calculated from Equation 3.3, where ρ is the density of air, V_h is the design gust wind speed at mid-roof height given in Equation 3.4 and C_{fig} is the aerodynamic shape factor. Quasi-steady, external pressure coefficients, C_{pe} , and internal pressure coefficients, C_{pi} , combined with factors for area-averaging, K_a , surface-combinations, K_c , permeable cladding, K_p , and local-pressure effects, K_l , are used to determine C_{fig} values for external and internal pressures as shown in Equations 3.5 and 3.6.

$$p_{design} = 0.5\rho V_h^2 C_{fig} \quad (3.3)$$

$$V_h = V_R M_d M_{z,cat} M_s M_t \quad (3.4)$$

$$C_{fig} = C_{pe} (K_a \times K_{c,e} \times K_l \times K_p) \quad (3.5)$$

$$C_{fig} = C_{pi} K_{c,i} \quad (3.6)$$

Where, V_R – Regional gust wind speed at 10m height in Terrain Category 2 for a specified return period, M_d . wind directional multiplier, $M_{z,cat}$ – terrain /height multiplier, M_s -. shielding multiplier, and M_t -. topographic multiplier

Nominal external and internal design pressures, p_N acting over the tributary area, A_N are combined to get the nominal, design wind load, W_N on the component as indicated in Equation 3.7.

$$W_N = p_N A_N \quad (3.7)$$

The most critical load combinations, S^* , which are used for ultimate limit state design as per AS/NZS 1170.0 (2002) is given in Equations 3.8 and 3.9.

$$1.2D_N + W_N \quad \text{-downwards} \quad (3.8)$$

$$0.9D_N + W_N \quad \text{-upwards} \quad (3.9)$$

Where, D_N is the nominal dead loads acting on the structure or particular connection being considered.

3.4 Reliability theory

A measure of resilience of a connection to wind loading is estimated by the probability of failure of the connection as a result of its strength being exceeded by the wind load. The load and the resistances are taken as random variables and the required statistical information is assumed to be available. In this process, the load effect, S and corresponding structural resistance, R are analysed statistically and the probability of failure calculated. The information required are the mean and coefficient of variation (COV) values of S and R or their probability density functions $f_S(S)$ and $f_R(R)$. Failure occurs when the load effect exceeds the resistance of the connection ($S > R$). This approach can be used for estimating the vulnerability of roofing components to wind loading as shown by Henderson and Ginger (2007). The dead load value is combined with the wind load in assessing these failures in this study.

Assuming that S and R are statistically independent, the probability of failure is given by

$$P_f = \int_{-\infty}^{\infty} F_R(S) f_S(S) dS \quad (3.10)$$

Where $F_R(R)$, is the cumulative probability distribution, such that $F_R(S) = \int_{-\infty}^S f_R(R) dR$.

3.4.1 Dead load

The dead loads influencing each connection type are based on the weight of cladding, battens and trusses. The dead load can be modelled by a Lognormal distribution with calculated mean value based on the material weights and an assumed coefficient of variation (0.1 was used by Holmes (1985) and Leicester *et al* (1985)). The following values are used in this study.

$$\text{Mean (D/D}_N) = 1.05 \quad \text{COV (D/D}_N) = 0.10$$

Where D - dead load, D_N -nominal value of dead load.

3.5 Wind load probabilistic model

Wind loads, W , acting on components of a building can be given by the probabilistic model in Equation 3.11, where V is the maximum gust velocity at 10m height in standard terrain category 2 in 50 yrs (life of structure) and the parameter B includes all the other parameters including the pressure coefficients used for calculating the wind load as described by Holmes (1985) and Henderson and Ginger (2007).

$$W = BV^2 \tag{3.11}$$

Here, B is a parameter combining all variables of the wind load except the basic wind speed.

The product of the variables shown in Equation 3.12, gives parameter B.

$$B = \lambda . A . (C . E^2 . \theta^2 . G . \rho / 2) \tag{3.12}$$

Where:

C is the quasi-steady pressure coefficient, (i.e C_{pe} or C_{pi})

E is a velocity height multiplier that accounts for the exposure and height, ($M_{z,cat}$)

θ is a factor for wind directionality effects (M_d)

G is a factor that accounts for gusting effects and is related to K_a and K_1 ,

ρ is the density of air,

A is the tributary area, and

λ is a factor to account for modelling inaccuracies and uncertainties in analysis methods (unknowns)

The nominal design load is made up of nominal values of all the above parameters together with the wind speed as shown in Equation 3.13. This probabilistic relationship can be presented in non dimensional form of Equation 3.14.

$$W_N = B_N V_N^2 \quad (3.13)$$

$$W/W_N = [B/B_N] [V/V_N]^2 \quad (3.14)$$

$$\text{Where, } [B/B_N] = [\lambda/\lambda_N] [A/A_N] [C/C_N] [E/E_N]^2 [\theta/\theta_N]^2 [G/G_N] [\rho/\rho_N]$$

Each of normalized terms in the brackets is treated as random variables with probability distributions, mean, and coefficient of variation obtained from analysing available data. The estimation of the values of mean and coefficient of variation is a difficult procedure. It requires statistical data which in many cases is virtually nonexistent. However, these can be estimated from survey data, Delphi analysis and wind tunnel model studies. In cases when this data does not exist, assumptions are made.

3.6 Summary and Discussion

The study identified the structural system, roofing components and connections of a common masonry block house, based on a survey of housing in the cyclonic region of Australia. The capacities of roofing connections (i.e. cladding fastener connection, batten-to-truss connection

and truss-to-wall connection) were obtained from available test data, and were found to be greater than the capacities specified in codes and product manuals. The strength capacities used in this study account for the fatigue strength of the connections determined according to the current test standards (i.e. Low-High-Low (L-H-L) test regime etc). It was also found that the uplift capacity of these connections can be described by Lognormal distribution.

This study focuses on commonly used connections related to these structural systems. The structural systems of contemporary Australian house roofs are made up of timber and steel materials with variability in engineering material properties. In addition, these structural systems are designed and fabricated with a range of connections and fastener details, and varying construction quality and code enforcement from building to building. Thus, the variability of the connection strength changes with these factors and should be considered to assess the vulnerability of these houses in more generalized manner. In order to achieve this, the strength capacity of these connections with different fixing types should be determined considering the full scale behaviour of the structure such as those used in this study. The laboratory conditions under which individual roof connections are tested may also significantly influence the resulting statistical parameters and probability distributions. This can be a major source of uncertainty for vulnerability assessments. The individual connection tests can be useful for specifying the connection design values which are usually conservative determinations.

4 WIND LOADING

This Chapter presents the wind load acting over the roof of the common masonry block house obtained from a wind tunnel model study. Furthermore, the variability of these loads and the probabilistic descriptions of wind loads over the connections on the roof are presented. These results are also compared with the loads obtained using AS/NZS 1170.2 (2011).

4.1 *Experimental setup*

Wind tunnel model studies were carried out in the 2.0m high 2.5m wide 22.0m long boundary layer wind tunnel at the School of Engineering and Physical Sciences, James Cook University. The approach atmospheric boundary layer was simulated at a length scale of 1/50 over a fetch by using a 250mm high trip board at the upstream end followed by an array of blocks on the tunnel floor. Figures 4.1 and 4.2 show that the mean velocity (referenced to mean velocity at 25m) and turbulence intensity profiles measured fall between terrain category 2 and 3 profiles at mid roof height as per AS/NZS1170.2 (2011), confirming the profiles obtained by Ginger *et al.* (2000).

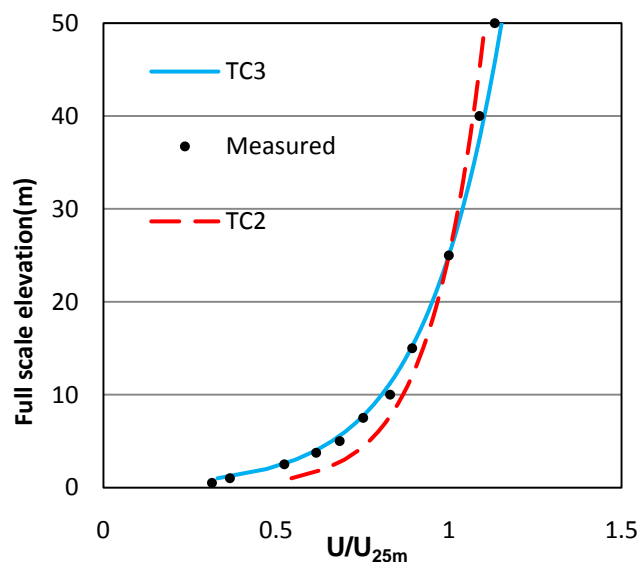


Figure 4.1: Mean velocity profile

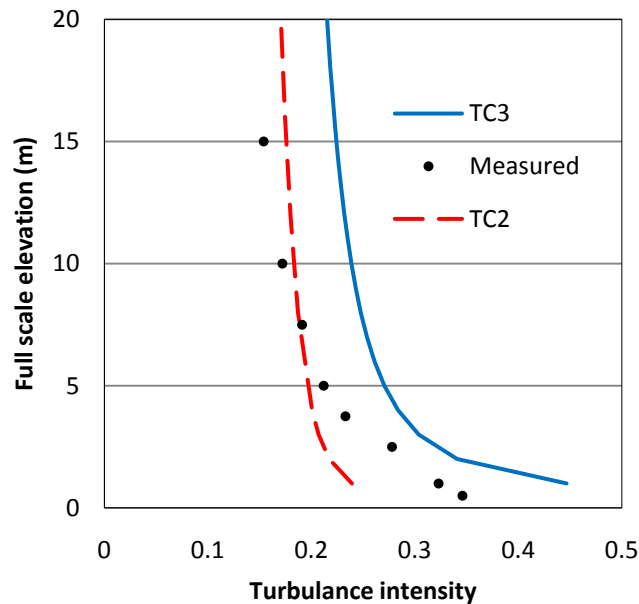


Figure 4.2: Turbulence intensity profile

The level of detail that can be incorporated in a wind tunnel model depends on the scale of model and its size. In case of the low rise house studied here, a model of 1/50 satisfactorily accommodates essential details such as the eaves, overhang etc. The information required for design is the peak loads acting over the tributary area of interest. This is a significant factor affecting to the structural behaviour.

A gable end $10\text{m} \times 19.8\text{m} \times 2.7\text{m}$ low rise house with 0.6m roof overhang and 22.5° pitch was constructed at a length scale of 1/50. The batten and truss layout and the pressure tap locations are shown in the Figure 4.3 (The isometric view is also shown in Appendix A). The battens spaced at 877mm in general areas and 650mm on eave and the roof trusses spaced at 900mm apart are identified from A to W. The wind pressures were measured on the pressure taps shown in Figures 4.3. Each roof truss tributary area was divided in to sixteen patches identified as 1...16 as shown in Figure 4.4. These patches are the typical batten-to-truss connection tributary areas that are named as B1...B16 for truss B, C1...C16 for truss C etc. The wind loads on tributary areas representing cladding fixings in regions; P, Q, R, S, T shown in Figure 4.4, are

also discussed in next section. Figure 4.5 shows the house model installed on the turn table in the wind tunnel.

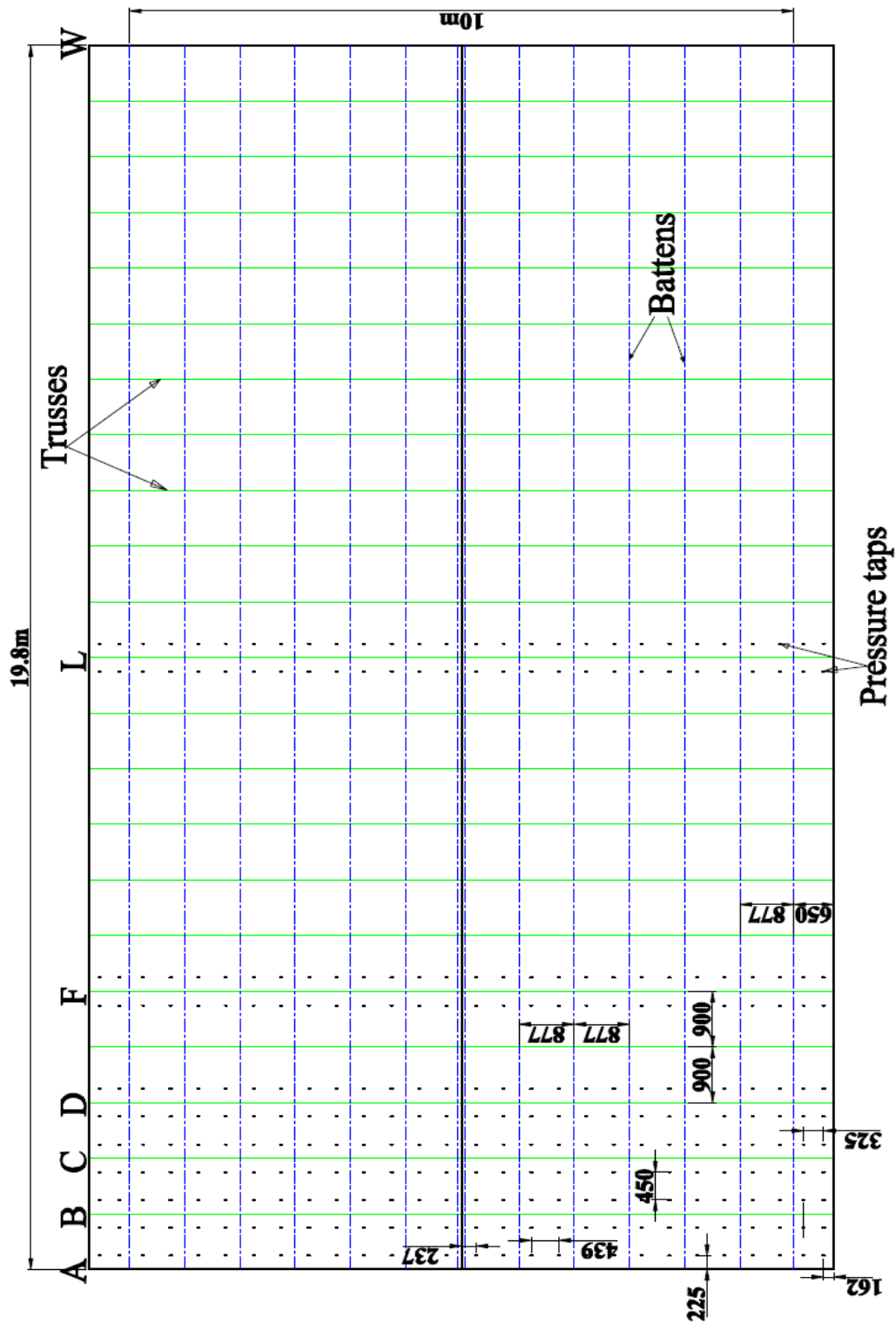


Figure 4.3: Pressure tap layout

(All dimensions are in 'mm' unless specified)

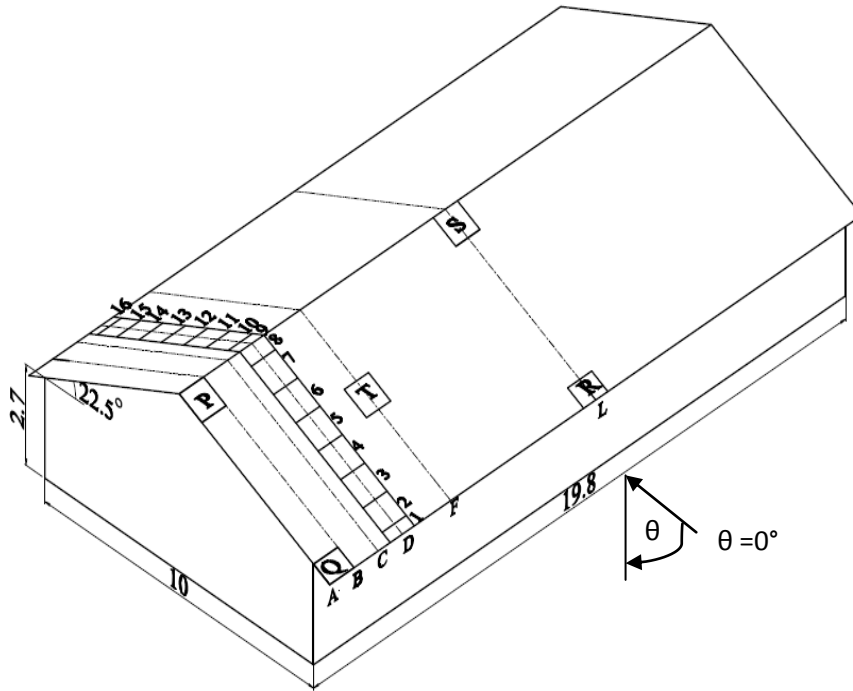


Figure 4.4: 10m x 19.8m x 2.7m gable end low rise house with 22.5° roof pitch



Figure 4.5: 1/50 scale model of the 10m x 19.8m x 2.7m house in the wind tunnel

External pressures were obtained for approach wind directions $\theta = 0^\circ$ to 360° in steps of 15° . Pressure taps on each patch were connected to a transducer using a tubing system via a pressure measurement system and pressures on 62 taps were measured simultaneously. The fluctuating

pressures were cut off at 625Hz and sampled at 1250 Hz for 30 seconds, and presented as pressure coefficients ($C_p(t) = p(t)/\frac{1}{2}\rho\bar{U}_h^2$). For a length scale ratio of 1/50 and velocity ratio of 2/5, this results in an equivalent full scale observation time of 10 minutes and a time scale of 1/20. These pressure coefficients were statistically analysed to obtain mean ($C_{\bar{p}}$), maximum ($C_{\hat{p}}$) and minimum ($C_{\check{p}}$) pressure coefficients in a single run;

$$C_{\bar{p}} = \frac{\bar{p}}{\frac{1}{2}\rho\bar{U}_h^2} \quad C_{\check{p}} = \frac{\check{p}}{\frac{1}{2}\rho\bar{U}_h^2} \quad C_{\hat{p}} = \frac{\hat{p}}{\frac{1}{2}\rho\bar{U}_h^2}$$

Where, $\frac{1}{2}\rho\bar{U}_h^2$ is the mean dynamic pressure at mid roof height h . Five runs were conducted for each angle to obtain repeat sets of pressure coefficients.

Henderson (2010) found that the wind pressure on series of cladding fixings can be represented by a single pressure tap. Therefore, the loads on cladding fixings in regions P, Q, R, S and T were obtained using the individual taps in each region. The loads on batten fixings were obtained by averaging simultaneous pressures acting on the group of taps representing each batten-to-truss connection tributary area. However, the load transmitted to the batten-to-truss connection is dependent on the cladding and structural support system including their directional stiffness properties. Therefore, this area averaged pressure may not give a satisfactory representation of the wind loads acting on the batten-to-truss connection. This is determined in Chapter 6 combining structural tests results in Chapter 5 with the wind loads.

4.2 Experimental results

4.2.1 Pressure distribution-cladding

The variation of external pressure coefficients $C_{\bar{p}}$, $C_{\hat{p}}$ and $C_{\check{p}}$ for all five runs on taps representative of cladding fixings with the wind approach direction (θ), for regions P, Q and T are shown in Figures 4.6, 4.7 and 4.8. The variation of external pressure coefficients for R and S are also shown in Appendix A. Wind loading standards typically provide design pressure

coefficients for wind directions perpendicular and parallel to the ridge. The nominal peak pressure coefficients (C_{p_N}) derived from Section 5 of AS/NZS1170.2 (2011) is $C_{p_N} = C_{p_e} \times K_l \times G_U^2$, where C_{p_e} is the external pressure coefficient, K_l is the local pressure factor and $G_U = \hat{U}_h/\bar{U}_h$ is the velocity gust factor which was taken as 1.875 in this study as per AS/NZS 1170.2 (1989). Here, \hat{U}_h and \bar{U}_h are gust wind speed and mean wind speed respectively at mid roof height. These C_{p_N} values for each region are also shown in Figures 4.6, 4.7 and 4.8 for wind approach directions 0° , 90° , 180° and 270° . It should be noted that there are 20 values of pressure in each region for each wind approach direction based on the number of repeat runs (five) and number of pressure taps in each area (four).

These Figures show that there was a large variability in wind load at each wind approach direction and the largest suction was expected in region P for wind approach directions 135° to 150° . The design of cladding fastener fixings are based on largest load stipulated in AS/NZS 1170.2. As shown in the Figures, the largest code design values occur at wind approach direction 90° in region Q. Figure 4.6 shows that the peak pressures obtained for region P exceeded the design values stipulated in AS/NZS 1170.2 (2011) for wind approach directions 120° to 150° . Hence, the design values underestimated the design of cladding fixing on region P. Compared to P and Q regions, R, S and T regions have lower suction. Thus, the roof cladding at roof corners experience larger wind loads compared to those at middle regions and cladding fixings in region P are more prone to failure.

These peak and mean values were in close agreement with values and patterns obtained from the previous wind tunnel model studies such as those by Holmes and Best (1977), Reardon and Holmes (1981), Meecham *et al.* (1991), and Lin and Surry (1998). However, there were some differences due to variations in the experimental set up in those studies (i.e. Changes to the basic dimensions of the houses such as roof pitch, height etc).

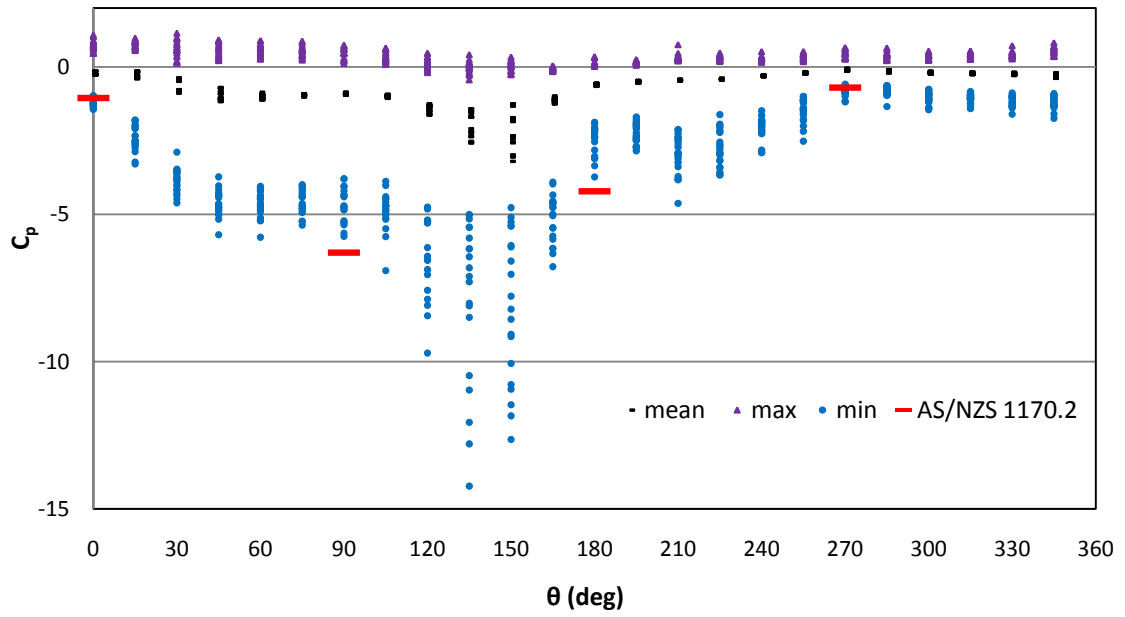


Figure 4.6: Pressure coefficients vs wind direction – P (cladding)

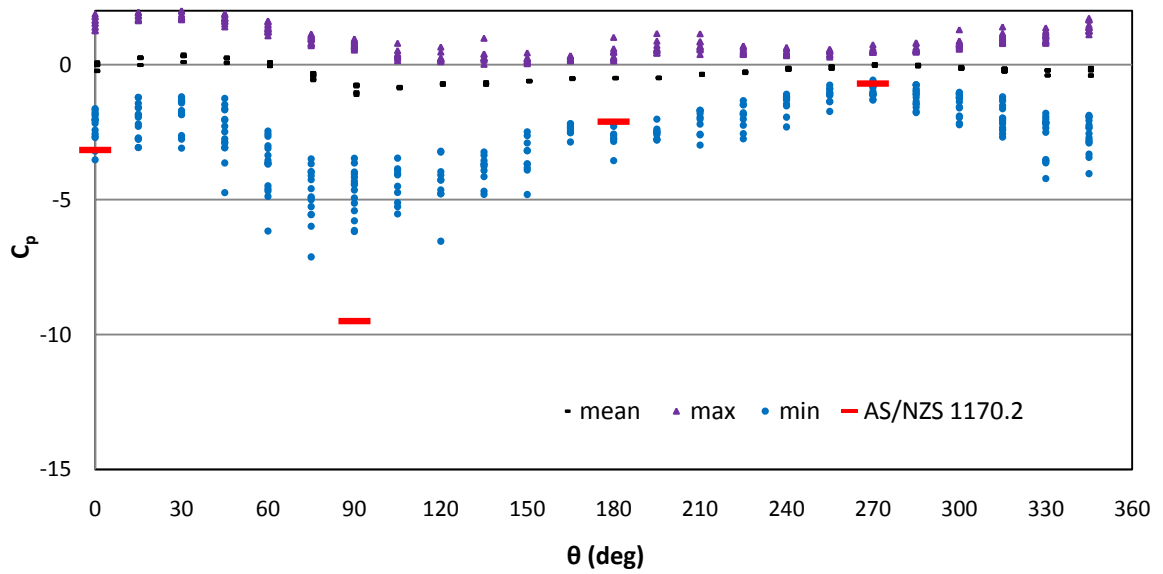


Figure 4.7: Pressure coefficients vs wind direction - Q (cladding)

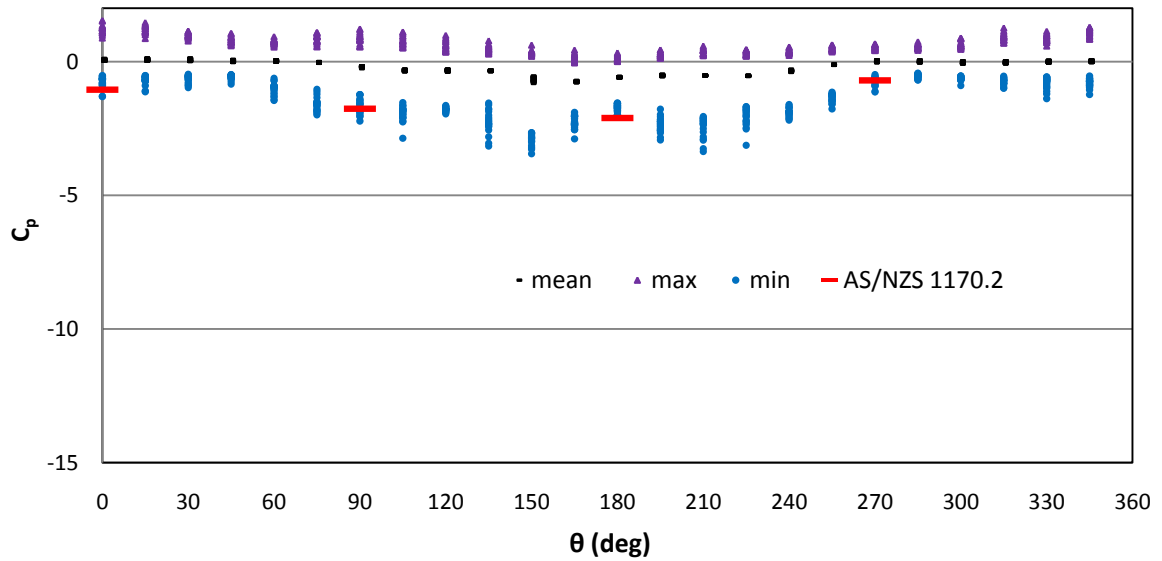


Figure 4.8: Pressure coefficients vs wind direction - T (cladding)

4.2.2 Pressure distribution-Battens

The variation of area-averaged external pressure coefficients $C_{p\bar{}}$ and $C_{p\bar{}}$ for all five runs with the wind approach direction on batten-to-truss patches B2, B7 and F5 are shown in Figures 4.9, 4.10 and 4.11, respectively. Further, the data for L2 and L7 are shown in Appendix A. These area-averaged pressures were obtained by averaging the pressure simultaneously at each tap on the patches. These Figures show the large variability of wind load on batten fixings with wind approach directions and the large peak suction pressure occurred in regions B2 and B7 for wind approach directions 90° and 135° to 150° respectively compared to F5, L2 and L7 regions. The corresponding AS/NZS 1170.2, C_{pN} values for batten-to-truss connection tributary areas are also given for wind approach directions of 0° , 90° , 180° and 270° . According to these Figures, AS/NZS 1170.2 (2011) gives a reasonable estimate for loads on batten fixings. The spatial area averaging produced a reduction in peak pressures on patch B7 compared to peak pressures on cladding fixings in region P. Jayasinghe and Ginger (2011) showed that taking the average of the peak pressure coefficients of each of the tap within the tributary area gives a conservative

(i.e larger) peak area-averaged pressure, but with a similar trend. These values were higher than the simultaneous peak pressure measurements obtained.

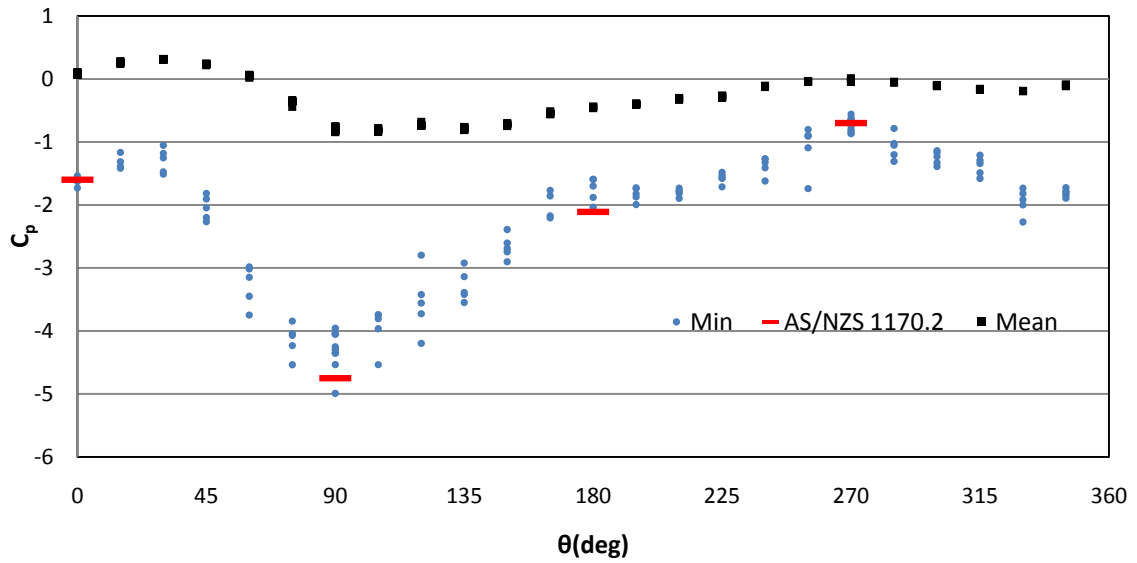


Figure 4.9: Pressure coefficients (C_p) vs wind direction – Batten-to-truss connection B2

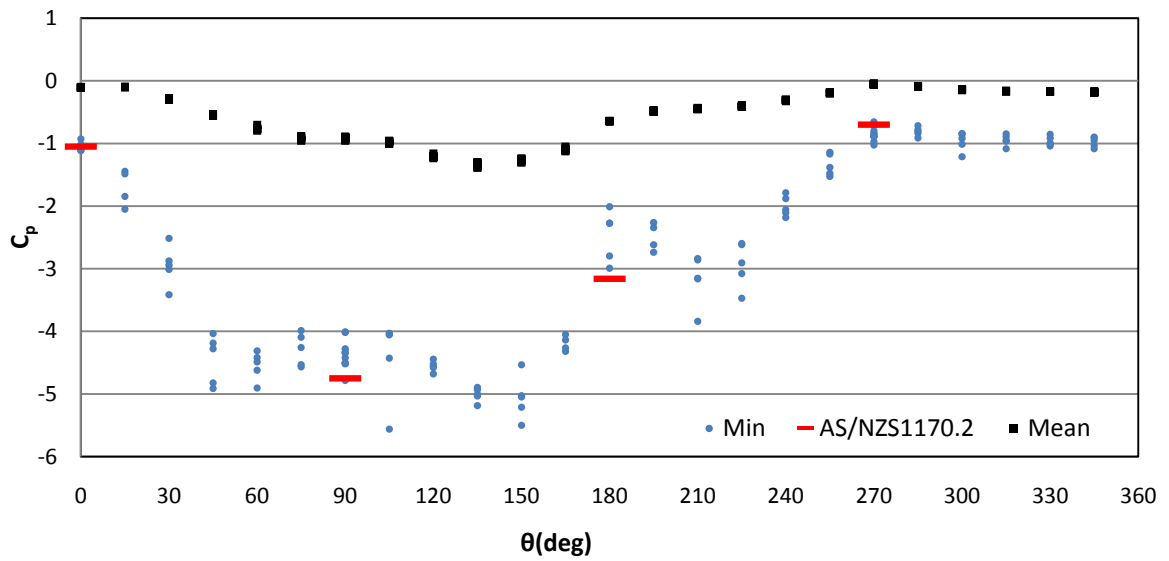


Figure 4.10: Pressure coefficients (C_p) vs wind direction – Batten-to-truss connection B7

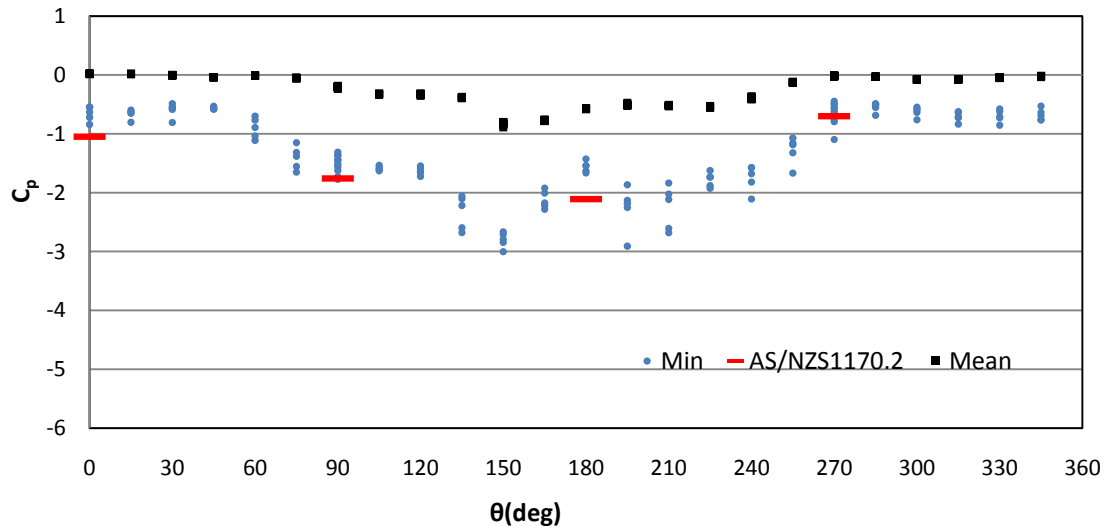


Figure 4.11: Pressure coefficients (C_p) vs wind direction – Batten-to-truss connection F5

4.3 Probability distributions

The peak pressure on cladding fixing tributary area in each region is represented as normalized pressure coefficients ($C_{\bar{p}}/C_{pN}$) for each wind approach direction. The variation in peak pressure coefficient is described in statistical terms by fitting the data to several standard probability distribution functions (PDF) including Normal (N), Lognormal (LN), Rayleigh (RE), Gamma (GM), Weibull (WB) and Generalized Extreme Value (GEV). These distributions accommodate the skewness of the data set (i.e. Gaussian or non-Gaussian). The distributions have several shapes with negative or positive skewness other than the normal distribution. The application of an appropriate distribution is important in order to sample wind load data satisfactorily. The assumed distribution was statistically verified by goodness-of-fit tests. The Kolmogorov-Smirnov (K-S) test was applied to determine the appropriate PDF. K-S test heavily favours the mean region of distributions where the probability weight is largest and is less sensitive to the tail regions. The Anderson-Darling test was also performed to determine whether the PDF was conservative in the tail regions.

Table 4.1 gives the probabilistic distributions of peak pressure coefficient for cladding fixings in P, Q and T regions for selected wind approach directions. The detailed probabilistic

descriptions for P, Q, R, S and T regions for each 15° interval are presented in Appendix A. However, the sample size of 20 values was used for this analysis and the best fit from the selected distributions are shown. The values are presented in normalized manner in order to identify the areas and wind directions exceeding the nominal values (i.e. the values greater than 1). The nominal pressure coefficients (C_{pN}) were obtained from external pressure values given in AS/NZS 1170.2 for wind approach directions 0°, 90°, 180° and 270°. In order to normalize pressures on the roof, the highest C_{pN} value from $\theta \pm 45^\circ$ wind approaching sector was used. For example, to normalize the wind pressure coefficients at 45° the larger value from 0° and 90° given in AS/NZS1170.2 (2011) was selected (90° had the larger value). Similarly for 135°, the value given in AS/NZS1170.2 for 90° was used (the higher value from 90° and 180°).

Table 4.1: The probabilistic distribution of peak pressure (C_p/C_{pN}) on cladding fixings at P, Q and T regions

Approach angle(θ°)	Region P			Region Q			Region T		
	Mean	COV	PDF	Mean	COV	PDF	Mean	COV	PDF
0	1.16	0.11	GM	1.08	0.25	GEV	0.74	0.29	GEV
45	0.73	0.10	GEV	0.40	0.36	GEV	0.33	0.16	GEV
90	0.74	0.13	GEV	0.75	0.18	GEV	0.95	0.17	GM
135	1.25	0.36	GEV	0.62	0.13	WB	1.07	0.19	WB
180	0.60	0.21	GEV	1.23	0.17	LN	0.81	0.08	GEV
225	0.66	0.22	GEV	0.92	0.24	GEV	0.99	0.17	GEV
270	1.15	0.21	N	1.34	0.26	WB	1.06	0.24	WB
315	1.01	0.13	WB	0.94	0.24	WB	1.06	0.17	GEV

Note: - GM - Gamma Distribution
 GEV - Generalized Extreme Value Distribution
 N - Normal Distribution
 WB - Weibull Distribution
 LN - Lognormal Distribution

As per the detailed analysis conducted (See Appendix A), the Generalized Extreme Value distribution was the best fit for most of the wind load data for cladding fixings. However, in some areas the data were fitted with other types of skewed distributions. This is due to the characteristic of the wind flow over these areas including separation and reattachment. Previous studies described in Chapter 2 (Holmes and Cochran (2003)), and studies by Cope *et al.* (2005) also indicated that the GEV is likely an appropriate distribution for peak wind load data. Similarly, the probabilistic distributions for area-averaged pressures on batten-to-truss connection tributary areas can also be found. These data provide the variability of wind load for all the connections with the wind approach direction.

4.4 Structural Load effects on Trusses

The fluctuating reaction force at the truss-to-wall connection shown in Figure 4.12, at time t can be determined from Equation 4.1.

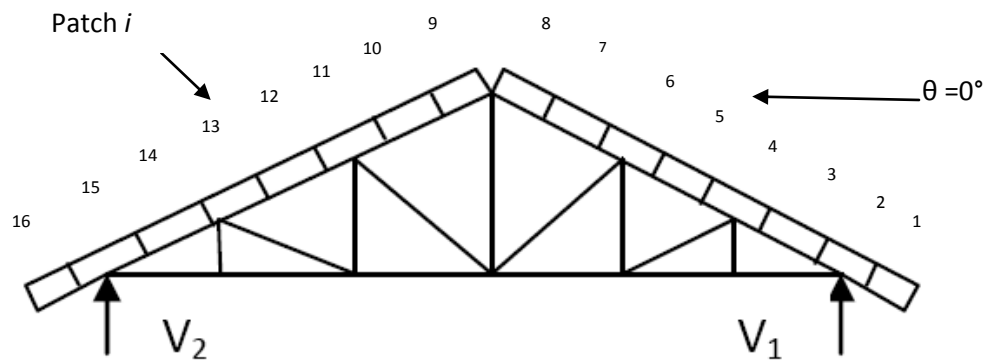


Figure 4.12: Schematic diagram of roof truss showing batten to truss connection patches and truss to wall reaction forces

$$X(t) = \sum_{i=1}^N \beta_i p_i(t) A_i \quad (4.1)$$

Where $X(t)$ - the fluctuating reaction force V_1 or V_2 , β_i - the influence coefficient for X , p_i - wind pressure, A_i - tributary area of patch i and N - is the total number of batten to truss patches on the tributary area of the truss.

The influence coefficients for truss reaction forces V_1 and V_2 shown in Figure 4.12 were found by applying an inward unit load at each batten-to-truss connection. The structural analysis package SPACEGASS version 10.81b was used for obtaining the reactions. These vertical reaction forces were presented in coefficient form, $C_X(t)$, as shown in Equation 4.2, where, $C_{p_i}(t)$ -pressure coefficient at panel i , and A_T -Total tributary area of the truss (i.e. Spacing of the trusses multiplied by the total chord length of the truss).

$$C_X(t) = \frac{X(t)}{\frac{1}{2}\rho\bar{U}_h^2 A_T} = \frac{\sum_{i=1}^N \beta_i A_i C_{p_i}(t)}{A_T} \quad (4.2)$$

The pressures measured simultaneously on the N patches of the truss for each approach wind direction were analysed to obtain $X(t)$ from which the peak value of C_X was determined. Figures 4.13, 4.14 and 4.15 show the variation of the peak (i.e. minimum) reaction coefficients \check{C}_{V_1} and \check{C}_{V_2} for all five runs with the wind approach direction, θ for trusses B, F and L respectively and the design values obtained from AS/NZS 1170.2. The Figures show that the reaction coefficients had a large variability with the wind approach direction. Truss B had a larger load compared to truss F and L and the largest peak reaction coefficients on truss B occurred for $\theta = 90^\circ$. Trusses F and L generally had similar loads with the wind approach direction and the largest loads occurred for $\theta = 30^\circ$ to -30° . These Figures also show that the reaction force V_2 was larger than the reaction force V_1 . Therefore, the reactions at leeward side of the trusses had larger loads compared to the windward side. However, V_1 and V_2 had approximately equal loads for wind approach directions 90° and -90° as expected. The reaction coefficients obtained from AS/NZS 1170.2 underestimated the reaction at V_2 for $\theta = 0^\circ$ but accommodated that for $\theta = 90^\circ$ on truss B. Hence, AS/NZS 1170.2 gave a reasonable estimate for design wind loads on truss-to-wall connections. The trusses towards the gable end of the houses had larger wind loads compare to middle region.

Probabilistic descriptions for truss reaction forces also can be found by using the method used in Section 4.3. The corresponding nominal (X_N) values can be obtained from AS/NZS 1170.2 (2011). The outcomes of this Chapter have been summarized by Jayasinghe and Ginger (2011).

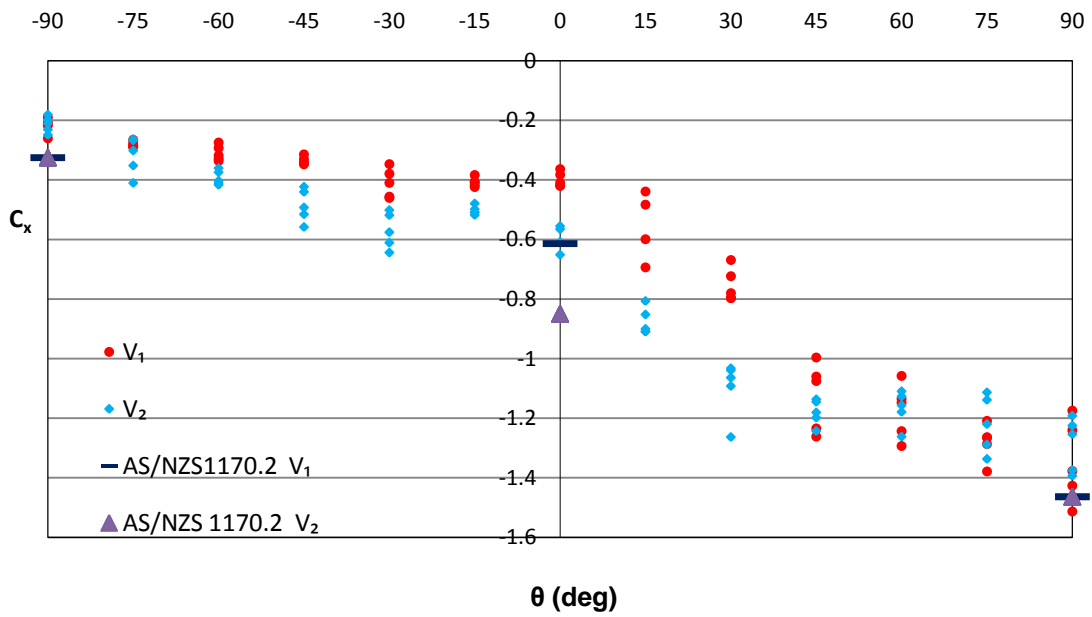


Figure 4.13: \check{C}_{V_1} and \check{C}_{V_2} vs wind approach angles -Truss B

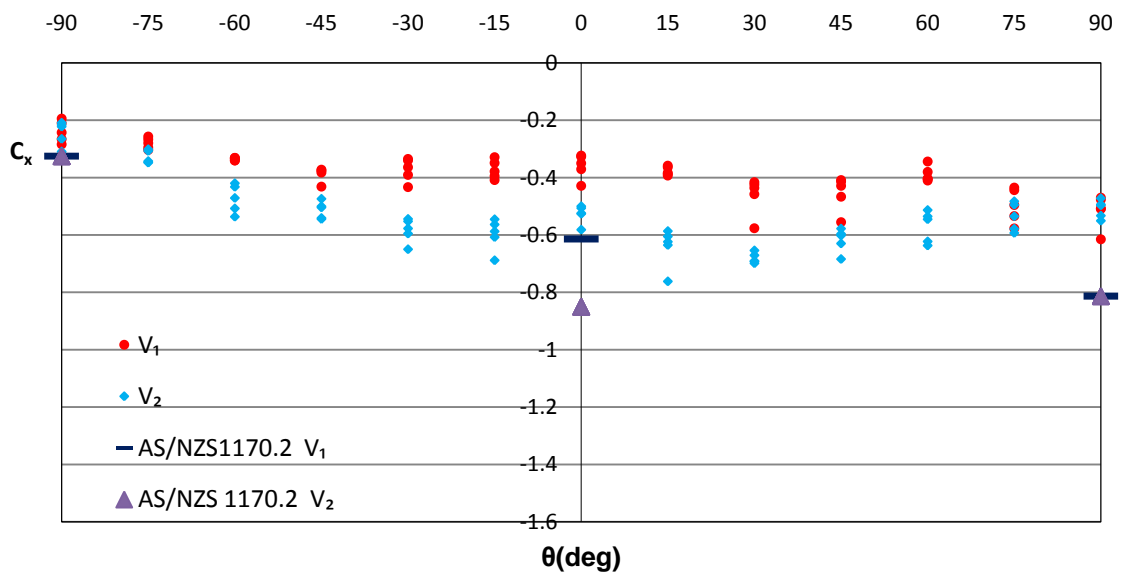


Figure 4.14: \check{C}_{V_1} and \check{C}_{V_2} vs wind approach angles -Truss F

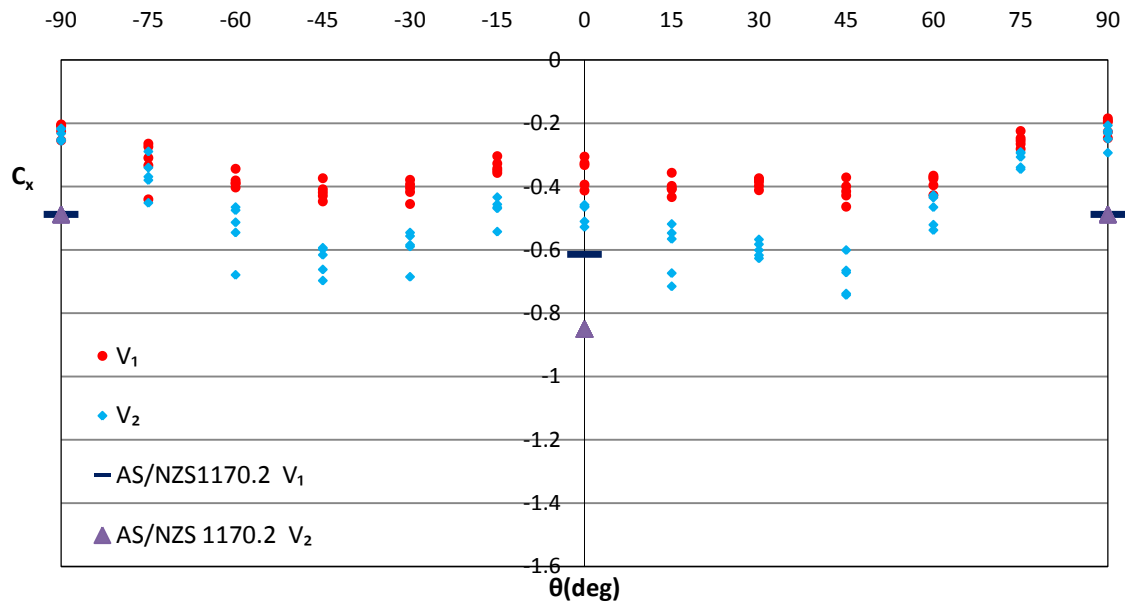


Figure 4.15: \check{C}_{V_1} and \check{C}_{V_2} vs wind approach angles -Truss L

4.5 Summary and Discussion

The study determined the wind load acting on the roofing connections and compared the results with the loads obtained from AS/NZS 1170.2 (2011). The probabilistic descriptions of wind loads over the cladding fixings on the roof were determined in terms of normalized values with the wind approach direction. These parameters can be used to determine the load action on a house with the wind approach direction.

In this chapter conventional wind engineering practice was used to detail the area-averaged patch load on a tributary area to calculate the load effects on batten-to-truss connection and truss-to-wall connection. However, the load effects will be dependent on the structural system response (tests in Chapter 5) and the spatial and temporal wind loads which may generate different loads.

The wind load data were obtained on an isolated house in a suburban environment and hence it was only simulating a situation where the houses are widely spaced in all directions. In practice most houses located in urban areas will be shielded to differing degrees by neighbouring houses that will provide reduced loads (Ho *et al.* (1991)). In addition, houses will also have variation in dimensions including roof shape, roof angle, width, length and height etc.

All these factors will result in a population of houses experience wind loads that will significantly vary compare to the data obtained. The use of normalized parameters may account for these variations to some extent. The wind loading standard AS/NZS 1170.2 (2011) specifies pressure coefficients C_{pN} based on those dimensions and roof slope. When these dimensions are changed in the range observed from the survey data, the corresponding code value is also changed. Therefore, the variations in peak pressure $C_{\bar{p}}/C_{pN}$ for a range of houses with the population of contemporary houses may be similar. This parameter is likely to increase the variability of $C_{\bar{p}}/C_{pN}$, which can be accounted for by the coefficient of variation. However, this should be confirmed with some rigorous testing on other geometries and using the results of previous studies. The wind load data on connections is usually obtained based on mean value, coefficient of variation and probability distribution function in vulnerability assessments. Therefore, the output results from this wind tunnel study can be used for obtaining the wind loads on roofing connections in a population of masonry block houses.

5 STRUCTURAL TESTING AND RESPONSE

The structural response of the roof of a house is dependent on the spatial and temporal variation of loads, load sharing and interdependency between components. The response changes with increasing wind speed, as the structural components and connections deteriorate from being elastic (linear) to plastic (non-linear) and progressive failures take place. Such an analysis requires an understanding of load sharing, possible modes of failure, and redistribution of loads as the loads increase. This Chapter presents a series of tests on roof subassembly systems subjected to a range of loads and comparisons with analytical data. The list of tests conducted is presented in Appendix B.

5.1 Load sharing and progressive failure

The loads applied on a house are shared by the structural elements and non-structural elements in a complex manner. Full scale testing provides a means of estimating load sharing and determining the coefficients or factors for the load effects of interest (i.e. batten-to-truss connection load). Increasing wind speed results in progressive failures and possible changes to the load sharing and load redistribution. As described in Chapter 2, tests conducted on full scale houses and building subassemblies provide an overview of these effects. However, those studies generally considered cumulative effects and the structural systems used were different from contemporary houses built in cyclonic region of Australia.

Test data on load sharing, progressive failure and interdependency between components of contemporary houses is scarce, thus limiting the ability to estimate load effects and assess their structural response. In order to address this lack of data, the behaviour of roofing connections of contemporary houses was studied by conducting a series of roofing subassembly tests. The sub assembly tests are designed with appropriate boundary conditions based on engineering decisions to accommodate the roofing system response. The results from these experiments were also compared with structural analysis, and then used as a basis to predict the response of

the roof structure. Both linear and non-linear behaviour of structural components and connections were tested in order to predict the progressive response of roofing components during wind events.

5.2 Experimental set up # 1

A roof system was set up with 90mm x 35mm, MGP 12 (Machine Graded Pine) top chord truss elements R1 to R5 spaced at 900mm, and 40 mm x 40mm, BMT 0.75mm (Base Metal Thickness) top hat battens b1 to b5 spaced at 700, 750, 750 and 600mm respectively, as shown in Figures 5.1 and 5.2. These non-uniform spacings represent the minimum batten spacing and typical eave spacing of contemporary houses. The battens were fixed to the trusses via calibrated tension/compression 'S' type load cells at selected batten-to-truss connections, as shown in Figures 5.3. The remaining connections were fixed with dummy blocks with a threaded rod to maintain consistent fixing type at each batten-to-truss connection, as shown in Figure 5.4. These fixings were assumed to satisfactorily replicate the batten-to-truss fixings on these types of roofs (i.e. based on stiffness of the connection etc). The roof cladding was fixed to the battens with Type-17 cladding fasteners (No14-10 x 50mm) at the crests of alternate corrugations, as shown in Figure 5.5. The equally spaced grid lines 1 to 12 and W, X, Y as shown in Figure 5.1, represent the load application locations on battens and cladding such that (b2, 5) describes the loading position on batten b2 halfway between timber truss members R2 and R3 (This is also illustrated in Appendix B with the test Matrix). Load cell locations are given in terms of the batten and supporting truss member such that (b3, R2) represents the connection of batten b3 with truss element R2 (See Appendix B). Each Panel between the batten and truss elements are identified as P1 to P16. A point load applied in the middle of the panel P6 (the area between b2, b3, R2 and R3) is represented by (P6, X, 5) (See Appendix B). The applied load and load on connections were measured with 'S' type load cells and the deflections were measured by using LVDTs (displacement transducers).

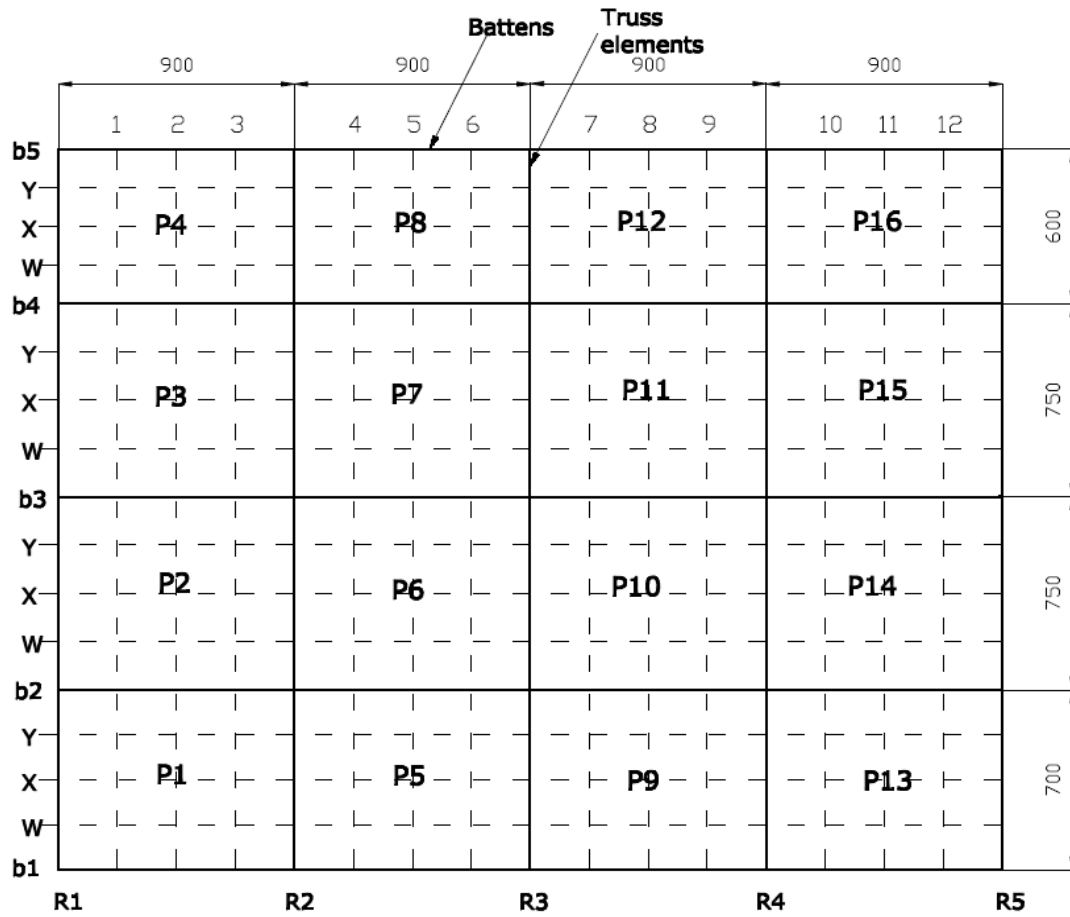


Figure 5.1: Schematic diagram of the test setup #1 (all dimensions are in mm)

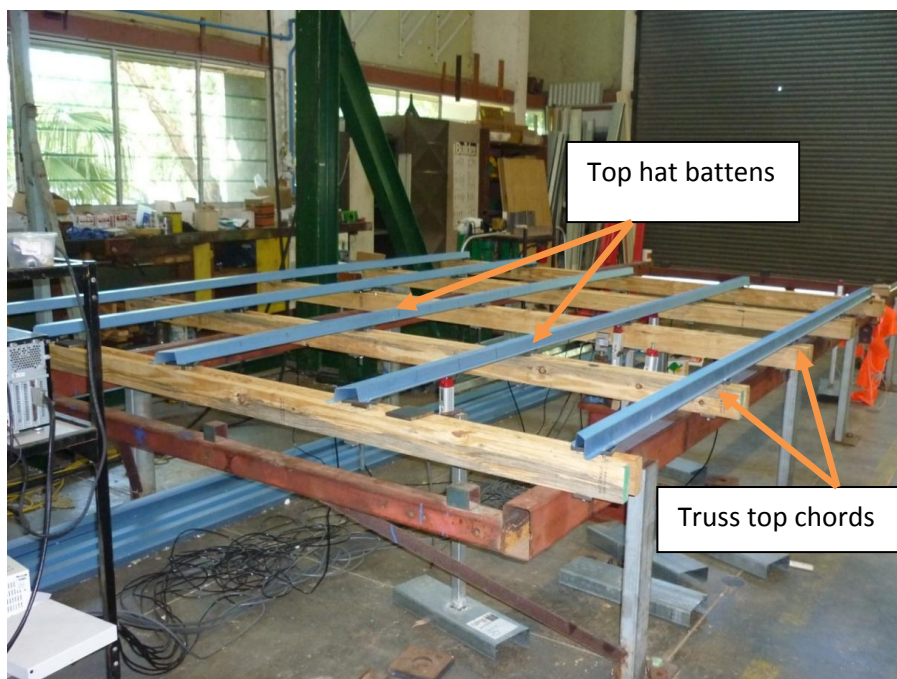


Figure 5.2: Test setup #1 before fixing the cladding

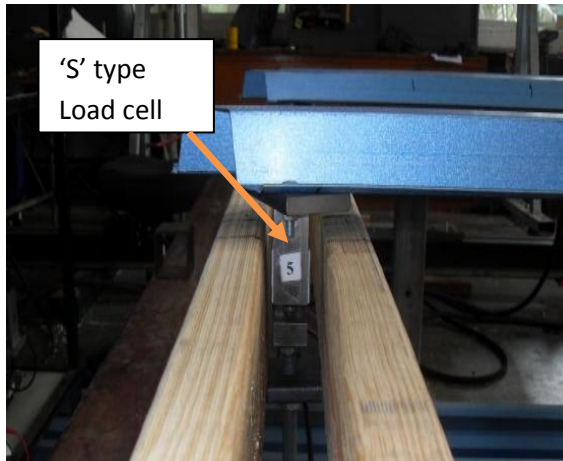


Figure 5.3: Batten-to-truss connection with load cell

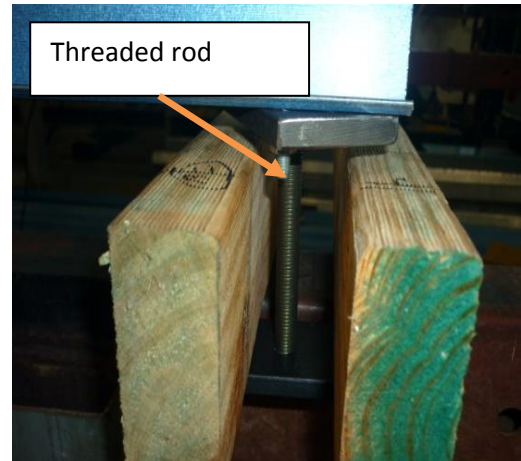


Figure 5.4: Dummy load cell



Figure 5.5: Test set up with cladding fixed

5.2.1 Test procedure

A range of tests were carried out and the reactions at batten-to-truss connections and deflections at selected locations were measured and compared with analytical solutions obtained from a similar setup using SPACEGASS version 10.85 (Integrated Technical software 2010). The

reaction coefficients (C) were obtained by dividing the load at each batten-to-truss connection with the applied load. The general procedure was to apply an uplift point load or a line load at selected locations on battens or roof cladding, and measure the loads at instrumented batten-to-truss connections. The load was applied from the bottom of the test setup using a jack. Timber blocks and foam moulds were shaped to match the profiles of the battens or the cladding at the locations of load application. Figure 5.6 shows a foam mould and the jack used for applying the point loads on cladding. Signal conditioning and data acquisition was carried out using LabVIEW software (version 8.5).

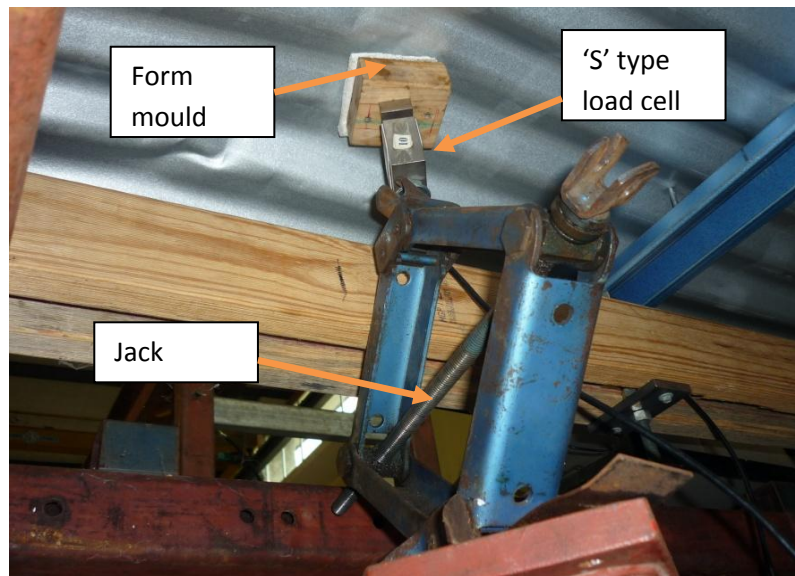


Figure 5.6: Load application to the bottom surface of cladding with a foam mould and jack

5.2.2 *Elastic range tests*

- *Point loads*

The first series of tests were carried out prior to installing the cladding, with only the battens connected to the truss elements. A series of point loads were applied along the battens and reactions and deflections were measured, as shown in Figure 5.7. The applied load was measured with an 'S' type load cell and the deflections were measured by using LVDTs (displacement transducers). Following this, the cladding was installed and loads applied at the

same points on the battens, in order to assess the effect of cladding on load sharing and transfer.

These tests were followed by the application of point loads at a range of positions on the cladding, to assess the load distribution from the cladding. During this stage, some selected cladding fasteners were removed to study the load transfer and sharing when these connections failed. Steadily increasing load to a maximum of 1kN was applied during this stage, where the structure was in the elastic range (linear region). The overall tests carried out are shown in Appendix B (Test Matrix).

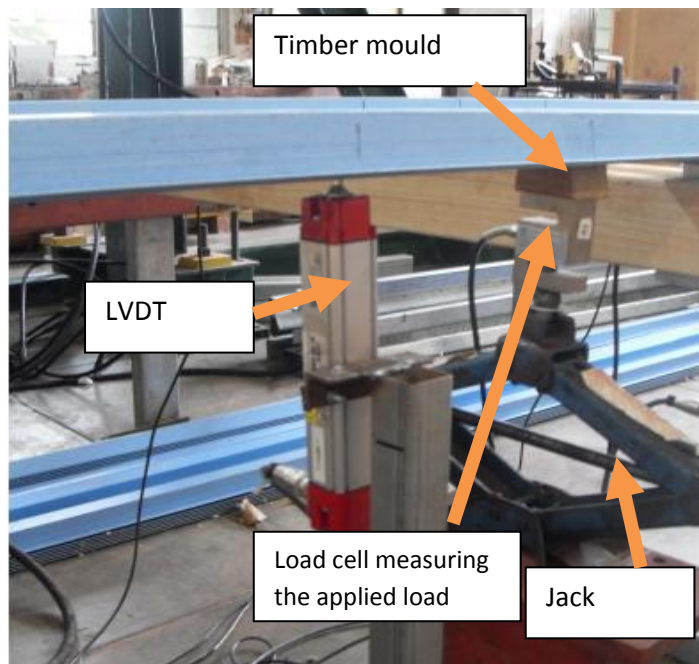


Figure 5.7: Load application to batten and deflection measurement

- *Line loads*

The point load tests were followed by line loads increasing up to 5kN per panel (i.e. 5.56 kN/m) applied on the cladding. The load application length was exactly the panel length (900mm) and the load was applied along W, X or Y lines in each panel. Following this, two adjacent panels along the battens (i.e for an example P1 and P5), were loaded simultaneously in each W, X or Y

lines with up to 5kN in each panel. In each case, the reactions at batten-to-truss connections were measured. Figure 5.8 shows the test arrangement for line loads. The overall tests carried out for line loads are also shown in Appendix B (Test Matrix).

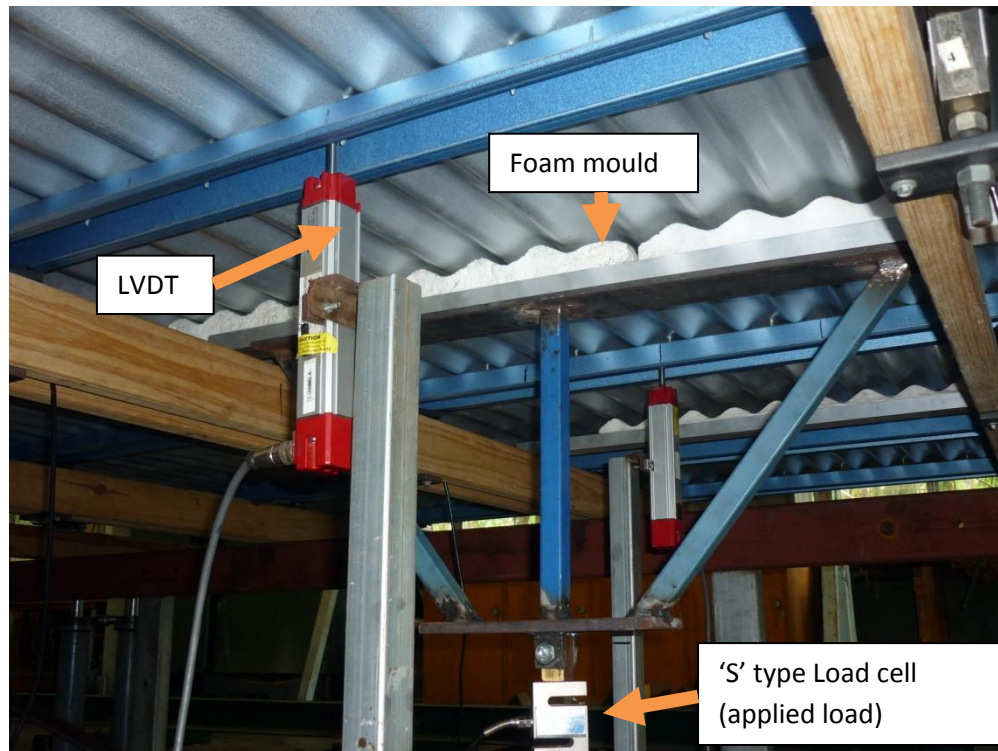


Figure 5.8: Line loads applied along a line over spacing between trusses

5.2.3 Loading until failure

In order to compare the reaction coefficients (the load at each batten-to-truss connection divided by the total applied load to obtain the reaction coefficient at each connection) in the linear and non-linear ranges, point loads were applied until failure of a cladding fastener and then the cladding was further loaded to observe how the load was distributed while approaching the next failure. Panels P1 and P6 were selected for this purpose and point load applied at positions (P1, X, 1) and (P6, X, 5) until failure. Similarly, line loads were also applied using a hydraulic jack at (P10, X) and (P13, X), until failure.

5.2.4 Analytical model

A SPACEGASS model (version 10.81b Integrated Technical software 2010) as shown in Figure 5.9 was developed to obtain analytical results for these tests and to compare the laboratory test results. Each pair of timber truss elements used in the test setup were modeled as one element with equivalent size (i.e. 90mm × 35mm pair was modeled as 90mm × 70mm single element) and the support condition of truss elements to the steel frame was taken as simply supported. The top-hat batten profile was modelled with beam elements to produce selected properties (i.e. moment of inertia of cross section) that matched those used in lab tests. The roof cladding was modeled with small beam elements to match the cladding profile. The width of the beam elements was taken as the spacing between cladding fasteners (i.e. every 2nd corrugation, 152mm). Since the load transfer occurs along the crests of cladding as shown by Henderson (2010), these small beam elements satisfactorily simulate the cladding behaviour. The shear forces/reactions were obtained in batten-to-truss connections of the model to compare with the test results.

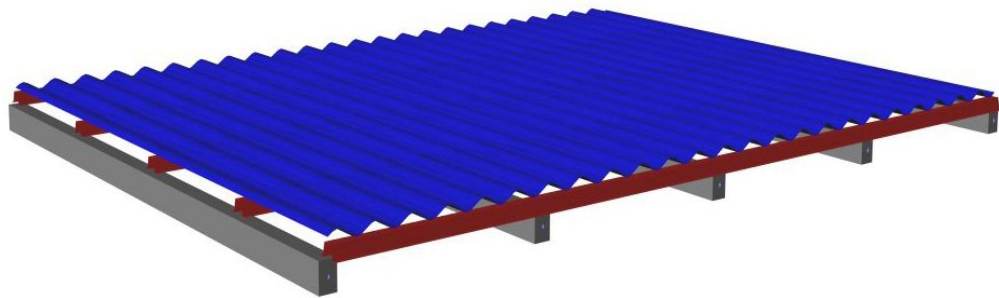


Figure 5.9: SPACEGASS 3D model of the Test setup #1

5.2.5 Results and Discussion

This section analyses the loads at batten-to-truss connections in terms of reaction coefficients. The reaction coefficient has a positive value when the connection has an upward load (tensile force in the connection) whereas it is negative when the connection has a downward load (i.e.

compressive force in the connection). The reaction coefficients and deflections for various load application states are compared with analytical solutions.

5.2.5.1 Point loads on batten (cladding not installed) - Elastic range

Figure 5.10 shows the variation of reaction coefficient at b2, R1 ($C_{b2, R1}$), when the load was applied along the batten b2 and the comparison with analytical results. There were some differences between analytical and measured values but both results followed the same trends supporting structural engineering principles. When the load was applied to the first span, the connection had a positive reaction coefficient (i.e. a tensile force in the connection) and the analytical values were closer to the measured values, while for the second span it was negative (i.e. compression) and there was a significant difference between analytical and measured values for some locations suggesting the batten is more flexible than that modelled. However, the reaction coefficients values were less than 0.06 in the negative region. There was a negligible load on the connection (b2, R1) when the load application was more than two spans away. The load was not applied exactly on the measurement point due to access restrictions. Similar results were obtained for $C_{b2, R2}$ and $C_{b2, R3}$ for point loads on batten b2, as shown in Appendix B. However, measured and analytical values for $C_{b2, R2}$ had a maximum of 10% difference in some locations when the load was applied in the adjacent spans. Furthermore, simultaneous load measurements were taken at batten-to-truss connections of adjacent battens b1 and b3 for load application on batten b2. It was found that a very small load is transferred to the adjacent battens when the load is applied close to the truss elements without the cladding attached. This occurs by load transfer through truss elements, but can be considered to be negligible, as the values were close to zero.

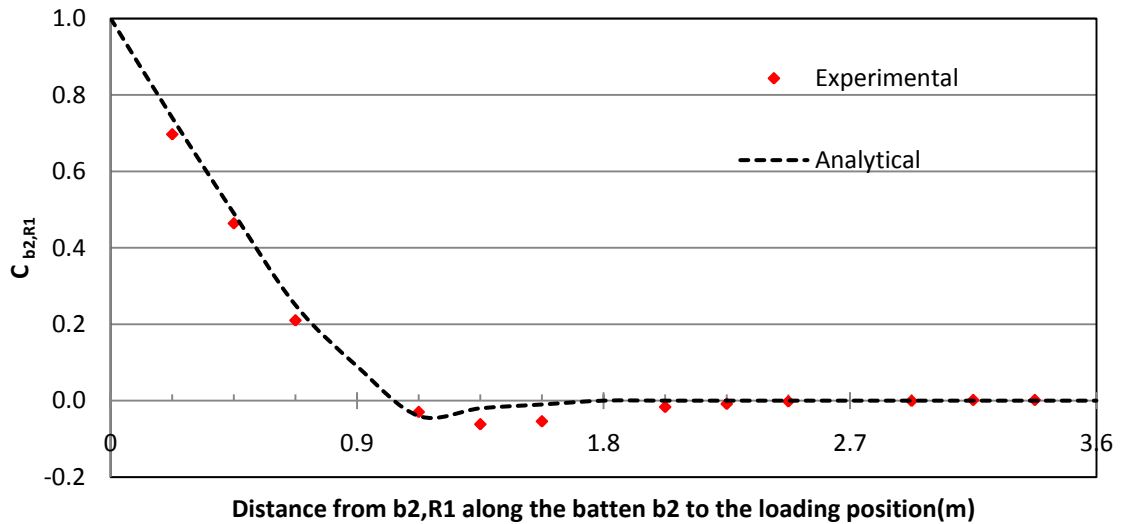


Figure 5.10: Reaction coefficient at b2, R1 ($C_{b2,R1}$) for point load on batten b2

The Figure 5.11 shows the deflection of different points for the application of load in the middle of the first span (i.e. point (b2, 2)). As shown, the measured values followed a similar trend with analytical values. However, the measured values were larger than the analytical values when the load was applied close to the measured point, and vice-versa. The deflections along b2 for the applied load at other positions are shown in Appendix B. These Figures indicated that the maximum measured deflections were always greater than the analytical calculated deflections in the locations expecting peak deflections with the maximum difference of 1mm confirming that the batten is more flexible than modelled.

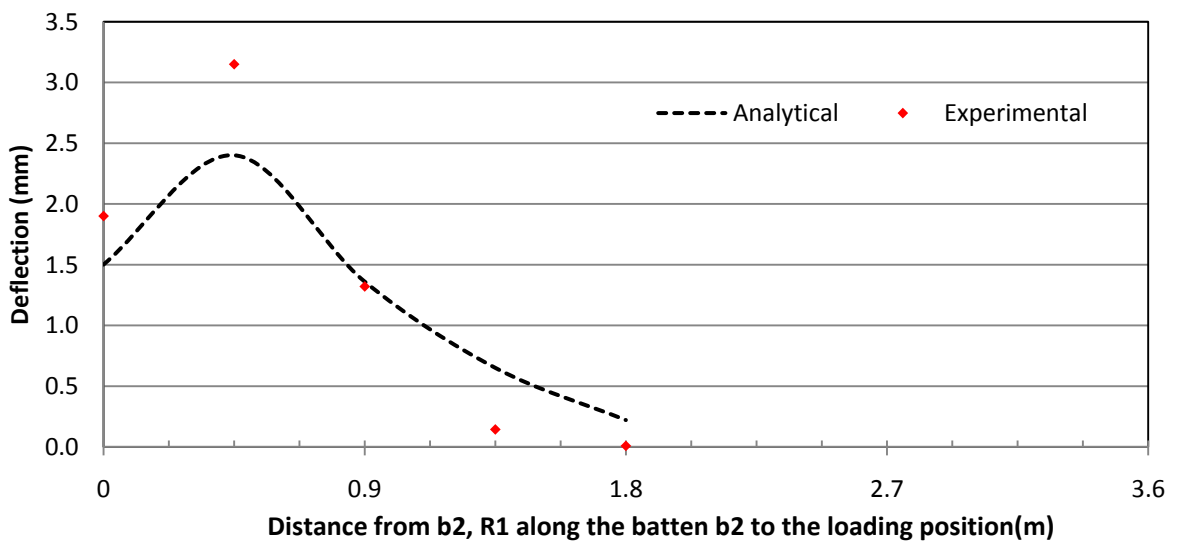


Figure 5.11: Deflection of batten b2 for load at (b2, 2)

At this stage, each batten-to-truss connection was disconnected one at a time to represent the failure of a connection and the load was applied along that batten before fixing the cladding. Figure 5.12 compares the reaction coefficient $C_{b2, R1}$ when the batten-to-truss connections at (b2, R2) and (b2, R3) were alternatively removed. As shown in Figure 5.12, the reaction coefficient, $C_{b2, R1}$, increased for (b2, R2) removed case when the load was applied on the first two spans, but returned close to the values for the undamaged intact case when the load was applied on spans three and four. When the batten-to-truss connection (b2, R3) was removed, $C_{b2, R1}$ values were closer to the intact case in the first span and the negative reaction coefficient (i.e. compressive load on the connection) was higher than the intact case values in the second and third spans. The variation of $C_{b2, R2}$, $C_{b2, R3}$, $C_{b2, R4}$, and $C_{b2, R5}$ with alternate removal of batten truss connections at (b2, R2) and (b2, R3), are shown in Appendix B.

These Figures show the reaction coefficients tend to have greater magnitudes (either positive or negative values) than values for the undamaged intact case when the load was applied adjacent to the spans of the removed connection. When the load was applied to the other spans, the reaction coefficients were approximately equal to the intact case values. The overall results showed that the reactions coefficients were increased at batten-to-truss connections adjacent to the removed connection.

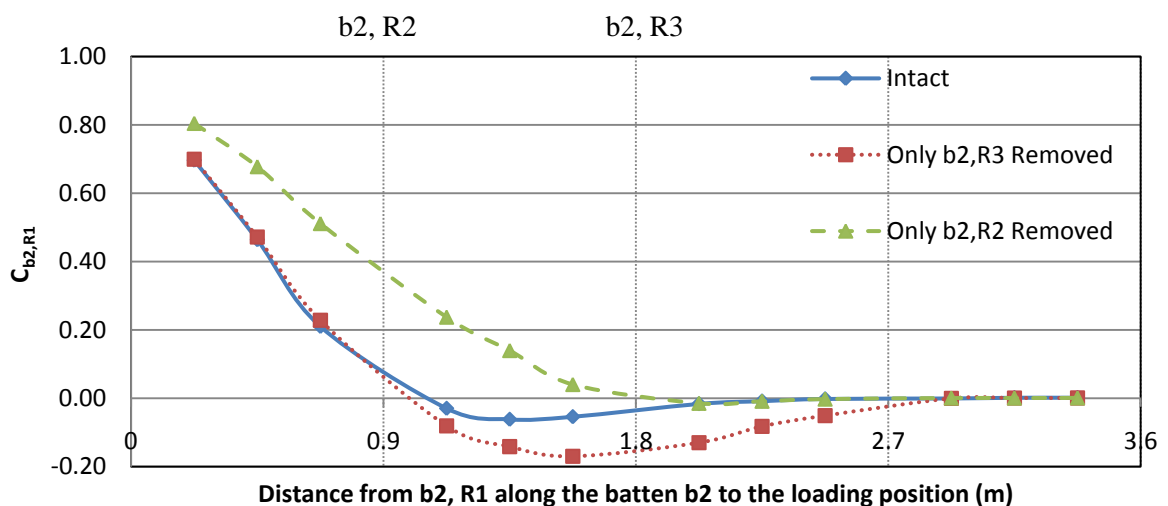


Figure 5.12: Reaction coefficient, $C_{b2, R1}$, for point load on batten b2

- *Effect of cladding*

Figure 5.13 shows the reaction coefficient, $C_{b2, R1}$ obtained from tests without cladding and with cladding attached. As shown, the magnitude of the reaction coefficients was generally reduced with the installation of cladding. This is due to the redistribution of load through cladding elements to the other panels of the structure. The effect of cladding on reaction coefficients, $C_{b2, R2}$ and $C_{b2, R3}$ are shown in Appendix B. These figures show, the installation of cladding resulted in the redistribution of the loads throughout the roof structure with approximately 10% reduction in large reaction coefficients of nearby supports compared to the case before the cladding was installed.

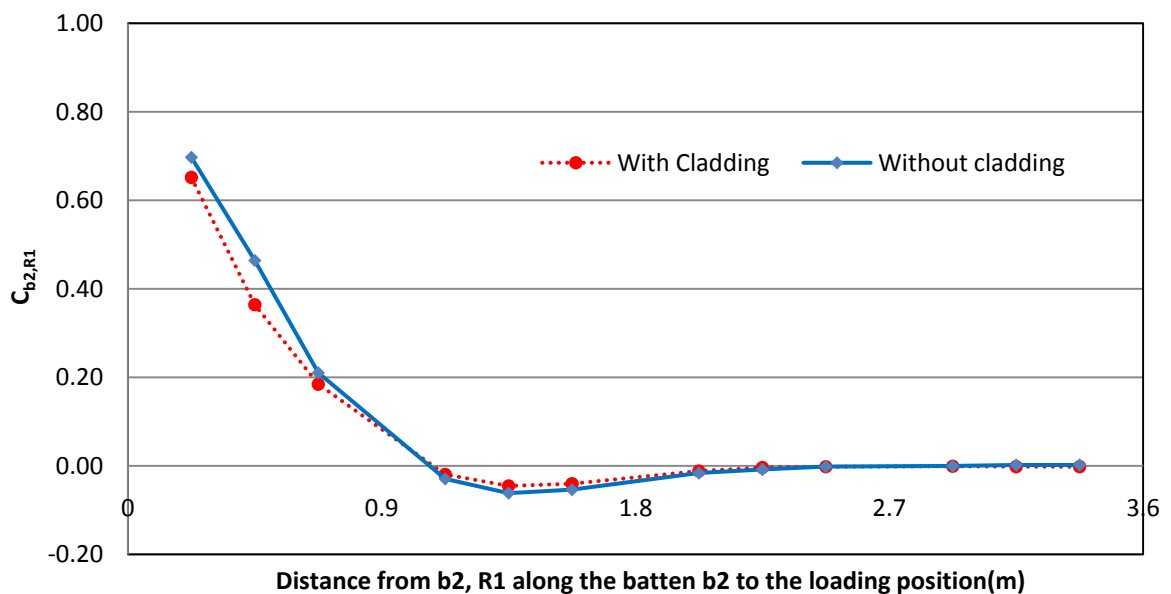


Figure 5.13: The effect of cladding on reaction coefficient, $C_{b2, R1}$

5.2.5.2 Point loads on cladding - Elastic range

Figure 5.14 shows the variation of reaction coefficient, $C_{b2, R2}$, when the load was applied on points along W, X and Y in Panels P6, P10 and P11 and the corresponding analytical values from SPACEGASS. Figure 5.14 shows that $C_{b2, R2}$ had larger measured and analytical values when the load was applied along W of Panels P6 and P10. When the load was applied along W, the theoretical analysis gave a larger coefficient than that measured for loads applied closer to the batten-to-truss connection. When the load was applied along X on panels P10 and P11, the

analytical and experimental values were in close agreement whereas that along Y showed the analytical values were lower than the experimental values. Furthermore, Figure 5.14 shows that the load application at any position of panels P10 and P11 had little effect on $C_{b2, R2}$. It should be noted that the load application along line Y which is outside the conventional tributary area of half panel width of the batten b2, has a significant effect on the connection (b2, R2) as shown in the Figure 5.14.

The variation of reaction coefficients for all the other batten-to-truss connections at Panels P6 and P10 also behaved in a similar manner, as shown in Appendix B. These Figures show that significant amount of the loads were resisted at the batten-to-truss connections nearest to the panels on which the load was applied. The reaction coefficients obtained from the analytical method were generally lower than the experimental data when the load was applied away from the measured point. However, the analytical values were larger than the measured values, when the load application was near the measurement point of interest and close to the measured value when the applied load was halfway between battens. Thus, the analytical method generally underestimates the load transfer when the load is applied away from the measured point of interest.

These differences could be due to many reasons. A sensitivity analysis showed that the main reason is due to the modelling inaccuracies. The roof cladding was modelled with small beam elements and the connections (i.e. cladding fastener and batten-to-truss connections) were taken as rigid connections in the analytical model. The results of the previous section showed that the batten is more flexible than that modelled. The model was further analysed by changing the assumed values of the Moment of Inertia (I) and the Young's modulus (E) of the battens and the analysis showed that the results are more sensitive to E than I. However, the analytical deflection values were closer to the measured experiment values, when E and I were close to half of the original values. This indicates that the deficiencies are not due to the modelled batten but the batten-to-truss connections. Therefore, the cladding fixings and the batten-to-truss connection fixings should be modelled with accurate support condition (not as rigid connections) in order to obtain accurate results. The current version of SPACE GASS cannot be

used for modelling this. Similarly, there can be unavoidable experimental factors that can cause some of these anomalies.

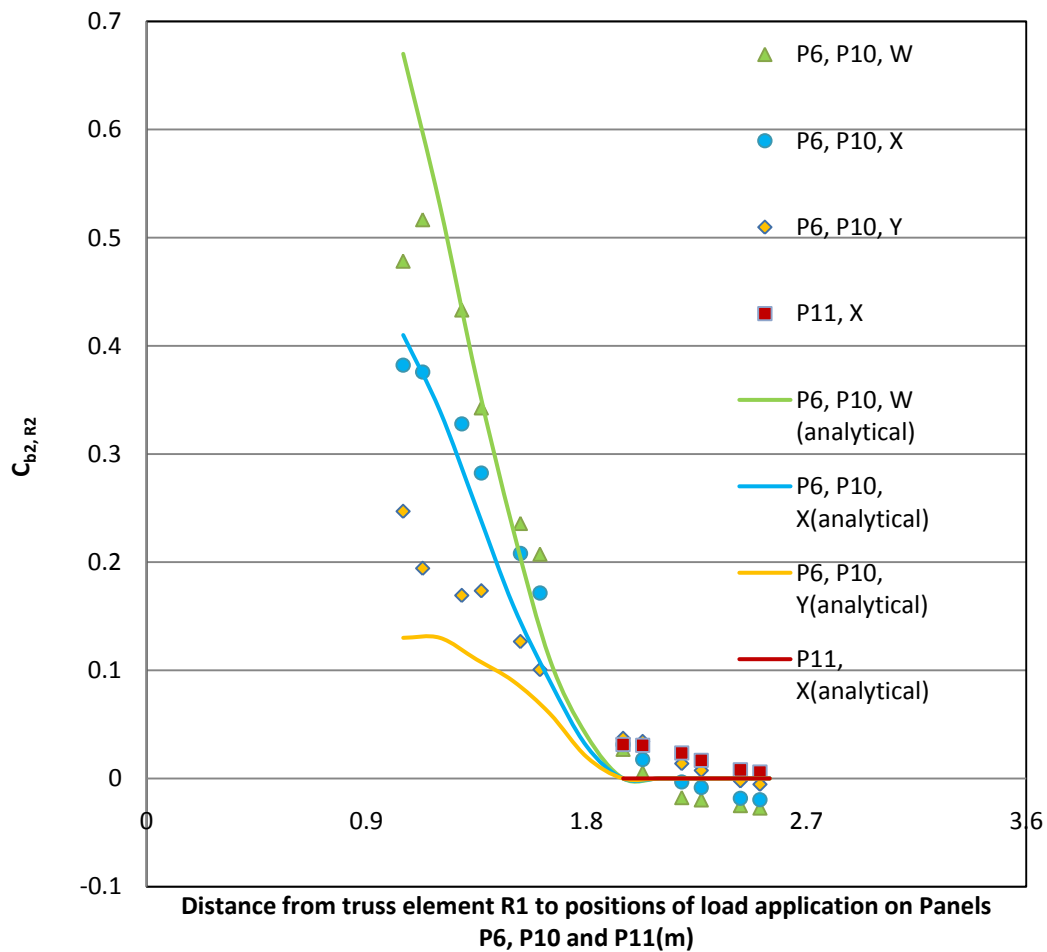


Figure 5.14: Reaction coefficient, $C_{b2, R2}$ with point loads along W, X and Y

- *Cladding fasteners removed*

Tests were conducted by alternatively removing a cladding fastener at locations (b1, 5), (b2, 5) and (b3, R3) and applying the loads same as before. Figure 5.15 shows the variation of reaction coefficient, $C_{b2, R2}$ when the load was on Panels P6 and P10 along line X. As shown in Figure 5.15, removing fasteners at (b3, R3) or (b1, 5) had small effect on the $C_{b2, R2}$. Removing (b2, 5) caused a reduction in $C_{b2, R2}$ when the applied load was close to (b2, 5). The largest reduction occurs when the load was at the crest of the removed connection (i.e. b2, 5). Thus, the load on the cladding was transferred primarily via this crest to either side of fasteners at battens b1 and b3.

The variation of reaction coefficients C_{b_2, R_3} , C_{b_2, R_4} , C_{b_3, R_2} , C_{b_3, R_3} , and C_{b_3, R_4} when cladding fasteners at (b1, 5), (b2, 5) and (b3, R3) were alternatively removed, are shown in Appendix B. These results showed that the load was transferred to either side of the batten, when the applied load was near to the crest of the removed fastener. The greatest change occurred when the load was applied to the crest from which the fastener was removed confirming that the applied loads are transferred along the crests (Henderson and Ginger (2011)).

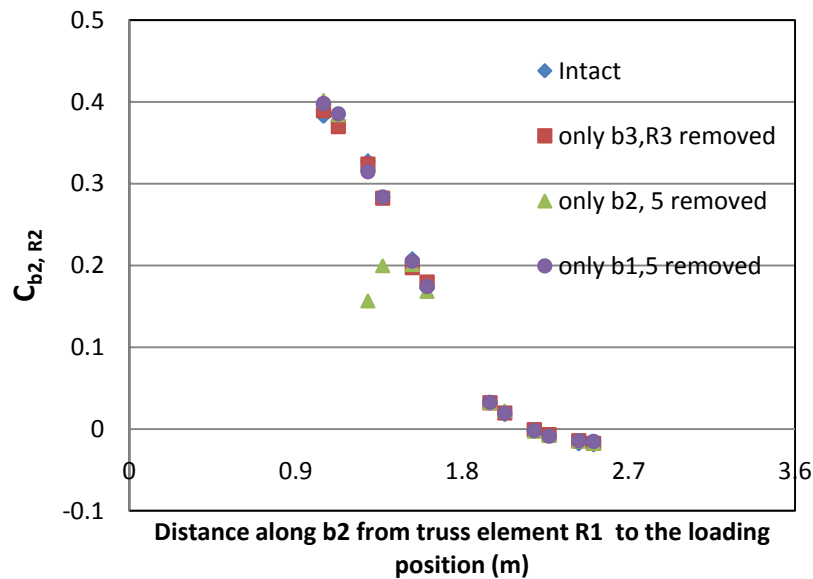


Figure 5.15: C_{b_2, R_2} for point load on X on Panels P6 and P10

5.2.5.3 Line loads - Elastic range

Reaction coefficients at batten-to-truss connections were measured with line loads applied along a range of lines on panels. These reaction coefficients were compared with those derived by superposing point loads applied along the same line. Table 5.1 shows the comparison done for point loads and line loads along X on Panels P6 and P10. As shown in the Table 5.1, the reaction coefficients for line loads produce the same values as the superposed point loads with a largest difference of 0.03 for applied load along X in panels P6 and P10. Furthermore, when the line load was applied on both panels together (i.e. P6, P10, X), the largest difference was 0.02 in comparison with superimposed point loads of both panels. These results indicate that the reaction coefficients at batten-to-truss connections (b2, R2), (b2, R3), (b2, R4), (b3, R2), (b3,

R3), and (b3, R4) obtained from superposing a series of discrete point loads on a line were similar to that form a line load. Further analysis of reaction coefficients showed that superposition of line loads in two adjacent panels were in agreement with the application of line loads in these two panels simultaneously, having a largest difference of 0.02 in reaction coefficients. Thus, the load transfer to the battens from the cladding is similar when a series of point loads are applied along a line and a line load is applied along the same line. However, this methodology is applicable only when the system is behaving linearly in terms of material behaviour and the deformations. If there are any significant nonlinearities (i.e. deformation), the superposition of series of point load instead of a line load may not be applicable.

Table 5.1: Comparison of reaction coefficients from line loads with point loads

Location	Load type	Reaction Coefficients					
		$C_{b2, R2}$	$C_{b2, R3}$	$C_{b2, R4}$	$C_{b3, R2}$	$C_{b3, R3}$	$C_{b3, R4}$
P6,X	Point loads	0.29	0.27	0.01	0.26	0.25	0.02
P6,X	Line loads	0.32	0.25	0.02	0.25	0.25	0.02
P10,X	Point loads	0.00	0.25	0.28	0.01	0.24	0.30
P10,X	Line loads	0.02	0.25	0.27	0.01	0.27	0.29
P6,P10,X	Point loads	0.15	0.26	0.14	0.13	0.24	0.16
P6,P10,X	Line loads	0.16	0.24	0.16	0.15	0.26	0.14

A point load can be applied to study the individual cladding fastener connection influence on the reaction coefficients of batten-to-truss connections while a line load can be used to study the influence of a series of cladding fasteners on the batten-to-truss connections. The frequencies of wind load fluctuations are lower than the natural frequency of the roof system of low rise buildings, hence, the temporal variation in dynamic loads is satisfactorily represented by static tests, as shown by Henderson (2010). The spatial variation can be captured by using the reaction coefficients of a series of point load tests. The application of a line load represents the average spatial wind load acting on cladding panels.

5.2.5.4 Loading until Failure

Figure 5.16 shows the variation of reaction coefficients with increasing load until failure, when a point load was applied in the middle of Panel P6. Stage 0 to 1 refers to the increasing load until first failure of a cladding fastener. Stage 1 to 2 refers to the continued loading at the same location until another fastener failure occurs. As shown in the Figure 5.16, the reaction coefficients decrease with the increasing load, as some of the load was distributed to adjoining panels. During the test, the cladding fastener at (b2, 5) failed first and the reaction coefficients at (b2, R2) and (b2, R3) decreased significantly transferring the loads to (b1, R2), (b1, R3), (b3, R2) and (b3, R3). At this stage, the applied load to the cladding dropped to some extent due to the reduction in stiffness of the roof system. Further loading resulted in failure of fastener at (b3, 5) transferring loads to the batten-to-truss connections at (b1, R2), (b1, R3), (b4, R2) and (b4, R3). The results in Figure 5.16 indicate that the loads are transferred to the adjoining panels as the plastic deformation takes place around the cladding fasteners. This is due to the reduction in stiffness of the system around cladding fasteners. Figure 5.17 shows how the cladding fasteners failed for the point load application, during these tests. It also shows that the load in the cladding may also be transferred by membrane forces as the corrugations have buckled significantly reducing their bending strength.

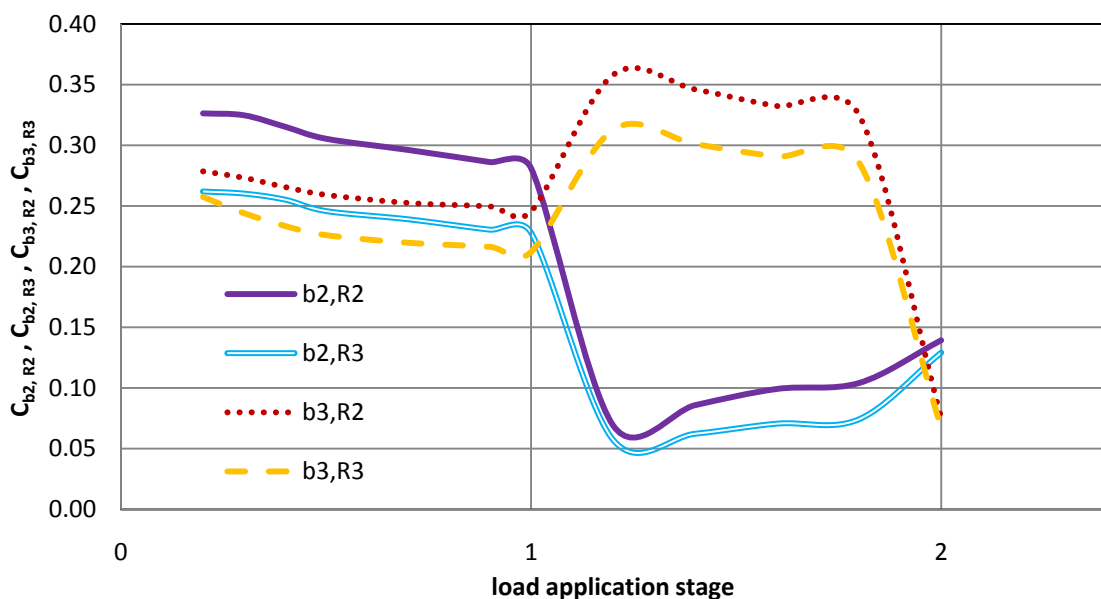


Figure 5.16: Reaction coefficients for loading at centre of Panel 6 until failure of fasteners

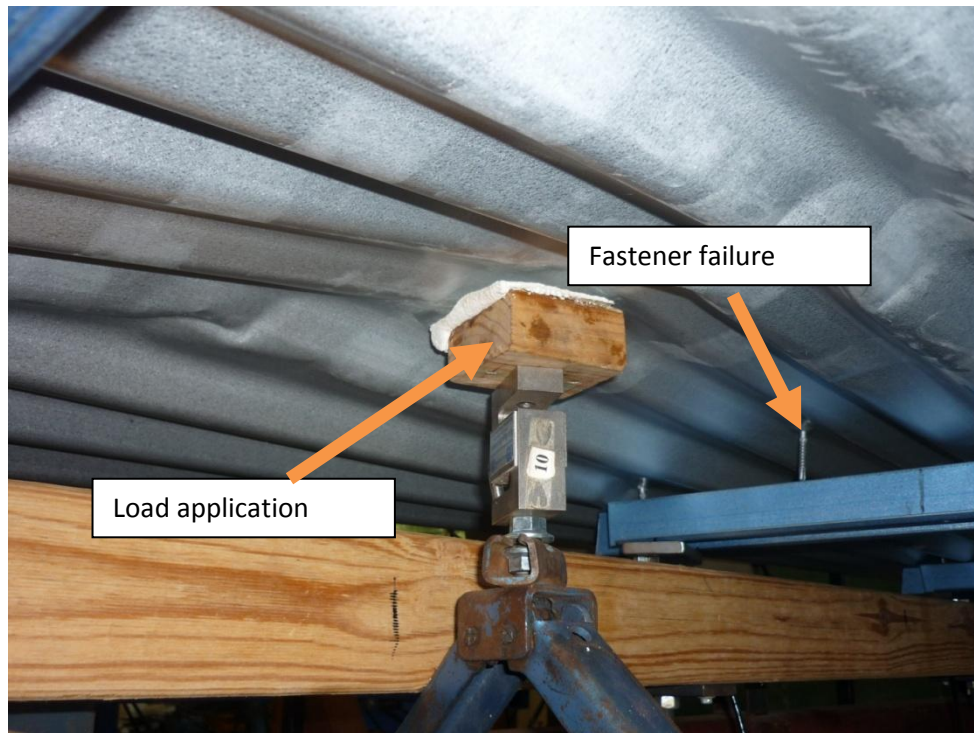


Figure 5.17: Application of point load showing a cladding fastener failure (pulling out of batten)

Similarly, line loads were also applied on selected Panels until failure of cladding fasteners. For these tests, Panels P10 and P13 were selected. The line load on Panel P10 along line X was progressively increased up to 9.5kN (Capacity of the load cell is 10kN). The reaction coefficients at $C_{b2, R3}$, $C_{b2, R4}$, $C_{b3, R3}$, and $C_{b3, R4}$ remained essentially unchanged with the increasing load. However, the plastic deformation of cladding was observed around fasteners as shown in Figure 5.18. At this stage, the maximum deflection in the middle of the panel was 60mm as shown in the Figure 5.19. The deflection in the middle of the panel (P10, X, 8) and the end (R4, X) increased linearly with increasing load up to 6.5kN, and then became non linear increasing at a progressively faster rate with plastic deformation of cladding. However, the deflections at positions (b2, 8), (b3, 8) and (P14, X, 11) were linear throughout the test as shown in the Figure 5.19.



Figure 5.18: Plastic deformation of cladding around fasteners

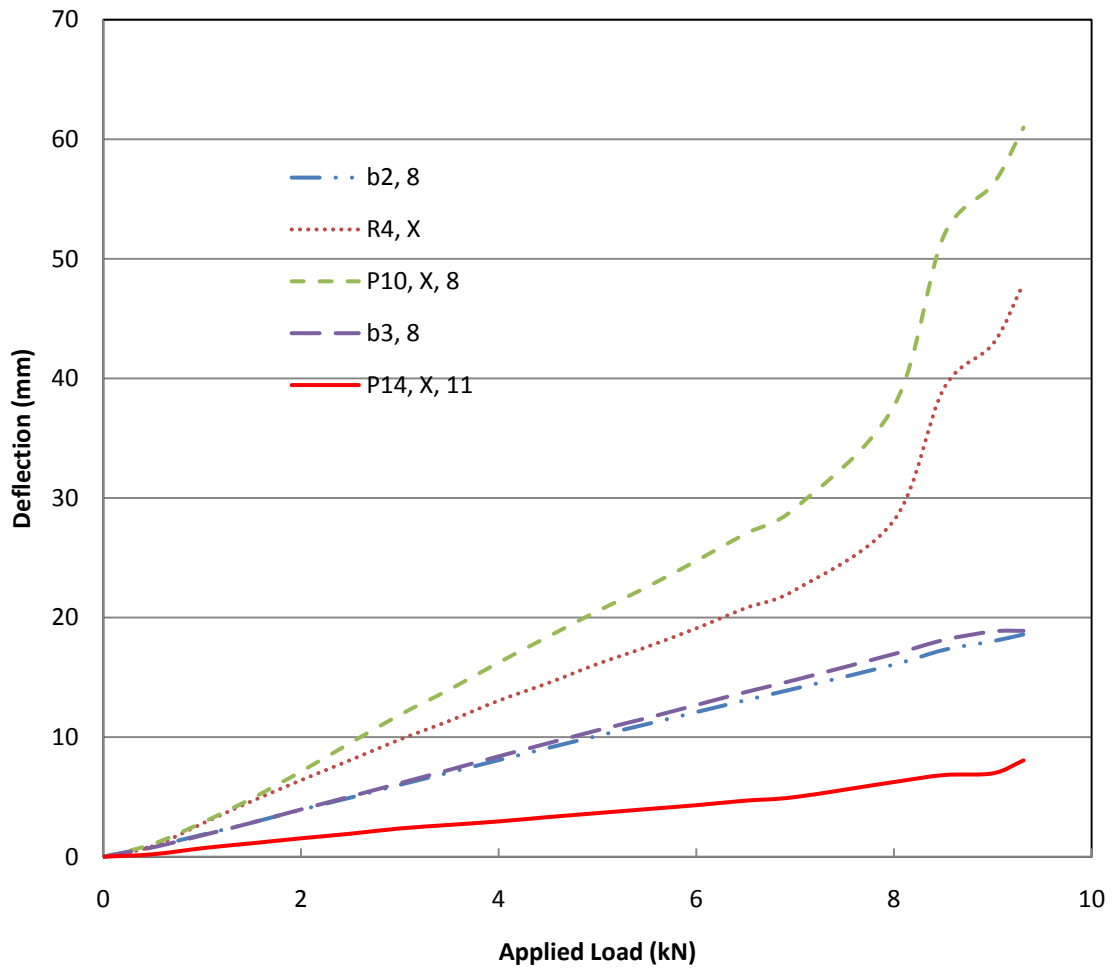


Figure 5.19: Deflections at selected positions with the applied load along line X of P10

Figure 5.20 shows the variation of reaction coefficients for line load application until failure of Panel 13. Stage 0-1 refers to the load application before the cladding fastener connection failure and Stage 1-2 refers to that following the failure of fasteners. Similar to the point load test, the majority of the applied load was taken by the batten-to-truss connections in P13. Being a corner panel, P13 had a lower capacity than P10, as it was connected to other panels on two sides only and hence it was only able to transfer load from two sides (majority of the load was transferred essentially to one side through the crests of cladding). During this test several fasteners started withdrawing from the batten b1 and b2 of Panel, P13, as shown in Figure 5.21. Furthermore, rotation of battens was also observed (shown in Figure 5.21). When the fasteners started failing, the loads were transferred to Panel, P14, increasing the downward loads (i.e. negative reaction coefficients) of $C_{b3, R4}$ and $C_{b3, R5}$ as shown in the Figure 5.20. Thus, the results show that the load transfer occurs via a range of crests of roof cladding to the next panels (i.e. P14). Therefore, the response on the connections due to line load application on Panels P10 and P13 until failure, behaved in a similar manner to that obtained from point loads (i.e. the loads were transferred to the adjacent panels).

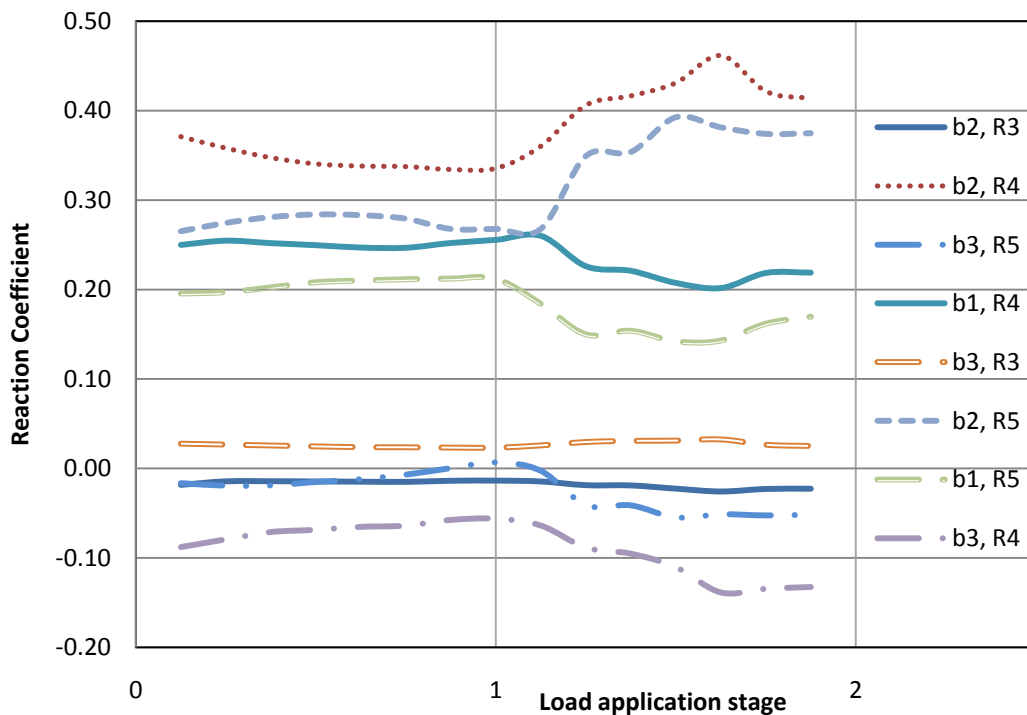


Figure 5.20: Reaction coefficient for a line load on P13 along line X

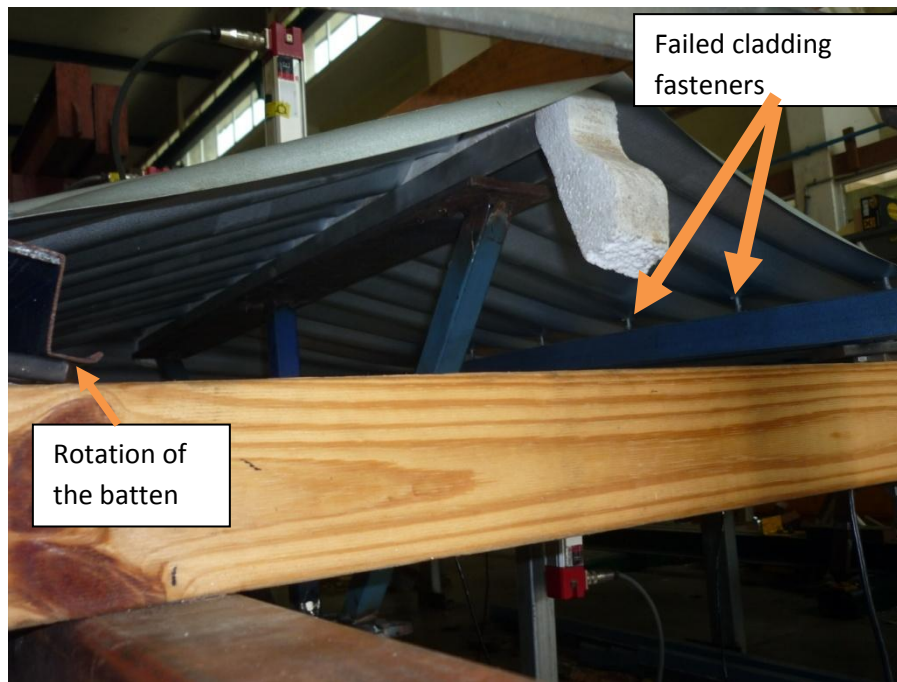


Figure 5.21: Line load on P13, X until failure of cladding fasteners

Further, the deflections were also measured at selected points on cladding and the variation of the deflection with the applied load is shown in Figure 5.22. The deflection in the middle of Panel, P13, was slightly lower than that of panel, P10, in elastic (linear) region. This may be due to the reduced area of the Panel P13 compared to P10 (i.e. the areas of Panels P10 and P13 are $900\text{mm} \times 750\text{mm}$ and $900\text{mm} \times 700\text{mm}$ respectively). However, it was higher in Panel P13 than P10 at the onset of plastic deformation around fasteners, thus enabling the dislodgment of fasteners at a lower load on Panel 13. The deflection at the middle of the Panel P13 increased with the applied load until the failure of fasteners that caused the reduction of the load to 5kN, as shown in Figure 5.22. Further loading increased the deflection in the middle of the panel significantly, as a result of failure of some of the fasteners on this panel. The Figure 5.22 also shows that the deflection at the interior batten (b2, 11) was larger compared to exterior (b1, 11), as a significant amount of the applied load is carried by the interior batten.

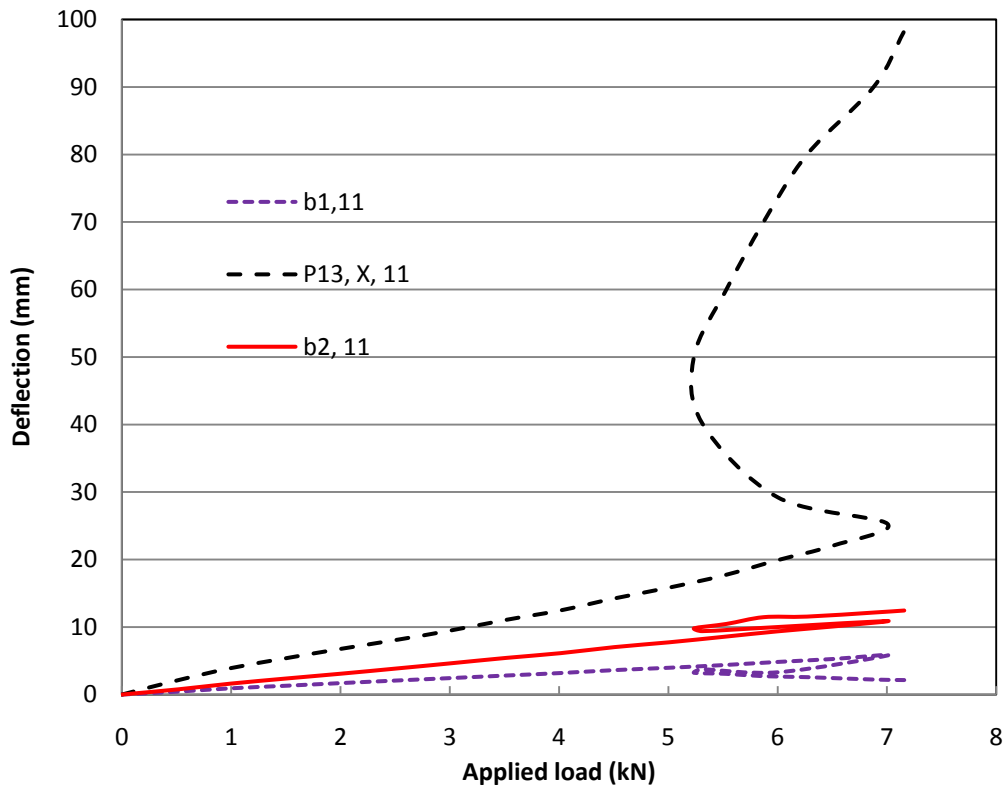


Figure 5.22: Deflection with the applied load on P13 along line X

5.3 Experimental test set up # 2

In the test set up #2, a roof frame was installed with batten spacings of 900mm as shown in Figure 5.23, closely representing the general batten spacing of new house construction. The Test set up #1 gave the variation of reaction coefficients for an average batten spacing of 750mm and the Test set up #2 can be used to obtain the reaction coefficients for batten spacing of 900mm. These values can be used to predict the reaction coefficients for a range of spacing between 750mm and 900mm. Thus, the effect of spacing on the reaction coefficients can be studied in order to predict the batten-to-truss connection behaviour for a population of houses. Test set up #1 focused on the effect of cladding fastener failures on batten-to-truss connection response. The main objective of the Test set up #2 was to focus on the changes in reaction coefficients with batten-to-truss connection failures, when the roof cladding was attached to the battens.

Figure 5.23 shows the battens identified as b1 to b4, truss elements identified as R1 to R5 and 12 panels named from P1 to P12 in Test set up #2. The load cells were installed on selected positions and the dummy load cells were installed at other connections. Furthermore, symmetry of the structural subassembly and associated connections allowed the system to be assessed by testing Panels P1, P2, P4 and P5. In addition, repeat tests enabled the collection of additional data. The load application procedure was also the same as that for Test set up #1. Thus, the load was applied from underneath of the roof set up (along grid X of each panel and on selected batten-to-truss connections) and the deflections were also measured from top and bottom (along grids X, 1, 2, 3, 4 and on battens) of the roofing elements wherever necessary. The list of tests carried out in this study is also shown in Appendix B.

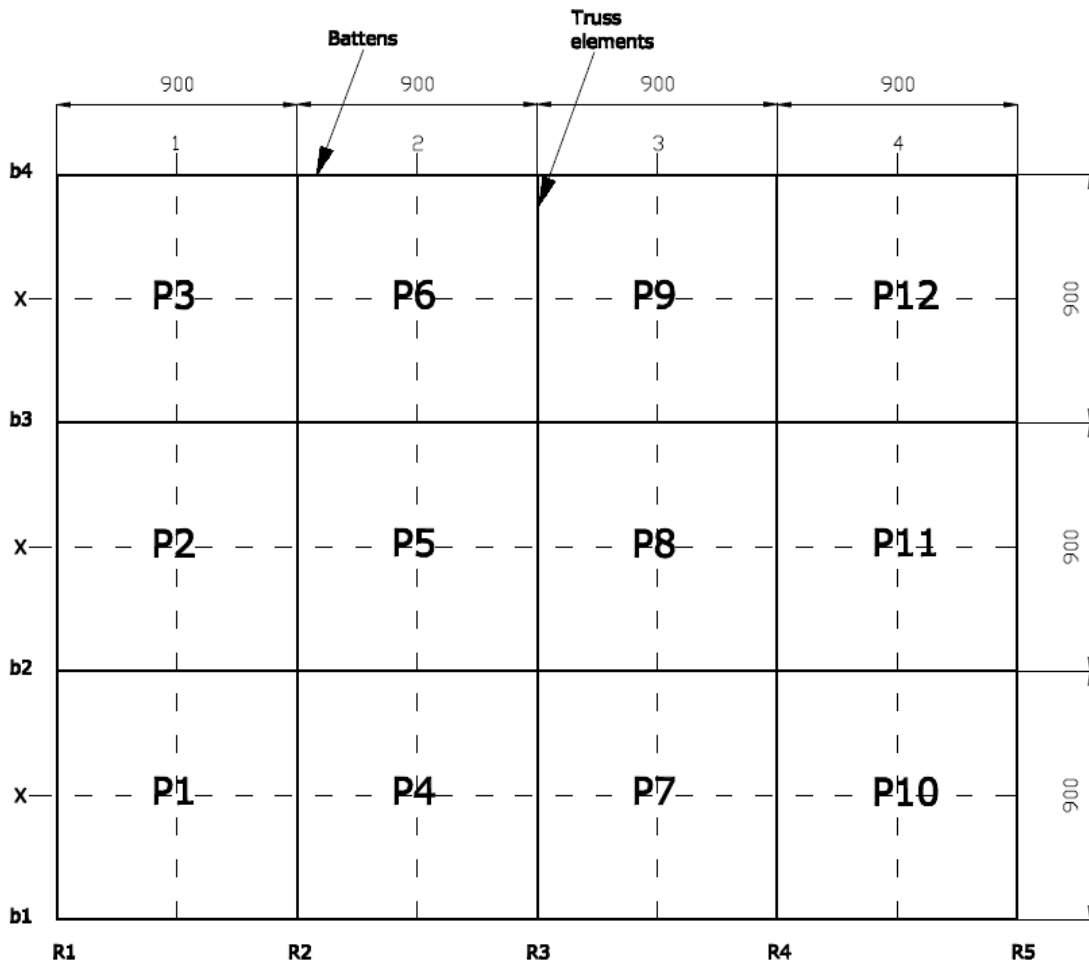


Figure 5.23: Schematic diagram of the Test Set up #2

5.3.1 Results and Discussions for Test Set up #2

A line load of up to 4kN was applied along the middle of each panel (i.e X) and the reactions and deflections were measured at various points. Table 5.2 shows the reaction coefficients for selected batten-to-truss connections, when the line load was applied sequentially on Panels P1 to P9. As shown on the Table 5.2, when the load was on the edge Panels (i.e. P1, P4...etc), a greater magnitude of the load was resisted by the interior connections. For an example, when the load was applied in the middle of Panel P4 (P4, X), reaction coefficients at the edge connections (b1, R2) and (b1, R3) were 0.23 and 0.25 respectively whereas that for interior connections (b2, R2) and (b2, R3) were 0.35 and 0.36 respectively. When the load was at the interior panels (i.e. P5, P8...etc), the four connecting supports shared the load about equally similar to the Test set up #1. These reaction coefficients were used to compare the variation of reaction coefficients with the spacing (i.e. with Test set up #1) and to compare several batten-to-truss connection damage scenarios discussed later in this chapter.

Table 5.2: Reaction coefficients of selected connections for load applied at P1 to P9

Applied load at	Reaction coefficients								
	C _{b1, R1}	C _{b1, R2}	C _{b1, R3}	C _{b2, R1}	C _{b2, R2}	C _{b2, R3}	C _{b3, R1}	C _{b3, R2}	C _{b3, R3}
P1,X	0.19	0.27	-0.04	0.28	0.42	-0.04	-0.04	-0.08	0.02
P2,X	-0.03	0.00	-0.02	0.26	0.29	0.00	0.25	0.30	0.00
P3,X	0.00	0.01	-0.01	-0.03	-0.07	0.02	0.28	0.42	-0.04
P4,X	-0.02	0.23	0.25	-0.03	0.35	0.36	0.01	-0.05	-0.07
P5,X	0.00	-0.01	-0.01	-0.01	0.28	0.29	-0.02	0.28	0.27
P6,X	0.00	0.01	0.01	0.01	-0.05	-0.06	-0.03	0.35	0.36
P7,X	0.00	-0.03	0.25	0.00	-0.04	0.36	0.00	0.02	-0.06
P8,X	0.01	-0.02	0.00	-0.01	0.00	0.29	-0.01	0.01	0.27
P9,X	0.00	0.00	0.10	0.00	0.01	-0.06	0.00	-0.03	0.36

Table 5.3 shows the deflections at selected points for a line load applied sequentially in the middle of Panels P1, P2, P4 and P5. As shown in the Table 5.3, the deflection in the middle of the panel on which the load was applied was similar magnitude in Panels P2, P4 and P5 and less

in Panel P1. The adjoining panels had lower deflection values and the deflections in the interior battens were larger compared to the batten at the edge similar to Test set up #1. For example when the load was applied at P1, the deflection was larger in the batten b2 than b1. Further, the deflections on the first internal batten were larger when the load was applied on a interior panel compared to that in an edge panel (i.e. the deflection at batten b2 was larger when the load was applied in Panel P5 than that in Panel P4). These values were also used to compare the deflections for several failure scenarios discussed later in this Chapter.

Table 5.3: Deflection at selected panels for line load application on panels

Loading Location		P1,X	P2,X	P4,X	P5,X
Applied load (kN)		3.5	4.0	3.9	4.06
Deflections(mm)	P1,X,1	15.6	-0.2	-0.0	
	P2,X,1	-0.1	20.7		1.9
	P4,X,2	0.1		19.3	-0.1
	P5,X,2		2.0	0.0	19.8
	P7,X,3			-0.3	
	P8,X,3				2.1
	b1,1	2.5			
	b1,2			2.3	
	b1,3			-0.4	
	b2,1	4.8	7.7		
	b2,2			4.9	7.7
	b2,3			0.2	1.8
	b3,1		7.8		
	b3,2				7.8
	b3,3				1.9

5.3.1.1 Comparison of reaction coefficients and deflections with the Test set up #1

Table 5.4 presents the reaction coefficients in selected batten-truss connections obtained from Test set up #1 and #2. When the load was applied at Panel P1, the reaction coefficient at batten-to-truss connection (b2, R2) in Test set up #2 was 0.07 greater than that in Test set up #1. The majority of the load at a corner panel was carried by the interior connection. When the spacing increases the load carried by the interior batten is larger and hence the connection (b2, R2) has a larger reaction coefficient. The reaction coefficients of other connections varied by up to 0.02.

When the load was applied at (P2, X), the reaction coefficient at (b3, R2) in Test set up #2 was 0.05 greater than that for Test set up #1. This is due to the distribution of load to the other panels in Test set up #1 which had an additional row of panels compared to the Test set up #2. Panel P5 of Test set up #1 and P4 of Test set up #2 were compared as shown in the Table 5.4 and the comparison showed a maximum difference of 0.04 for the reaction coefficients. Similarly, P6 and P5 of Test set ups #1 and #2 respectively had a maximum difference of 0.04 in reaction coefficients. Therefore, the results indicate that the variation in reaction coefficients was not significant with the spacing in most of the connections except for some locations which had a maximum of 20% variation (i.e reaction coefficient at (b2, R2) changed from 0.35 to 0.42). These results can be used to predict the reaction coefficients on batten-to-truss connections spaced from 750mm to 900mm. It should be noted that the accuracy error in each load cell is 0.09% of its total capacity and that for each LVDT is 0.02% of its total range. The resolutions in load and deflection measurements are found to be 0.305N and 0.0015mm respectively. Thus, the system is satisfactorily accurate.

Table 5.4: Comparison of reaction coefficients for line loads applied in test set up #1 and #2

Location	Test set up	Reaction coefficients								
		$C_{b1, R1}$	$C_{b1, R2}$	$C_{b1, R3}$	$C_{b2, R1}$	$C_{b2, R2}$	$C_{b2, R3}$	$C_{b3, R1}$	$C_{b3, R2}$	$C_{b3, R3}$
P1,X	#1	0.20	0.25	-0.03	0.28	0.35	-0.02	-0.02	-0.06	0.02
P1,X	#2	0.19	0.27	-0.04	0.28	0.42	-0.04	-0.04	-0.08	0.02
P2,X	#1	-	-	0.00	0.26	0.32	0.00	-	0.25	0.01
P2,X	#2	-0.03	0.00	-0.02	0.26	0.29	0.00	0.25	0.30	0.00
P5,X	#1	-	-	0.27	-0.02	0.31	0.32	-	-0.04	-0.06
P4,X	#2	-0.02	0.23	0.25	-0.03	0.35	0.36	0.01	-0.05	-0.07
P6,X	#1	0.00	-0.03	-0.01	-0.01	0.28	0.25	0.00	0.27	0.26
P5,X	#2	0.00	-0.01	-0.01	-0.01	0.28	0.29	-0.02	0.28	0.27

Further, the deflections measured on selected parts were also compared for Test set ups #1 and #2. Table 5.5 shows the comparison of deflections on two selected panels located at the edge and the middle of the Test set ups #1 and #2. The deflections were measured at representative locations in each set up for the same load application. The positions where the deflections were measured in each test set up are indicated in Table 5.5 showing the test set up number in the

bracket following the measured location. The results indicate that the deflections in the middle of the panels were larger in Test set up #2 compared to the setup #1. This is due to the larger spacing of battens in Test set up #2. However, the difference in deflections of the adjacent battens to the panels where the load was applied was not significant.

Table 5.5: Comparison of deflections in Test set up #1 and #2

Loading location		P1,X	P1,X	P6,X	P5,X
Test set up		#1	#2	#1	#2
Applied load(kN)		3.52	3.52	4.06	4.06
Deflection(mm)	b1,2 (#1) & b1,1 (#2)	2.82	2.52		
	b2,2 (#1)& b2,1 (#2)	5.43	4.84		
	P1, X,1 (#1& #2)	11.08	15.60		
	b2,5 (#1)& b2,2 (#2)			8.10	7.66
	b3,5 (#1)& b3,2 (#2)			8.40	7.82
	P6,X,5 (#1)& P5,X,2 (#2)			16.25	19.78

5.3.1.2 Batten Failure

Test setup #2 also studied the failure of batten-to-truss connection and the resulting load transfer. First, the load distribution and the deflections were obtained for failure of four connections circled as shown in the Figure 5.24. The failure of each connection was assessed followed by reinstalling the connection before failing the next connection. In each connection, the screw towards the roof edge was named as screw “E” and the internal screw was named as screw “I”. The screws at each connection were removed or loosened separately or together and the load was applied in the middle of adjacent panels of the connection. Removal of both screws in a connection represents the failure of a connection. Fowler (2003) observed that the batten-to-truss connection failure occurred after a partial failure (i.e. failure of one leg of the top hat batten). Thus, removing one screw represents the partial failure of a connection. Sometimes these connection screws can be loosened when it is subjected to a wind event or poor workmanship. In order to represent this behaviour, one or both screws were loosened at a time and the reaction coefficients and deflections were obtained by applying load on the adjacent panels.

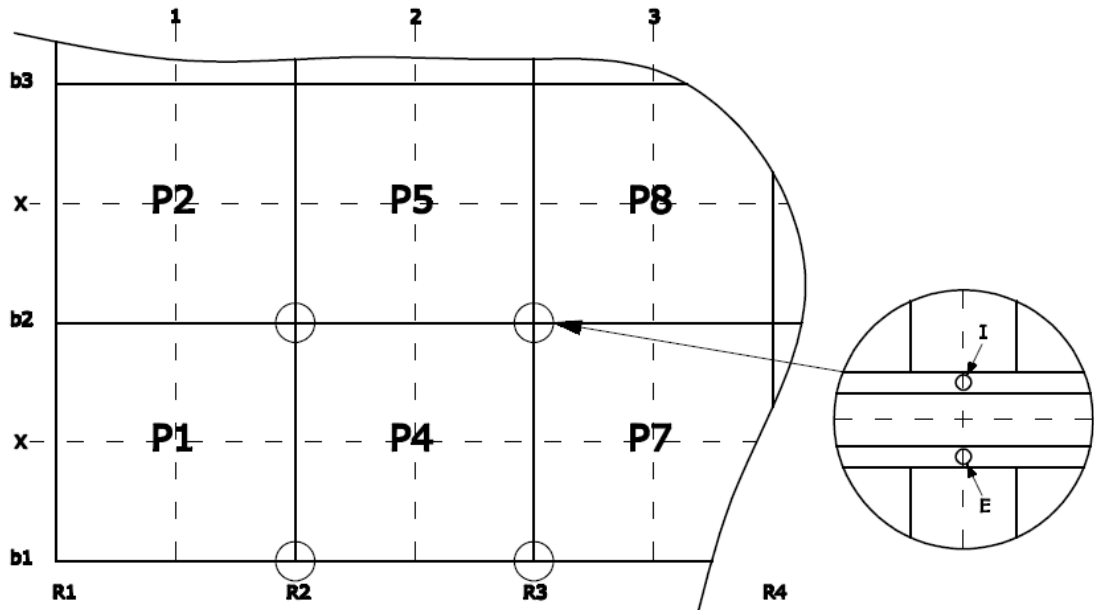


Figure 5.24: Schematic diagram of the connections studied

5.3.1.3 Both screws removed

Table 5.6 shows the variation of reaction coefficients, when both screws 'I' and 'E' were removed on a connection and the load was applied on the adjacent panels. These reaction coefficients were compared with the values without failure given in Table 5.2.

Table 5.6: Reaction coefficients for removing both screws in selected connections

Connection removed	Load Applied at	Reaction coefficients								
		$C_{b1, R1}$	$C_{b1, R2}$	$C_{b1, R3}$	$C_{b2, R1}$	$C_{b2, R2}$	$C_{b2, R3}$	$C_{b3, R1}$	$C_{b3, R2}$	$C_{b3, R3}$
b1,R2	P1,X	0.30	0.00	0.17	0.30	0.41	0.00	-0.04	-0.12	0.03
b1,R2	P4,X	0.06	0.00	0.40	-0.01	0.37	0.39	0.01	-0.09	-0.06
b1,R3	P4,X	-0.05	0.36	0.00	-0.03	0.37	0.35	0.00	-0.05	-0.10
b2,R2	P1,X	0.22	0.27	0.01	0.39	0.00	0.15	-0.05	0.09	-0.02
b2,R2	P2,X	-0.02	0.01	0.01	0.34	0.00	0.12	0.28	0.39	-0.03
b2,R2	P4,X	-0.01	0.26	0.23	0.04	0.00	0.54	0.01	0.09	-0.11
b2,R2	P5,X	0.01	0.00	0.02	0.05	0.00	0.40	-0.01	0.43	0.25
b2,R3	P4,X	-0.03	0.30	0.17	-0.07	0.54	0.00	0.01	-0.09	0.07

When the connection (b1, R2) was removed and the load was applied at (P1, X), the reaction coefficient at (b1, R1), $C_{b1, R1}$, increased from 0.19 to 0.30 and $C_{b1, R3}$ increased from -0.04 to 0.17. However, there was not a significant change in $C_{b2, R1}$ and $C_{b2, R2}$. This indicates that a significant amount of load is distributed to the adjacent batten connections. However, when the load was applied to (P4, X), there was a small increase in $C_{b2, R2}$ and $C_{b2, R3}$ 0.02 and 0.03 respectively in addition to the adjacent batten connections. As shown in the Table 5.2 and 5.6, when the screws of the connection (b2, R2) were removed, the reaction coefficients at (b2, R1) increased from 0.28 to 0.39 and the coefficient at (b2, R3) increased from -0.04 to 0.15 for applied load at (P1, X). Further, the reaction coefficient at (b3, R2) increased from -0.08 to 0.09 indicating the load transfers through cladding. When the load was applied at (P2, X), the reaction coefficients changed in the similar manner as that for (P1, X). However, when the load was applied at (P4, X) and (P5, X), a greater magnitude of load was resisted by the connection (b2, R3) than (b2, R1) and part of the load was transferred to the connection (b3, R2) via the roof cladding. When the connection (b2, R3) was removed, $C_{b2, R2}$, $C_{b2, R4}$ and $C_{b3, R3}$ increased in a similar manner.

These results indicate that a significant amount of load is redistributed to the connections next to the failed connection either via the batten or the crests of the cladding. However, the reaction coefficients of connections at the edge do not change significantly due to the failure of middle connections. Figure 5.25 shows the changes to the reaction coefficients, when the connection (b2, R2) failed and equal loads were applied to the middle of Panels P1, P2, P4 and P5 simultaneously (this is for connection (b1, R2) also shown in Table B.9 of Appendix B). These values were obtained by superposing the reaction coefficients of connections for the loads applied separately at each panel. The reaction coefficients before the failure of connection (b2, R2) are shown within the brackets for each connection. This is also illustrated graphically in Figures 5.26 and 5.27 respectively for before and after failure of the connection (b2, R2) respectively.

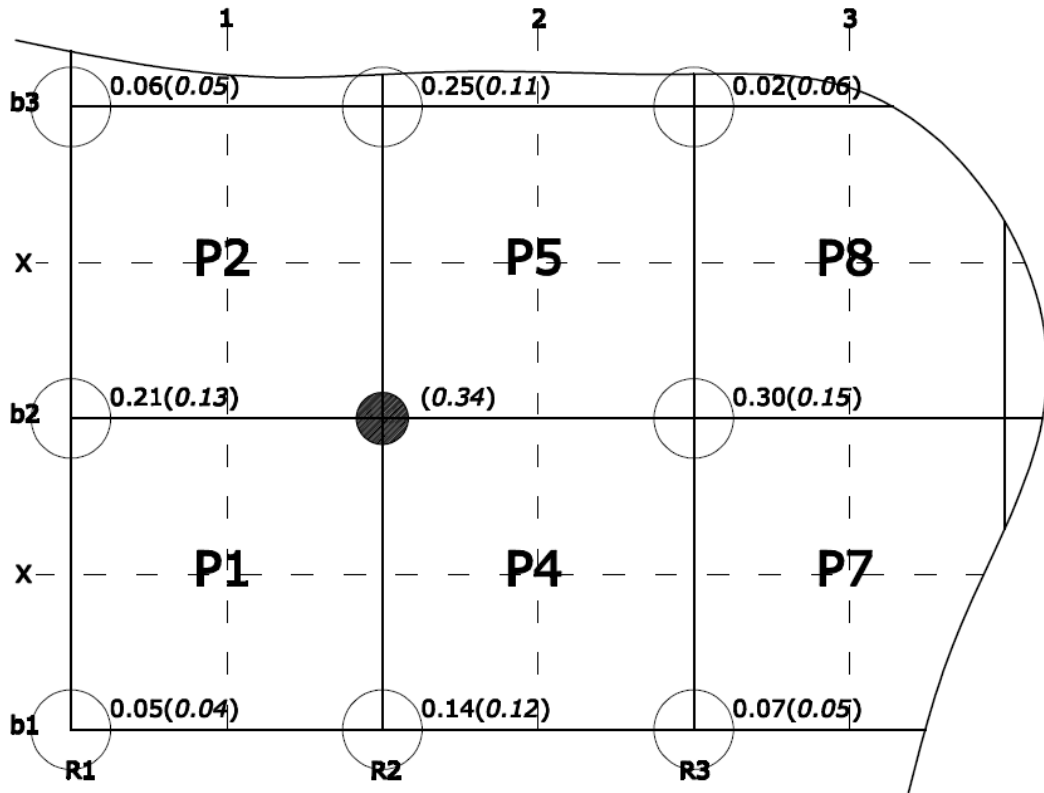


Figure 5.25: Reaction coefficients of adjacent connections when b2, R2 Failed

Note: Values in () are prior to failure

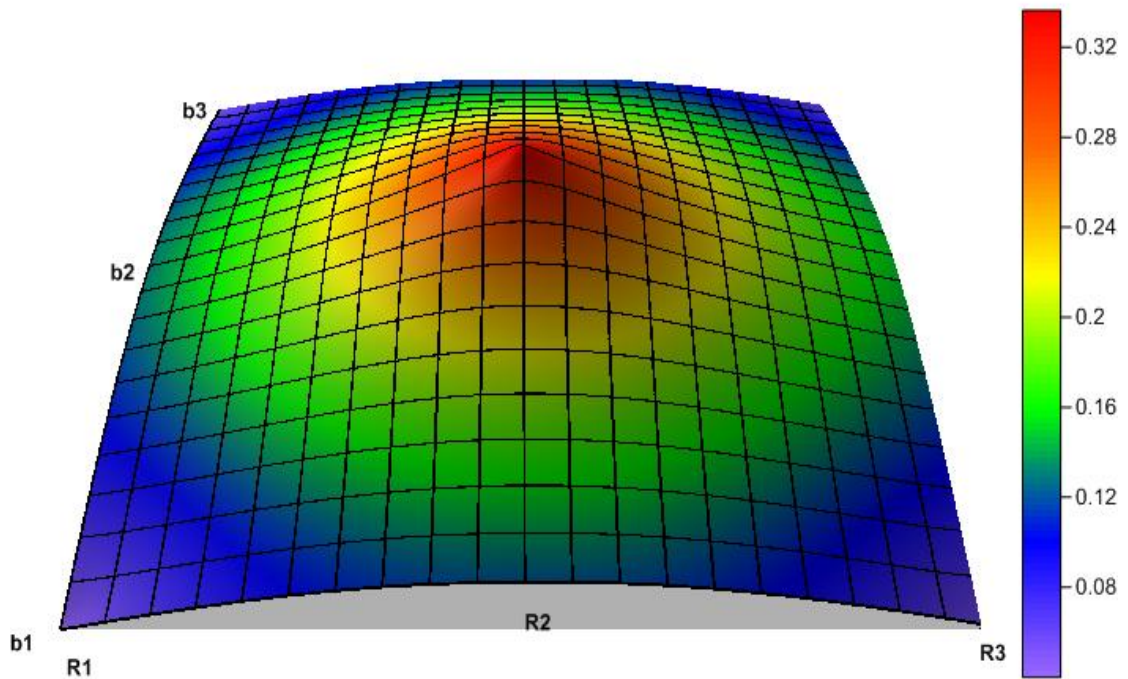


Figure 5.26: Reaction coefficients on connections for equal loads applied on P1, P2, P4 and P5

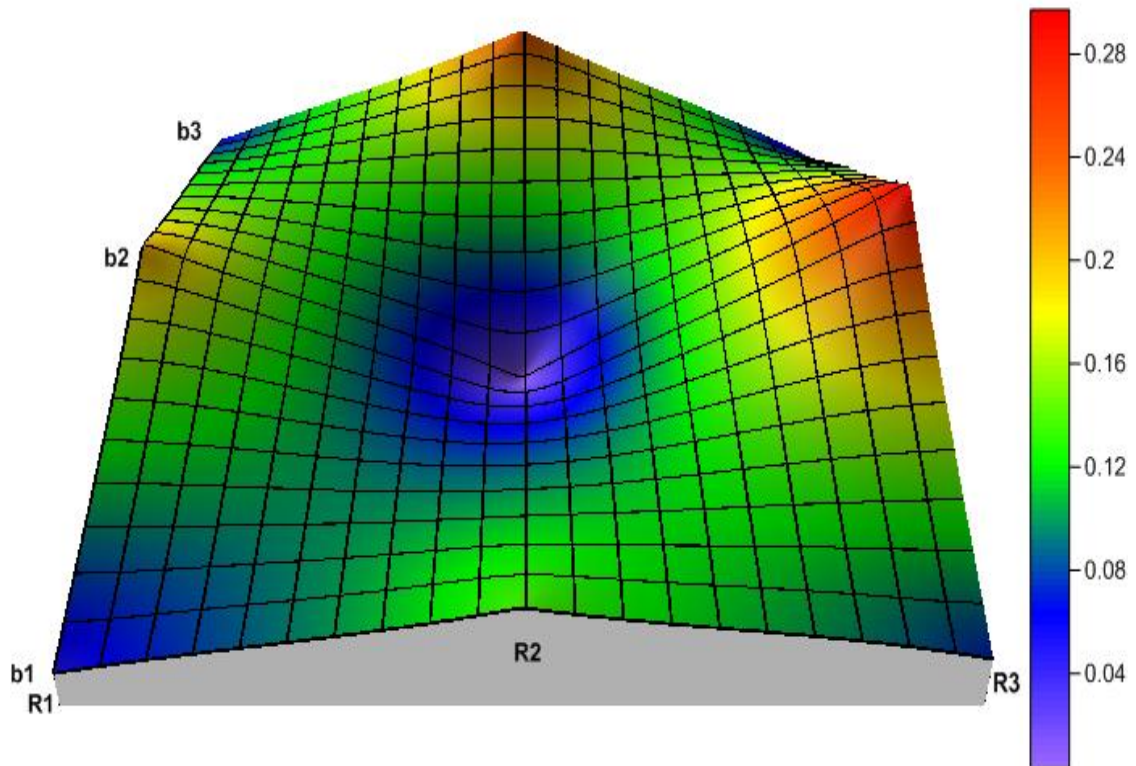


Figure 5.27: Reaction coefficients on connections when (b2, R2) failed for equal loads applied on P1, P2, P4 and P5

The variation to the deflections with failure of connections (i.e. both screws removed) are tabulated in the Appendix B. Comparison of deflections with data in Table 5.3 shows that the deflections generally increase in the middle of the panels and in the batten which had a connection failure. The difference of the deflections was higher in the battens compared to the middle of the cladding. However, the difference of the deflections was negligible for battens in some locations. The deflections of the failed connections are also indicated in the same table and it was found that the connections located in the middle had a larger deflections compared to the connections at the edge. The deflections of the adjacent panels were also increased during these tests.

5.3.1.4 Screw 'E' or 'I' removed



Figure 5.28: Batten-to-Truss connection with one screw connection removed

The changes to reaction coefficients were obtained when screw 'E' or 'I' was removed on selected connections as shown in the Figure 5.28. Table 5.7 shows the variation of reaction coefficients for selected connections when the screw 'I' was removed (the same for screw 'E' is also shown in Appendix B). These values were compared with the undamaged intact case given in the Table 5.2. Generally, the reaction coefficients vary in a similar manner for both cases with some minor variations. When the inner screw was removed from (b1, R2) the reaction coefficients on the connection from which the screw was removed, dropped from 0.27 to 0.19 and the reaction coefficients of the adjacent connections of the loaded panel increased (i.e. $C_{b1, R1}$ increased from 0.19 to 0.22 and $C_{b1, R3}$ increased from 0.24 to 0.29 when the applied load was at (P1, X) and (P4, X) respectively). When the screw 'I' was removed in connection (b2, R2), the reaction coefficient $C_{B2, R2}$ dropped from 0.42 to 0.29, 0.29 to 0.23, 0.34 to 0.27 and 0.28 to 0.21 for the load applied at P1, P2, P4 and P5 respectively, increasing the reaction coefficient at the adjacent connection in each panel on which the load was applied. The reaction coefficients in the connections for similar load applications at adjacent panels simultaneously are also shown in the Table B.9 of Appendix B and Figure 5.29 shows that for connection (b2, R2) (This can be compared with the Figure 5.26). These results indicated that the load transferred in a similar manner when a single screw was removed at a connection to that when both screws were removed (Note that the values were different in both cases). The reaction

coefficient of the connection from which the screw was removed, was reduced to some extent (i.e. up to a maximum of 31%) distributing a fraction of the carried the load to the adjacent connections. Thus, when only one screw is removed, the connection is still able to carry the load but the connection has a lower strength capacity.

Table 5.7: Reaction coefficients for removing screw ‘I’ of selected connections

Connection	Location	Reaction coefficients								
		$C_{b1,R1}$	$C_{b1,R2}$	$C_{b1,R3}$	$C_{b2,R1}$	$C_{b2,R2}$	$C_{b2,R3}$	$C_{b3,R1}$	$C_{b3,R2}$	$C_{b3,R3}$
b1,R2	P1,X	0.22	0.19	0.01	0.30	0.41	-0.03	-0.04	-0.09	0.02
	P4,X	0.00	0.17	0.29	-0.02	0.35	0.37	0.01	-0.07	-0.07
b1,R3	P4,X	-0.03	0.26	0.18	-0.03	0.38	0.35	0.01	-0.06	-0.07
	P7,X	0.00	0.00	0.21	0.00	-0.03	0.37	0.00	0.02	-0.07
b2,R2	P1,X	0.21	0.26	-0.02	0.32	0.29	0.00	-0.04	-0.03	0.01
	P2,X	-0.03	0.00	-0.01	0.28	0.23	0.03	0.24	0.33	-0.01
	P4,X	-0.02	0.27	0.19	-0.01	0.27	0.39	0.01	-0.01	-0.08
	P5,X	0.00	-0.01	-0.01	0.00	0.21	0.28	-0.01	0.33	0.27
b2,R3	P4,X	-0.03	0.27	0.18	-0.04	0.41	0.24	0.01	-0.06	-0.02
	P5,X	-0.01	-0.01	-0.01	-0.02	0.32	0.17	-0.01	0.29	0.31
	P7,X	-0.01	0.01	0.20	-0.01	0.02	0.26	0.00	0.01	-0.01
	P8,X	0.00	-0.01	0.00	-0.02	0.04	0.22	-0.01	0.00	0.30

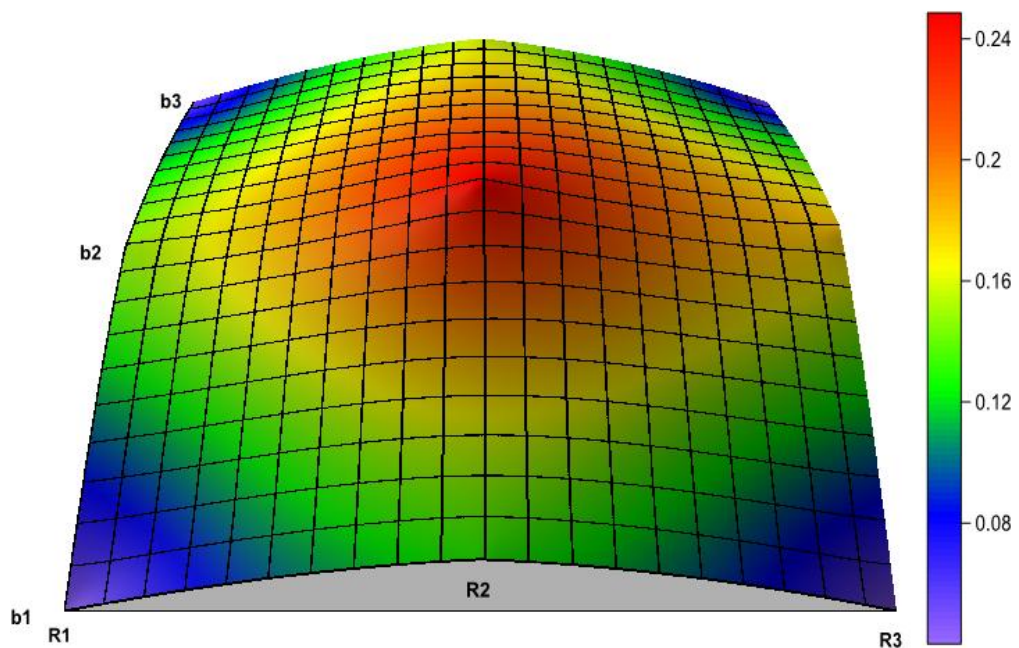


Figure 5.29: Reaction coefficients for a partial failure of the connection b2, R2 for equal loads applied on P1, P2, P4 and P5

The detailed deflection values for screw ‘E’ and ‘I’ failures are also shown in the Appendix B and the values behaved in a similar manner for both cases. The results indicated that the difference of the deflections in the middle of the panels where the load was applied was not significant with the values given for intact case (Table 5.3). However, the deflections were increased in the battens where the connection was failed. Further, the deflections at the connections were generally less than that for both screws removed condition.

5.3.1.5 Screws loosened

Both screws at a batten-to- truss connection were loosened as shown in Figure 5.30 to simulate partial screw withdrawal of a connection. Table 5.8 presents the reaction coefficients when the connections at selected locations were loosened. When the screws at connection (b2, R2) were loosened, the reaction coefficient at (b2, R2) reduced from 0.42 to 0.21 for load applied at (P1, X) increasing $C_{b2, R1}$ from 0.28 to 0.35 and $C_{b2, R3}$ from -0.04 to 0.06. The results indicated that the reaction coefficient of the loosened connection drops to a certain level (It can be more than 50%) distributing fraction of the load to the adjacent connections in a similar manner to that of a failed connection.

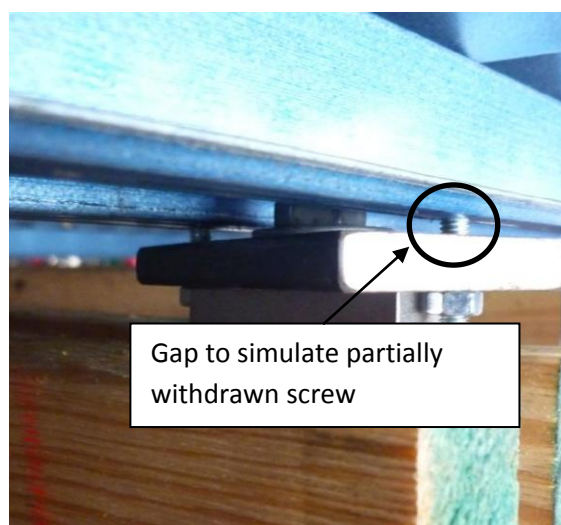


Figure 5.30: A connection with loose screws

Table 5.8: Reaction coefficients for loosening both screws on selected connections

Loose screw Connection	Applied Load at	Reaction coefficients								
		$C_{b1,R1}$	$C_{b1,R2}$	$C_{b1,R3}$	$C_{b2,R1}$	$C_{b2,R2}$	$C_{b2,R3}$	$C_{b3,R1}$	$C_{b3,R2}$	$C_{b3,R3}$
b1,R2	P1,X	0.23	0.19	0.03	0.29	0.40	-0.03	-0.04	-0.09	0.02
	P4,X	0.01	0.16	0.30	-0.02	0.35	0.36	0.01	-0.07	-0.06
b1,R3	P4,X	-0.03	0.30	0.14	-0.03	0.36	0.35	0.01	-0.05	-0.08
	P7,X	-0.01	0.03	0.17	0.00	-0.02	0.37	-0.01	0.02	-0.07
b2,R2	P1,X	0.21	0.25	-0.01	0.35	0.21	0.06	-0.04	0.00	0.00
	P2,X	-0.03	0.01	-0.01	0.29	0.17	0.06	0.26	0.34	-0.01
	P4,X	-0.02	0.25	0.19	0.01	0.21	0.44	0.01	0.01	-0.09
	P5,X	0.00	-0.01	0.00	0.01	0.16	0.31	-0.01	0.35	0.25
b2,R3	P4,X	-0.03	0.26	0.18	-0.04	0.41	0.26	0.01	-0.07	-0.03
	P5,X	-0.01	0.00	-0.01	-0.03	0.34	0.14	-0.01	0.28	0.31

Similarly, when the screws ‘E’ or ‘I’ were loosened, the reaction coefficients were higher in the connections than that for the screw ‘E’ or ‘I’ were fully removed condition. The values for reaction coefficients are shown in the Appendix B. The maximum difference in reaction coefficients was 0.05. Thus, the reaction coefficient of the connection from which the screw ‘E’ loosened was less than the intact values and greater than the fully removed condition. The reaction coefficients in the connections for similar load applications at adjacent panels simultaneously are shown in the Table B.9 of Appendix B.

The deflections were also recorded at this stage and are shown in the Appendix B for all three cases. The deflection results showed that there was not significant variation in the difference with the intact values but in some cases variations were observed in the middle of the panels where the load was applied for both screws removed case. Similar to previous tests, the deflections on the battens from which the screws were loosened had a larger deflection compared to the intact case values in Table 5.3. The deflections measured for single screw loosened cases were similar to fully removed condition except for some variations.

5.3.1.6 Loading until failure of batten-truss connections

The load was applied to the batten on either side of the support using a ‘U’ shaped steel frame as shown in the Figure 5.31. In order to simulate the screw washer of the batten fastener, the 12 gauge screw washers were used in each connection. These washers correctly represented the batten fastener screw washer (Fowler (2003)).



Figure 5.31: Applied load on batten-truss connection

First, the load was applied to the batten-to-truss connection (b2, R2) and the loads were measured at selected connections. The loading was stopped when the applied load was at 9.8kN since the capacity of load cell is 10kN. At this stage, there was not any apparent failure of the connection. However, plastic deformation of batten at the connection (b2, R2) was observed. There was not any significant variation of reaction coefficients at this stage with the applied load. Figure 5.32 shows the distribution of reaction coefficients at the adjacent connections for the total applied load. As shown, the total applied load was not taken by the connection (b2, R2) and a considerable amount of load was shared by the adjacent connections.

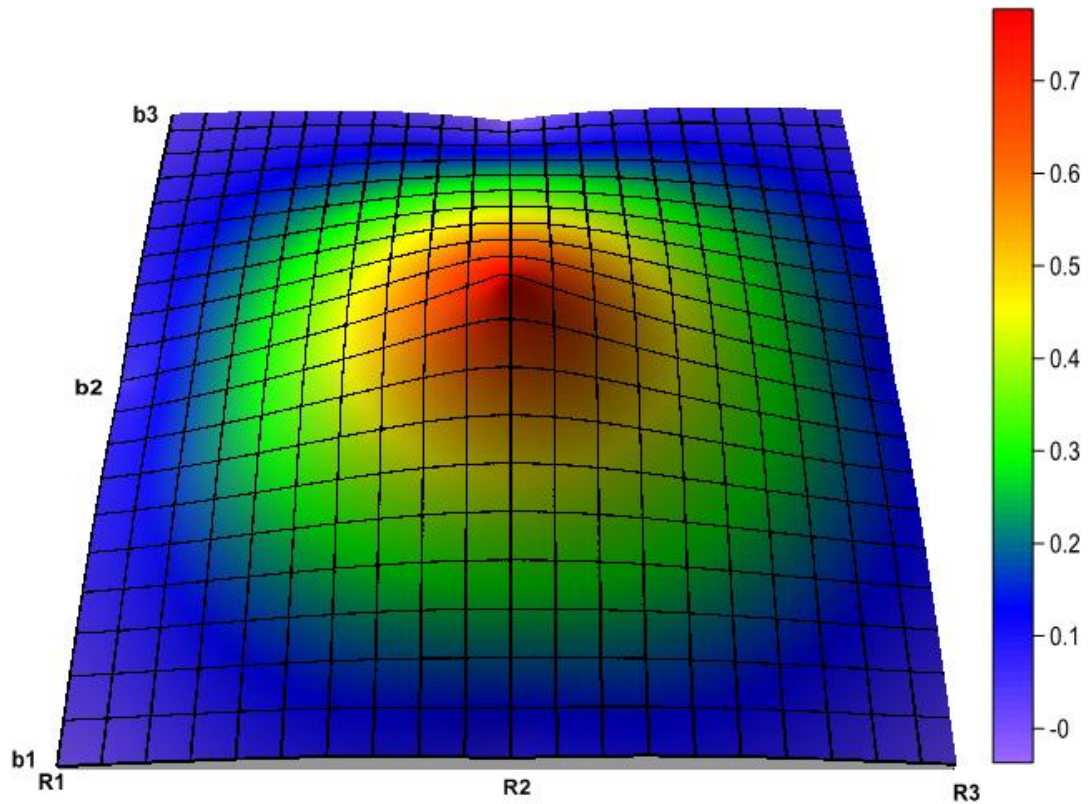


Figure 5.32: Reaction coefficients for total applied load on (b2, R2)

The deflections were also measured at selected points as shown in the Figure 5. 33. Figure 5.34 shows the deflections of the connection (b2, R2) and the points (b2, 1) and (b2, 2) along the batten b2 with the applied load. The connection had the largest deflection as expected and the deflection at (b2, 1) had larger deflection compared to that for (b2, 3). Thus, the edge of the batten has higher deflection compared to the middle. However, the difference was only 2mm. The deflection of the point (b2, 3) was also measured and it was negligible compared to other points (less than 0.5mm).



Figure 5.33: Deflection measurement

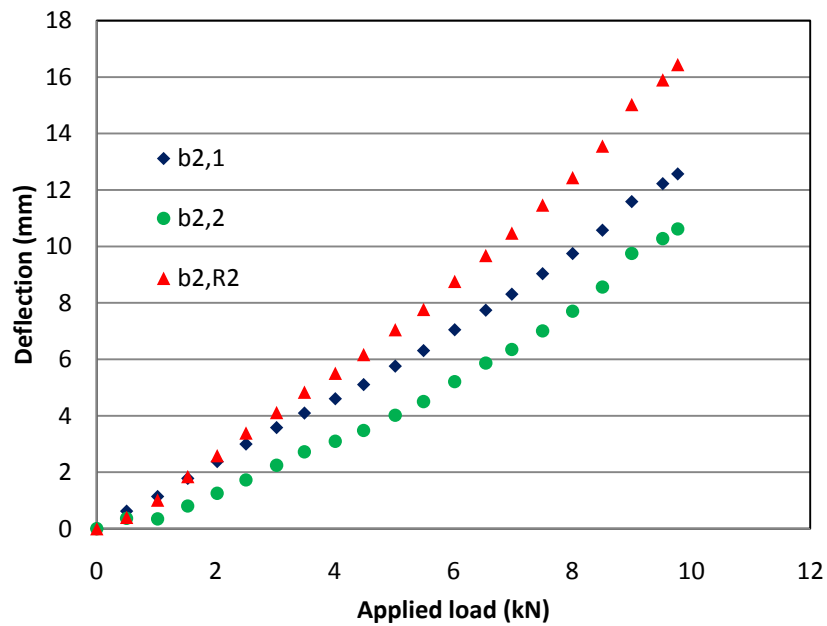


Figure 5.34: The applied load vs deflection at (b2, R2)

Then the load cell of the hydraulic jack was removed and the load was applied to the connection until the connection load become just less than 10kN. At this stage, there was not any failure of the batten except for plastic deformation around the connection, as shown in the Figure 5.35 similar to the previous test. During this stage there were not many changes to the reaction coefficients and the load deflection curve. The maximum deflection was observed at the connection around 20mm for 10kN load in the connection.



Figure 5.35: Plastic deformation of a batten-to-truss connection

Then the screw ‘E’ of batten-truss connection (b2, R2) was removed and loaded until failure. Figure 5.36 shows the variation of deflection at selected points with the load on the connection (b2, R2). The batten-to-truss connection (b2, R2) failed around the screw ‘I’ as shown in Figure 5.37 for the load at connection 5.2kN. The failure mode of the batten was cutting out a semi circular shape around the washer and angling out towards the edge of the batten.

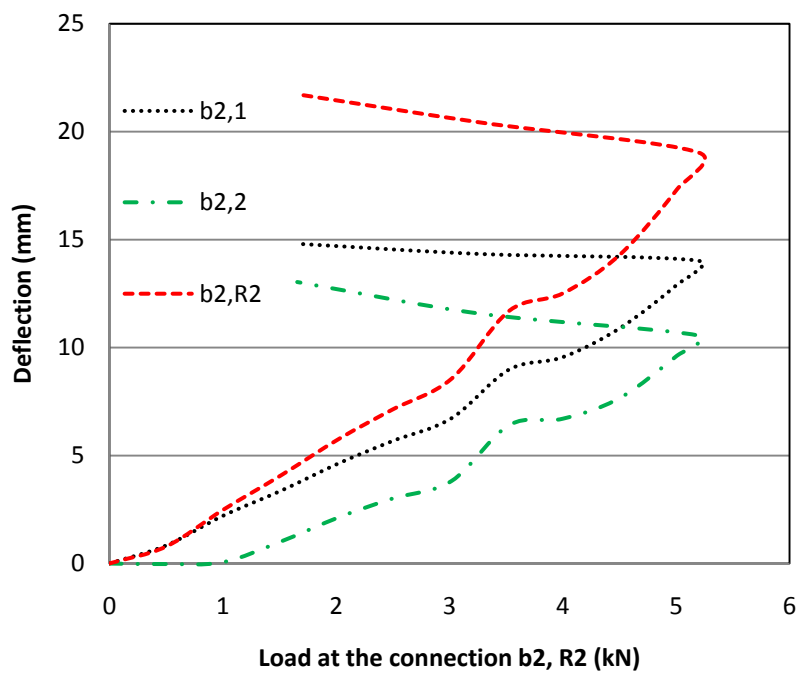


Figure 5.36: Applied load vs Deflection on connection (b2, R2)



Figure 5.37: Failure of the connection (b2, R2)

Similarly, the connection (b3, R3) was loaded until failure (this connection is equivalent to (b2, R3) due to the symmetry). The load was increased to 9.9kN and the connection did not fail as was the case with connection (b2, R2). The variation of the deflections at selected points with the applied load is shown in Appendix B. Then, the screw 'E' (the screw towards connection (b4, R3)) of batten-to-truss connection (b3, R3) was removed and loaded until failure. Figure 5.38 shows the variation of reaction coefficients at selected points with the load application stages. Stage 0-1 refers to the reaction coefficients before the total failure of the connection. As shown in the Figure 5.38, the majority of the applied load was taken by the connection (b3, R3) as expected and the rest of the load was shared by the connections (b3, R2), (b3, R4) and (b4, R3). At stage one, the connection (b3, R3) failed but the batten was still connected to the connection. The load at (b3, R3) dropped significantly from 5.15kN to 2.1kN and at the same time the load was taken by (b3, R2), (b3, R4) and (b2, R3) connections as shown in the Figure 5.38. Then, the connection was further loaded (stage 1-2) and the batten was entirely removed from the connection at stage 2. The reaction coefficients at (b3, R2), (b3, R4) and (b2, R3) connections further increased during this stage. The reaction coefficient at (b4, R3) was consistent throughout the whole process having a small increase at each stage. Thus, the interior connections carried the majority of the load. The failure mode of the batten was cutting out a semi circular shape around the washer and angling out towards the edge of the batten. A

similar failure mode was observed by Fowler (2003) for cyclic tests on top hat battens. The variation of the deflection at selected points with the total applied load is also shown in the Figure 5.39.

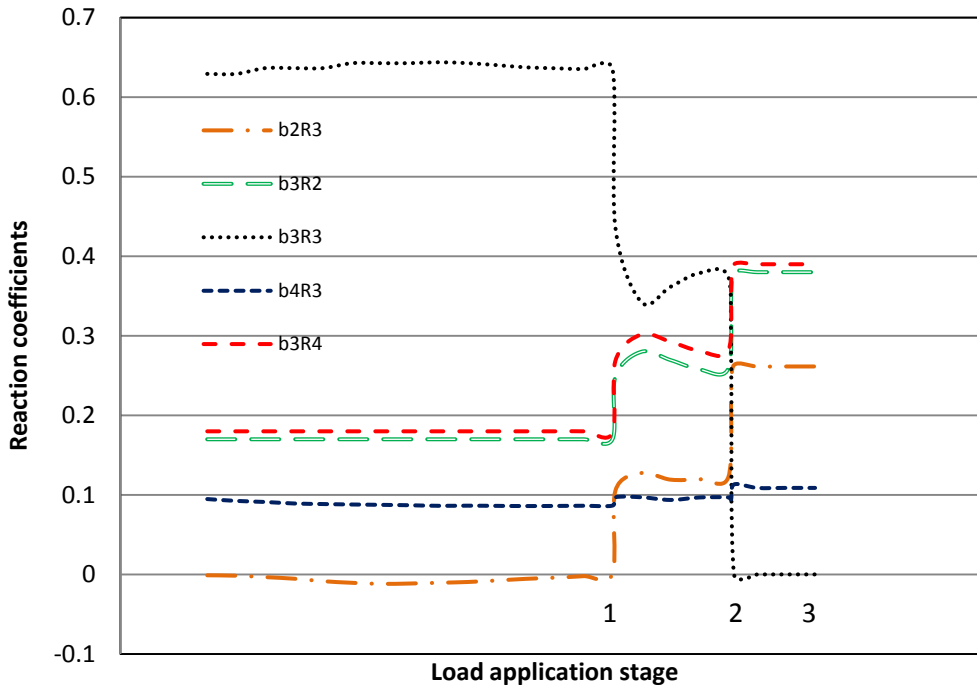


Figure 5.38: Variation of reaction coefficients with the applied load

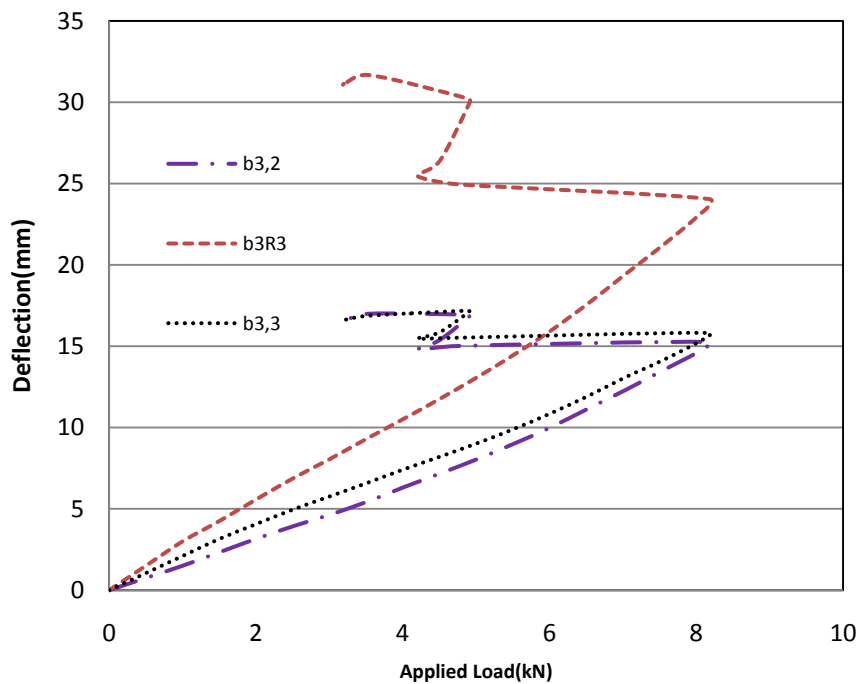


Figure 5.39: Variation of deflections with the applied load

These results showed that the connection (b2, R2) had larger reaction coefficient than the connection (b3, R3) which can be taken as a connection in the middle area of a roof (i.e. When the load applied to (b2, R2) the reaction coefficient was 0.79 and that for connection (b3, R3) was 0.75). This is due to the distribution of load in the middle connection (b3, R3). Thus, the first internal batten-to-truss connection subjected to failure first, when the applied load is equal on the total roofing panels.

5.4 Summary and Discussion

A series of tests on roof subassembly systems subjected to a range of loads were presented. The reaction coefficients at batten-to-truss connections and deflections were measured and analysed. The distribution of loads among the batten-to-truss connections was determined for various scenarios in the linear response region. The deflections of the cladding and battens were also obtained. The results of these tests were compared with structural analysis for a linear elastic system and were found to agree well, with some differences (especially when the load is applied to the claddings). The repeat tests carried out to measure loads and deflections were in close agreement. The accuracy error in each load cell is 0.09% of its total capacity and that for each LVDT is 0.02% of its total range. The resolutions in load and deflection measurements are found to be 0.305N and 0.0015mm respectively. Therefore, the experimental errors due to the load and deflection measurements were assumed to be negligible in this study. The reaction coefficients were obtained for point loads and line loads applied to the undamaged system and for several damage scenarios of failed cladding fasteners and failed batten-to-truss connections. The effect of cladding fastener failure and batten-to-truss connection failures with the increasing load (from linear to non-linear region of components/connection) on the batten-to-truss connections were studied. Furthermore, the redistribution of load and the changes to the deflections in cladding and battens were also determined. The results show that the load acting outside the conventional tributary area has a significant effect on the batten-to-truss connection loads, indicating that the area of the adjoining panels should be considered in order to obtain the

load effect on batten-to-truss connections. The outcomes of this chapter (i.e. the reaction coefficients) are used in Chapter 6, for determining the wind load distribution on batten-to-truss connections. The results can be used to describe the performance of contemporary houses built in cyclonic region of Australia.

The failure of roofing connections (i.e. cladding fixings and batten-to-truss connections) usually occur due to fatigue producing characteristics of wind loads (i.e. cycles of loading of various amplitudes). The failure of these connections is caused by a combination of number of load cycles and their magnitude. Henderson (2010) showed that the cladding fixing respond in a quasi-steady manner to the applied wind loads, and that static load can be used to satisfactorily measure the response of the roofing to wind loads. Hence, the tests carried out can accurately represent the response of the roof structure to wind loads during different stages of loading up to failure.

The analytical study conducted in this chapter was basically carried out to confirm that the experimental set up follows the structural engineering principals and also to compare the experimental results. The results of this chapter such as distribution of loads and load-deflection curves are important for carrying out linear/ non-linear analysis of the roofing system. The boundary conditions used in these test setups can be incorporated in the structural engineering software and the analysis can be performed for the total structure being considered. Such an analysis can be used for predicting the loads on connections for various scenarios.

6 VULNERABILITY OF THE ROOF SYSTEM

The wind loads measured on the wind tunnel model and presented in Chapter 4 are combined with the roof structure response given in Chapter 5 to determine the distribution of load in the roof system of contemporary houses. These results are also compared with the data obtained from conventional methods. A method for developing vulnerability curves for cladding fastener, batten-to-truss and truss-to-wall connections on selected parts of the roof using the reliability method and probability theories are also presented.

6.1 Load distribution on Roof system

The wind load acting on structural components vary with the wind approach direction. The complex and fluctuating nature of wind loads can pose significant challenges for structural design and the assessment of structural vulnerability. As shown in the literature review, the wind load effects on the roof components are influenced by the spatial distribution of wind pressure and underlying structural system. Thus, the behaviour of load action and structural response should be taken in to account when determining the load distribution among the components and assessing their vulnerabilities.

The peak loads on the batten-to-truss connections on the part of the roof experiencing large loads were studied. The structural system of the common contemporary house was discussed in previous chapters and the segment comprising batten-to-truss connections A5 to A8, B5 to B8, C5 to C8 and D5 to D8 of trusses, A, B, C and D shown in Figure 6.1 (i.e. from Figure 4.3 in Chapter 4) was analysed for loading from a range of wind directions. The distribution of pressures and the peak loads on these batten-to-truss connections were determined for each wind direction. It should be noted that the connection loads presented in this chapter are based on the instantaneous wind pressure measurements on the pressure taps in this region.

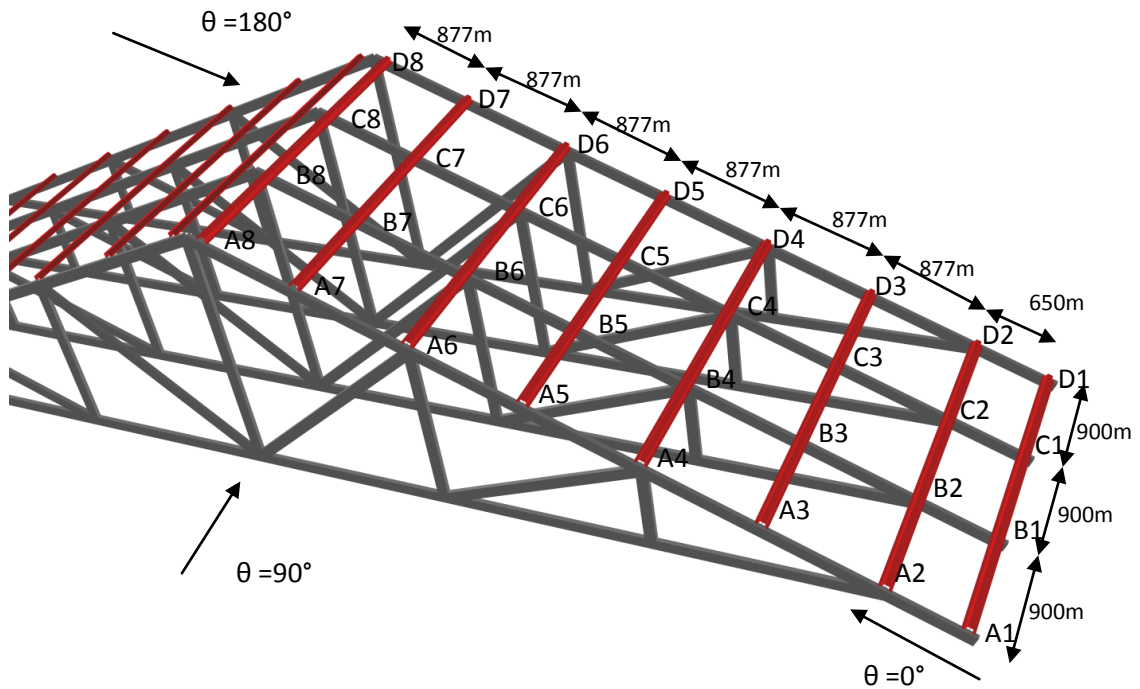


Figure 6.1: Schematic Diagram of connections considered

Figures 6.2, 6.3 and 6.4 show the plan view of the selected connections on trusses A, B, C and D and the pressure tap locations. As shown in these figures (and also Figure 4.3 of Chapter 3), each panel consists of four pressure taps. The shaded area on Figures 6.2 and 6.3 shows the typical tributary areas conventionally used for calculating design loads on batten-to-truss connections or assessing their vulnerability. In these figures the tributary areas for connection B7 is shown for each case. The area defined for the conventional method #2 (i.e. Tributary area of half panel width either side of the batten b2) is basically considered for the purlin/batten design, as specified in product manuals (Stramit (2000)). The load on each connection of the beam is obtained by analysing the load acting on overall tributary area along the total batten. The area specified in Figure 6.3 affects connection B7, and the tributary areas related to other connections (i.e. C7, B6, A7...etc) were also taken in a similar manner.

However, the structural testing results from Chapter 5 indicated that the wind loads on shaded area shown in Figure 6.4 has a significant effect on connection B7. Based on test data from Chapter 5, the loads on the other connections (i.e. C7, B6, A7...etc) were also considered using the panels in a similar manner. Thus, the area of the adjoining panels of each connection was considered for each connection. For example, the tributary areas for connections B8 and B6 are also shown in Appendix C (Figures C1 and C2). This section compares the peak instantaneous load acting on these connections from each method.

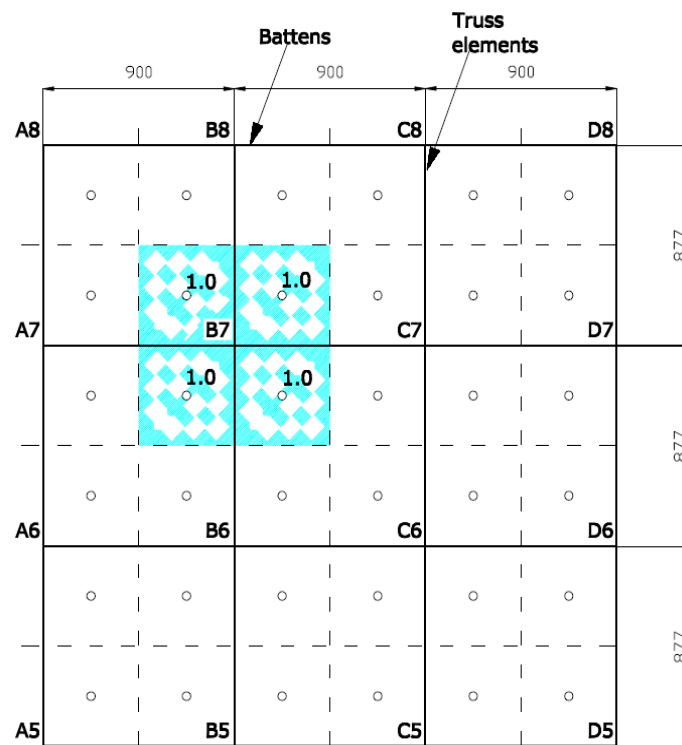


Figure 6.2: Conventional method #1-Tributary area for connection B7

Note: o - Pressure taps
 The values shown next to the pressure taps are reaction coefficients

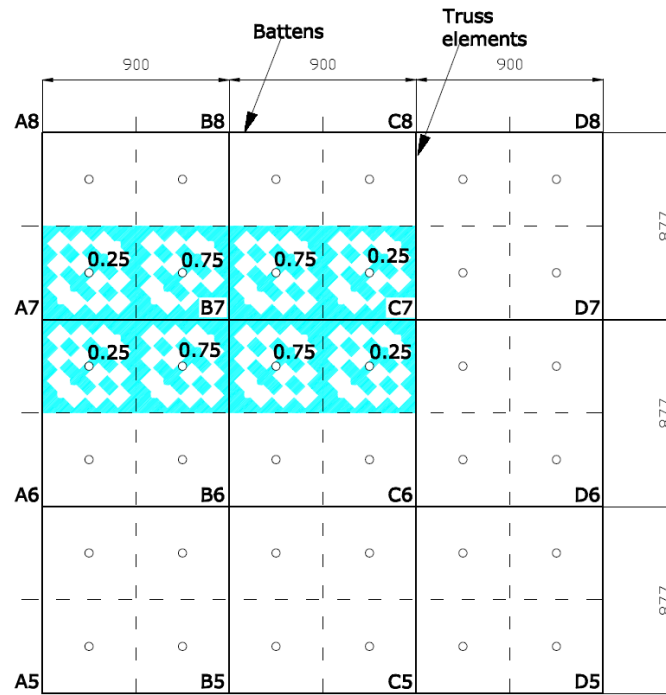


Figure 6.3: Conventional method #2-Tributary area for connection B7
 Note: o - Pressure taps
 The values shown next to the pressure taps are reaction coefficients

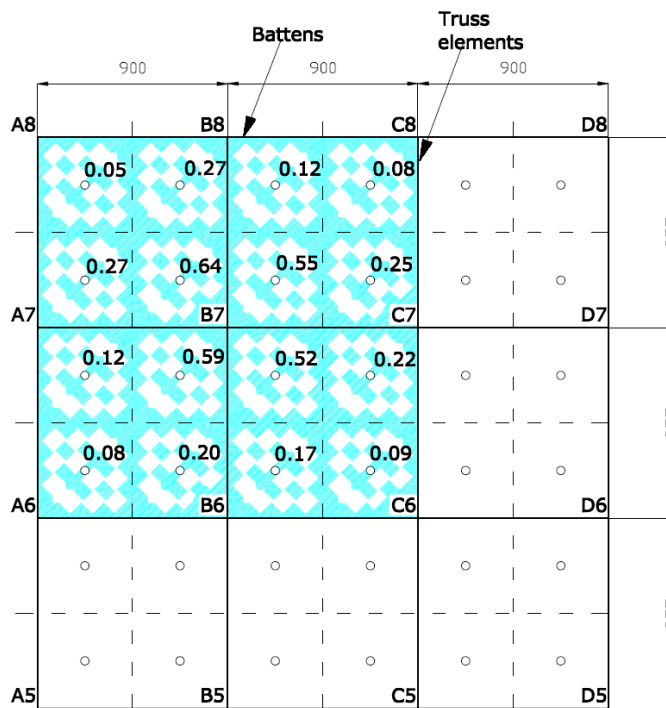


Figure 6.4: Proposed method - Tributary area for connection B7
 Note: o - Pressure taps
 The values shown next to the pressure taps are reaction coefficients

The load at a given batten-to-truss connection ($X_b(t)$) is given by

$$X_b(t) = \left(\sum_{i=1}^N \beta_i A_i C_{p_i}(t) \right) * 1/2 \rho \bar{U}_h^2 \quad (6.1)$$

Where

β_i -Reaction coefficient for load applied at pressure tap location, i

A_i - Tributary area for pressure tap, i $C_{p_i}(t)$ - Pressure coefficient at pressure tap, i at time t .

N - Number of pressure taps affecting on the connection being considered

For the conventional method #1, the reaction coefficient β was taken as 1.0, as shown in Figure 6.2 for connection B7. For conventional method #2, the reaction coefficients, were obtained by analysing the load along each batten using structural analysis, are also shown in Figure 6.3. For the proposed method, the reaction coefficient in linear elastic region on each batten-truss connection for loads applied at each panel measured from Test set up #1 and #2 in Chapter 5 were used to obtain the load distribution among the batten-truss connections. The reaction coefficients only for connection B7 are shown in Figure 6.4 and the reaction coefficients for other connections were also obtained (i.e. considered a large tributary area for each connection).

The conventional methods #1 and #2, and the proposed method with the load distribution effect were analysed and compared for spatially varying wind pressure for several wind approach directions. The peak load (i.e. \check{X}_b) of each connection was obtained combining reaction coefficients with the simultaneous measurement of wind pressure on each pressure tap (i.e. using Equation 6.1) for each wind approach direction.

The batten-to-truss connection load acting normal to the connection is represented in coefficient form as shown in Equation 6.2. Where, A_N is the nominal area related to batten-to-truss connections in contemporary houses and it was taken as 0.81m^2 for all the connections (This was done to present the results in non-dimensional coefficient form).

$$C_{X_b}(t) = \frac{x(t)}{\frac{1}{2}\rho\bar{U}_h^2.A_N} = \frac{\sum_{i=1}^N \beta_i A_i C_{p_i}(t)}{A_N} \quad (6.2)$$

Table 6.1 shows the load distribution on connections calculated using the proposed method in terms of peak values of C_{X_b} , \check{C}_{X_b} for 150° wind approach direction (i.e. wind direction that generated the largest load effect). The external pressure coefficients were used in the analysis and the negative values of \check{C}_{X_b} represent an uplift load (in coefficient form) on the connections. The connection at B7 was the most critical connection for wind approach direction 150° (shown in bold). The load distributions for other directions including the critical connection for each wind approach direction are shown in Appendix C (Table C.1 to C.22). Figure 6.5 shows the variation of load on the connection B7 in terms of mean and peak values with the wind approach direction. As shown in the Figure 6.5, the maximum load occurs for 150° wind approach direction. The detailed results (See Appendix C) indicated that the largest load occurred on connection B7 for 135° and 150° wind approach directions.

Table 6.1: \check{C}_{X_b} for $\theta = 150^\circ$ - Undamaged roof using load distribution effects

Connection Number	\check{C}_{X_b}		
	Truss A	Truss B	Truss C
5	-2.45	-3.84	-2.69
6	-3.18	-3.99	-3.18
7	-3.86	-5.12	-4.59
8	-2.54	-4.44	-3.72

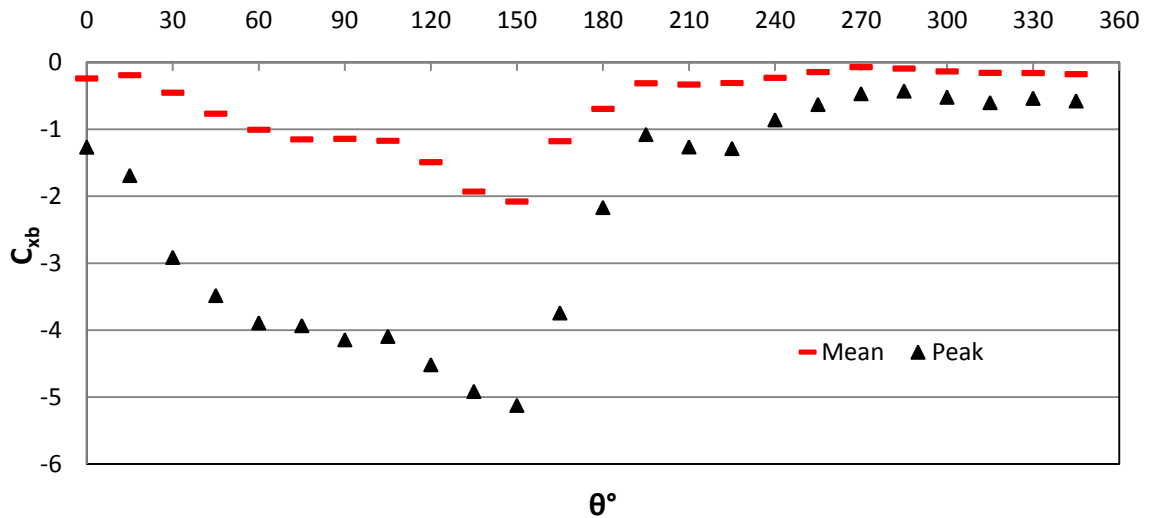


Figure 6.5: Variation of C_{x_b} at B7 with the wind approach direction

Tables 6.2 and 6.3 shows the loads on connection for 150° wind approach direction obtained using the conventional methods #1 and #2. The critical connection was identified as B8 for both methods and the load on connections obtained using both methods were close to each other. These values were also determined by using instantaneous pressure of each time step of wind pressure recordings (i.e. not from the maximum recorded pressure at each pressure tap).

Table 6.2: \check{C}_{x_b} for $\theta=150^\circ$ - Undamaged roof using conventional method #1

Connection Number	\check{C}_{x_b}		
	Truss A	Truss B	Truss C
5	-2.09	-3.54	-2.35
6	-2.92	-3.58	-2.74
7	-4.13	-3.65	-3.92
8	-2.78	-4.38	-3.46

Table 6.3: \check{C}_{x_b} for $\theta=150^\circ$ - Undamaged roof using conventional method #2

Connection Number	\check{C}_{x_b}		
	Truss A	Truss B	Truss C
5	-2.02	-3.28	-2.29
6	-2.56	-3.38	-2.67
7	-3.52	-3.75	-3.76
8	-2.51	-4.01	-3.34

However, comparison of these loads on connections with the values obtained from the proposed method with load distribution effect shows a significant difference for some connections, as

shown in Figure 6.6 (The \check{C}_{X_b} values on the Tables 6.1, 6.2 and 6.3 related to each connection are incorporated in Figure 6.6). For example, the \check{C}_{X_b} for B7 using methods #1 and #2 were 3.65 (Red) and 3.75 (pink) respectively and that obtained using the load distribution effects was 5.12 (Black), as shown in the Figure 6.6. Therefore, the use of conventional method #1 and #2 can significantly underestimate the loads on some connections for the same wind direction.

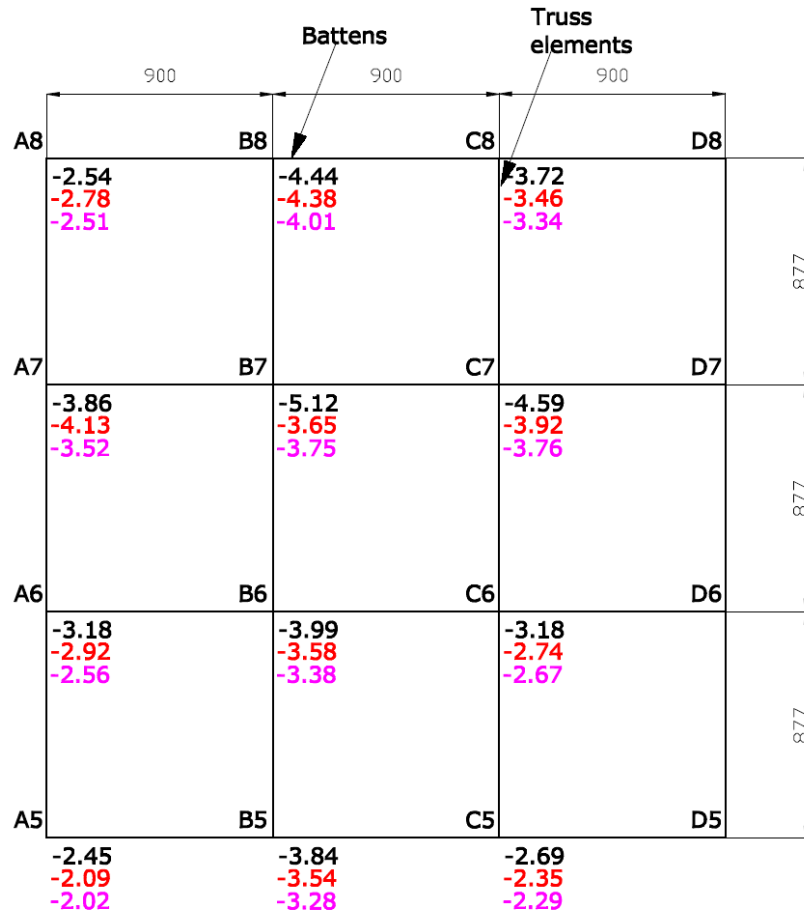


Figure 6.6: \check{C}_{X_b} for undamaged system for $\theta = 150^\circ$

- Black -Proposed method
- Red -Conventional method #1
- Pink -Conventional method #2

The reason for this significant difference is due to the occurrence of large correlated negative pressure outside the conventional tributary area and the flexibility of the batten contributing to the distribution of loads via the reaction coefficients. Figures 6.7, 6.8 and 6.9 show the

instantaneous pressure distribution (in pressure coefficients) obtained from wind tunnel study around the connection B7 for each method, when it experienced the peak load at 150° wind approach direction. It should be noted that the peak load for each method occurred at different instances in the time signals. The conventional tributary areas are shown in dotted lines in Figures 6.8 and 6.9. It should be noted that the colour scale is different for each Figure. As discussed in Chapter 2, the large suctions occur in roof corner due to the formation of edge vortices. Figure 6.7 shows the formations of classic vortices in the corner of the roof.

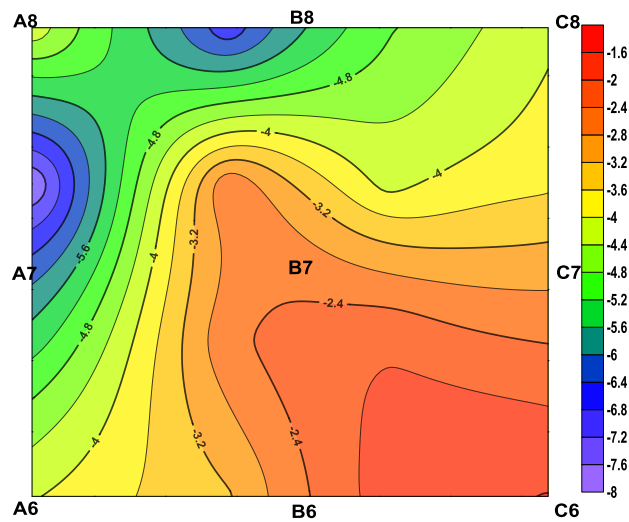


Figure 6.7: Pressure distribution around B7-Proposed method

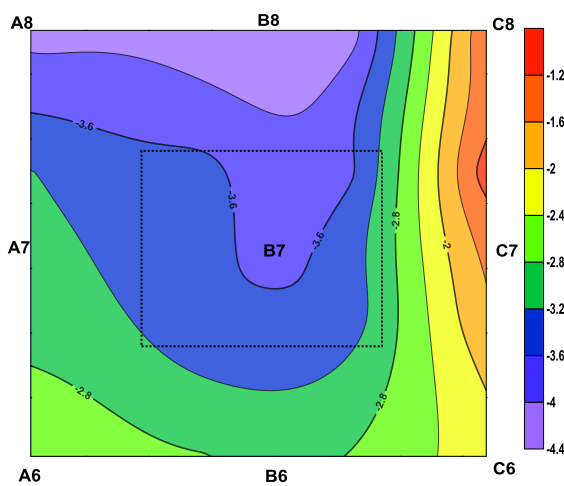


Figure 6.8: Pressure distribution around B7-Conventional Method #1

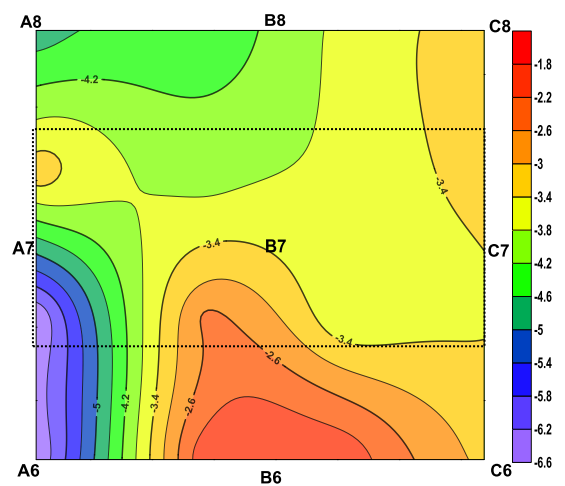


Figure 6.9: Pressure distribution around B7-Conventional Method #2

Similarly, Figure 6.10 shows the load distributions for 90° wind approach direction from the three methods. The most critical connection for this wind approach direction is B7 for each method. The comparison shows that some values obtained from conventional methods #1 and #2 significantly underestimate the load on some connections. These differences could be mainly due to the flexibility of battens of contemporary houses. However, a stiffer roof system may not have such a large discrepancy. Henderson (2010) showed that the load on a cladding fixing is given by the pressure acting on the conventional tributary area (i.e. conventional method #1). However, this study shows that approach is not applicable for calculating the load on batten-to-truss connections on contemporary houses. Thus, the tributary area defined in Figure 6.4 should be considered in order to obtain the load on batten-to-truss connections.

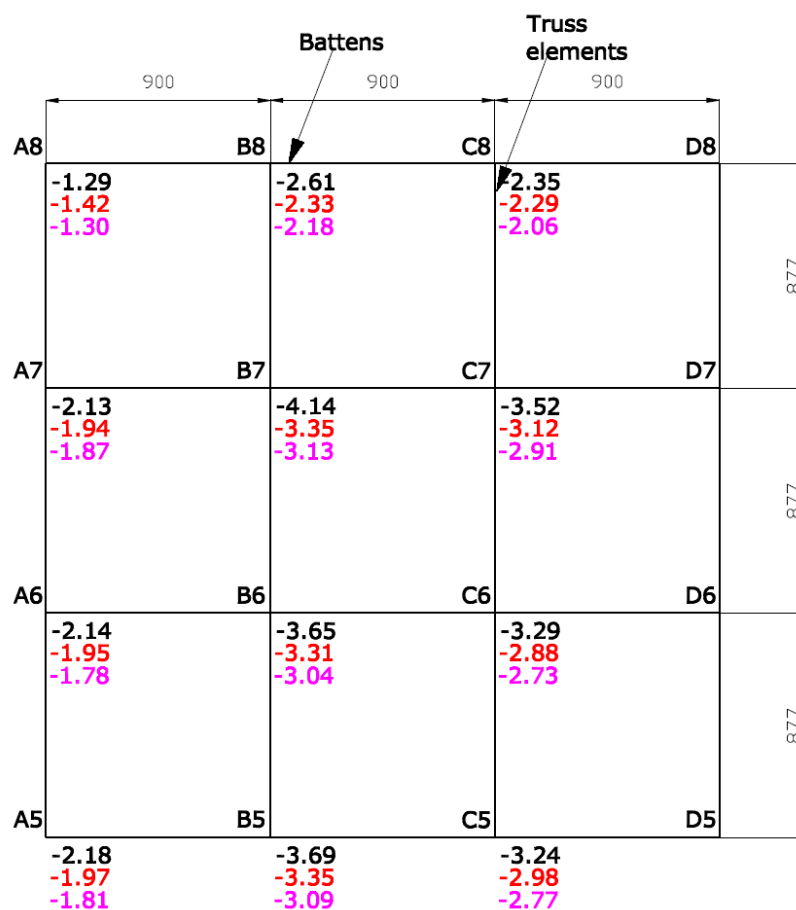


Figure 6.10: \check{C}_{X_b} for undamaged system for $\theta = 90^\circ$

Black -Proposed method, Red -Conventional method #1, Pink -Conventional method #2

6.2 The effect of cladding fastener failure

As shown in Chapter 5, the failure of cladding fastener redistributes the loads along the corrugations of cladding to the adjacent panels. It was also found that the greatest effect on load transfer occurs when the load is applied on the crest of the failed connection during the structural testing in Chapter 5. These reaction coefficients from point load tests were combined with the pressure in each tap to obtain the redistribution of loads to batten-to-truss connections, assuming a cladding fastener failure between B7 and C7, as shown in Figure 6.11. Thus, the failed fastener was in the same line with the pressure taps leading to the greatest effect on batten-to-truss connections.

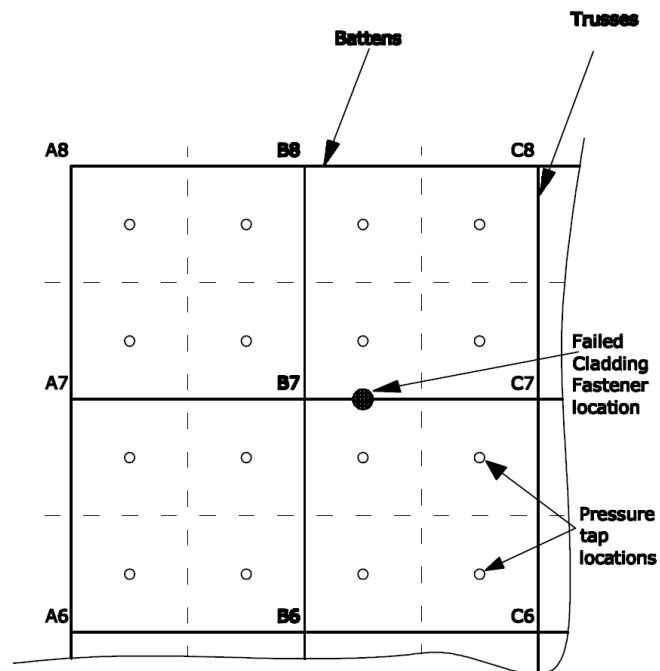


Figure 6.11: Failure of a cladding fastener

Table 6.4 shows the redistribution of loads when the cladding fastener failed for 150° wind approach direction combining instantaneous wind pressure with the results of load redistributions from Chapter 5. The batten-to-truss connection, B8, was the most critical connection when this cladding fastener failed. The results indicate that the loads on B7 and C7 were reduced to some extent (load on connection B7 dropped from 5.12 to 4.49) increasing the

loads on B6 and B8 transferring the load through the crests of the claddings. The loads on C6 and C8 were also slightly increased. Thus, the failure of a cladding fastener (during a wind event or from a previous wind event or poor workmanship) redistributes some of the loads to the batten-to-truss connections of the adjacent battens, increasing their probability of failure. However, it reduces the failure probability of the batten-to-truss connections of the batten from which the cladding fastener failed due to the lower load carried.

Table 6.4: \check{C}_{x_b} for $\theta = 150^\circ$ - Cladding fastener failure (between B7 and C7)

Connection Number	\check{C}_{x_b}		
	Truss A	Truss B	Truss C
5	-2.45	-3.84	-2.69
6	-3.18	-4.44	-3.30
7	-3.86	-4.49	-4.35
8	-2.54	-4.70	-3.85

6.3 The effect of batten-to-truss connection failure

Similarly, the load redistribution was obtained for a batten-to-truss connection failure. Since the connection B7 experienced the largest load, it was assumed to fail in this analysis. Table 6.5 shows the distribution of loads, when the connection B7 failed indicating the connection C7 was the next critical connection and then connections B6 and A7, respectively. The results are also shown in graphical manner in Figures 6.12 and 6.13 for undamaged and damaged system respectively. These results indicate that the failure of batten-to-truss connection has a significant effect on the adjacent connections as the load experienced by the connection it transferred to the adjacent connections.

Table 6. 5: \check{C}_{X_b} for $\theta = 150^\circ$ - Batten-to-truss connection B7 failed

Connection Number	\check{C}_{X_b}		
	Truss A	Truss B	Truss C
5	-1.98	-3.11	-2.18
6	-2.57	-4.27	-2.58
7	-4.13		-5.38
8	-2.06	-3.69	-3.01

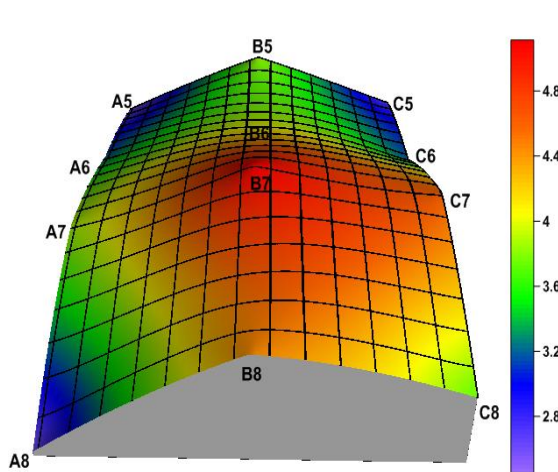


Figure 6.12: Load distribution-Undamaged system

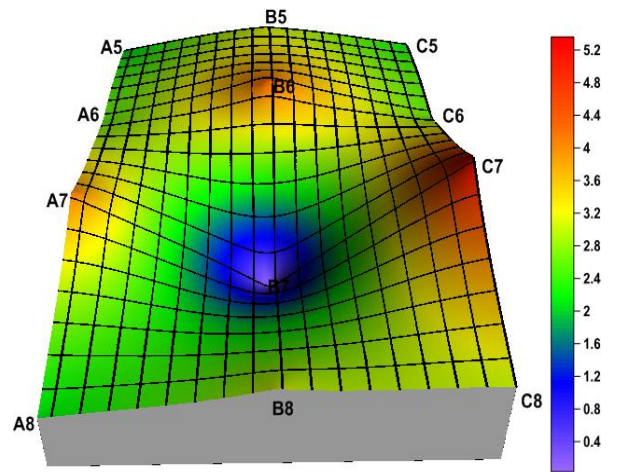


Figure 6.13: Load distribution-B7 failed

6.4 Reliability Analysis

The load distribution discussed in the previous section was obtained by applying deterministic values for patch loads and building response results. The development of vulnerability models require these parameters to be analysed in a probabilistic manner.

The failure of each connection in this study is defined as the point at which wind load combined with dead loads exceeds the capacity of the connection. The probability of failure of roofing components is determined with increasing wind speed. The wind load acting on a batten-to-truss connection can be obtained from Equation 6.3. For wind uplift, the limit state of each connection is expressed as shown in Equation 6.4.

$$W = 1/2 \rho V^2 \times C_{xb} \times A_N \quad (6.3)$$

$$R - (W - D) = 0 \quad (6.4)$$

Where, R - Strength capacity of the connection, D -Dead load and V - is the gust wind speed at 10m height in Terrain Category 2.5.

Failure occurs when $R - (W - D) < 0$.

The vulnerability of each connection is assessed for selected batten-to-truss connections on the roof locations based on Equations 6.3 and 6.4. The strength capacity statistics and the wind load statistics determined in Chapter 3 and 4 were used in the analysis. The probability of failure of connections in each region was calculated for increasing steps of wind speeds by repeating the reliability analysis described in Chapter 3, at each wind speed increment step.

The vulnerability analysis is conducted in this section to assess the effect of load distribution, and compare values with engineering assessment made using simplistic tributary area. It should be noted that the passage of a cyclone would generate an extremely complex loading regime on parts of a roof as described by Jancauskas *et al.* (1994). In addition to progressively increasing winds that reach a maximum and then drop off depending on the orientation of the house to the track of the cyclone, it would also vary the wind direction. This would generate varying load cycles and fatigue response.

Figure 6.14 shows the probability of failure of batten-truss connections B6, B7, B8, A7 and C7 by incorporating the load distribution effects described in Chapter 5 for 150° wind approach direction. Figure 6.15 shows the curves obtained using the conventional method #1 for the same connections. These figures give the probability of failure of each connection type with the approach gust wind speed at 10m height in Terrain Category 2.5. The comparison of the vulnerability of connections in Figures 6.14 and 6.15 show an increase in vulnerability due to the proposed method with load distribution effects (The vulnerability of connection B7 increased from 0% to 2% at 75m/s). Similar to the connection load distribution, the connection B7 was the most vulnerable connection from the proposed methodology and that from the conventional method #1 was B8. However, this analysis did not consider the internal pressure acting on connections (i.e. internal pressure coefficient is assumed to be zero) and assumed that cladding fasteners have not failed.

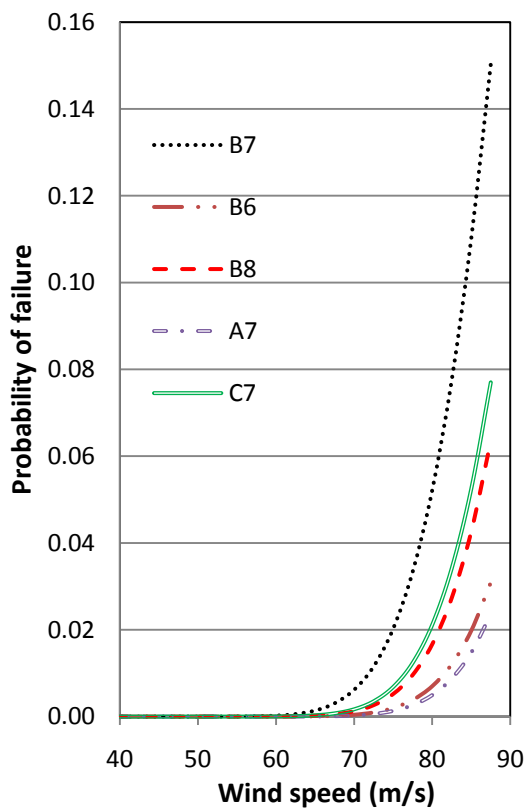


Figure 6.14: Vulnerability of batten connections for $\theta=150^\circ$ in TC 2.5

-with load distribution method

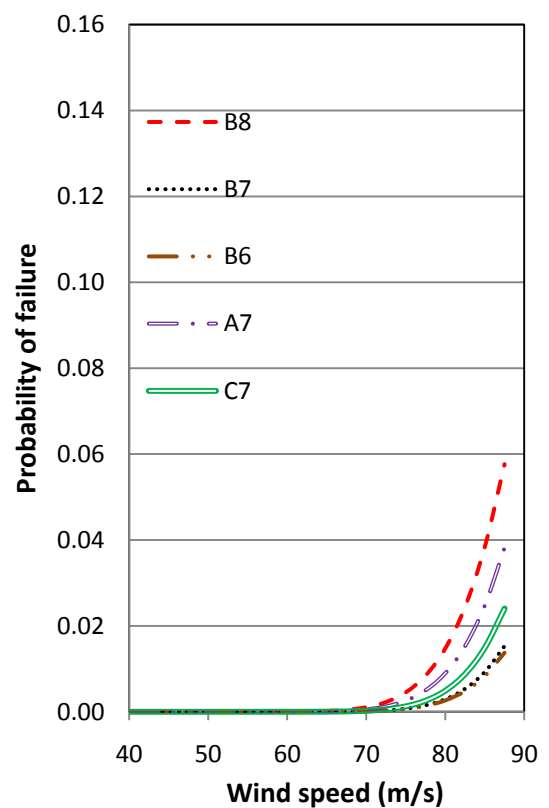


Figure 6.15: Vulnerability of batten truss connections for $\theta=150^\circ$ in TC 2.5

-Conventional method #1

Failure of a door or a window can create a dominant opening in contemporary houses leading to a significant increase in internal pressure. Failure of ceiling elements or the ceiling access manholes will transmit these high internal pressures to the roof cladding and as a result the wind loads on roofing components are increased. The house subjected to internal pressure coefficients 0.2, 0.4 and 0.7 were determined in this study. The maximum internal pressure coefficient specified in AS/NZS 1170.2 (2011) is 0.7. The internal pressure coefficient was the same for each wind speed step in this analysis. Figures 6.16 and 6.17 show the vulnerability of the batten-to-truss connections using the largest internal pressure coefficient (i.e. 0.7) for load distribution method and conventional method #1 respectively for 150° wind approach direction. These figures show that when internal pressures are included, connection B7 is still the most vulnerable using the load distribution method, but the connection C7 is the most vulnerable using conventional method #1. At a wind speed of 75m/s, the probability of failure of connection B7 has increased up to 25% as shown in the Figure 6.16 and that from the conventional method #1 has increased up to 6%. The figures for 0.2 and 0.4 internal pressure coefficients are also shown in Appendix C. Thus, the conventional method #1 significantly underestimates the vulnerability of some connections. Hence, the load distribution effects must be incorporated when determining the vulnerability of these connections. However, these curves are based on the wind direction giving the largest loads and assuming that cladding fasteners have not failed.

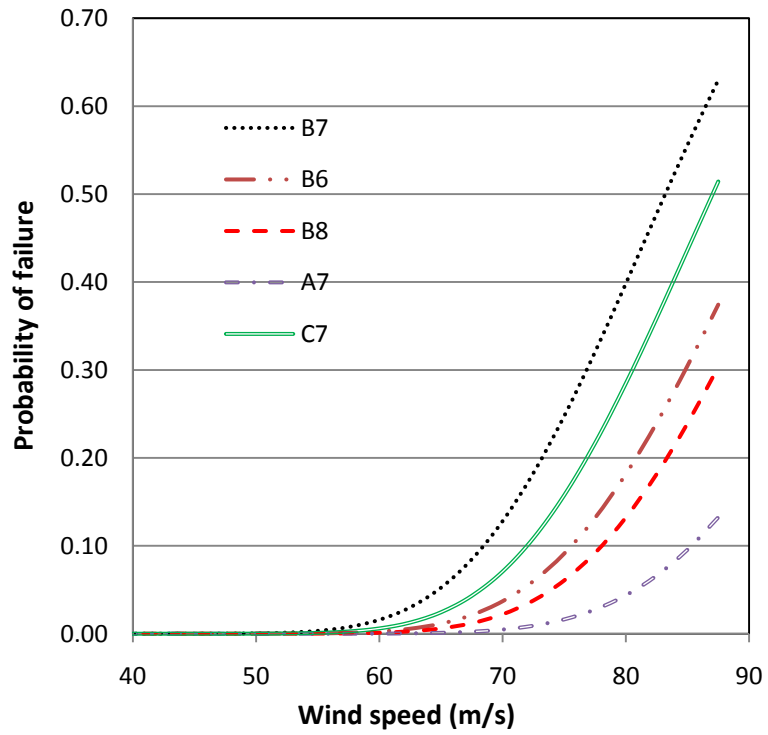


Figure 6.16: Vulnerability of batten connections for $\theta=150^\circ$ in TC 2.5
 -with load distribution method- internal pressure coefficient- +0.7

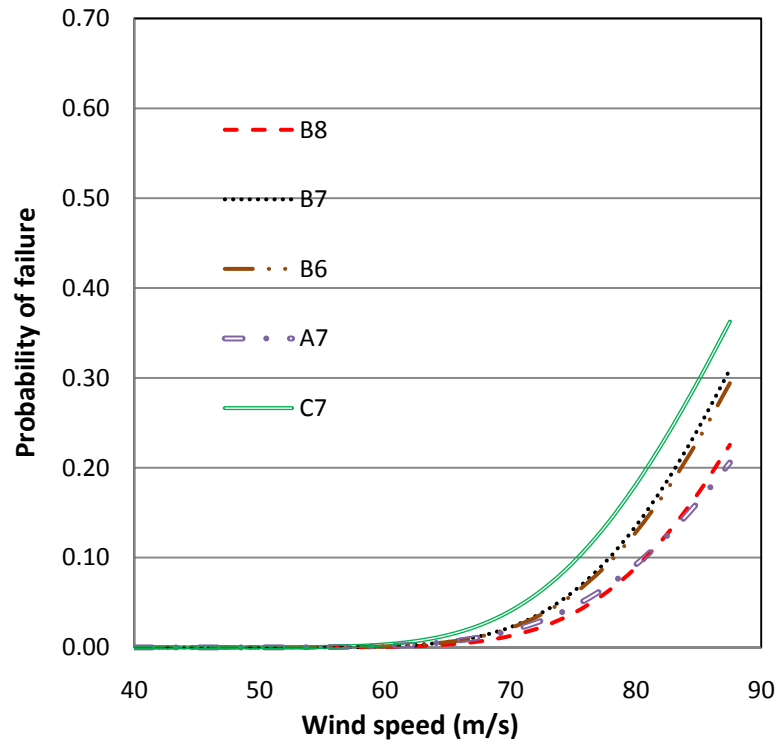


Figure 6.17: Vulnerability of batten truss connections for $\theta=150^\circ$ in TC 2.5
 - Conventional method #1- internal pressure coefficient- +0.7

- ***With failed batten-truss connection B7***

Figure 6.18 shows the probability of failure for connections B6, B8, A7 and C7 in the roof with a failed connection B7, for 150° wind approach direction based on the load distribution method. The results reflect the data in Table 6.5 which shows the connection C7 becomes more vulnerable. For example, the probability of failure of C7 increases from 1% (from Figure 6.14) to 11% at 75m/s. This analysis assumed that the internal pressure coefficient was zero.

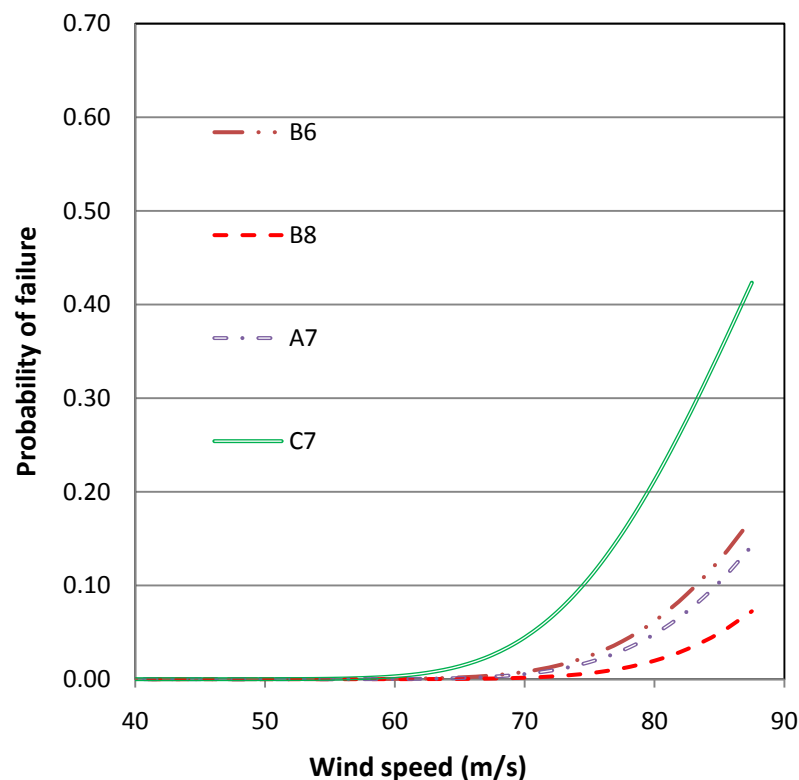


Figure 6.18: Probability of batten-truss connection failure vs wind speed following the failure of B7 in TC 2.5- internal pressure coefficient- 0

- ***The effect of other parameters***

The application of this test data for a population of houses that are located in the community requires consideration of the parameters defined in Equation 3.14 and the directional variability of wind pressure during a cyclone (Jancauskas *et al.* (1994)). Such an analysis will also need to account for variation in house geometry, terrain, topography and shielding in addition to the variation in batten and truss layouts and fixings.

Each of normalized terms in the brackets in Equation 3.14 was treated as random variables with probability distributions (Lognormal distribution was used), mean values, and coefficient of variation obtained from analysing available data. This study incorporated the values used by previous studies such as those by Henderson and Ginger (2007) for the parameters shown in Table 6.6. The C/C_N values for the connections were obtained from the wind tunnel model study for this analysis.

Table 6.6: Statistical parameters for normalized values

Factor	Mean Value	COV
λ/λ_N	1	0
A/A_N	1	0.10
E/E_N	0.95	0.10
θ/θ_N	0.95	0.10
G/G_N	0.95	0.10
ρ/ρ_N	1	0.02

Furthermore, the percentage of houses subjected to higher internal pressure as a result of dominant opening in the envelope was taken to increase from 0% to a maximum of 90% for approach gust wind speed of 40m/s to 80m/s. These values were based on limited survey results and expert opinion. The internal pressure coefficient of 0.7 was applied. Figure 6.19 shows the vulnerability of batten-to-truss connections incorporating above factors for 150°wind approach direction. The analysis used the load distribution effects including the factors in the Table 6.6. The vulnerability of the connections generally reduced compared to the curves obtained in Figure 6.16 due to the effect of other factors (the vulnerability of the connection B7 drops from 25% to 11% at 75 m/s). Thus, these factors have a significant impact on the connection

vulnerability and should be used for assessing the overall vulnerability of the houses. It should be noted that this analysis assumed that cladding fasteners have not failed.

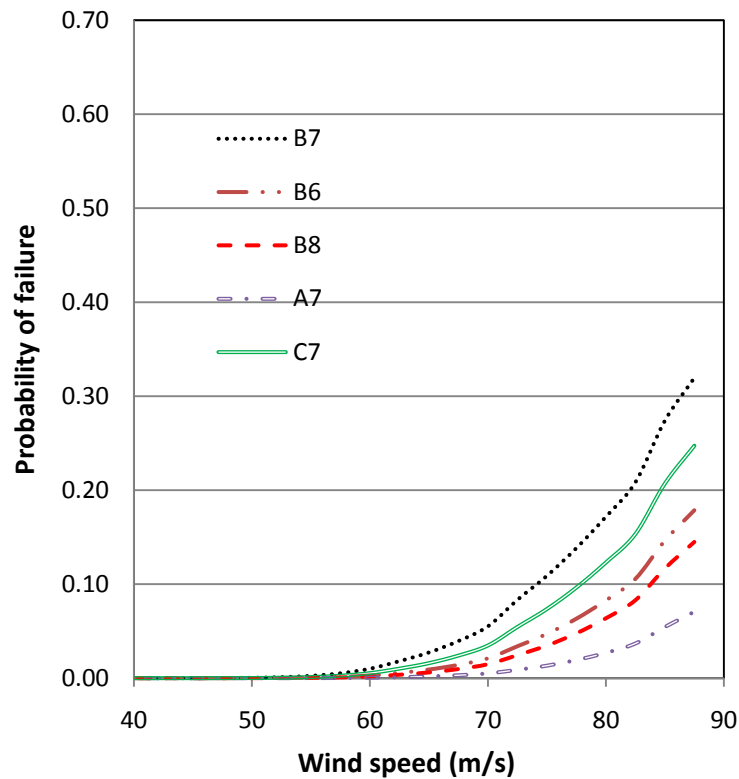


Figure 6.19: The effect of factors in Eqn 3.14 on batten-to-truss connection vulnerability for $\theta=150^\circ$ in TC 2.5- internal pressure coefficient- +0.7

- ***Vulnerability of cladding and truss to wall connections***

Similarly, the vulnerability of cladding fastener connections and truss-to-wall connections in selected regions of the roof for different wind approach direction was estimated. The cladding fixings in regions P, Q, R, S and T as shown in Figure 6.20 (i.e. Figure 4.4) were analysed. In this case, the wind loads acting on the tributary area for cladding fasteners was to be supported by the relevant connection (i.e. Reaction coefficient was taken as one), as shown by Henderson (2010). The truss-to-wall connections on truss B, F and L shown in Figure 6.20 were also analysed using the wind load data described in Chapter 4. These analyses were conducted assuming that the related other connections have not failed. For example, the vulnerability for cladding failures was determined assuming that no failures in batten-to-truss connections and

truss-to-wall connections. Figures 6.21 and 6.22 show the vulnerability of cladding fastener connections and truss-to-wall connections respectively, over selected regions of the roofs for the wind approach direction generating the largest load effect (i.e. worst direction indicated for each region in each Figure). These figures also give the probability of failure of each connection type with the approach gust wind speed at 10m height in Terrain Category 2.5 and the analysis used incorporated the effect of other factors. Figure 6.21 shows that the cladding fixings are more vulnerable in regions P and Q.

Figure 6.22 shows that truss B near the gable end was the most vulnerable and the trusses at middle regions of the roof were less vulnerable. This analysis incorporated the internal pressure coefficient of 0.7. The vulnerability without the internal pressure and without the effect of other parameters is also shown in Appendix C for these connections. The Figures 6.19, 6.21 and 6.22 indicate that the cladding fixing is the most vulnerable followed by batten-to-truss connection and then the truss-to-wall connection.

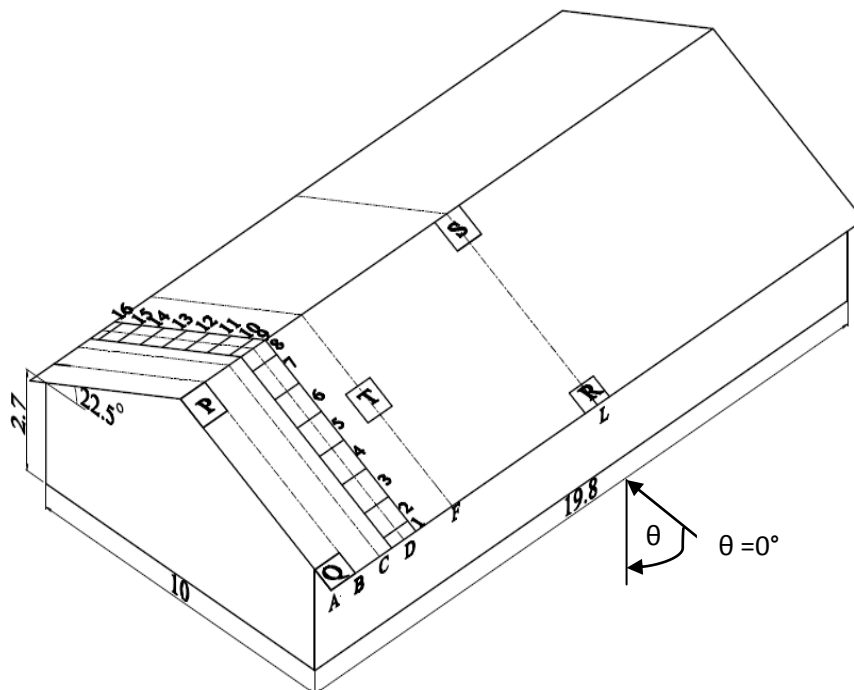


Figure 6.20: Typical contemporary house (i.e. Figure 4.4)

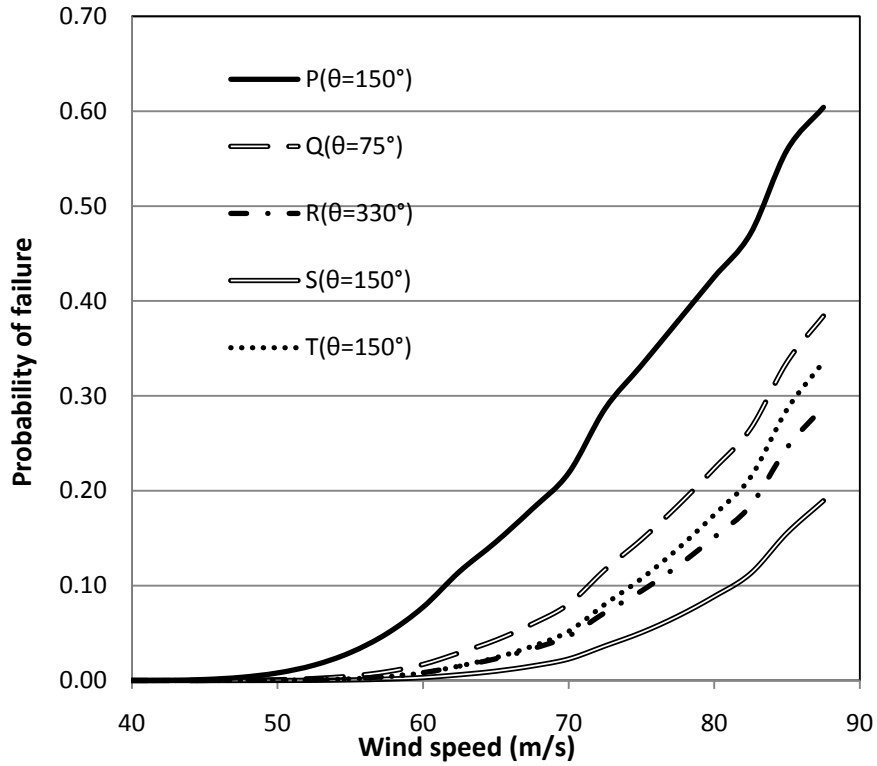


Figure 6.21: Probability of failure vs Basic Wind speed- Cladding connections for house in TC 2.5- internal pressure coefficient- +0.7

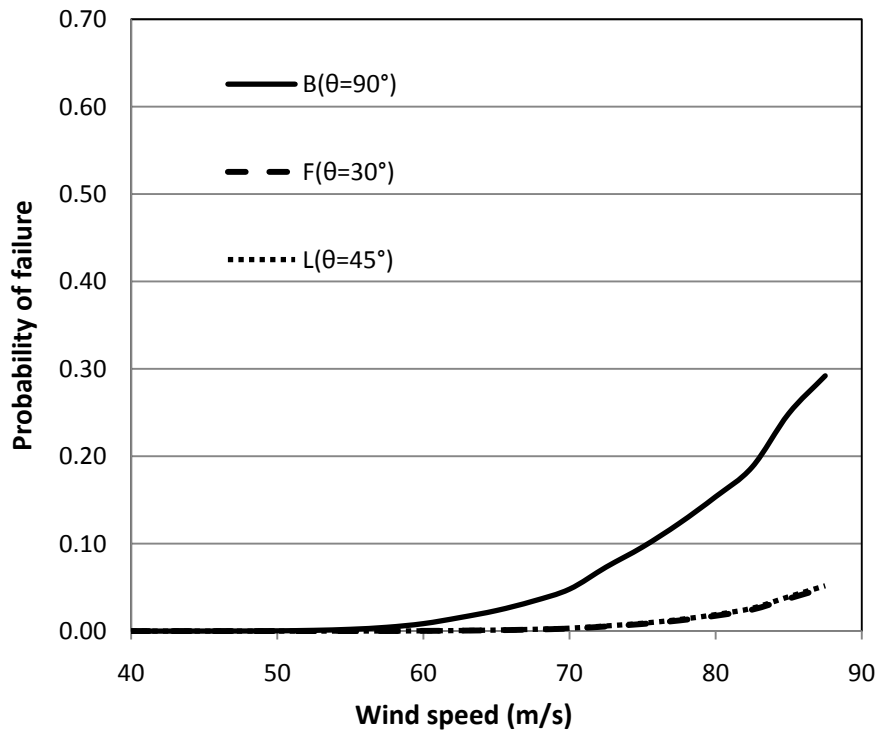


Figure 6.22: Probability of failure vs Basic Wind speed-Truss-to-wall connections for house in TC 2.5- internal pressure coefficient- +0.7

6.5 Summary and Discussion

The study compared the load distributions on batten-to-truss connections and found that the use of conventional methods underestimate the wind loads on batten-to-truss connections. As discussed in Chapter 2, most studies use the conventional tributary area for design and vulnerability/fragility analysis of structural components of houses. These studies do not satisfactorily incorporate the load distribution effects, and hence may under estimate the vulnerability of these connections to windstorms. This chapter shows that the application of current simplistic tributary area approach in association with instantaneous wind pressure is unreliable. However, the structural systems used in other studies were different to the structural system used in this study. Therefore, the approach used in this study should be employed with other structural systems to determine the effects of the load distribution when assessing their vulnerability.

The procedure that is proposed in this study is that, the reaction coefficients related to the response of each connection type in a structural system should be determined for the undamaged system and then for several damage scenarios. This would enable the tributary area related to each connection type in a structural system to be identified. Then, the connection load should be assessed combining the reaction coefficients and the associated tributary area with the wind pressure considering the variation of wind pressures both spatially and timewise. This proposed procedure is applicable for any structural system to determine reliable loads on connection.

Following this procedure, the vulnerability assessment can be undertaken using reliability and probability theories incorporating Monte Carlo Simulation methods. This study did not incorporate Monte Carlo simulation techniques to account for the consequent failures of other connections (only reliability theory and probability theories considered for a single connection type failure). This study determined the vulnerability of each connection type assuming the other connections do not fail. In reality failure of one connection negates the failure of

dependent connections. However, the procedure described is applicable to a wide range of systems and geometries for assessing the building vulnerability.

This study also analysed the vulnerability of connections for deterministic values of internal pressure (internal pressure coefficients of 0.2, 0.4 and 0.7). It also used assumptions for the internal pressure with increasing wind speed based on limited survey results and expert opinion. However, the more accurate internal pressure values should be incorporated with increasing wind speed as it has a significant effect on the failure of the connections.

The vulnerability obtained for cladding fixings here appear to be over-estimating the damage, since recent windstorms such as Cyclone Yasi (Boughton *et al.* (2011) did not indicate such significant failures for wind events less than the design wind speed. Henderson (2010) showed that cladding systems designed in cyclone region to cyclic test regime (L-H-L) are able to withstand significantly large loads in simulated design cyclone suctions. These systems have a significantly larger strength than that specified by design, because of the cyclone L-H-L strength requirements for cladding fixings. Therefore, the analysis may over-estimate the vulnerability of the cladding fixings. Furthermore, this analysis was carried out for the worst direction with large internal pressures. It might have not occurred in actual conditions due to the directional variability of wind pressure during a cyclone, as described by Jancauskas *et al.* (1994). The region of gable end towards the ridge (i.e. Region P) might have had additional strength due to the ridge capping of the houses and hence the failure might have not occurred during these windstorms.

The use of normalized parameters in the analysis method reduces the variability that occurs due to the house dimensions, shielding, topography and terrain category etc. The uncertainties can also be accounted with the use of probabilistic parameters in the analysis. However, these parameters should be validated with further research. In order to obtain reliable vulnerability curves, it is necessary to consider the probabilistic nature of the load action and response of the housing components.

7 CONCLUSIONS AND RECOMMENDATIONS

7.1 *Conclusions*

This study determined the transmission of wind loads through roofing components, including the effect of local failures, and the impact on the overall structural performance of the roof system. Specifically the distribution of applied loads and associated structural response of a batten-to-truss connection from contemporary houses built in cyclonic region of Australia was investigated and its application to design and vulnerability was determined. This was achieved by obtaining; a common structural system, the spatial and temporal variation of wind loads acting on the roofing connections from a wind tunnel study, and the effect of load sharing and interdependency between components and progressive failure by conducting a series of tests on selected sub-assemblies of the roof system.

The main conclusion drawn from this study is that loads on the batten-to-truss connections are strongly influenced by the behaviour of the entire structural system and the wind pressure distribution on roof. The study showed that load transferred to batten-to-truss connections are influenced by the flexibility of the battens and cladding used in the roof, and the directional stiffness characteristics of the cladding. The redistribution of batten-to-truss connection loads following failure of connections also depends on these properties. Furthermore, these connection loads are dependent on the instantaneous distributions of the wind pressure (i.e. spatial correlation of pressures) on the cladding panels supported by these fixings. As a result, estimates based on the application of wind pressures to the conventional connection tributary area, which is normal design practice, can be unreliable and can lead to underestimation of connection loads. The study showed that a larger tributary area should be considered to obtain the batten-to-truss connection loads on these structural systems. Furthermore, the study also showed that consideration of the wind pressure distribution and the load transfer is important for the assessment of the vulnerability of the type of roof system investigated.

A primary outcome of the thesis is the establishment of an improved procedure for analysing the variation of the connection loads with time, taking account of the spatial and temporal variation in wind pressures and the structural response characteristics of the roof system, which is a necessary first step in the assessment of their vulnerability.

The study established a useful tool for establishing the fatigue loads on the connections which would be the next step required in the development of the relationship between vulnerability and wind speed. The procedure proposed in this study can be used for evaluating the tributary area and the associated reaction coefficients for other roof geometries and structural systems, in order to carry out the connection design and to assess their vulnerability. The outcomes from this study can be used for roof systems similar to that used in this study.

Other conclusions are as follows:

- The uplift load on a connection is dependent on the characteristics of the fluctuating wind load on the area of influence. The study shows that the batten-to-truss connection load is affected by loads acting outside the conventional tributary area. It also shows that the majority of the load on a panel is distributed among the batten-to-truss connections supporting the loaded panel. The failure or partial failure of a batten-to-truss connection redistributes the majority of load to the adjoining batten-to-truss connections either via battens or crests of the cladding. Further, the reaction coefficients of the batten-to-truss connections in the linear and non-linear response of cladding are not the same, but the difference is not significant. These results indicate the extent of load distribution and redistribution that should be incorporated in structural analysis and vulnerability assessments of these types of structural systems. The subassembly tests also show that;

- The strength capacity of the cladding panels in corner regions (i.e. Panels near eave and ridge) is less than the panels in the inner regions, causing failure of fasteners or batten-to-truss connections at a lower load in the corner panels due to their reduced capability to share the load.
 - The deflection on the cladding increases linearly with increasing load and then becomes non-linear increasing the deflection at a progressively faster rate with the onset of plastic deformation of cladding. When the cladding fastener failure occurs, the deflection of the cladding increases significantly. Thus, failure of a batten-to-truss connection generally increases the deflections and hence reduces the stiffness of the roof.
 - The variation in reaction coefficient was not significant with the spacing of the battens in most of the connections except for some locations which had a maximum of 20% variation (i.e. reaction coefficient of the interior connection of corner panel). Thus, the results obtained can be used to describe the load distribution of batten-to-truss connections for a range of masonry block houses with typical batten and truss spacings.
 - The partial failure of a batten-to-truss connection (i.e. removal of one screw) indicated that the reaction coefficient of the connection is reduced to some extent (i.e. up to a maximum of 31%) and transfers the loads to the adjoining connections. Thus, it is still able to carry the load but the connection has a lower strength capacity.
- The variability of uplift capacity of the cladding fastener connections, batten-to-truss connection and truss-to-wall connection of common contemporary houses in cyclonic regions of Australia, were well fitted by a Lognormal probability distribution which can be used to assess the reliability of the roof system.

- The wind tunnel study also showed that for the house geometry studied, which is typical of current housing construction in North Queensland;
 - The largest cladding and batten connections loads occurred for wind approach directions 120°-150° and that for truss-to-wall connection was 90° confirming results obtained from previous studies.
 - AS/NZS 1170.2 (2011) underestimates the external pressures on cladding fixings at roof corners towards the ridge at a gable end.
 - The Generalized Extreme Value distribution with a negative shape parameter (Type III distribution) gives the best fit for wind loads on cladding fixings for most of the wind approach directions.

- The vulnerability analysis showed that for the house geometry and roof construction studied;
 - The internal batten-to-truss connection of the corner panel towards the ridge experienced the largest load for 150° wind approach direction due to a combination of wind load action and structural response.
 - The cladding fasteners are the most vulnerable to wind loads followed by the batten-to-truss connections and then the truss-to-wall connections. In particular, the cladding fixings and the internal batten-to-truss connection in the roof corner towards the ridge is the most vulnerable. The first internal truss near the gable end was the most vulnerable while trusses in middle regions of the roof were less vulnerable to wind loads.

These outcomes make a significant contribution to the aim of understanding the wind load distribution and developing vulnerability functions for houses.

7.2 Recommendations

This study developed a general procedure and produced useful data for design and for developing an engineering-based vulnerability model by considering the probabilistic nature of load actions and building response of cladding fasteners and batten-to-truss connections. The study recommends that the simplistic approach of applying wind pressure to a conventional tributary area is unreliable for metal clad roof systems supported by metal battens. The structural flexibility and temporal and spatial variability of pressures need to be taken into account to determine the loads on connections.

Furthermore, the study also recommends using the type of procedure proposed in this study for evaluating the characteristics of the connection loads. Thus, the reaction coefficients related to the response of each connection type in a structural system should be determined for the undamaged system and for several damage scenarios. This would enable the tributary area related to each connection type of a structural system to be identified. Then, the connection load should be assessed combining the reaction coefficients and the associated tributary area with the wind pressure considering the variation of wind pressures both spatially and temporally.

However, any approach for developing reliable vulnerability and wind speed relationships for roof systems needs to take the influence of fatigue into account since the relationship between fatigue strength and wind speed is highly non-linear and very dependent on the actual nature and duration of the load fluctuations. As the wind speed and direction changes in a cyclone (i.e. Jancauskas *et al.* (1994)), a specific area on a roof will experience the wind pressure from different directions (For example, as the wind speed increases during a cyclone, the direction can change from say 200° at time =0hr, to 150° when the wind speed is the highest at time =2.5hr, and then to 100° at time = 5hr when the wind has dropped off again). Consequently, the wind load data described in this study cannot be used directly for vulnerability analysis for cyclone winds, although it would be relevant for thunderstorm winds. However, the procedure developed in this study could be used for developing the temporal

variation of loadings on a connection during the passage of a cyclone which is needed as input for any study of vulnerability incorporating fatigue. Therefore, further studies with this focus are recommended. Furthermore, this procedure can be applied to Database-Assisted Design (DAD) process described by Whalen *et al.* (2002).

These studies also can be extended to analyse the response of truss-to-wall connections to obtain reaction coefficients, deflections, etc, for various damage scenarios. Furthermore, components such as ceiling and cornices should be incorporated in any future test setups. The failure of individual elements and the redistribution of loads through the structure as a result of local failures including time dependant effect such as fatigue could be incorporated. This will lead to a better understanding of the overall structural behaviour under wind loads. The results, such as distribution of loads and load-deflection curves are important to carry out linear/ non-linear analysis of the roofing system. The boundary conditions used in these test set ups can be incorporated in structural engineering software and the analysis can be performed for the total structure being considered. These results should be validated through tests on a complete full scale house.

The analysis conducted in this study for assessing the vulnerability did not use Monte Carlo simulation methods. Therefore, it is recommended to use Monte Carlo simulation techniques for future studies. The data obtained and the methodologies used in this study provide information for the development of more accurate software models for assessing building vulnerability. An example of a preliminary version of such a product, VAWS is discussed in the Appendix D. This software incorporates structural behaviour using structural analysis and uses conventional tributary areas for obtaining the load on connections. Therefore, the output results will need to be calculated to account for the load distribution effect. However, the methodology used in the software and the techniques such as reliability and probability methods incorporating Monte Carlo simulation are very important for extending the studies for obtaining an overall vulnerability of contemporary house. The use of such techniques is necessary in engineering

vulnerability models to determine more reliable vulnerability assessments. The outcomes of this study make a significant contribution to the ultimate objective of developing vulnerability functions for contemporary houses.

Finally, this research can be expanded to incorporate the response of other residential construction to wind events considering the large variety of structural systems of buildings, shapes and sizes etc through better understanding of approach wind speed including analysis of uncertainties in structural system behaviour, loading, damage and cost for loss estimation and decision making. Such models require a considerable amount of investment in research and development.

8 REFERENCES

- Ang, A. H.-S. and Tang, W. H. (2007). *Probability Concepts in Engineering: Emphasis on Applications in Civil and Environmental Engineering*, John Wiley & Sons, Inc.
- ASCE 7-10 (2010). *Minimum Design Loads for Buildings and Other Structures*
- BCA (2011). *Building Code of Australia*, ABCB, Canberra.
- Ben Ayed, S., Aponte-Bermudez, L. D., Hajj, M. R., Tieleman, H. W., Gurley, K. R. and Reinhold, T. A. (2011). "Analysis of hurricane wind loads on low-rise structures." *Engineering Structures* In Press, Corrected Proof.
- Boughton, G. N., Henderson, D. J., Ginger, J. D., Holmes, J. D., Walker, G. R., Leitch, C., Somerville, L. R., Frye, U., Jayasinghe, N. C. and Kim, P. (2011). "Tropical Cyclone Yasi Structural Damage to Buildings." TR 57.
- Boughton, G. N. and Reardon, G. F. (1982). *Simulated Wind Tests On a House*, Cyclone Testing Station, James Cook University, Townsville. TR 14.
- Boughton, G. N. and Reardon, G. F. (1983). *Testing a High Set House Designed for 42m/s Winds*, Cyclone Testing Station, James Cook University, Townsville. TR 19.
- Boughton, G. N. and Reardon, G. F. (1984). *Simulated Wind Load Tests on the Tongan Hurricane House*, Cyclone Testing Station, James Cook University, Townsville. TR 23.
- Case, P. C. and Isyumov, N. (1998). "Wind loads on low buildings with 4 : 12 gable roofs in open country and suburban exposures." *Journal of Wind Engineering and Industrial Aerodynamics* 77-78: 107-118.
- Cochran, L. S. and Cermak, J. E. (1992). "Full- and model-scale cladding pressures on the Texas Tech University experimental building." *Journal of Wind Engineering and Industrial Aerodynamics* 43(1-3): 1589-1600.
- Cope, A. D., Gurley, K. R., Gioffre, M. and Reinhold, T. A. (2005). "Low-rise gable roof wind loads: Characterization and stochastic simulation." *Journal of Wind Engineering and Industrial Aerodynamics* 93(9): 719-738.
- Cummins, W. (2002). *Bond beam truss hold down connections*. BSc Thesis, James Cook University, Townsville.
- Datin, P. L. and Prevatt, D. O. (2007). *Wind uplift reactions at roof to wall connections of wood framed gable roof assembly*. 12th International Conference on Wind Engineering, Cairns, Australia.
- Datin, P. L., Prevatt, D. O. and Cook, R. A. (2011). *Wind load design using ASCE 7 Main Wind Force Resisting System in Light Frame Wood Construction*. 13th International Conference on Wind Engineering, Amsterdam, Netherlands.
- Eaton, K. J. and Mayne, J. R. (1975). "The measurement of wind pressures on two-storey houses at Aylesbury." *Journal of Wind Engineering and Industrial Aerodynamics* 1: 67-109.
- Ellingwood, B. R., MacGregor, J. G., Galambos, T. V. and Cornell, C. A. (1982). "Probability-Based Load Criteria: Load Factors and Load Combinations." *Journal of Structural Division ASCE* 108(5): 978-997.
- Ellingwood, B. R., Rosowsky, D. V., Li, Y. and Kim, J. H. (2004). "Fragility Assessment of Light-Frame Wood Construction Subjected to Wind and Earthquake Hazards." *Journal of Structural Engineering* 130(12): 1921-1930.
- Ellingwood, B. R. and Tekie, P. B. (1999). "Wind Load Statistics for Probability-Based Structural Design." *Journal of Structural Engineering* 125(4): 453-463.

- Fowler, R. (2003). Fatigue damage to metal battens subjected to simulated wind loads. BE Thesis, James Cook University, Townsville.
- Galambos, T. V., Ellingwood, B. R., MacGregor, J. G. and Cornell, C. A. (1982). "Probability-Based Load Criteria: Assessment of Current Design Practice." *Journal of Structural Division ASCE* 108(5): 959-977
- Geoscience Australia (2007). Natural Hazards in Australia - Identifying risk analysis requirements, by Geoscience Australia, DOTARS, Bureau of Meteorology and CSIRO.
- Ginger, J. D. and Holmes, J. D. (2005). "Design wind loads on gable-ended low-rise buildings with moderate and steep roof slopes." *Australian Journal of Structural Engineering* 6(2): 89-102.
- Ginger, J. D., Holmes, J. D. and Kim, P. Y. (2010). "Variation of Internal Pressure with Varying Sizes of Dominant Openings and Volumes." *Journal of Structural Engineering* 136(10): 1319-1326.
- Ginger, J. D., Holmes, J. D. and Kopp, G. A. (2008). "Effect of building volume and opening size on fluctuating internal pressure." *Wind & Structures* 11: 361-376.
- Ginger, J. D., Mehta, K. C. and Yeatts, B. B. (1997). "Internal pressures in a low-rise full-scale building." *Journal of Wind Engineering and Industrial Aerodynamics* 72: 163-174.
- Ginger, J. D., Reardon, G. F. and Whitbread, B. J. (2000). "Wind load effects and equivalent pressures on low-rise house roofs." *Engineering Structures* 22(6): 638-646.
- Hamid, S., Golam Kibria, B. M., Gulati, S., Powell, M., Annane, B., Cocke, S., Pinelli, J.-P., Gurley, K. and Chen, S.-C. (2010). "Predicting losses of residential structures in the state of Florida by the public hurricane loss evaluation model." *Statistical Methodology* 7(5): 552-573.
- Henderson, D. J. (2010). Response of pierced fixed metal roof cladding to fluctuating wind loads. PhD Thesis, James Cook University, Townsville.
- Henderson, D. J. and Ginger, J. D. (2007). "Vulnerability model of an Australian high-set house subjected to cyclonic loading." *Wind & Structures* 10(3): 269-285.
- Henderson, D. J. and Ginger, J. D. (2011). "Response of pierced fixed corrugated steel roofing systems subjected to wind loads." *Engineering Structures* 33(12): 3290-3298.
- Henderson, D. J., Ginger, J. D., Leitch, C., Boughton, G. and Falck, D. (2006). Tropical Cyclone Larry – Damage to buildings in the Innisfail area, Cyclone Testing Station, James Cook University, Townsville. TR51.
- Henderson, D. J. and Harper, B. (2003). Detailed Modeling of the Vulnerability of Domestic Housing to Tropical Cyclone winds Proc. 11th AMOS International conference on storms and disaster mitigation, Brisbane, Australia.
- Henderson, D. J., Leitch, C., Frye, U., Ginger, J. D., Kim, P. and Jayasinghe, N. C. (2010). Investigation of Housing and Sheds in Proserpine, Midge point, and Airlie Beach, Following Tropical Cyclone Ului, Cyclone Testing Station, James Cook University, Townsville. TR 56.
- Henderson, D. J., Morrison, M. J. and Kopp, G. A. (2011). Spatially and temporarily varying wind loads applied to a full-scale, timber-framed, hip roof. 13th International Conference on Wind Engineering, Amsterdam, Netherlands.
- Hill, K., Datin, P., Prevatt, D. O., Gurley, K. R. and Kopp, G. A. (2009). A Case for Standardized Dynamic Wind Uplift Pressure Test for Wood Roof Structural Systems. 11th Americas Conference on Wind Engineering, San Juan, Puerto Rico.

- Ho, T. C. E., Surry, D. and Davenport, A. G. (1990). "The variability of low building wind loads due to surrounding obstructions." *Journal of Wind Engineering and Industrial Aerodynamics* 36(Part 1): 161-170.
- Ho, T. C. E., Surry, D. and Davenport, A. G. (1991). "Variability of low building wind loads due to surroundings." *Journal of Wind Engineering and Industrial Aerodynamics* 38(2-3): 297-310.
- Ho, T. C. E., Surry, D. and Davenport, A. G. (1992). "Low building wind load variability with application to codes." *Journal of Wind Engineering and Industrial Aerodynamics* 43(1-3): 1787-1798.
- Ho, T. C. E., Surry, D., Morrish, D. and Kopp, G. A. (2005). "The UWO contribution to the NIST aerodynamic database for wind loads on low buildings: Part 1. Archiving format and basic aerodynamic data." *Journal of Wind Engineering and Industrial Aerodynamics* 93(1): 1-30.
- Holmes, J. D. (1979). Mean and fluctuating internal pressures induced by wind. Proc. 5th Int. Conf. on Wind Engineering, Colorado, USA.
- Holmes, J. D. (1981). Wind Pressures on Houses with High Pitched Roofs. Wind Engineering reports 4/81, James Cook University, Townsville.
- Holmes, J. D. (1983). Comparative Studies of Wind Pressures on a Low-rise Building. Eighth Australian Fluid Mechanics Conference University of New Castle, N.S.W.
- Holmes, J. D. (1985). "Wind loads and limit states design." *Civ.Eng.Trans, IE Aust CE27*: 21-25.
- Holmes, J. D. (2007). *Wind Loading of Structures*, Spon Press, London, UK.
- Holmes, J. D. and Best, R. J. (1977). Wind Tunnel Measurement of Mean Pressures on House Model and Comparison with Full Scale Data 6th Australasian Hydraulics and Fluid Mechanics Conference, Adelaide, Australia.
- Holmes, J. D. and Best, R. J. (1979). A wind Tunnel Study of Wind Pressures on grouped tropical houses. Wind Engineering Report 5/79, James Cook University, Townsville.
- Holmes, J. D. and Best, R. J. (1981). "An approach to the determination of wind load effects on low-rise buildings." *Journal of Wind Engineering and Industrial Aerodynamics* 7(3): 273-287.
- Holmes, J. D. and Cochran, L. S. (2003). "Probability distributions of extreme pressure coefficients." *Journal of Wind Engineering and Industrial Aerodynamics* 91(7): 893-901.
- Holmes, J. D., Wehner, M., Sandland, C. and Edwards, M. (2010). Modelling damage to residential buildings from wind-borne debris-Part 1.Methodology. 14th Australasian Wind Engineering Workshop, Geosciences Australia, Canberra.
- Jancauskas, E. D., Mahendran, M. and Walker, G. R. (1994). "Computer simulation of the fatigue behaviour of roof cladding during the passage of a tropical cyclone." *Journal of Wind Engineering and Industrial Aerodynamics* 51(2): 215-227.
- Jayasinghe, N. C. and Ginger, J. D. (2011). "Vulnerability of Roofing Components to Wind Loads." *Wind & Structures* 14(4): 321-335.
- Kasperski, M. and Hoxey, R. (2008). "Extreme-value analysis for observed peak pressures on the Silsoe cube." *Journal of Wind Engineering and Industrial Aerodynamics* 96(6-7): 994-1002.
- Kasperski, M. and Niemann, H. J. (1992). "The L.R.C. (load-response-correlation) - Method A General Method of Estimating Unfavourable Wind Load Distributions for Linear and

- Non-linear Structural Behaviour." *Journal of Wind Engineering and Industrial Aerodynamics* 41-44: 1753-1763.
- Kopp, G. A., Morrison, M. J. and Henderson, D. J. (2011). Full-scale testing of low-rise building using realistically simulated wind loads. 13th International Conference on Wind Engineering, Amsterdam, Netherlands.
- Lee, K. H. and Rosowsky, D. V. (2005). "Fragility assessment for roof sheathing failure in high wind regions." *Engineering Structures* 27(6): 857-868.
- Leicester, R. H., Pham, L. and Kleeman, P. W. (1985). "Use of reliability concepts in the conversion of codes to limit state design." *Civ.Eng.Trans CE27*: 1-7.
- Leicester, R. H. and Reardon, G. F. (1976). *A Statistical Analysis of the Structural Damage by Cyclone Tracy*, The institution of Engineers Australia.
- Leitch, C., Ginger, J. D., Harper, B., Kim, P., Jayasinghe, N. C. and Somerville, L. R. (2010). "Performance of Housing in Brisbane Following Storms on 16 November 2008." *Australian Journal of Structural Engineering* Vol 11(No 1).
- Letchford, C. W., Iverson, R. E. and McDonald, J. R. (1993). "The application of the Quasi-steady Theory to full scale measurements on the Texas Tech building." *Journal of Wind Engineering and Industrial Aerodynamics* 48(1): 111-132.
- Levitan, M. L., Mehta, K. C., Vann, W. P. and Holmes, J. D. (1991). "Field measurements of pressures on the Texas tech building." *Journal of Wind Engineering and Industrial Aerodynamics* 38(2-3): 227-234.
- Li, Q. S., Calderone, I. and Melbourne, W. H. (1999). "Probabilistic characteristics of pressure fluctuations in separated and reattaching flows for various free-stream turbulence." *Journal of Wind Engineering and Industrial Aerodynamics* 82(1-3): 125-145.
- Li, Q. S., Hu, S. Y., Da, Y. M. and Li, Z. N. (2009). Extreme-value analysis for field measured peak pressure coefficients on a low-rise building. 7th Asia-Pacific conference on wind engineering, Taipei, Taiwan.
- Li, Y. and Ellingwood, B. R. (2006). "Hurricane damage to residential construction in the US: Importance of uncertainty modeling in risk assessment." *Engineering Structures* 28(7): 1009-1018.
- Li, Y. and Ellingwood, B. R. (2009). "Framework for Multihazard Risk Assessment and Mitigation for Wood-Frame " *Journal of Structural Engineering* 135(2): 159-168.
- Lin, J. X. and Surry, D. (1998). "The variation of peak loads with tributary area near corners on flat low building roofs." *Journal of Wind Engineering and Industrial Aerodynamics* 77-78: 185-196.
- Lindt, J. W. v. d. and Dao, T. N. (2009). "Performance-Based Wind Engineering for Wood-Frame Buildings." *Journal of Structural Engineering* 135(2): 169-177.
- Liu, H. and Saathoff, P. J. (1981). "Building Internal Pressure:Sudden Change." *Journal of Engineering Mechanics Division* 107(EM2): 309-321.
- Mahendran, M. (1989). *Fatigue behaviour of corrugated roofing under cyclic wind loading*, Cyclone Testing Station, James Cook University, Townsville, TR 35.
- Mahendran, M. (1995). "Towards an appropriate fatigue loading sequence for roof claddings in cyclone prone areas." *Engineering Structures* 17(7): 476-484.
- Meecham, D., Surry, D. and Davenport, A. G. (1991). "The magnitude and distribution of wind-induced pressures on hip and gable roofs." *Journal of Wind Engineering and Industrial Aerodynamics* 38(2-3): 257-272.

- Mehta, K. C., Levitan, M. L., Iverson, R. E. and McDonald, J. R. (1992). "Roof corner pressures measured in the field on a low building." *Journal of Wind Engineering and Industrial Aerodynamics* 41(1-3): 181-192.
- Melchers, R. E. (1985). "Reliability Calculation for Structures." *Civ.Eng.Trans CE27*: 124-129.
- Melchers, R. E. (1987). *Structural Reliability Analysis and Predictions*, Ellis Horwood Ltd, England.
- Mensah, A. F., Datin, P. L., Prevatt, D. O., Gupta, R. and van de Lindt, J. W. (2011). "Database-assisted design methodology to predict wind-induced structural behavior of a light-framed wood building." *Engineering Structures* 33(2): 674-684.
- Morrison, M. J., Henderson, D. J. and Kopp, G. A. (2011). Response of a Wood-Frame Gable Roof, Under Realistic Fluctuation Wind Loads. 13th International Conference on Wind Engineering, Amsterdam, Netherlands.
- Morrison, M. J. and Kopp, G. A. (2009). Application of Realistic Wind Loads to the Roof of a Full-scale, Wood-Frame House. 11th Americas Conference on Wind Engineering, San Juan, Puerto Rico.
- Morrison, M. J. and Kopp, G. A. (2011). "Performance of toe-nail connections under realistic wind loading." *Engineering Structures* 33(1): 69-76.
- Pham, L. (1985). "Load Combinations and Probabilistic Load Models for Limit State Codes." *Civ. Eng. Trans CE27*: 62-67.
- Pham, L., Holmes, J. D. and Leicester, R. H. (1983). "Safety indices for wind loading in Australia." *Journal of Wind Engineering and Industrial Aerodynamics* 14(1-3): 3-14.
- Pielke, R. A., Jr and Pielke, R. A., Sr (1997). *Hurricanes: Their Nature and Impacts on Society*, John Wiley and Sons, U.K.
- Pinelli, J.-P., Simiu, E., Gurley, K., Subramanian, C., Zhang, L., Cope, A., Filliben, J. J. and Hamid, S. (2004). "Hurricane Damage Prediction Model for Residential Structures." *Journal of Structural Engineering* 130(11): 1685-1691.
- Pinelli, J. P., Gurley, K. R., Subramanian, C. S., Hamid, S. S. and Pita, G. L. (2008). "Validation of a probabilistic model for hurricane insurance loss projections in Florida." *Reliability Engineering & System Safety* 93(12): 1896-1905.
- Pita, G. L., Pinelli, J. P., Cocke, S., Gurley, K., Weekes, J. and Mitrani-Reiser, J. (2011). Assessment of hurricane-induced internal damage to low-rise buildings in the Florida Hurricane Loss Model. 13th International Conference of Wind Engineering, Amsterdam, Netherlands.
- Pita, G. L., Pinelli, J. P., Gurley, K. R., Subramanian, C. S. and Hamid, S. S. (2009). Vulnerability of low-rise commercial-residential buildings in the Florida Public Hurricane Loss Model. 11th Americas Conference on Wind Engineering, San Juan, Puerto Rico.
- Reardon, G. F. (1986). Simulated Cyclone Wind Loading of a Brick Veneer House, Cyclone Testing Station, James Cook University, Townsville, TR 28.
- Reardon, G. F. (1990). Simulated Cyclone Wind Loading of a Nu-Steel House, Cyclone Testing Station, James Cook University, Townsville, TR 36.
- Reardon, G. F. (1996). Simulated Wind Load Testing of Full size Houses. Joint IStructE/City University International Seminar, City University, London.
- Reardon, G. F. and Henderson, D. J. (1996). Simulated Wind Loading of a Two storey Test house. International Wood Engineering Conference, New Orleans, Louisiana, USA.

- Reardon, G. F. and Holmes, J. D. (1981). Wind Tunnel Research on Low Rise Buildings, Cyclone Testing Station, James Cook University, Townsville, TR 11.
- Reardon, G. F. and Mahendran, M. (1988). Simulated Cyclone Wind Loading of a Melbourne style Brick Veneer House, Cyclone Testing Station, James Cook University, Townsville, TR 34.
- Reardon, G. F., Walker, G. R. and Jancauskas, E. D. (1986). Effects of Cyclone Winifred on Buildings TR27, Cyclone Testing Station. James Cook University, Townsville.
- Richards, P. J. and Hoxey, R. P. (2008). "Wind loads on the roof of a 6 m cube." *Journal of Wind Engineering and Industrial Aerodynamics* 96(6-7): 984-993.
- Richardson, G. M. and Blackmore, P. A. (1995). "The silsoe structures building: Comparison of 1 : 100 model-scale data with full-scale data." *Journal of Wind Engineering and Industrial Aerodynamics* 57(2-3): 191-201.
- Richardson, G. M., Robertson, A. P., Hoxey, R. P. and Surry, D. (1990). "Full-scale and model investigations of pressures on an industrial/agricultural building." *Journal of Wind Engineering and Industrial Aerodynamics* 36(Part 2): 1053-1062.
- Richardson, G. M. and Surry, D. (1991). "Comparisons of wind-tunnel and full-scale surface pressure measurements on low-rise pitched-roof buildings." *Journal of Wind Engineering and Industrial Aerodynamics* 38(2-3): 249-256.
- Richardson, G. M. and Surry, D. (1992). "The Silsoe Building: a comparison of pressure coefficients and spectra at model and full-scale." *Journal of Wind Engineering and Industrial Aerodynamics* 43(1-3): 1653-1664.
- Richardson, G. M. and Surry, D. (1994). "The Silsoe structures building: Comparison between full-scale and wind-tunnel data." *Journal of Wind Engineering and Industrial Aerodynamics* 51(2): 157-176.
- Robertson, A. P. (1991). "Effect of eaves detail on wind pressures over an industrial building." *Journal of Wind Engineering and Industrial Aerodynamics* 38(2-3): 325-333.
- Rosowsky, D. V. and Cheng, N. (1999a). "Reliability of Light-Frame Roofs in High-Wind Regions. I: Wind Loads." *Journal of Structural Engineering* 125(7): 725-733.
- Rosowsky, D. V. and Cheng, N. (1999b). "Reliability of Light-Frame Roofs in High-Wind Regions. II: Reliability Analysis." *Journal of Structural Engineering* 125(7): 734-739.
- Rosowsky, D. V. and Ellingwood, B. R. (2002). "Performance-Based Engineering of Wood Frame Housing: Fragility Analysis Methodology." *Journal of Structural Engineering* 128(1): 32-38.
- Sadek, F. and Simiu, E. (2002). "Peak Non-Gaussian Wind Effects for Database-Assisted Low-Rise Building Design." *Journal of Engineering Mechanics* 128(5): 530-539.
- Shanmugam, B., Nielson, B. G. and Prevatt, D. O. (2009). "Statistical and analytical models for roof components in existing light-framed wood structures." *Engineering Structures* 31(11): 2607-2616.
- Sill, B. L., Cook, N. J. and Blackmore, P. A. (1989). "IAWE Aylesbury Comparative Experiment -- Preliminary results of wind tunnel comparisons." *Journal of Wind Engineering and Industrial Aerodynamics* 32(3): 285-302.
- Sill, B. L., Cook, N. J. and Fang, C. (1992). "The Aylesbury Comparative Experiment: A final report." *Journal of Wind Engineering and Industrial Aerodynamics* 43(1-3): 1553-1564.
- Standards Australia. (2006). "AS 4055 Wind Load for Housing." Standard Australia, Sydney, NSW.

- Standards Australia. (2002). "AS/NZS 1170.0. Structural Design Actions Part 0: General Principles." Standard Australia, Sydney, NSW.
- Standards Australia. (2002). "AS/NZS 1170.1. Structural Design Actions Part 1: Permanent, imposed and other actions." Standard Australia, Sydney, NSW.
- Standards Australia. (1989). "AS/NZS 1170.2 . Structural Design Action Part 2: Wind Action." Standard Australia, Sydney, NSW.
- Standards Australia. (2011). "AS/NZS 1170.2 (2011). Structural Design Action Part 2: Wind Action." Standard Australia, Sydney, NSW.
- Stewart, M. G. (2003). "Cyclone damage and temporal changes to building vulnerability and economic risks for residential construction." *Journal of Wind Engineering and Industrial Aerodynamics* 91(5): 671-691.
- Stramit (2000). *Stramit perlins: Design member moment capacities*, Stramit Building Products, Sydney.
- Surry, D. (1991). "Pressure measurements on the Texas tech building: Wind tunnel measurements and comparisons with full scale." *Journal of Wind Engineering and Industrial Aerodynamics* 38(2-3): 235-247.
- Tang, L. K. and Melchers, R. E. (1985). "Reliability of Large Structural Systems." *Civ.Eng.Trans* CE27(124-129).
- Thoft-Christensen, P. and Baker, M. J. (1982). *Structural Reliability Theory and Its Applications*, Springer-Verlag, New York.
- Tieleman, H. W., Surry, D. and Mehta, K. C. (1996). "Full/model-scale comparison of surface pressures on the Texas Tech experimental building." *Journal of Wind Engineering and Industrial Aerodynamics* 61(1): 1-23.
- Unanwa, C. O., McDonald, J. R., Mehta, K. C. and Smith, D. A. (2000). "The development of wind damage bands for buildings." *Journal of Wind Engineering and Industrial Aerodynamics* 84(1): 119-149.
- Vickery, B. J. (1986). "Gust-Factors for Internal Pressure in Low rise Buildings." *Journal of Wind Engineering and Industrial Aerodynamics*: 259-271.
- Vickery, P. J., Kopp, G. A. and Tewisdale, L. A. (2011). *Component and cladding wind pressures on hip and gable roofs: Comparisons to the US wind loading provisions*. 13th International Conference on Wind Engineering, Amsterdam, Netherlands.
- Vickery, P. J., Lin, J., Skerlj, P. F., Twisdale, J. L. A. and Huang, K. (2006a). "HAZUS-MH Hurricane Model Methodology. I: Hurricane Hazard, Terrain, and Wind Load Modeling." *Natural Hazards Review* 7(2): 82-93.
- Vickery, P. J., Skerlj, P. F., Lin, J., Twisdale, J. L. A., Young, M. A. and Lavelle, F. M. (2006b). "HAZUS-MH Hurricane Model Methodology. II: Damage and Loss Estimation." *Natural Hazards Review* 7(2): 94-103.
- Vickery, P. J., Skerlj, P. F., Steckley, A. C. and Twisdale, L. A. (2000). "Hurricane Wind Field Model for Use in Hurricane Simulations." *Journal of Structural Engineering* 126(10): 1203-1221.
- Walker, G. R. (1975). *Report on Cyclone Tracy-Effect on buildings-* Dec 1974, Australian Dept of Housing and Construction
- Walker, G. R. (1995). *Wind Vulnerability curves for Queensland houses*, Alexander Howden Reinsurance Brokers (Australia) Ltd., Sydney.
- Walker, G. R. (2010). "A review of the impact of cyclone Tracy on building regulations and insurance." *Australian Meteorological and oceanographic Journal* 60: 199-206.

- Walker, G. R. (2011). "Modelling the vulnerability of buildings to wind — a review." *Canadian Journal of Civil Engineering* 38(8): 1031-1039.
- Wehner, M., Sandland, C., Holmes, J. D., Henderson, D. J. and Edwards, M. (2010). Modelling damage to residential buildings from wind-borne debris-Part 2.Implimentation. 14th Australasian Wind Engineering Workshop, Geosciences Australia, Canberra.
- Wehner, M., Sandland, C., Holmes, J. D., Kim, P., Jayasinghe, N. C. and Edwards, M. (2010b). Development of a software tool for quantitative assessment of the vulnerability of Australian residential building stock to severe wind. 14th Australasian Wind Engineering Workshop, Geosciences Australia, Canberra.
- Whalen, M. T., Sadek, F. and Simiu, E. (2002). "Database-assisted design for wind: basic concepts and software development." *Journal of Wind Engineering and Industrial Aerodynamics* 90: 1349-1368.
- Xu, Y. L. (1995a). "Determination of Wind-Induced Fatigue Loading on Roof Cladding." *Journal of Engineering Mechanics* 121(9): 956-963.
- Xu, Y. L. (1995b). "Fatigue Performance of Screw-Fastened Light-Gauge-Steel Roofing Sheets." *Journal of Structural Engineering* 121(3): 389-398.
- Xu, Y. L. and Reardon, G. F. (1996). Full scale and Model scale Wind Pressure and Fatigue Loading on the Texas Tech University Building, Cyclone Testing Station, James Ciik University, Townsville,TR 42.
- Xu, Y. L. and Reardon, G. F. (1998). "Variations of wind pressure on hip roofs with roof pitch." *Journal of Wind Engineering and Industrial Aerodynamics* 73(3): 267-284.

APPENDIX A

- *Pressure Distribution-Cladding*

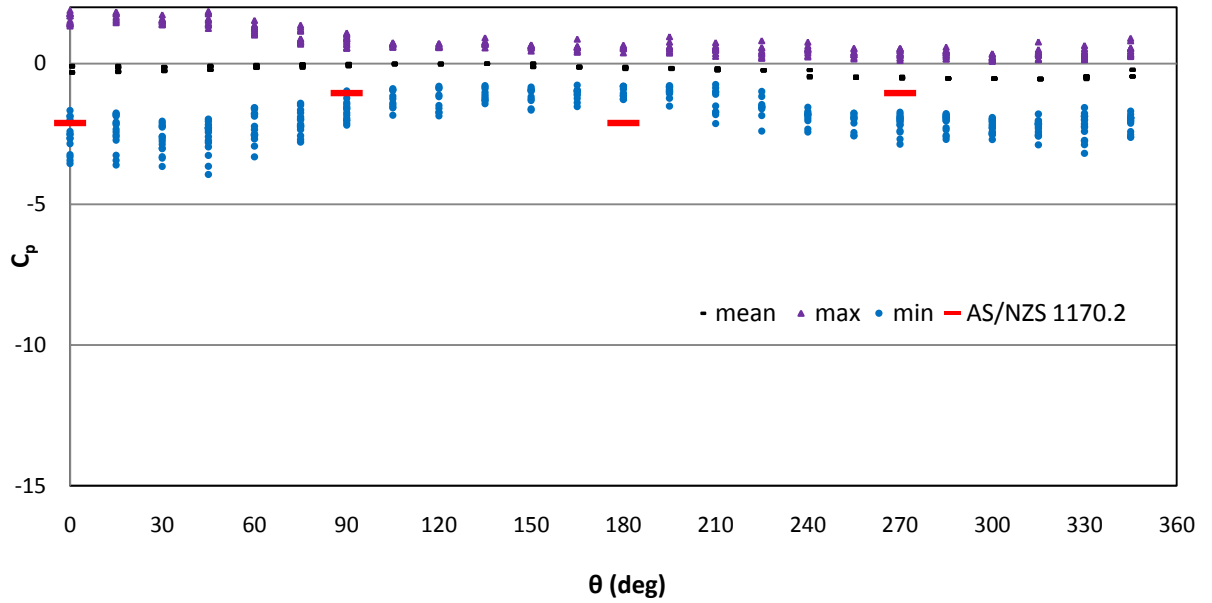


Figure A.1: Pressure coefficients vs wind direction - R (cladding)

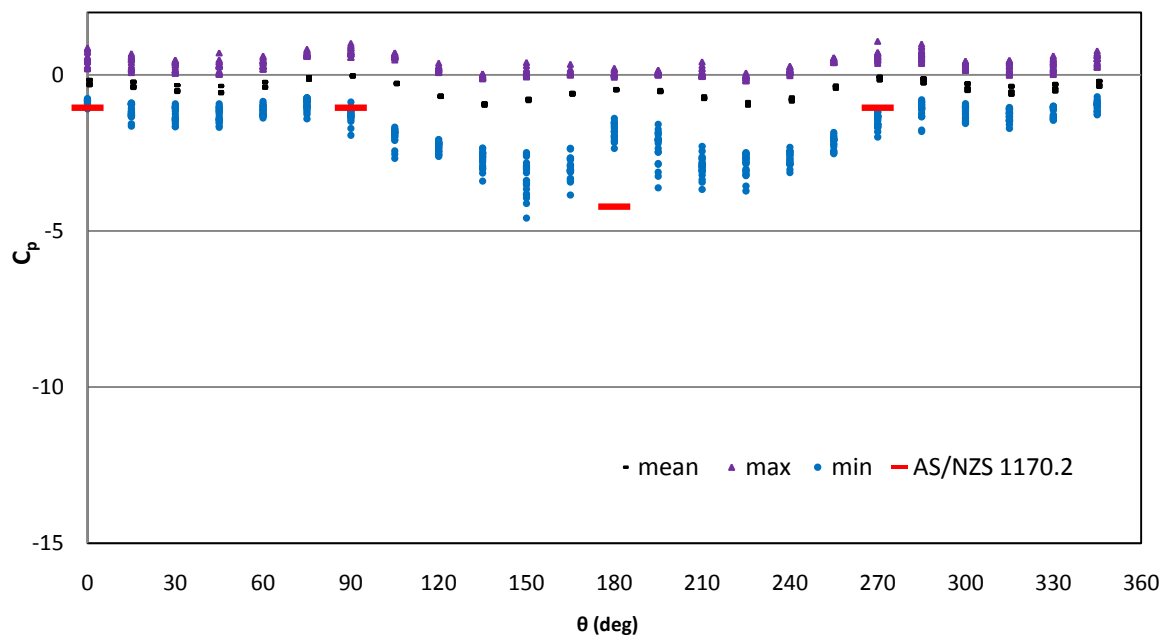


Figure A.2: Pressure coefficients vs wind direction - S (cladding)

- *Pressure Distribution-Battens*

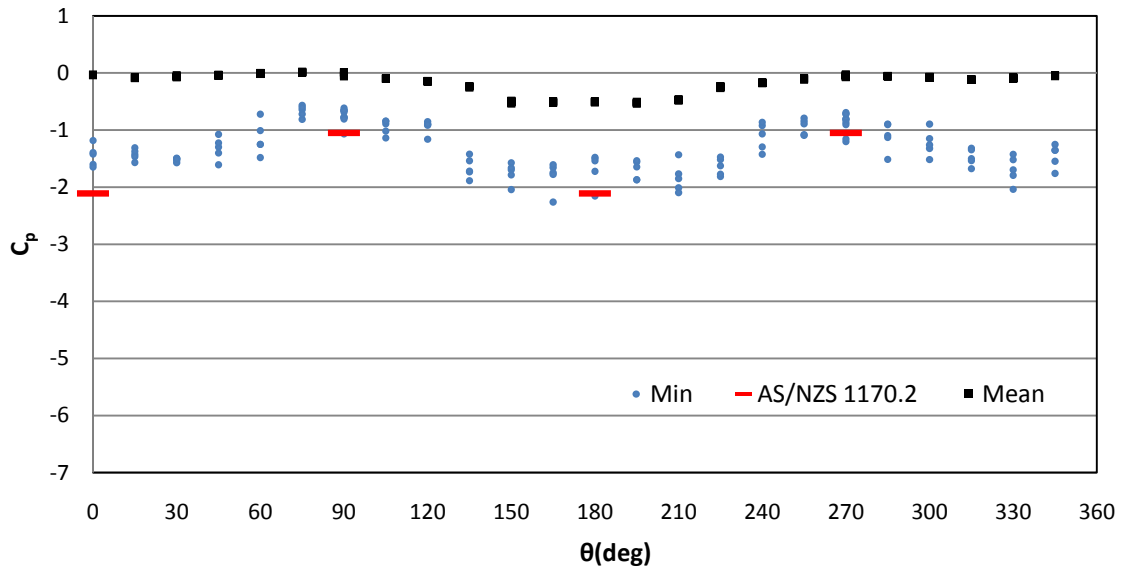


Figure A.3: Pressure coefficients (C_p) vs wind direction – Batten to truss connection L2

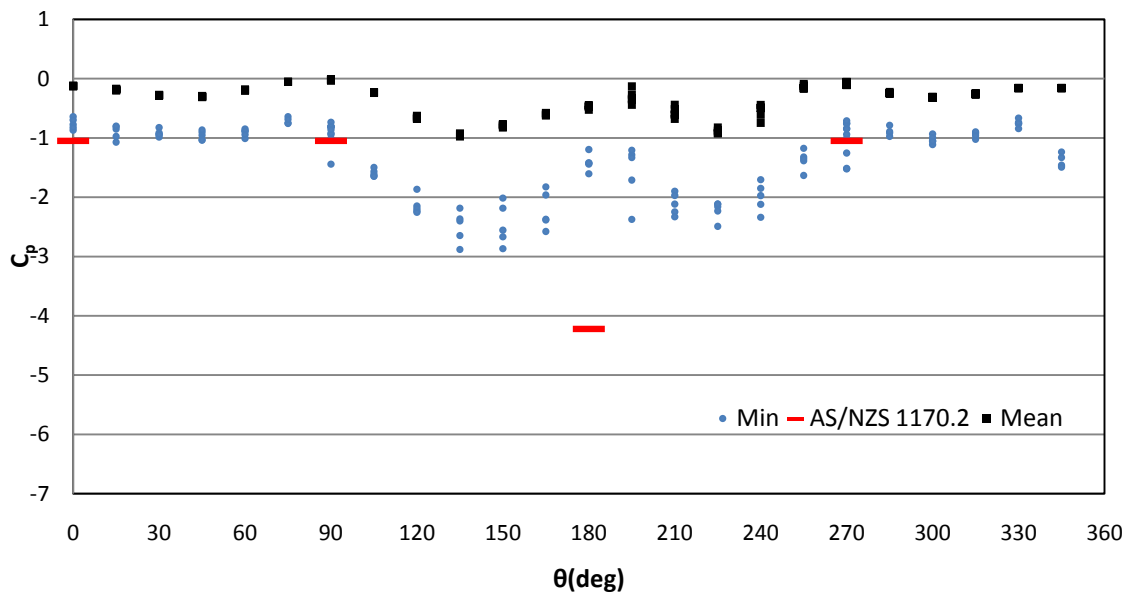


Figure A.4: Pressure coefficients (C_p) vs wind direction – Batten to truss connection L7

Table A.1: Probabilistic description of wind load for cladding fixing regions

(θ°)	Region P			Region Q			Region T			Region R			Region S		
	Mean	COV	PDF												
0	-1.16	-0.11	GM	-1.08	-0.25	GEV	-0.74	-0.29	GEV	-1.18	-0.23	GEV	-0.90	-0.12	GEV
15	-2.28	-0.19	GEV	-1.00	-0.31	GEV	-0.66	-0.24	GEV	-1.23	-0.23	GEV	-1.12	-0.19	RL
30	-3.68	-0.11	LN	-0.87	-0.35	GEV	-0.62	-0.22	GEV	-1.28	-0.20	GEV	-1.21	-0.19	GEV
45	-0.73	-0.10	GEV	-0.40	-0.36	GEV	-0.33	-0.16	GEV	-1.06	-0.23	GEV	-1.23	-0.17	GEV
60	-0.74	-0.10	GEV	-0.60	-0.27	GEV	-0.58	-0.22	WB	-1.76	-0.24	GEV	-1.10	-0.13	GEV
75	-0.73	-0.09	GEV	-0.77	-0.20	GEV	-0.91	-0.17	GEV	-1.31	-0.29	GEV	-0.91	-0.19	GEV
90	-0.74	-0.13	GEV	-0.75	-0.18	GEV	-0.95	-0.17	GM	-1.16	-0.24	GEV	-1.23	-0.18	WB
105	-0.78	-0.13	WB	-0.71	-0.15	GEV	-1.10	-0.15	WB	-1.05	-0.18	GEV	-1.88	-0.14	GEV
120	-1.01	-0.22	GEV	-0.70	-0.22	WB	-1.02	-0.04	GM	-0.92	-0.18	WB	-2.22	-0.07	GEV
135	-1.25	-0.36	GEV	-0.62	-0.13	WB	-1.07	-0.19	WB	-0.80	-0.21	WB	-0.64	-0.10	GEV
150	-1.92	-0.31	GEV	-1.63	-0.20	LN	-1.39	-0.08	GEV	-0.99	-0.15	GEV	-0.78	-0.17	GEV
165	-1.22	-0.16	GEV	-1.14	-0.08	WB	-1.08	-0.10	GM	-1.02	-0.15	GEV	-0.71	-0.12	WB
180	-0.60	-0.21	GEV	-1.23	-0.17	LN	-0.81	-0.08	GEV	-1.04	-0.12	GEV	-0.43	-0.15	GEV
195	-0.53	-0.15	GEV	-1.20	-0.09	N	-1.13	-0.12	N	-1.07	-0.16	WB	-0.55	-0.23	GEV
210	-0.70	-0.22	GEV	-1.01	-0.21	GEV	-1.16	-0.16	GEV	-1.01	-0.17	WB	-0.70	-0.11	WB
225	-0.66	-0.22	GEV	-0.92	-0.24	GEV	-0.99	-0.17	GEV	-0.89	-0.17	GEV	-0.69	-0.12	GEV
240	-2.99	-0.18	WB	-2.08	-0.27	WB	-2.70	-0.08	GM	-1.12	-0.19	GM	-2.56	-0.08	N
255	-2.11	-0.28	GEV	-1.62	-0.25	WB	-1.94	-0.12	GEV	-1.13	-0.28	WB	-2.07	-0.10	GEV
270	-1.15	-0.21	N	-1.34	-0.26	WB	-1.06	-0.24	WB	-1.23	-0.19	GEV	-1.43	-0.14	N
285	-1.17	-0.20	GEV	-1.71	-0.30	GEV	-0.78	-0.14	GEV	-1.95	-0.37	GEV	-1.08	-0.24	GEV
300	-1.49	-0.19	GEV	-2.09	-0.29	GEV	-0.90	-0.13	WB	-1.99	-0.33	WB	-1.18	-0.17	GEV
315	-1.01	-0.13	WB	-0.94	-0.24	WB	-1.06	-0.17	GEV	-1.25	-0.17	GEV	-1.25	-0.14	GEV
330	-1.11	-0.16	GEV	-1.26	-0.30	GEV	-1.15	-0.28	GEV	-1.31	-0.19	GEV	-1.15	-0.14	GEV
345	-1.15	-0.18	WB	-1.24	-0.24	GEV	-0.38	-0.20	GEV	-1.23	-0.25	GEV	-0.94	-0.16	GEV

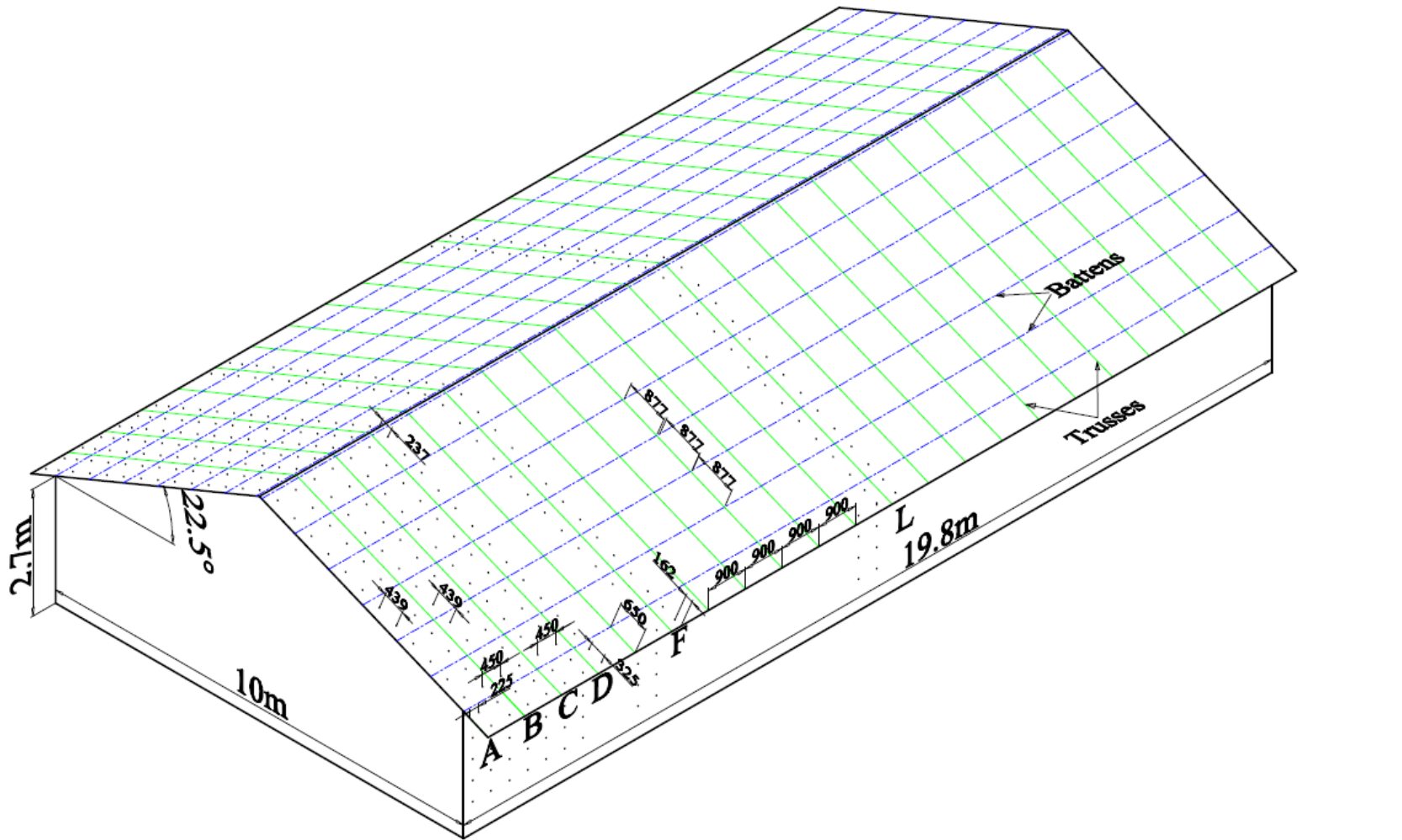


Figure A.5: Isometric view of the pressure tap locations

APPENDIX B- Test Matrix

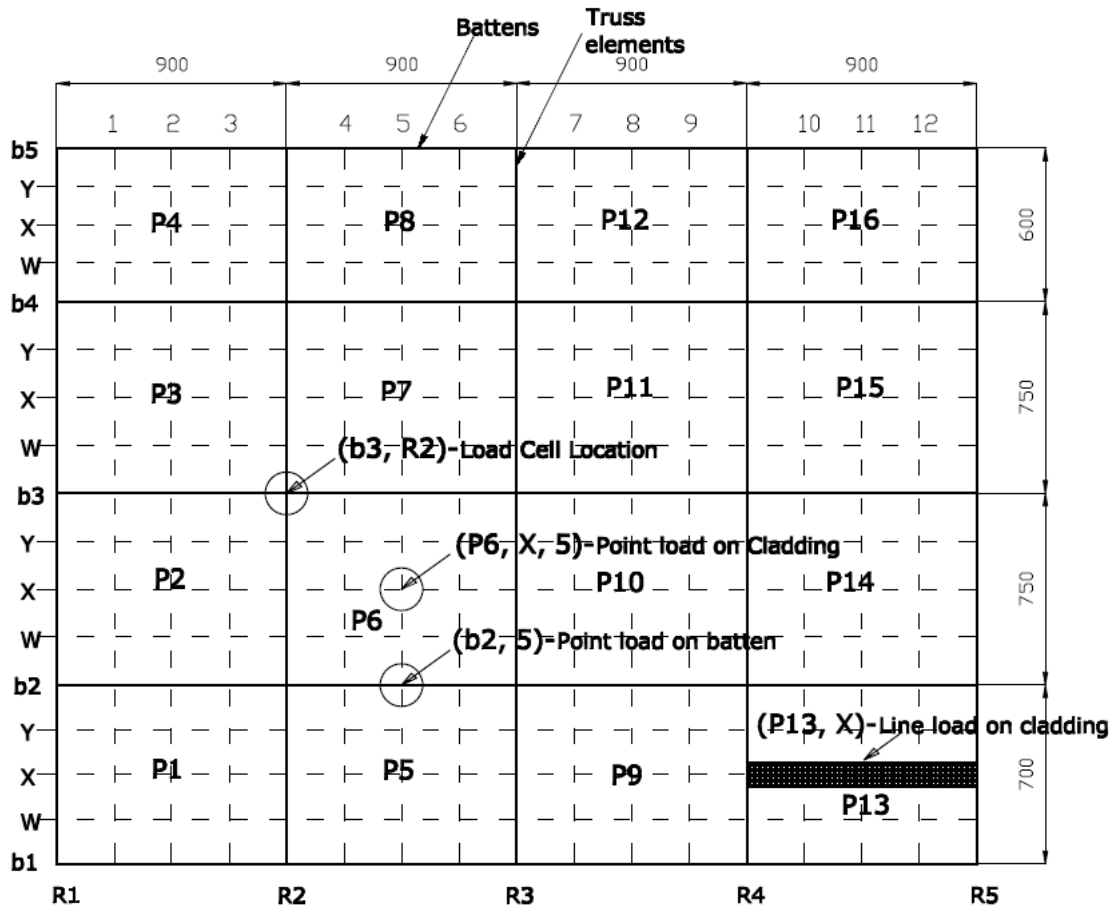


Figure B.1: Terminology for load application and load cell locations in the Test set up #1

Table B.1: Test setup #1- Point load on batten-Linear region

Location	Scenario
b2,1	Without cladding
b2,2	Without cladding
b2,3	Without cladding
b2,4	Without cladding
b2,5	Without cladding
b2,6	Without cladding
b2,7	Without cladding
b2,8	Without cladding
b2,9	Without cladding
b2,10	Without cladding
b2,11	Without cladding
b2,12	Without cladding
b3,1	Without cladding
b3,2	Without cladding
b3,3	Without cladding
b3,4	Without cladding
b3,5	Without cladding
b3,6	Without cladding
b3,7	Without cladding
b3,8	Without cladding
b3,9	Without cladding
b2,1	Without cladding-only b2,R2 removed
b2,2	Without cladding-only b2,R2 removed
b2,3	Without cladding-only b2,R2 removed
b2,4	Without cladding-only b2,R2 removed
b2,5	Without cladding-only b2,R2 removed
b2,6	Without cladding-only b2,R2 removed
b2,7	Without cladding-only b2,R2 removed
b2,8	Without cladding-only b2,R2 removed
b2,9	Without cladding-only b2,R2 removed
b2,10	Without cladding-only b2,R2 removed
b2,11	Without cladding-only b2,R2 removed
b2,12	Without cladding-only b2,R2 removed
b2,1	Without cladding-only b2,R3 removed
b2,2	Without cladding-only b2,R3 removed
b2,3	Without cladding-only b2,R3 removed
b2,4	Without cladding-only b2,R3 removed
b2,5	Without cladding-only b2,R3 removed
b2,6	Without cladding-only b2,R3 removed
b2,1	With cladding
b2,2	With cladding
b2,3	With cladding
b2,4	With cladding
b2,5	With cladding
b2,6	With cladding
b3,1	With cladding
b3,2	With cladding
b3,3	With cladding
b3,4	With cladding
b3,5	With cladding
b3,6	With cladding

Table B.2: Test setup #1- Point load on cladding-Linear region

Location	Scenario
P6,W,4F	Undamaged system
P6,W,4N	Undamaged system
P6,X,4F	Undamaged system
P6,X,4N	Undamaged system
P6,Y,4F	Undamaged system
P6,Y,4N	Undamaged system
P6,W,5F	Undamaged system
P6,W,5N	Undamaged system
P6,X,5F	Undamaged system
P6,X,5N	Undamaged system
P6,Y,5F	Undamaged system
P6,Y,5N	Undamaged system
P6,W,6F	Undamaged system
P6,W,6N	Undamaged system
P6,X,6F	Undamaged system
P6,X,6N	Undamaged system
P6,Y,6F	Undamaged system
P6,Y,6N	Undamaged system
P10,W,7F	Undamaged system
P10,W,7N	Undamaged system
P10,X,7F	Undamaged system
P10,X,7N	Undamaged system
P10,Y,7F	Undamaged system
P10,Y,7N	Undamaged system
P10,W,8F	Undamaged system
P10,W,8N	Undamaged system
P10,X,8F	Undamaged system
P10,X,8N	Undamaged system
P10,Y,8F	Undamaged system
P10,Y,8N	Undamaged system
P10,W,9F	Undamaged system
P10,W,9N	Undamaged system
P10,X,9F	Undamaged system
P10,X,9N	Undamaged system
P10,Y,9F	Undamaged system
P10,Y,9N	Undamaged system
P11,X,7F	Undamaged system
P11,X,7N	Undamaged system
P11,X,8F	Undamaged system
P11,X,8N	Undamaged system
P11,X,9F	Undamaged system
P11,X,9N	Undamaged system

Table B.3: Test setup #1- Point load on cladding-Linear region

Location	Scenario
P6,X,4F	Fastener at b3,R3 only removed
P6,X,4N	Fastener at b3,R3 only removed
P6,X,5F	Fastener at b3,R3 only removed
P6,X,5N	Fastener at b3,R3 only removed
P6,X,6F	Fastener at b3,R3 only removed
P6,X,6F	Fastener at b3,R3 only removed
P10,X,7F	Fastener at b3,R3 only removed
P10,X,7N	Fastener at b3,R3 only removed
P10,X,8F	Fastener at b3,R3 only removed
P10,X,8N	Fastener at b3,R3 only removed
P10,X,9F	Fastener at b3,R3 only removed
P10,X,9N	Fastener at b3,R3 only removed
P11,X,7F	Fastener at b3,R3 only removed
P11,X,7N	Fastener at b3,R3 only removed
P11,X,8F	Fastener at b3,R3 only removed
P11,X,8N	Fastener at b3,R3 only removed
P11,X,9F	Fastener at b3,R3 only removed
P11,X,9N	Fastener at b3,R3 only removed
P6,X,4F	Fastener at b2,5 only removed
P6,X,4N	Fastener at b2,5 only removed
P6,X,5F	Fastener at b2,5 only removed
P6,X,5N	Fastener at b2,5 only removed
P6,X,6F	Fastener at b2,5 only removed
P6,X,6F	Fastener at b2,5 only removed
P10,X,7F	Fastener at b2,5 only removed
P10,X,7N	Fastener at b2,5 only removed
P10,X,8F	Fastener at b2,5 only removed
P10,X,8N	Fastener at b2,5 only removed
P10,X,9F	Fastener at b2,5 only removed
P10,X,9N	Fastener at b2,5 only removed
P6,X,4F	Fastener at b1,5 only removed
P6,X,4N	Fastener at b1,5 only removed
P6,X,5F	Fastener at b1,5 only removed
P6,X,5N	Fastener at b1,5 only removed
P6,X,6F	Fastener at b1,5 only removed
P6,X,6F	Fastener at b1,5 only removed
P10,X,7F	Fastener at b1,5 only removed
P10,X,7N	Fastener at b1,5 only removed
P10,X,8F	Fastener at b1,5 only removed
P10,X,8N	Fastener at b1,5 only removed
P10,X,9F	Fastener at b1,5 only removed
P10,X,9N	Fastener at b1,5 only removed

Table B.4: Test setup #1- Point load on cladding

Location	Scenario
P1,X,2	Linear region
P1,X,2	Non linear region
P1,W,2	Linear region
P1,W,2	Non linear region
P1,Y,2	Linear region
P1,Y,2	Non linear region
P1,Y,3	Linear region
P1,Y,3	Non linear region
P1,X,3	Linear region
P1,X,3	Non linear region
P1,W,3	Linear region
P1,W,3	Non linear region
P1,X,1	Linear region
P1,X,1	Non linear region
P1,Y,1	Linear region
P1,Y,1	Non linear region
P2,X,2	Linear region
P2,X,2	Non linear region
P2,W,2	Linear region
P2,W,2	Non linear region
P2,Y,3	Linear region
P2,Y,3	Non linear region
P2,X,3	Linear region
P2,X,3	Non linear region
P2,X,1	Linear region
P2,X,1	Non linear region
P2,Y,1	Linear region
P2,Y,1	Non linear region
P3,X,2	Linear region
P3,X,2	Non linear region
P3,X,3	Linear region
P3,X,3	Non linear region
P3,X,1	Linear region
P3,X,1	Non linear region

Table B.5: Test setup #1- Line load on cladding

Location	Scenario
P1,W	Undamaged system
P5,W	Undamaged system
P1,P5,W	Undamaged system
P9,P13,W	Undamaged system
P1,X	Undamaged system
P5,X	Undamaged system
P1,P5,X	Undamaged system
P9,X	Undamaged system
P13,X	Undamaged system
P9,P13,X	Undamaged system
P1,Y	Undamaged system
P5,Y	Undamaged system
P1,P5,Y	Undamaged system
P9,P13,Y	Undamaged system
P2,W	Undamaged system
P6,W	Undamaged system
P2,P6,W	Undamaged system
P10,W	Undamaged system
P14,W	Undamaged system
P10,P14,W	Undamaged system
P2,X	Undamaged system
P6,X	Undamaged system
P2,P6,X	Undamaged system
P10,X	Undamaged system
P14,X	Undamaged system
P10,P14,X	Undamaged system
P2,Y	Undamaged system
P6,Y	Undamaged system
P2,P6,Y	Undamaged system
P10,Y	Undamaged system
P10,P14,Y	Undamaged system
P3,W	Undamaged system
P7,W	Undamaged system
P3,P7,W	Undamaged system
P11,W	Undamaged system
P15,W	Undamaged system
P11,P15,W	Undamaged system
P3,X	Undamaged system
P7,X	Undamaged system
P3,P7,X	Undamaged system
P11,X	Undamaged system
P15,X	Undamaged system
P11,P15,X	Undamaged system
P3,Y	Undamaged system
P7,Y	Undamaged system
P3,P7,Y	Undamaged system
P11,Y	Undamaged system
P15,Y	Undamaged system
P11,P15,Y	Undamaged system
P5,P9,W	Undamaged system
P5,P9,X	Undamaged system
P5,P9,Y	Undamaged system
P6,P10,W	Undamaged system
P6,P10,X	Undamaged system
P6,P10,Y	Undamaged system
P7,P11,W	Undamaged system
P7,P11,X	Undamaged system
P7,P11,Y	Undamaged system

Table B.6: Test setup #1- Failure of cladding fasteners-non linear region

Location	Scenario
P6,X,5	Point load until failure
P1,X,1	Point load until failure
P10,X	Line load until failure
P13,X	Line load until failure

Table B.7: Test setup #2-Line load

Location	Scenario
P1, X	Undamaged system
P2, X	Undamaged system
P3, X	Undamaged system
P4, X	Undamaged system
P5, X	Undamaged system
P6, X	Undamaged system
P7, X	Undamaged system
P8, X	Undamaged system
P9, X	Undamaged system
P1,X	B1, R2 Both screws removed
P4,X	B1, R2 Both screws removed
P4,X	B1, R3 Both screws removed
P7,X	B1, R3 Both screws removed
P1,X	B2, R2 Both screws removed
P2,X	B2, R2 Both screws removed
P4,X	B2, R2 Both screws removed
P5,X	B2, R2 Both screws removed
P4,X	B3, R3 Both screws removed
P5,X	B3, R3 Both screws removed
P7,X	B3, R3 Both screws removed
P8,X	B3, R3 Both screws removed
P1,X	B1, R2 Both screws 'E' removed
P4,X	B1, R2 Both screws 'E' removed
P4,X	B1, R3 Both screws 'E' removed
P7,X	B1, R3 Both screws 'E' removed
P1,X	B2, R2 Both screws 'E' removed
P2,X	B2, R2 Both screws 'E' removed
P4,X	B2, R2 Both screws 'E' removed
P5,X	B2, R2 Both screws 'E' removed
P4,X	B3, R3 Both screws 'E' removed
P5,X	B3, R3 Both screws 'E' removed
P7,X	B3, R3 Both screws 'E' removed
P8,X	B3, R3 Both screws 'E' removed
P1,X	B1, R2 Both screws 'T' removed
P4,X	B1, R2 Both screws 'T' removed
P4,X	B1, R3 Both screws 'T' removed
P7,X	B1, R3 Both screws 'T' removed
P1,X	B2, R2 Both screws 'T' removed
P2,X	B2, R2 Both screws 'T' removed
P4,X	B2, R2 Both screws 'T' removed
P5,X	B2, R2 Both screws 'T' removed
P4,X	B3, R3 Both screws 'T' removed
P5,X	B3, R3 Both screws 'T' removed
P7,X	B3, R3 Both screws 'T' removed
P8,X	B3, R3 Both screws 'T' removed

Table B.8: Test setup #2-line load and point load

Location	Scenario
P1,X	B1, R2 Both screws loosened
P4,X	B1, R2 Both screws loosened
P4,X	B1, R3 Both screws loosened
P7,X	B1, R3 Both screws loosened
P1,X	B2, R2 Both screws loosened
P2,X	B2, R2 Both screws loosened
P4,X	B2, R2 Both screws loosened
P5,X	B2, R2 Both screws loosened
P4,X	B3, R3 Both screws loosened
P5,X	B3, R3 Both screws loosened
P7,X	B3, R3 Both screws loosened
P8,X	B3, R3 Both screws loosened
P1,X	B1, R2 screw 'E' loosened
P4,X	B1, R2 screw 'E' loosened
P4,X	B1, R3 screw 'E' loosened
P7,X	B1, R3 screw 'E' loosened
P1,X	B2, R2 screw 'E' loosened
P2,X	B2, R2 screw 'E' loosened
P4,X	B2, R2 screw 'E' loosened
P5,X	B2, R2 screw 'E' loosened
P4,X	B3, R3 screw 'E' loosened
P5,X	B3, R3 screw 'E' loosened
P7,X	B3, R3 screw 'E' loosened
P8,X	B3, R3 screw 'E' loosened
P1,X	B1, R2 screw 'T' loosened
P4,X	B1, R2 screw 'T' loosened
P4,X	B1, R3 screw 'T' loosened
P7,X	B1, R3 screw 'T' loosened
P1,X	B2, R2 screw 'T' loosened
P2,X	B2, R2 screw 'T' loosened
P4,X	B2, R2 screw 'T' loosened
P5,X	B2, R2 screw 'T' loosened
P4,X	B3, R3 screw 'T' loosened
P5,X	B3, R3 screw 'T' loosened
P7,X	B3, R3 screw 'T' loosened
P8,X	B3, R3 screw 'T' loosened
b2, R2	Loading until failure
b3, R3	Loading until failure

Point loads on batten - Elastic range

- Loads

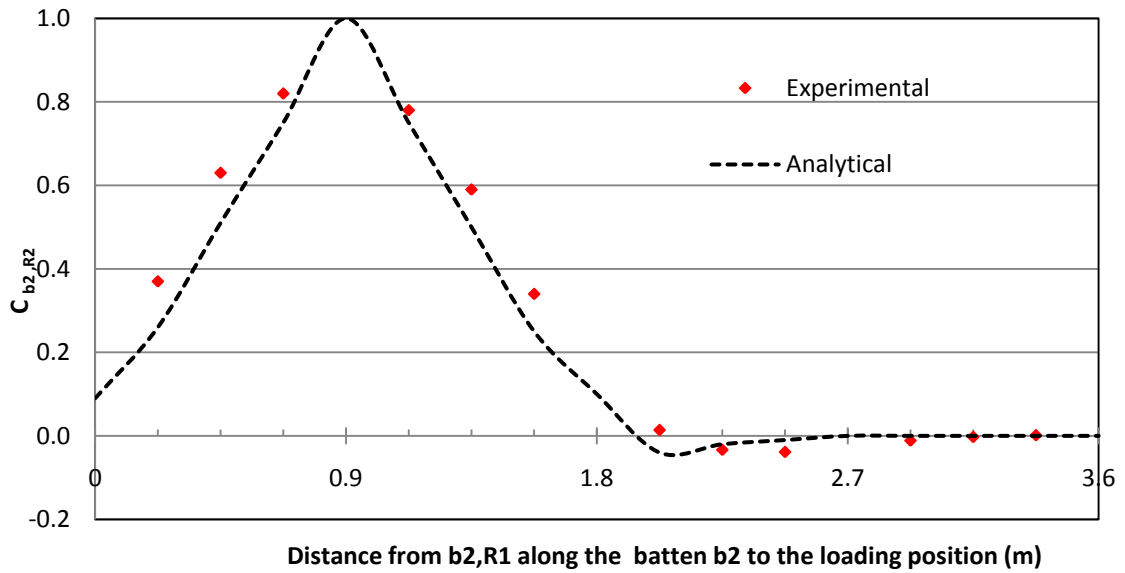


Figure B.2: $C_{b2,R2}$ for point load on batten b2

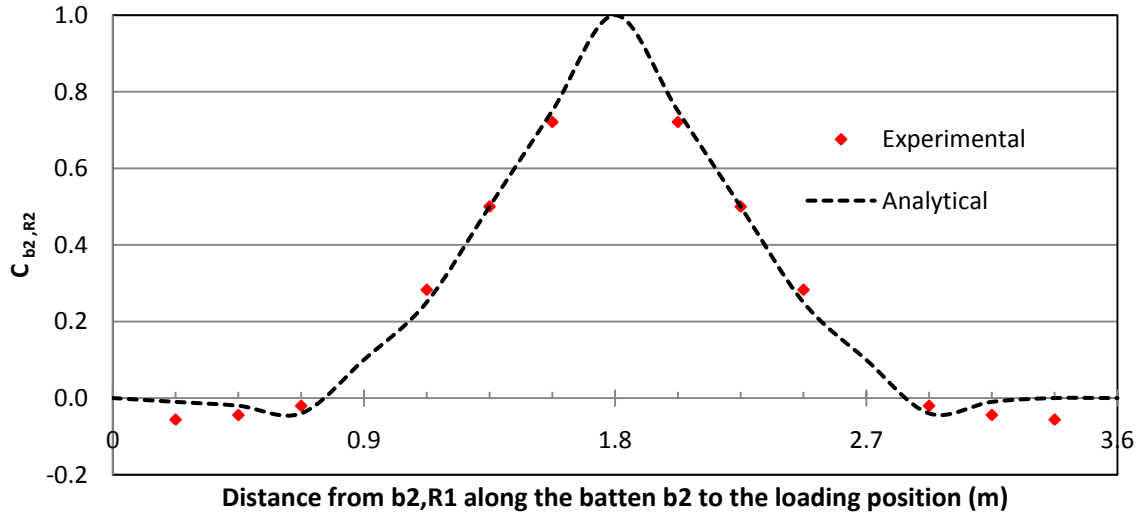


Figure B.3: $C_{b2,R3}$ for point load on batten b2

- *Deflections*

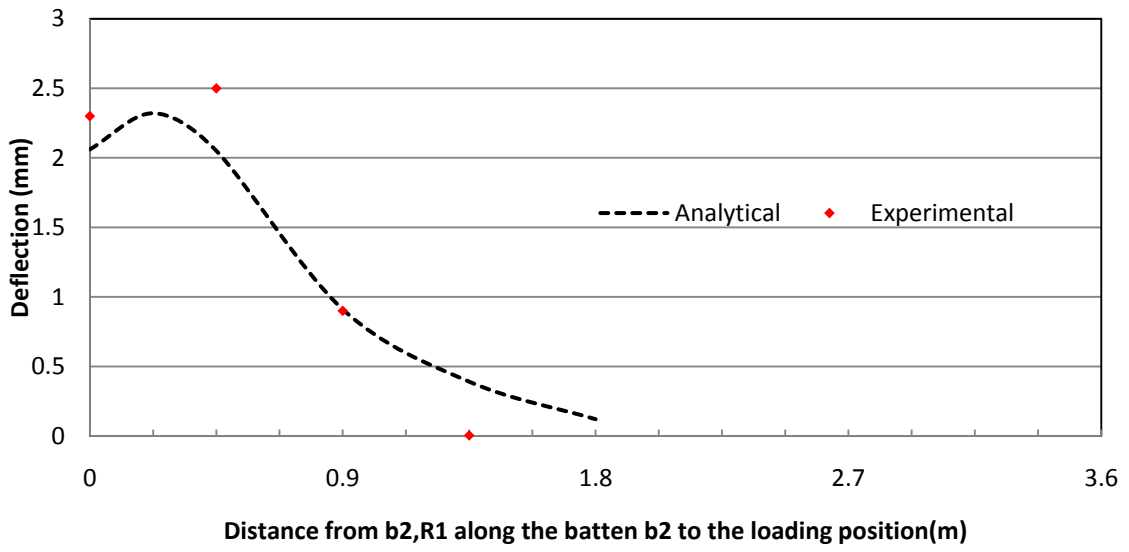


Figure B.4: Deflection of batten b2 for load at (b2, 1)

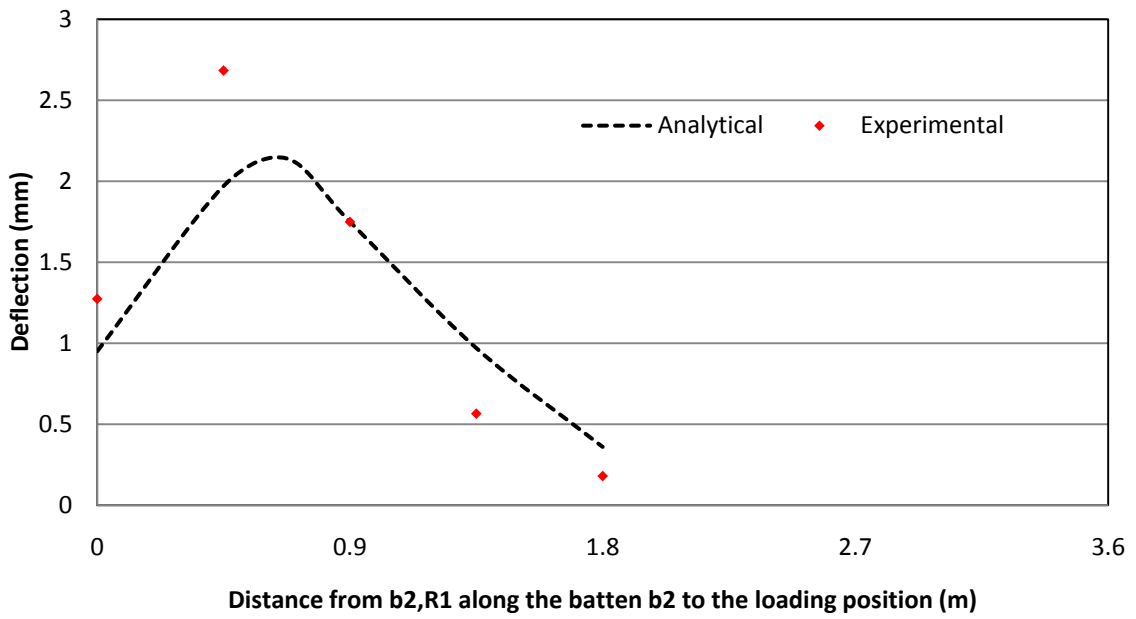


Figure B.5: Deflection of batten b2 for load at (b2, 3)

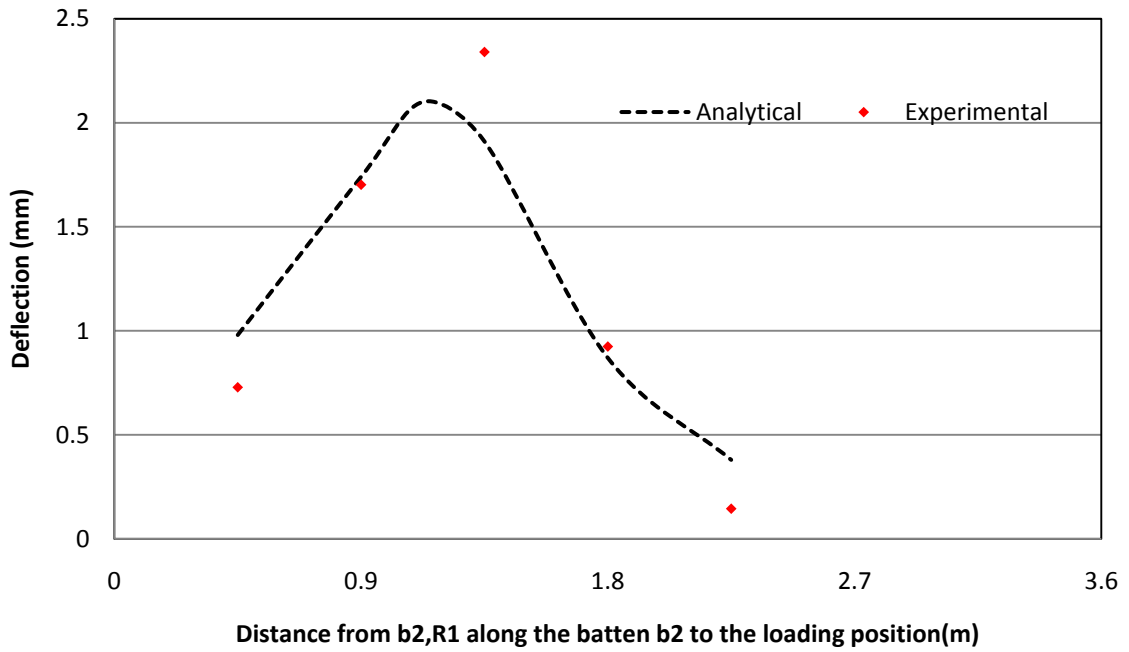


Figure B.6: Deflection of batten b2 for load at (b2, 4)

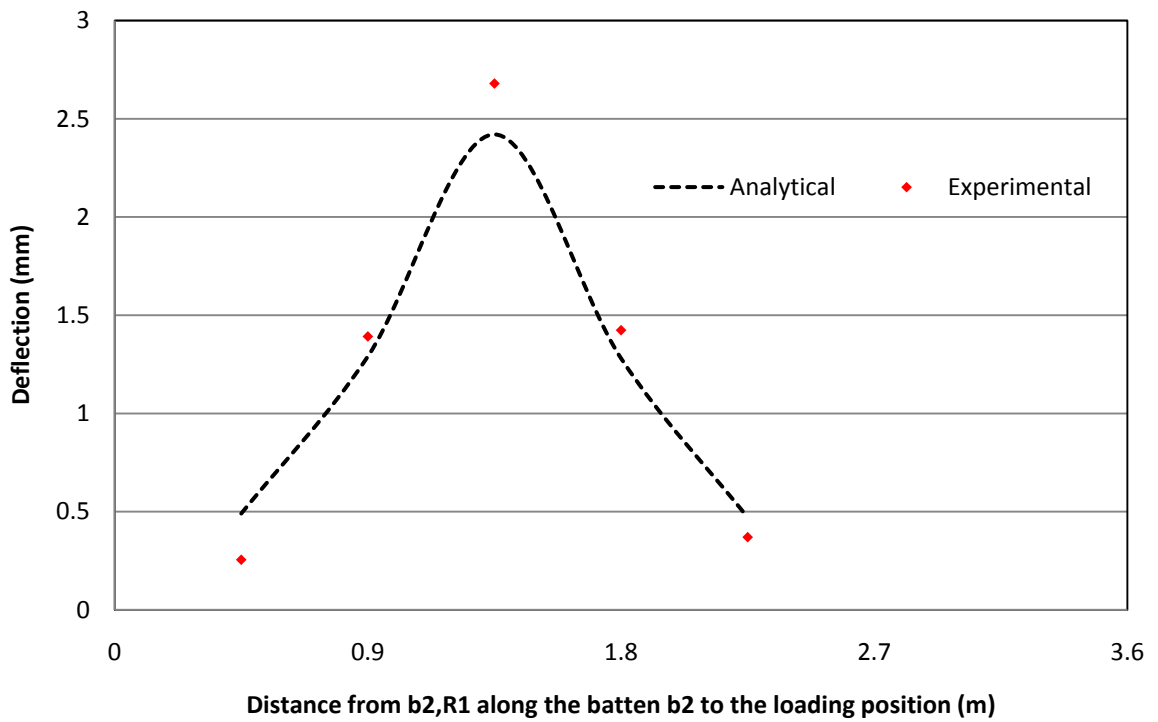


Figure B.7: Deflection of batten b2 for load at (b2, 5)

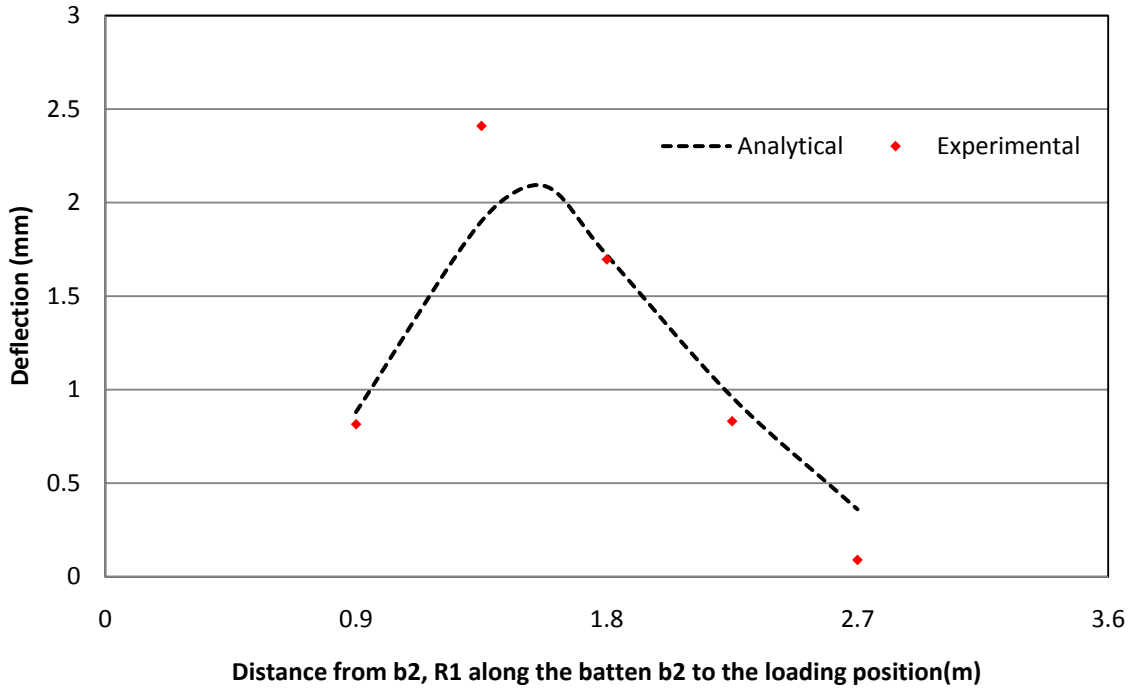


Figure B.8: Deflection of batten b2 for load at (b2, 6)

- *Batten failure without cladding*

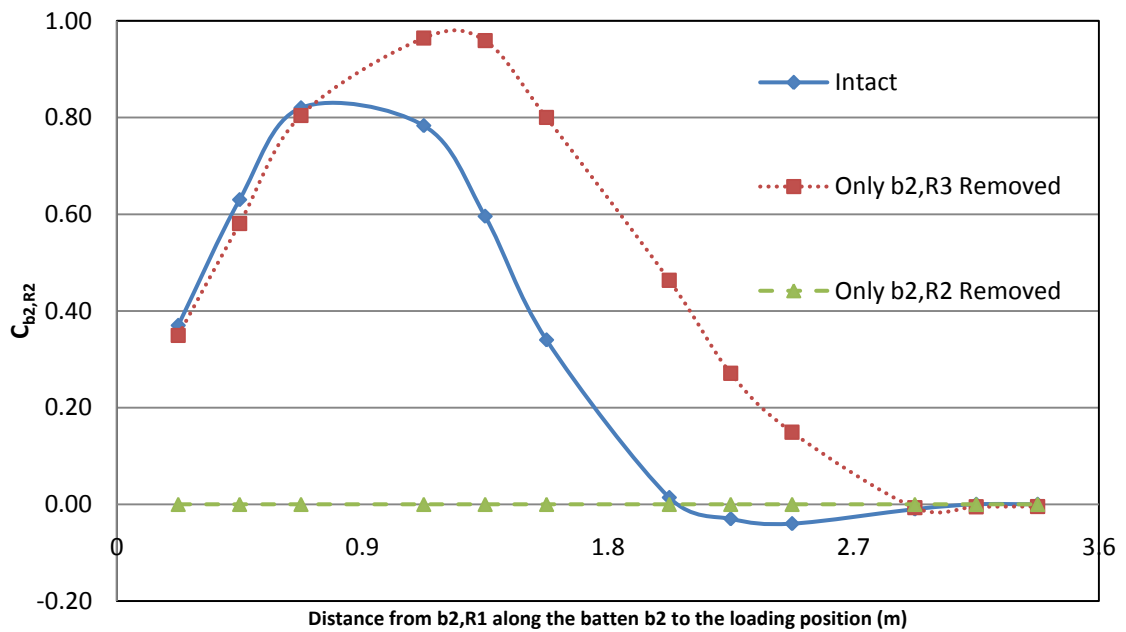


Figure B.9: $C_{b2,R2}$ for point load on batten b2

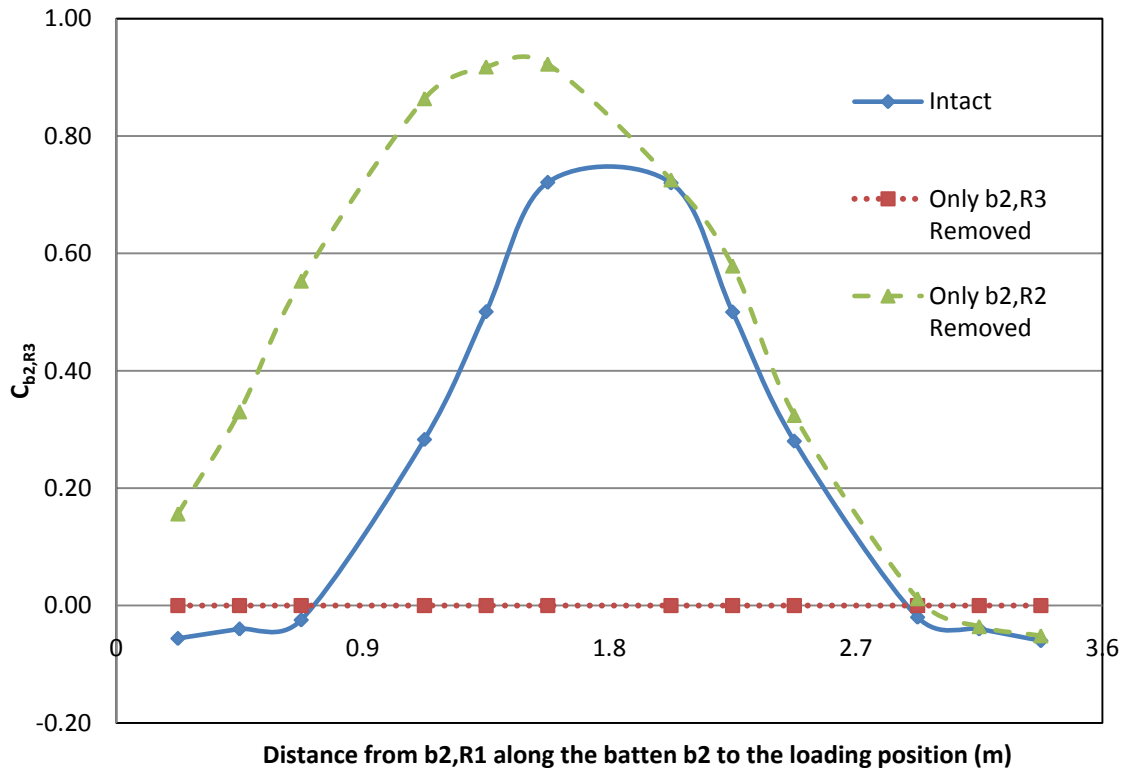


Figure B.10: $C_{b2,R3}$ for point load on batten B2

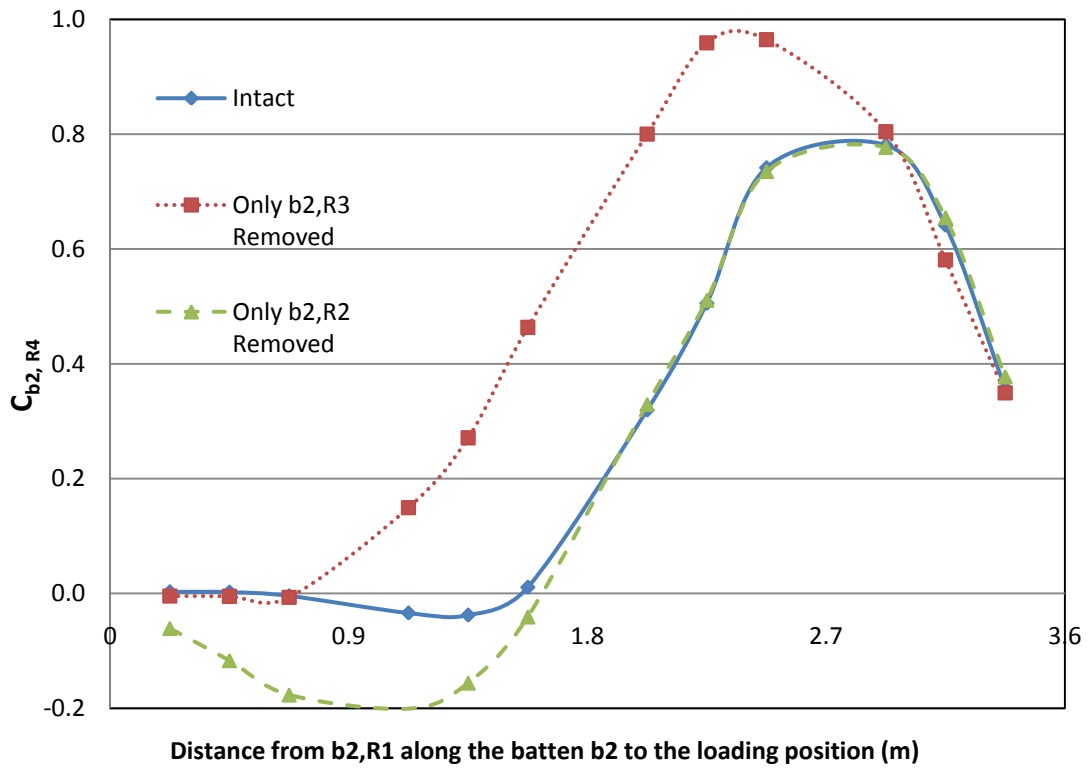


Figure B.11: $C_{b2,R4}$ for point load on batten b2

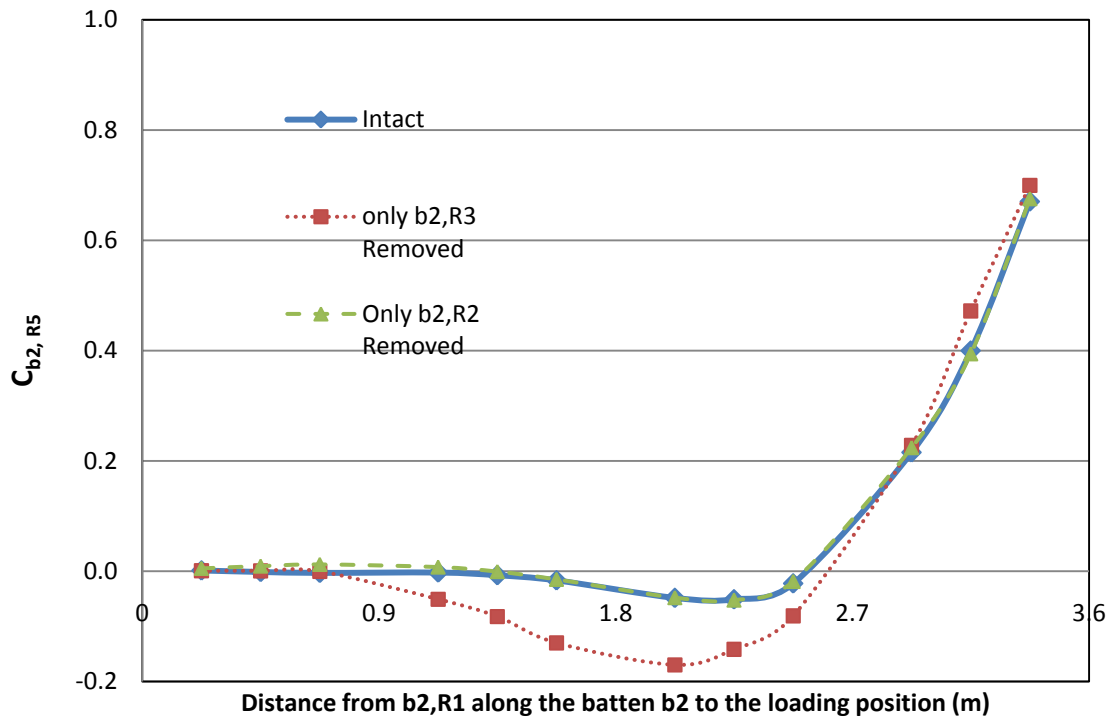


Figure B.12: $C_{b2, R5}$ for point load on batten b2

- *Effect of cladding on battens*

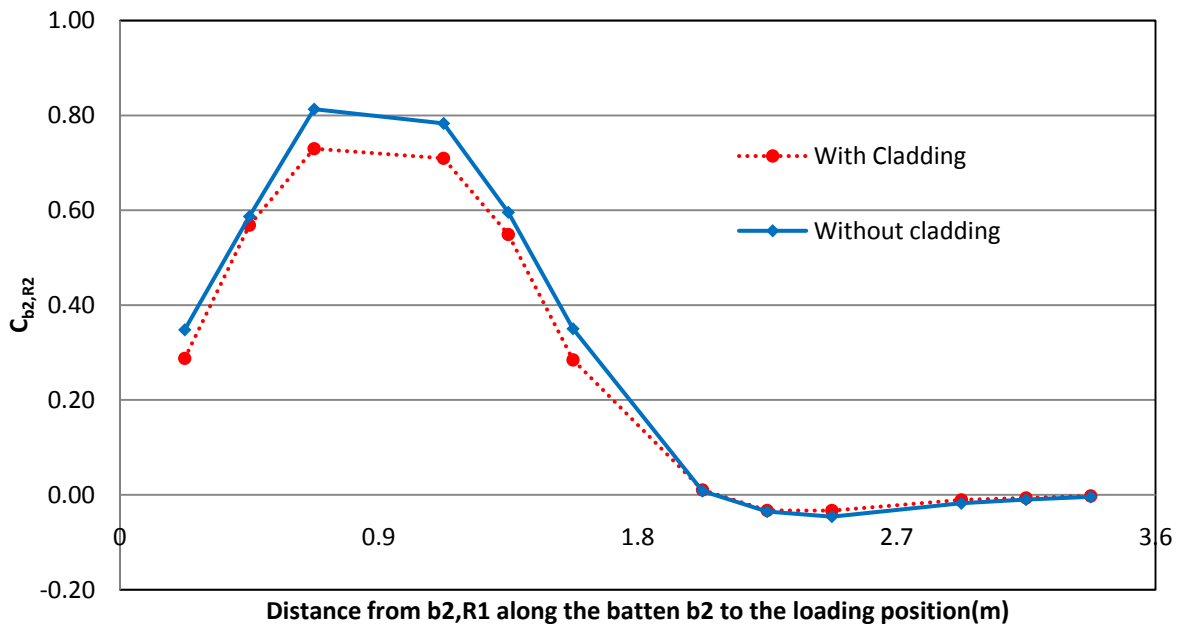


Figure B.13: The effect of cladding on $C_{b2, R2}$

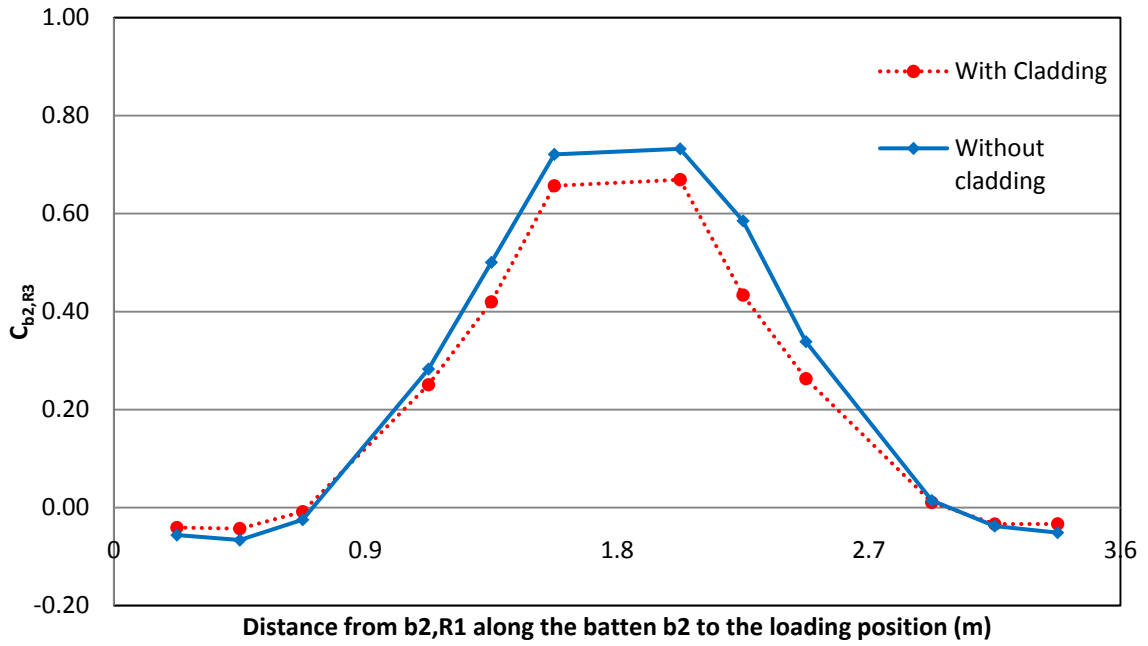


Figure B.14: The effect of cladding on $C_{b2, R3}$

- *Load on cladding*

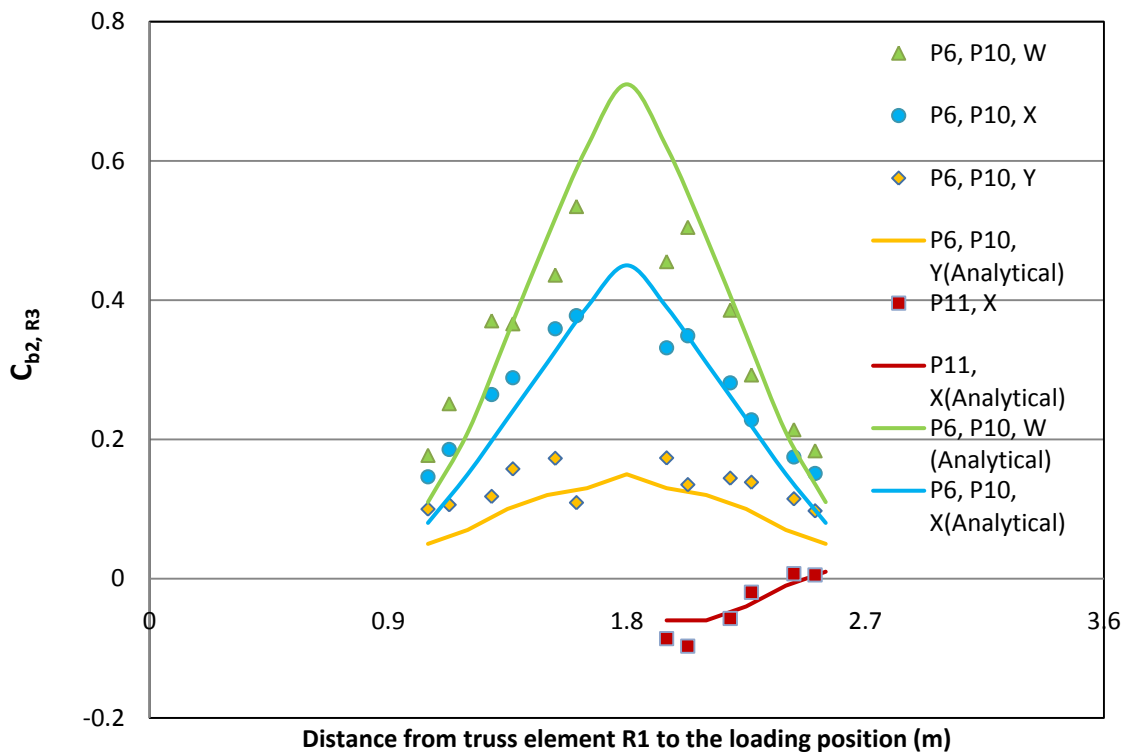


Figure B.15: $C_{b2, R3}$ point load on W, X, Y

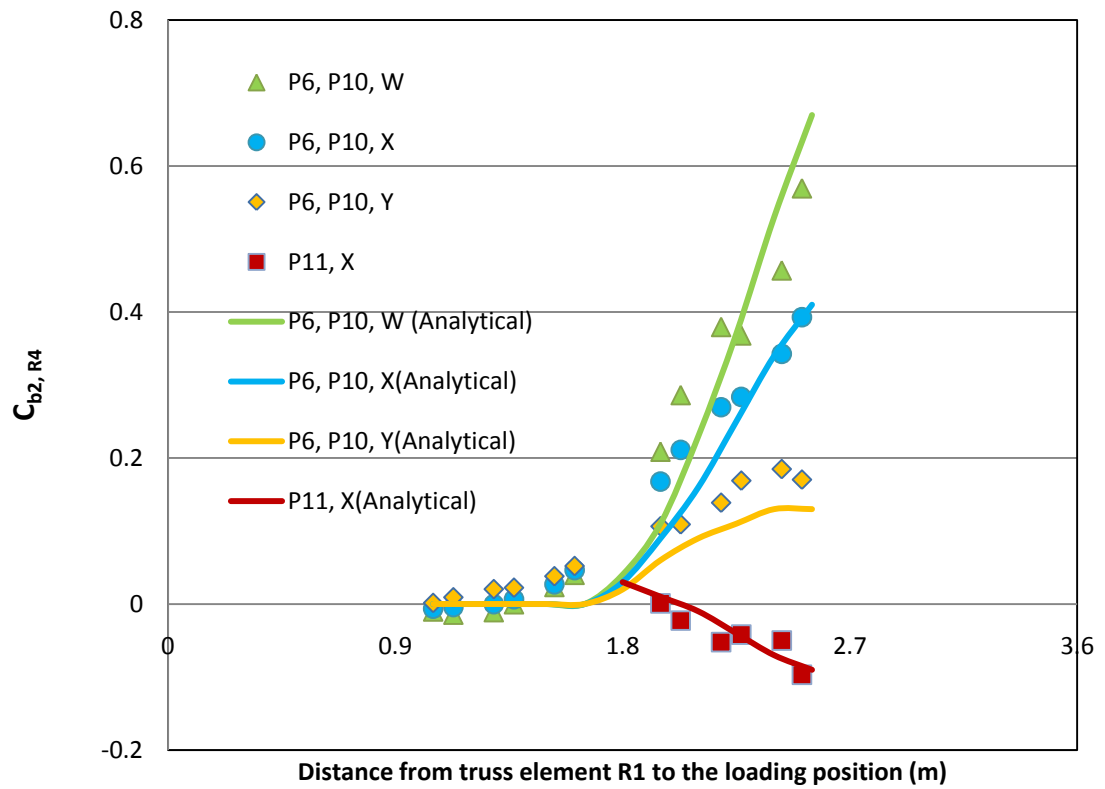


Figure B.16: $C_{b2, R4}$ point load on W, X, Y

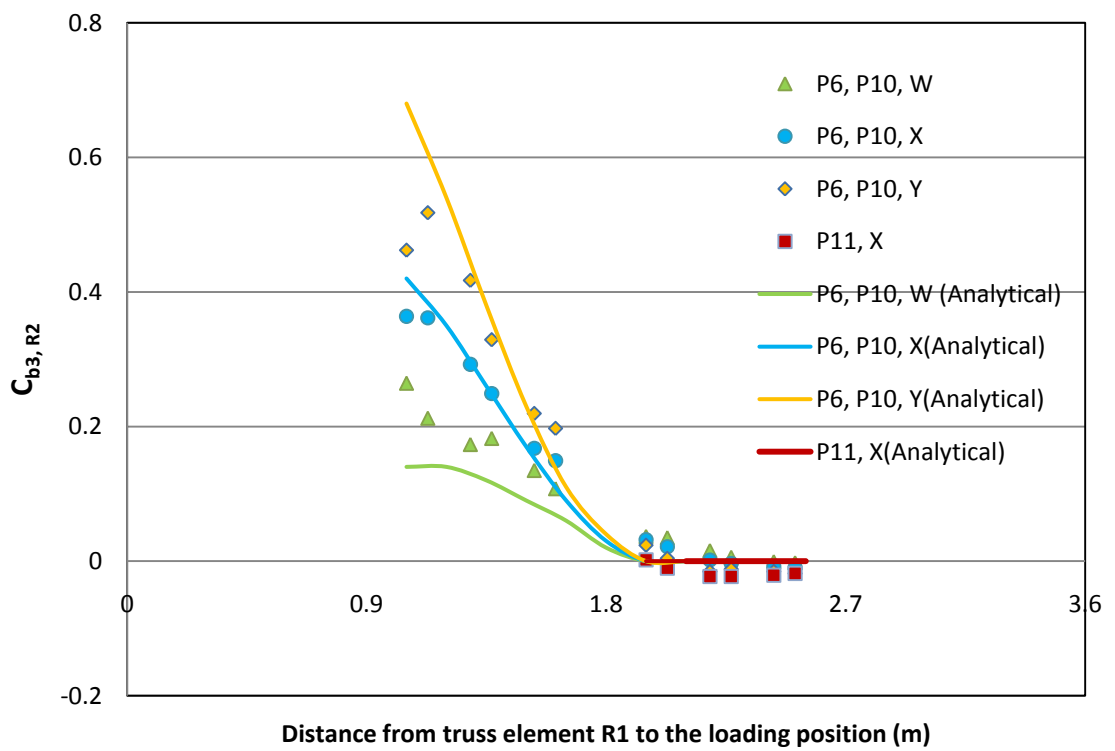


Figure B.17: $C_{b3, R2}$ point load on W, X, Y

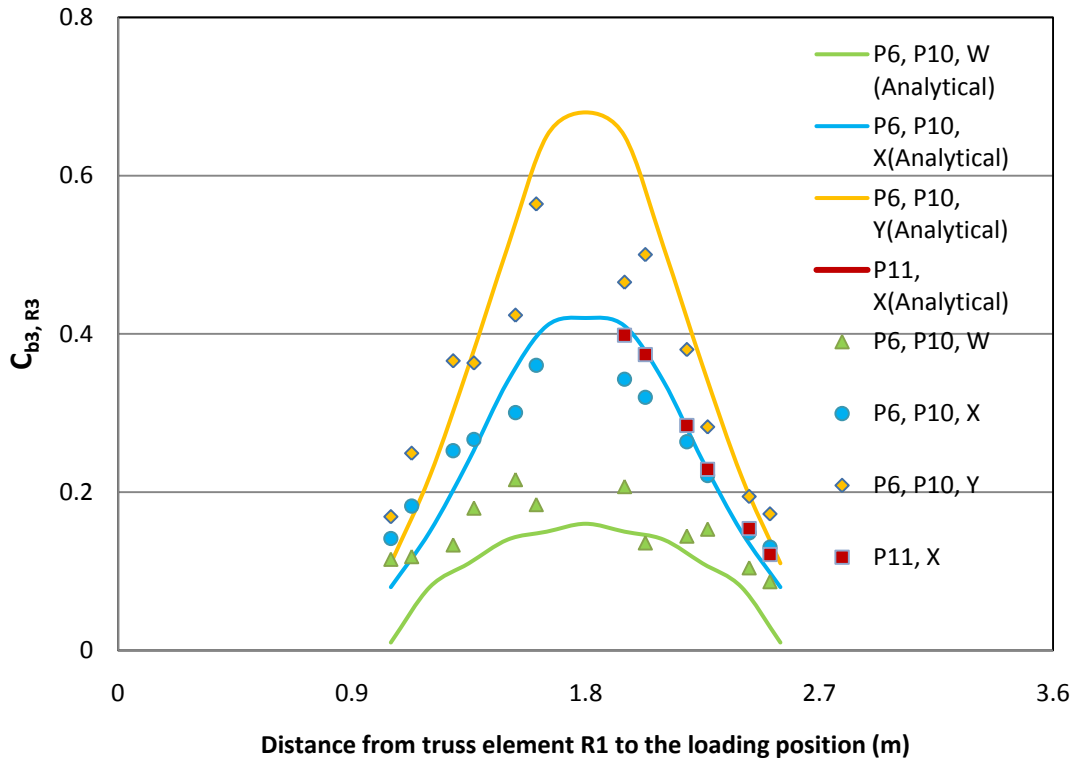


Figure B.18: $C_{b3, R3}$ point load on W, X, Y

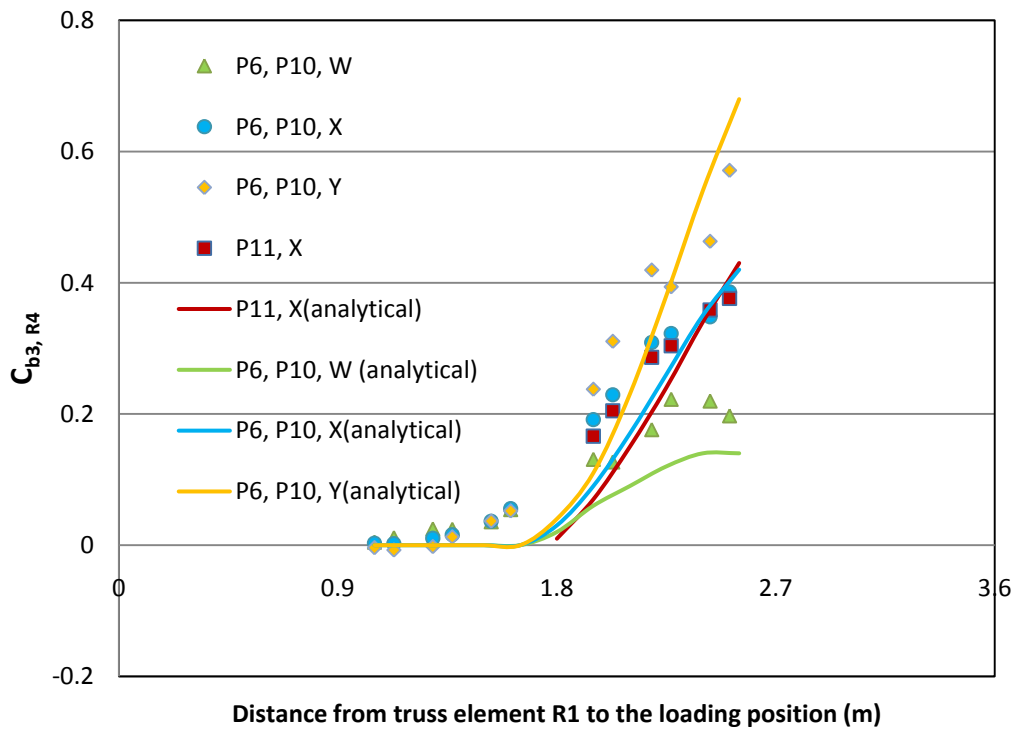


Figure B.19: $C_{b3, R4}$ point load on W, X, Y

- *Removal of cladding fasteners*

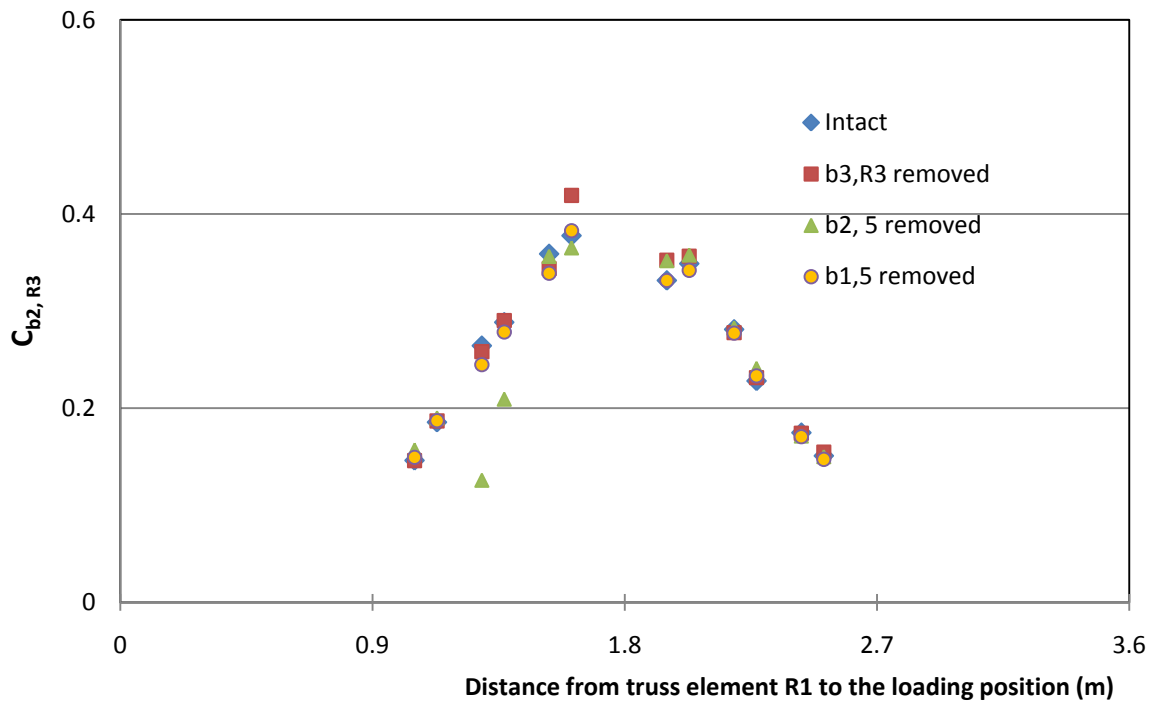


Figure B.20: $C_{b2, R3}$ for point load on X

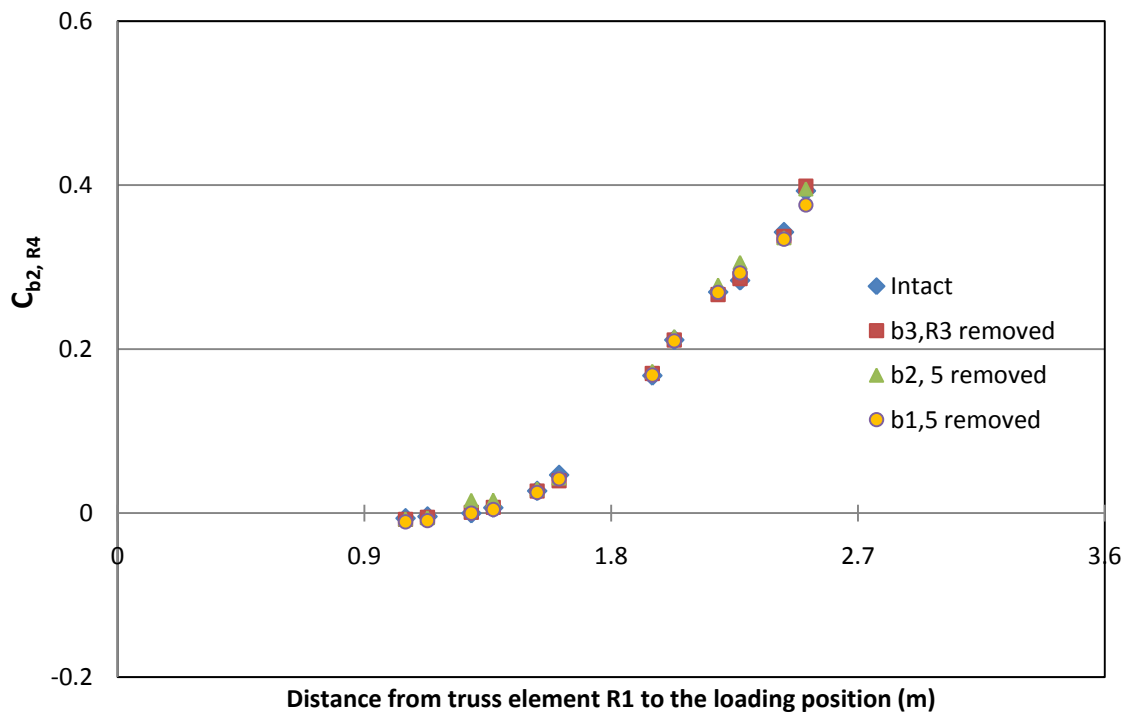


Figure B.21: $C_{b2, R4}$ for point load on X

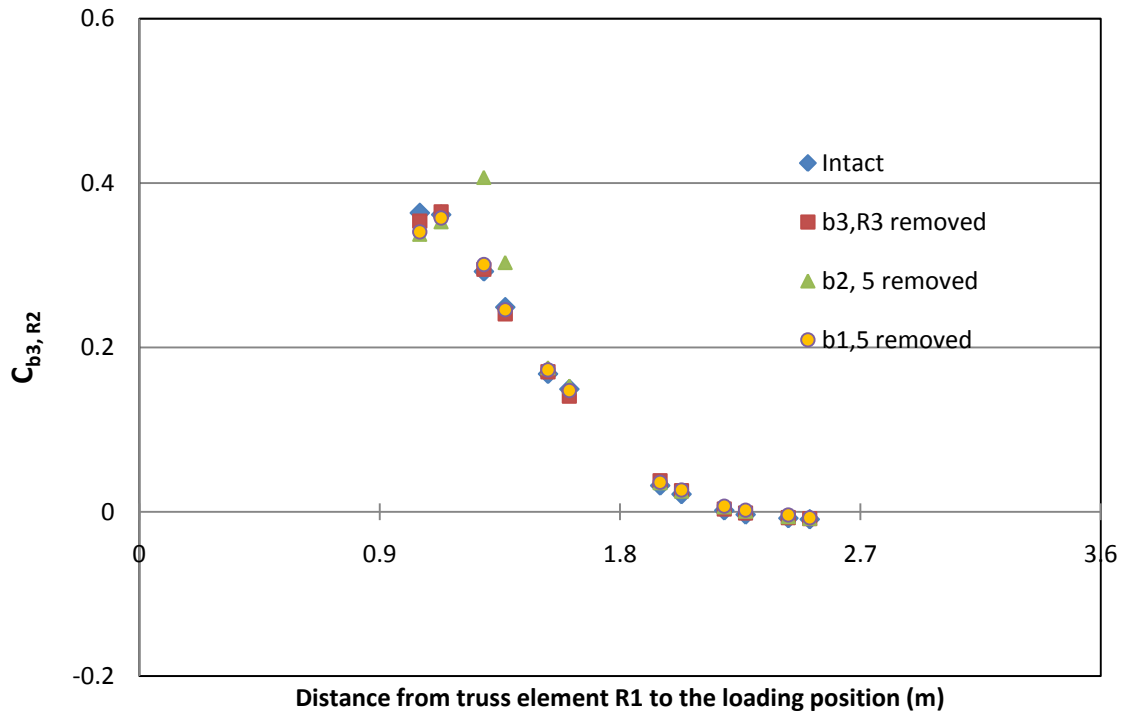


Figure B.22: $C_{b3, R2}$ for point load on X

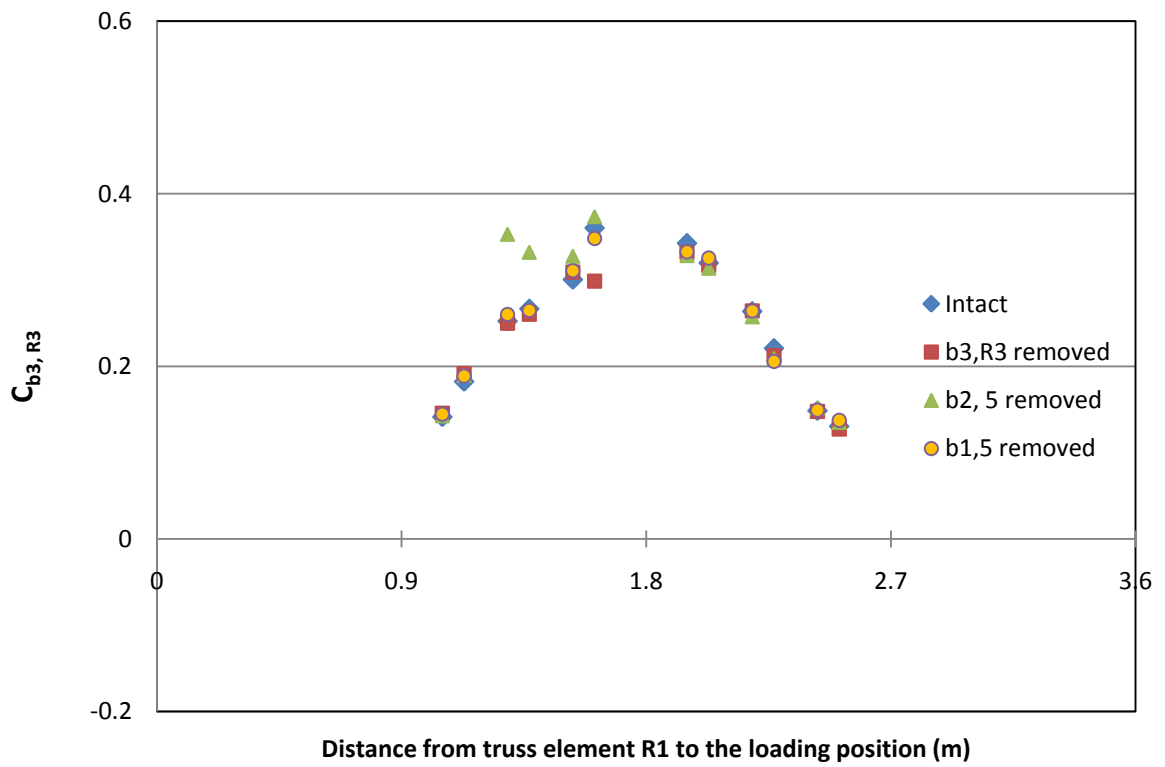


Figure B.23: $C_{b3, R3}$ for point load on X

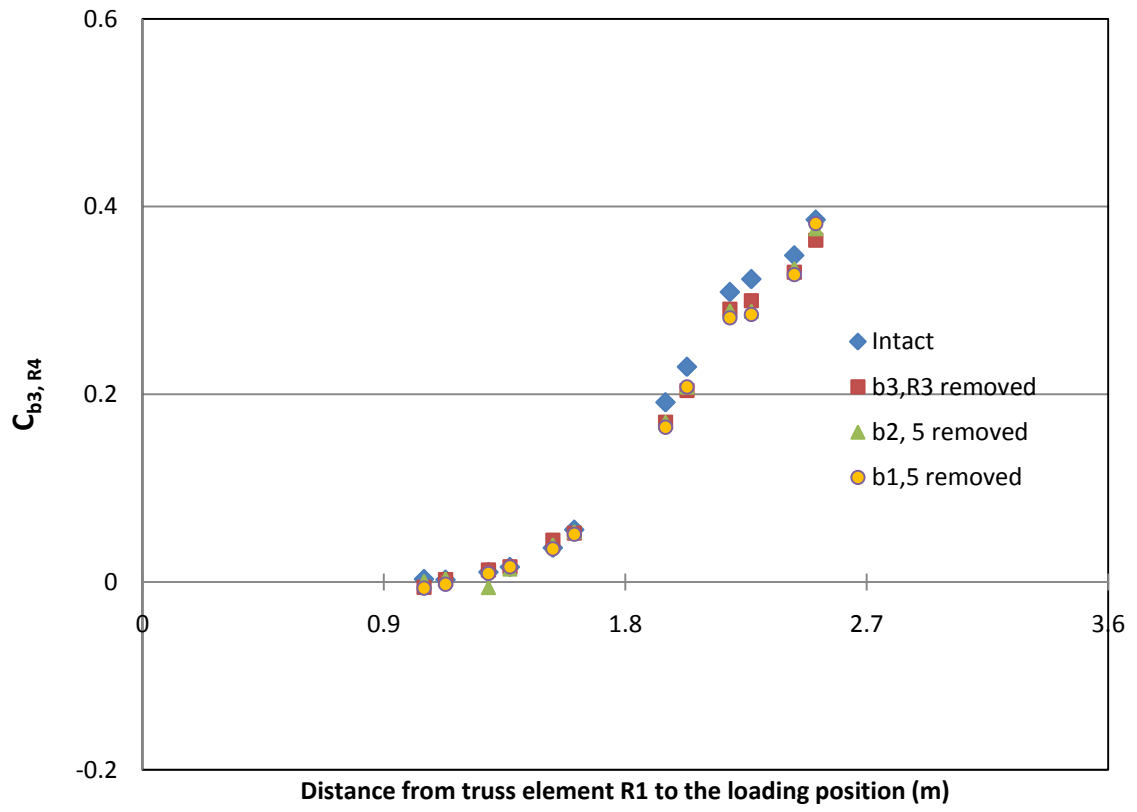


Figure B.24: $C_{b3, R4}$ for point load on X

Table B.9: Variation of reaction coefficient for unit load application at adjacent panels simultaneously

Location	Condition	Reaction coefficients								
		$C_{b1, R1}$	$C_{b1, R2}$	$C_{b1, R3}$	$C_{b2, R1}$	$C_{b2, R2}$	$C_{b2, R3}$	$C_{b3, R1}$	$C_{b3, R2}$	$C_{b3, R3}$
b1,R2	No failure	0.09	0.25	0.11	0.13	0.39	0.16	-0.02	-0.07	-0.03
	Both screw removed	0.18	0.00	0.29	0.15	0.39	0.20	-0.02	-0.11	-0.02
	Screw 'E' removed	0.10	0.19	0.16	0.13	0.39	0.17	-0.02	-0.08	-0.03
	Screw 'T' removed	0.11	0.18	0.15	0.14	0.38	0.17	-0.02	-0.08	-0.03
	Both screws loosened	0.12	0.18	0.17	0.14	0.38	0.17	-0.02	-0.08	-0.02
	screw 'E' loosened	0.11	0.21	0.15	0.14	0.37	0.17	-0.02	-0.08	-0.02
	screw 'T' loosened	0.11	0.20	0.14	0.14	0.38	0.17	-0.02	-0.08	-0.03
b2,R2	No failure	0.04	0.12	0.05	0.13	0.34	0.15	0.05	0.11	0.06
	Both screw removed	0.05	0.14	0.07	0.21	0.00	0.30	0.06	0.25	0.02
	Screw 'T' removed	0.04	0.13	0.04	0.15	0.25	0.18	0.06	0.15	0.05
	Screw 'E' removed	0.04	0.13	0.04	0.15	0.25	0.18	0.05	0.16	0.05
	Both screws loosened	0.04	0.13	0.04	0.17	0.19	0.22	0.06	0.18	0.04
	screw 'E' loosened	0.04	0.13	0.04	0.15	0.28	0.18	0.06	0.14	0.05
	screw 'T' loosened	0.04	0.12	0.03	0.15	0.28	0.17	0.05	0.14	0.05

Table B.10: Reaction coefficients for removing screw 'E' of selected connections

Conne ction	Locati on	Reaction coefficients								
		$C_{b1,R1}$	$C_{b1,R2}$	$C_{b1,R3}$	$C_{b2,R1}$	$C_{b2,R2}$	$C_{b2,R3}$	$C_{b3,R1}$	$C_{b3,R2}$	$C_{b3,R3}$
b1,R3	P4,X	-0.02	0.26	0.21	-0.03	0.35	0.35	0.01	-0.05	-0.08
	P7,X	0.00	-0.01	0.22	0.00	-0.03	0.37	-0.01	0.02	-0.07
b2,R2	P1,X	0.21	0.27	-0.02	0.33	0.29	0.01	-0.05	-0.04	0.01
	P2,X	-0.03	0.01	-0.01	0.29	0.21	0.03	0.28	0.32	-0.01
	P4,X	-0.02	0.26	0.20	-0.01	0.27	0.40	0.01	-0.02	-0.08
	P5,X	0.00	-0.01	0.00	0.00	0.22	0.29	-0.01	0.33	0.26

Table B.11: Reaction coefficients for loosening screw 'E' on selected connections

Connection	Location	Reaction coefficients								
		$C_{b1,R1}$	$C_{b1,R2}$	$C_{b1,R3}$	$C_{b2,R1}$	$C_{b2,R2}$	$C_{b2,R3}$	$C_{b3,R1}$	$C_{b3,R2}$	$C_{b3,R3}$
b1,R2	P1,X	0.22	0.22	0.01	0.29	0.39	-0.03	-0.04	-0.09	0.02
	P4,X	0.00	0.19	0.28	-0.02	0.34	0.36	0.01	-0.07	-0.06
b1,R3	P4,X	-0.02	0.26	0.21	-0.03	0.35	0.35	0.01	-0.06	-0.07
b2,R2	P1,X	0.19	0.25	-0.02	0.32	0.34	0.00	-0.04	-0.05	0.01
	P2,X	-0.03	0.00	-0.01	0.28	0.22	0.03	0.26	0.32	-0.01
	P4,X	-0.02	0.26	0.18	-0.01	0.31	0.39	0.01	-0.03	-0.08
	P5,X	0.00	-	-0.01	0.00	0.23	0.28	-0.01	0.32	0.26
b2,R3	P4,X	-0.03	0.26	0.18	-0.03	0.39	0.31	0.01	-0.06	-0.05
	P5,X	-0.01	-	-0.01	-0.02	0.30	0.23	-0.01	0.29	0.28

Table B.12: Reaction coefficients for loosening screw 'I' on selected connections

Connection	Location	Reaction coefficients								
		C _{b1} , R1	C _{b1} , R2	C _{b1} , R3	C _{b2} , R1	C _{b2} , R2	C _{b2} , R3	C _{b3} , R1	C _{b3} , R2	C _{b3} , R3
b1,R2	P1,X	0.22	0.19	0.01	0.30	0.41	-0.03	-0.04	-0.09	0.02
	P4,X	0.00	0.20	0.27	-0.02	0.35	0.36	0.01	-0.06	-0.07
b1,R3	P4,X	-0.02	0.25	0.19	-0.03	0.36	0.37	0.01	-0.05	-0.07
	P7,X	0.00	-0.01	0.21	0.00	-0.03	0.36	0.00	0.02	-0.06
b2,R2	P1,X	0.19	0.25	-0.02	0.32	0.34	0.00	-0.04	-0.05	0.01
	P2,X	-0.03	0.00	-0.02	0.28	0.24	0.02	0.26	0.32	-0.01
	P4,X	-0.02	0.25	0.18	-0.02	0.31	0.37	0.01	-0.03	-0.07
	P5,X	0.00	-0.01	-0.01	0.00	0.24	0.27	-0.01	0.33	0.26

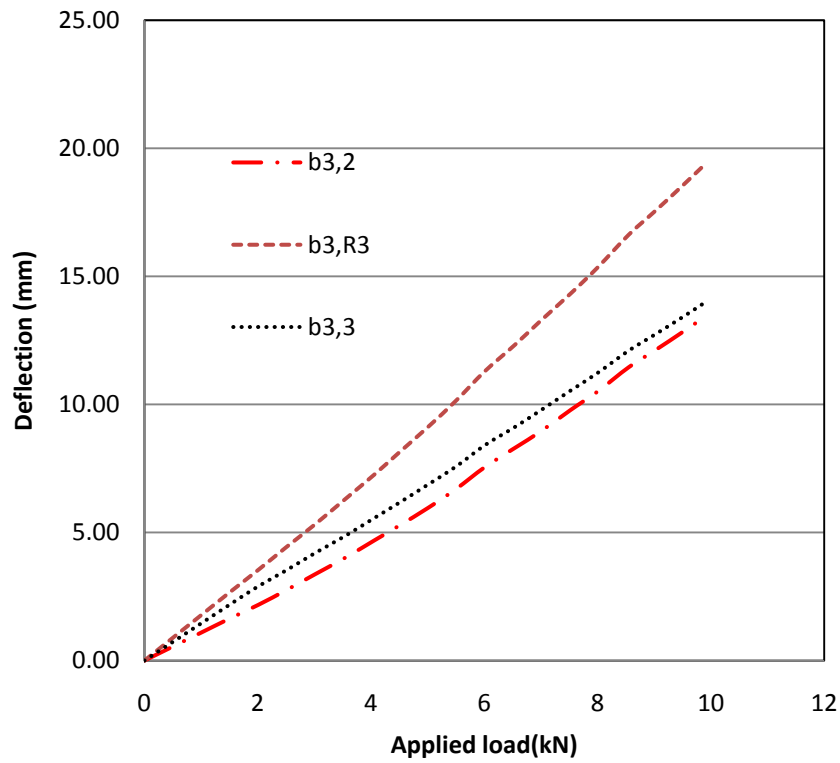


Figure B.25: Variation of the deflection with the applied load at (b3, R3)

Table B.13: The deflections for both Screws removed case

Connection	Location	Applied load(kN)	Deflections(mm)															
			Connection	P1,X,1	P2,X,1	P4,X,2	P5,X,2	P7,X,3	P8,X,3	b1,1	b1,2	b1,3	b2,1	b2,2	b2,3	b3,1	b3,2	b3,3
b1,R2	P1,X	3.25	5.50	17.97							9.38			4.78				
	P4,X	3.96	8.26	2.72		18.53					6.39				5.26			
b1,R3	P4,X	4.05	7.87			19.73						7.25			5.34			
	P7,X	3.97	8.17			1.92		23.22				4.93			0.45			
b2,R2	P1,X	3.39	13.43	20.72		2.84					2.86				11.92			
	P2,X	3.91	13.20		20.76		3.99							12.99			7.30	
	P4,X	3.98	11.99	3.84		22.20						4.26			11.93			
	P5,X	3.83	7.94		8.45		25.92								7.53			3.86
b3,R3	P4,X	3.98	11.03	-0.60	23.12							0.00			11.50			
	P7,X	4.03	12.69		4.53			27.01					3.72			12.11		
	P8,X	4.05	14.04				4.82		24.98							13.71		8.00

Table B.14: The deflections for screw 'E' removed case

Connection	Location	Applied load(kN)	Deflections(mm)															
			Connection	P1,X,1	P2,X,1	P4,X,2	P5,X,2	P7,X,3	P8,X,3	b1,1	b1,2	b1,3	b2,1	b2,2	b2,3	b3,1	b3,2	b3,3
b1,R2	P1,X	4.11	0.48	15.05		0.20					3.19			4.38				
	P4,X	3.88	2.91	0.00		16.75					0.66			5.15				
b1,R3	P4,X	4.00	2.64			18.50		0.12				3.66		5.10				
	P7,X	4.07	3.73			-0.09		22.40				0.27		0.36				
b2,R2	P1,X	3.50	5.41	17.16		0.21					2.42			6.15				
	P2,X	4.03	7.22		20.70		1.87							9.29			7.72	
	P4,X	4.15	4.49	1.02		20.56						4.03		7.08				
	P5,X	4.14	6.66		1.29		20.89							9.70			8.02	
b2,R3	P4,X	4.50	4.39			21.60		1.38				3.47		7.39				
	P5,X	4.47	6.39		2.21		21.67							9.65			8.30	
	P7,X	3.94	5.33			1.17		23.32					3.17		7.48			
	P8,X	4.22	8.30				1.86		22.06						10.65			8.15

Table B.15: The deflections for Inner screw 'I' removed case

Connection	Location	Applied load(kN)	Deflections(mm)															
			Connection	P1,X,1	P2,X,1	P4,X,2	P5,X,2	P7,X,3	P8,X,3	b1,1	b1,2	b1,3	b2,1	b2,2	b2,3	b3,1	b3,2	b3,3
b1,R2	P1,X	3.31	1.36	16.60		0.14					3.34			4.58				
	P4,X	4.07	3.51	0.80		18.60					1.70			4.97				
b1,R3	P4,X	4.01	1.94			17.94		0.04				3.25			5.31			
	P7,X	3.93	1.54			0.06		20.64			0.64			0.12				
b2,R2	P1,X	3.43	5.50	17.84		0.01					2.40			6.08				
	P2,X	3.92	7.72		20.37		2.73							9.22			7.52	
	P4,X	4.16	4.70			20.31						3.20			7.43			
	P5,X	4.11	6.04		2.90		20.40							9.55			7.91	
b2,R3	P4,X	4.00	4.42			19.41		1.26				3.68			6.82			
	P5,X	4.00	6.26				20.57		2.75					9.69			7.74	
	P7,X	4.04	5.59			1.78		23.70				3.46			7.86			
	P8,X	4.13	8.55				2.68		22.37						10.72			8.00

Table B.16: The deflections for both screws half loosened case

Connection	Location	Applied load(kN)	Deflections(mm)											
			Connection	P1,X,1	P2,X,1	P4,X,2	P5,X,2	P7,X,3	b1,1	b1,2	b2,1	b2,2	b3,1	b3,2
b1,R2	P1,X	3.83	3.57	19.32		0.68			4.75		5.24			
	P4,X	4.00	4.60	0.50		18.59				4.48		4.74		
b1,R3	P4,X	4.22	3.28	-0.12		19.84				4.75		4.94		
	P7,X	4.24	4.23			0.55		26.14		1.77		0.29		
b2,R2	P1,X	3.19	7.07	17.23							7.48			
	P2,X	4.03	8.84		20.95						10.05		7.32	
	P4,X	4.06	6.31			20.17				2.93		8.61		
	P5,X	4.08	8.12				20.19					10.20	7.63	
b2,R3	P4,X	4.16	9.23			16.83		3.00		8.12		10.78		
	P5,X	4.06	7.95				20.19					10.58	7.70	

Table B.17: The deflections for screw “E” loosened case

Connection	Location	Applied load(kN)	Deflections(mm)												
			Connection	P1,X,1	P2,X,1	P4,X,2	P5,X,2	P7,X,3	P8,X,3	b1,1	b1,2	b2,1	b2,2	b3,1	b3,2
b1,R2	P1,X	4.11	3.82	20.45		0.48					4.45		5.60		
	P4,X	4.07	4.64	0.21		18.46						3.65		4.80	
b1,R3	P4,X	4.06	2.23	-0.01		19.67						3.51		5.00	
	P7,X														
b2,R2	P1,X	3.44	5.81	17.37									6.33		
	P2,X	4.06	8.50		21.21								9.04		7.34
	P4,X	4.19	4.01			19.69						2.88		6.60	
	P5,X	4.48	6.91				21.56							9.90	8.34
b2,R3	P4,X	4.24	4.10			19.99		0.80				3.22		6.35	
	P5,X	4.14	6.69				20.81		2.07					9.29	7.99

Table B.18: Deflections for screw “I” loosened case

Connection	Location	Applied load(kN)	Deflections (mm)											
			Connection	P1,X,1	P2,X,1	P4,X,2	P5,X,2	P7,X,3	b1,1	b1,2	b2,1	b2,2	b3,1	b3,2
b1,R2	P1,X	3.31	1.36	16.60		0.12				3.34		4.58		
	P4,X	4.16	3.92	0.08		18.83					3.46		4.81	
b1,R3	P4,X	4.31	2.31	0.31		19.93					3.25		5.37	
	P7,X	4.36	3.33			-0.03		23.69			0.55		0.15	
b2,R2	P1,X	3.32	5.53	16.47		0.00				0.00		5.69		
	P2,X	3.94	7.74		19.68							8.24		7.19
	P4,X	4.38	4.10			20.53					3.01		6.96	
	P5,X	4.01	6.41				20.15						8.70	7.55

APPENDIX C

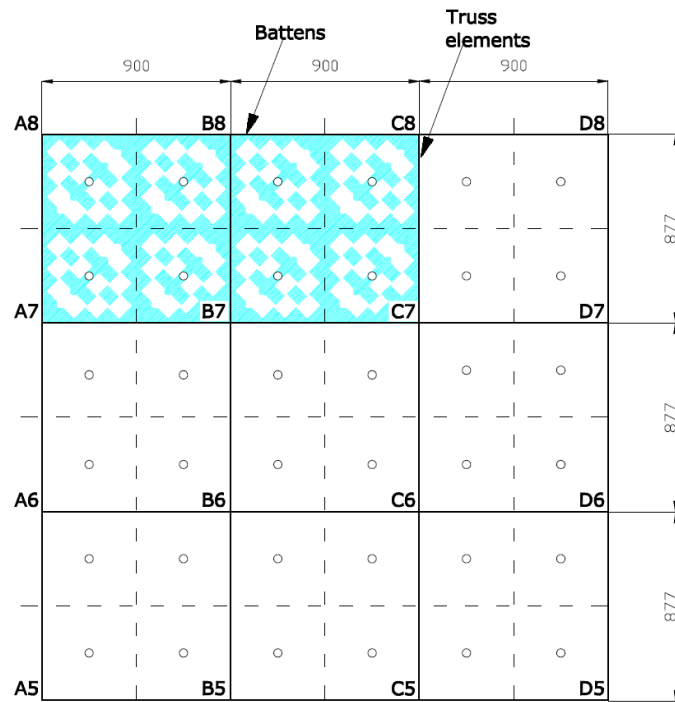


Figure C.1: Tributary area for connection B8-Proposed method

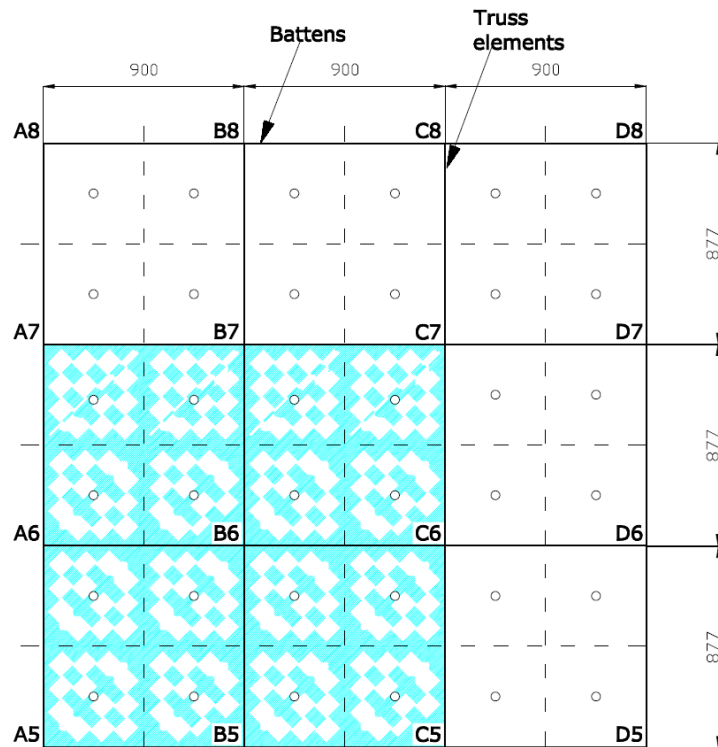


Figure C.2: Tributary area for connection B6-Proposed method

Table C.1: \check{C}_{X_b} for $\theta = 0^\circ$ - Undamaged roof

Connection Number	\check{C}_{X_b} Values		
	Truss A	Truss B	Truss C
5	-0.73	-1.02	-0.85
6	-0.74	-1.04	-0.89
7	-0.72	-1.27	-1.06
8	-0.43	-0.87	-0.83

Table C.4: \check{C}_{X_b} for $\theta = 45^\circ$ - Undamaged roof

Connection Number	\check{C}_{X_b} Values		
	Truss A	Truss B	Truss C
5	-1.74	-3.10	-1.75
6	-1.75	-3.13	-2.22
7	-1.80	-3.48	-2.59
8	-1.31	-2.34	-1.93

Table C.2: \check{C}_{X_b} for $\theta = 15^\circ$ - Undamaged roof

Connection Number	\check{C}_{X_b} Values		
	Truss A	Truss B	Truss C
5	-0.82	-0.93	-0.77
6	-0.95	-1.12	-0.83
7	-1.07	-1.69	-1.11
8	-0.76	-1.25	-1.01

Table C.5: \check{C}_{X_b} for $\theta = 60^\circ$ - Undamaged roof

Connection Number	\check{C}_{X_b} Values		
	Truss A	Truss B	Truss C
5	-2.05	-3.60	-3.09
6	-2.13	-3.41	-2.98
7	-2.22	-3.89	-3.09
8	-1.41	-2.49	-1.99

Table C.3: \check{C}_{X_b} for $\theta = 30^\circ$ - Undamaged roof

Connection Number	\check{C}_{X_b} Values		
	Truss A	Truss B	Truss C
5	-1.29	-1.82	-0.92
6	-1.40	-2.13	-1.15
7	-1.57	-2.91	-1.63
8	-1.23	-2.11	-1.55

Table C.6: \check{C}_{X_b} for $\theta = 75^\circ$ - Undamaged roof

Connection Number	\check{C}_{X_b} Values		
	Truss A	Truss B	Truss C
5	-2.08	-3.52	-3.18
6	-2.15	-3.43	-3.05
7	-2.03	-3.93	-3.22
8	-1.24	-2.49	-2.04

Table C.7: \check{C}_{X_b} for $\theta = 105^\circ$ - Undamaged roof

Connection Number	\check{C}_{X_b} Values		
	Truss A	Truss B	Truss C
5	-1.90	-3.40	-3.01
6	-1.90	-3.45	-3.02
7	-1.98	-4.09	-3.26
8	-1.40	-2.77	-2.45

Table C.8: \check{C}_{X_b} for $\theta = 120^\circ$ - Undamaged roof

Connection Number	\check{C}_{X_b} Values		
	Truss A	Truss B	Truss C
5	-1.99	-3.33	-2.88
6	-2.21	-3.64	-2.92
7	-2.77	-4.52	-3.46
8	-2.03	-3.73	-3.05

Table C.9: \check{C}_{X_b} for $\theta = 135^\circ$ - Undamaged roof

Connection Number	\check{C}_{X_b} Values		
	Truss A	Truss B	Truss C
5	-2.06	-3.52	-2.90
6	-2.74	-3.99	-2.92
7	-3.37	-4.91	-4.41
8	-2.39	-4.45	-3.82

Table C.11: \check{C}_{X_b} for $\theta = 180^\circ$ - Undamaged roof

Connection Number	\check{C}_{X_b} Values		
	Truss A	Truss B	Truss C
5	-0.93	-1.74	-1.75
6	-1.01	-1.84	-1.77
7	-1.02	-2.17	-1.92
8	-0.67	-1.41	-1.25

Table C.10: \check{C}_{X_b} for $\theta = 165^\circ$ - Undamaged roof

Connection Number	\check{C}_{X_b} Values		
	Truss A	Truss B	Truss C
5	-1.51	-2.54	-2.32
6	-1.84	-2.95	-2.77
7	-2.19	-3.74	-3.19
8	-1.43	-2.66	-2.23

Table C.12: \check{C}_{X_b} for $\theta = 195^\circ$ - Undamaged roof

Connection Number	\check{C}_{X_b} Values		
	Truss A	Truss B	Truss C
5	-0.55	-1.06	-0.98
6	-0.53	-1.04	-1.02
7	-0.51	-1.08	-0.99
8	-0.31	-0.71	-0.65

Table C.13: \check{C}_{X_b} for $\theta = 210^\circ$ - Undamaged roof

Connection Number	\check{C}_{X_b} Values		
	Truss A	Truss B	Truss C
5	-0.58	-1.11	-1.13
6	-0.56	-1.03	-1.17
7	-0.54	-1.26	-1.26
8	-0.35	-0.89	-0.80

Table C.16: \check{C}_{X_b} for $\theta = 255^\circ$ - Undamaged roof

Connection Number	\check{C}_{X_b} Values		
	Truss A	Truss B	Truss C
5	-0.26	-0.55	-0.60
6	-0.26	-0.53	-0.58
7	-0.27	-0.63	-0.66
8	-0.18	-0.46	-0.52

Table C.14: \check{C}_{X_b} for $\theta = 225^\circ$ - Undamaged roof

Connection Number	\check{C}_{X_b} Values		
	Truss A	Truss B	Truss C
5	-0.49	-0.95	-1.04
6	-0.51	-1.08	-1.16
7	-0.44	-1.29	-1.22
8	-0.34	-0.88	-0.77

Table C.17: \check{C}_{X_b} for $\theta = 270^\circ$ - Undamaged roof

Connection Number	\check{C}_{X_b} Values		
	Truss A	Truss B	Truss C
5	-0.21	-0.42	-0.44
6	-0.21	-0.39	-0.41
7	-0.21	-0.47	-0.48
8	-0.13	-0.34	-0.37

Table C.15: \check{C}_{X_b} for $\theta = 240^\circ$ - Undamaged roof

Connection Number	\check{C}_{X_b} Values		
	Truss A	Truss B	Truss C
5	-0.38	-0.77	-0.84
6	-0.39	-0.76	-0.80
7	-0.36	-0.86	-0.86
8	-0.25	-0.60	-0.60

Table C.18: \check{C}_{X_b} for $\theta = 285^\circ$ - Undamaged roof

Connection Number	\check{C}_{X_b} Values		
	Truss A	Truss B	Truss C
5	-0.20	-0.37	-0.39
6	-0.21	-0.39	-0.36
7	-0.21	-0.43	-0.39
8	-0.14	-0.29	-0.29

Table C.19: \check{C}_{X_b} for $\theta = 300^\circ$ - Undamaged roof

Connection Number	\check{C}_{X_b} Values		
	Truss A	Truss B	Truss C
5	-0.24	-0.44	-0.40
6	-0.23	-0.43	-0.43
7	-0.24	-0.52	-0.49
8	-0.15	-0.35	-0.37

Table C.21: \check{C}_{X_b} for $\theta = 330^\circ$ - Undamaged roof

Connection Number	\check{C}_{X_b} Values		
	Truss A	Truss B	Truss C
5	-0.24	-0.43	-0.42
6	-0.24	-0.43	-0.44
7	-0.26	-0.54	-0.53
8	-0.17	-0.40	-0.42

Table C.20: \check{C}_{X_b} for $\theta = 315^\circ$ - Undamaged roof

Connection Number	\check{C}_{X_b} Values		
	Truss A	Truss B	Truss C
5	-0.24	-0.44	-0.46
6	-0.25	-0.47	-0.48
7	-0.27	-0.60	-0.55
8	-0.17	-0.43	-0.42

Table C.22: \check{C}_{X_b} for $\theta = 345^\circ$ - Undamaged roof

Connection Number	\check{C}_{X_b} Values		
	Truss A	Truss B	Truss C
5	-0.31	-0.48	-0.47
6	-0.32	-0.49	-0.49
7	-0.30	-0.58	-0.55
8	-0.19	-0.41	-0.42

- *Internal pressure coefficient - +0.2*

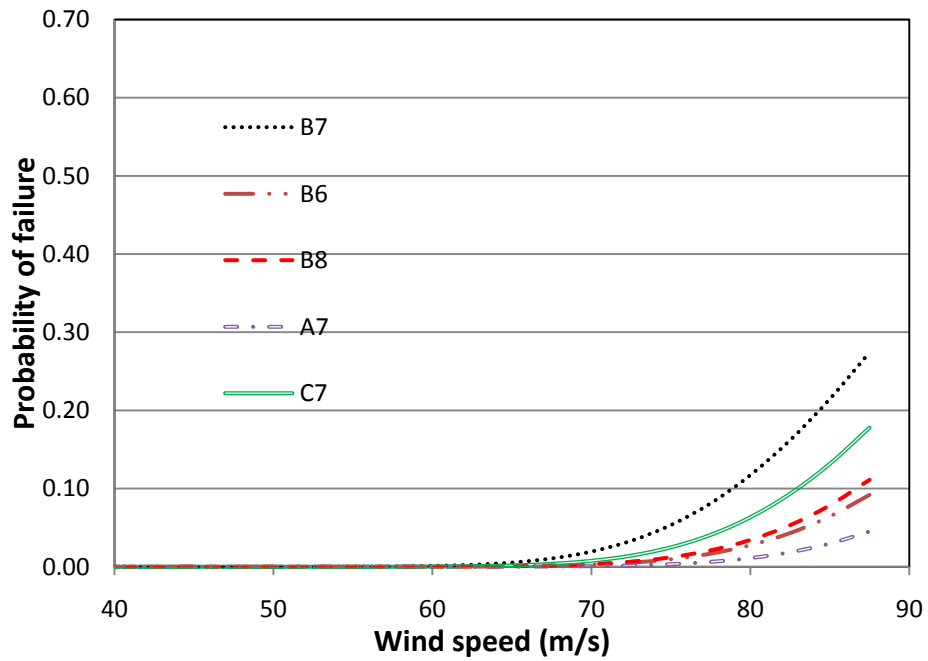


Figure C.3: Vulnerability of batten connections for $\theta=150^\circ$ in TC 2.5
-with load distribution method

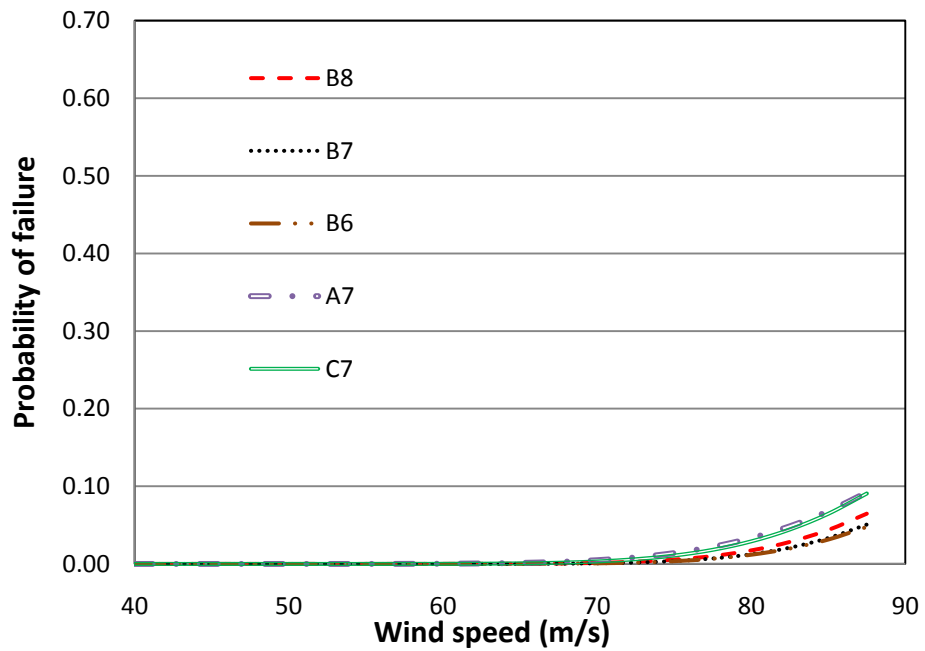


Figure C.4: Vulnerability of batten truss connections for $\theta=150^\circ$ in TC 2.5-Conventional method #1

- *Internal pressure coefficient - +0.4*

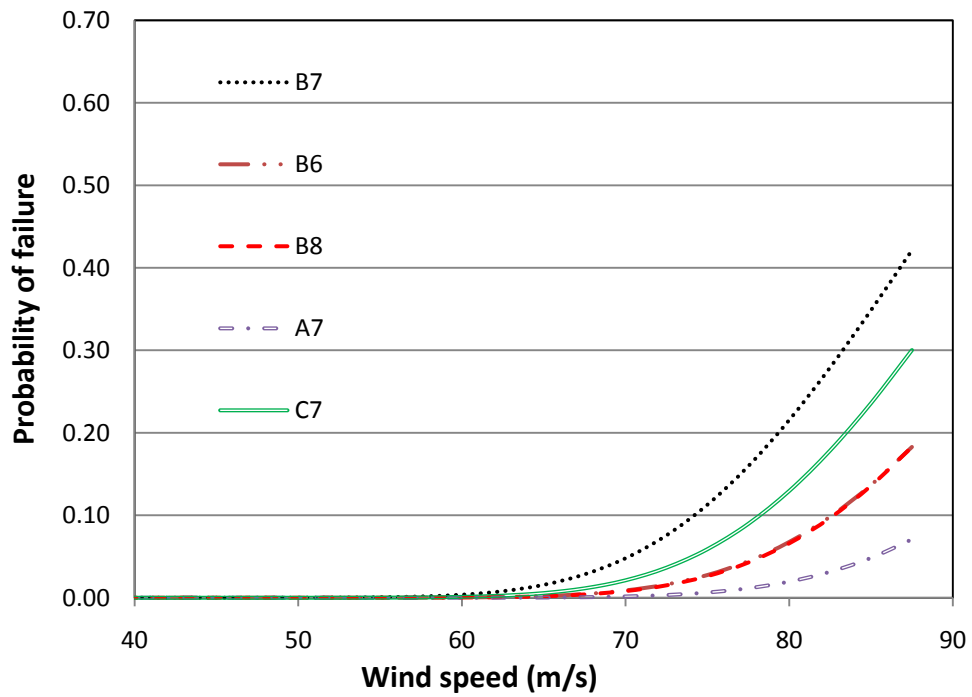


Figure C.5: Vulnerability of batten connections for $\theta=150^\circ$ in TC 2.5-with load distribution method

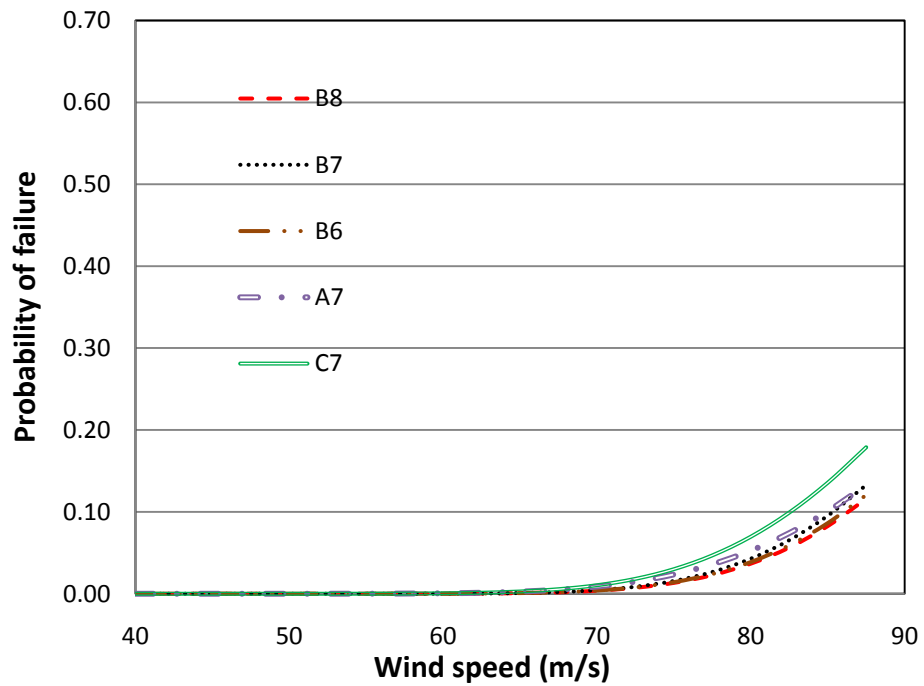


Figure C.6: Vulnerability of batten truss connections for $\theta=150^\circ$ in TC 2.5-Conventional method #1

- *No internal pressure*

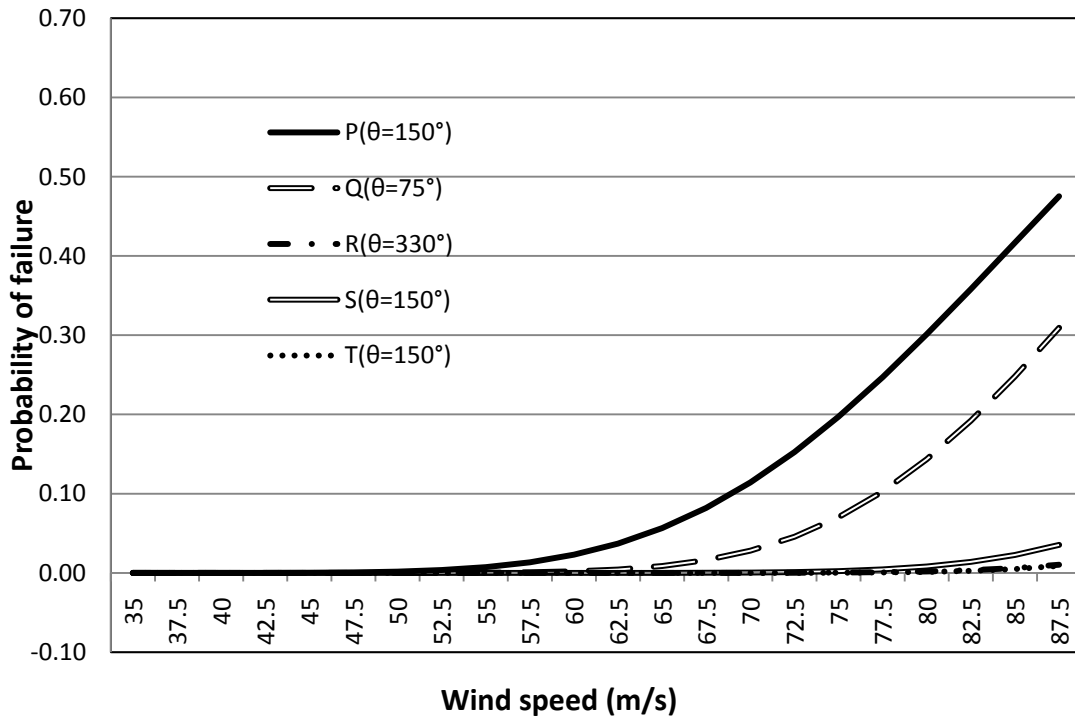


Figure C.7: Probability of failure vs Basic Wind speed- Cladding connections for house in TC 2.5

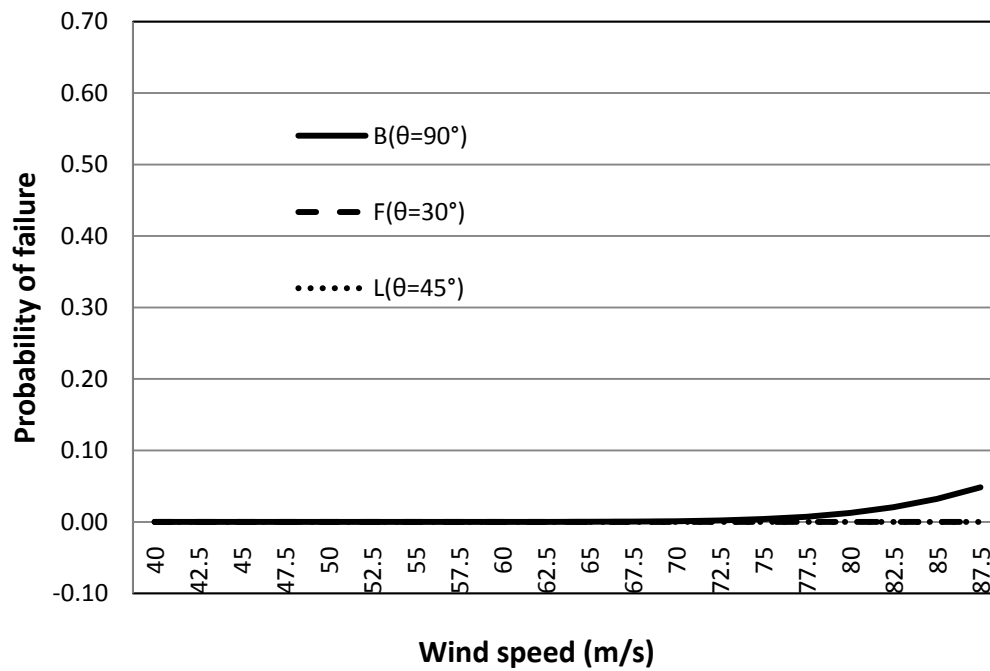


Figure C.8: Probability of failure vs Basic Wind speed-Truss to wall connections for house in TC 2.5

APPENDIX D- Vulnerability and Adaptation to Wind Simulation (VAWS)

Geosciences Australia in collaboration with Cyclone Testing Station and JDH Consulting has produced an alpha version of software (VAWS) to estimate the vulnerability of a range of house types. The author of this thesis was also involved in this project to provide engineering inputs. VAWS assesses the vulnerability of buildings by using reliability theory incorporating Monte Carlo Simulation. This section demonstrates the application of data obtained in this study to VAWS for obtaining an overall vulnerability curve for a masonry block house.

The details of the roof of a masonry block house were input to VAWS, as this research focuses only on roof damage. As described in Chapter 3, the roof has dimensions 10m x 19.8m with roof pitch and overhang 22.5° and 0.6m respectively. The batten spacing was taken as 650mm and 877mm in the roof eave and other areas respectively and the truss spacing was taken as 900mm. Figure D.1 shows the truss and batten layout of the structure having 23 trusses identified as A to W and 16 battens. Each truss tributary area was divided into 16 panels according to batten-truss connection tributary area. These Panels were identified as A1 to A16, B1 to B16, W1 to W16 to represent the roof.

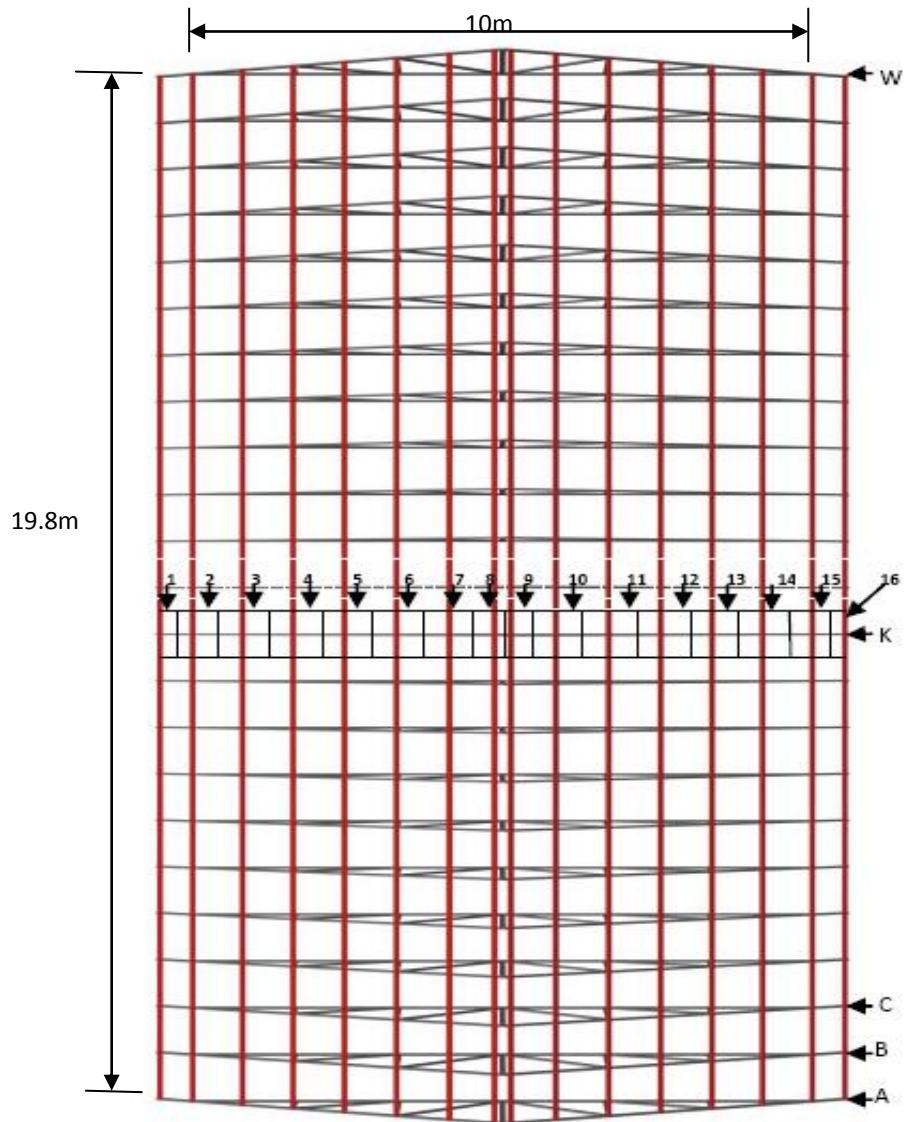


Figure D.1: Layout of trusses and battens

The probabilistic descriptions of external pressure coefficients related to each panel were given for eight wind approach directions ($\theta=0^\circ, 45^\circ, 90^\circ, \dots, 315^\circ$) based on the wind tunnel model study described in Chapter 4. However, the software uses constant coefficient of variation (COV) to sample zone pressures by means of Extreme Value Type III distribution. The internal pressure in the software was based on the debris model described by Holmes *et al.* (2010) and Wehner *et al.* (2010). This analysis used the same debris model.

The strength data related to each patch was input for the three connection types in terms of means and COVs. The number of cladding fasteners in each patch was obtained according to the survey data and the strength data was given accordingly. The software randomly generates strength data of the connections. As described in previous chapters, the progressive failure with increasing wind speed depends on the load-sharing and structural inter-dependency and strengths of the components. For example, the failure of one of the connections in a house can prevent the occurrence of a dependent connection failing or alternatively accelerate another failure mode. These effects have been incorporated in VAWS based on test data, damage investigation reports and expert opinions.

- ***Structural/ component response***

The response of components and connections that contribute to the specified failures with increasing wind speed, were considered in terms of reaction coefficients (i.e. linear region) for load effects of interest, x by Equation D.1.

$$x = \sum_{i=1}^N \beta_i p_i A_i = \sum_{i=1}^N \beta_i P_i \quad \text{Eq.(D.1)}$$

where,

x – Load effect at each wind speed step

i – Patch identifier

N -Total number of Patches influencing the load effect of interest

p_i – pressure on patch i

A_i – Tributary area of patch i

P_i – Load on patch i

β_i – Reaction coefficient (i.e. Value of load effect due to unit load applied on Patch i)

The load effects cases considered were:

1. Force on roof cladding fastener
2. Force on batten-truss connection

3. Hold-down force on truss to wall connection

The software uses the reaction coefficients for cases 1 and 2 above as 1.0 such that the pressure acting on connection is multiplied by the tributary area to get the wind loads. For example, tributary area for cladding fastener is $0.152 \times 0.9 = 0.137\text{m}^2$ and for batten truss connection, it is $0.9 \times 0.877 = 0.79\text{m}^2$. Furthermore, the failure of roof cladding fixing(s) in a Patch was considered to transfer loads to the adjoining Patches along the cladding sheet equally. The failure of a batten-truss connection was considered to share the loads to the adjoining Patches along the batten equally. This analysis used the same reaction coefficients.

The next step was to obtain the damaged and undamaged influence matrices for truss to wall connections. Five pairs of trusses placed next to each other were considered as part of a repeating structural grid pattern along the length of the roof. The five truss structure was modelled with battens and claddings on them using SPACEGASS. Reaction coefficients of the truss to wall connections were obtained by applying a unit load at each batten-truss connection (linear elastic region). The load transfer of truss to wall connections was observed and the reaction coefficients were obtained for undamaged system and for various damage scenarios (such as failure of truss to wall connection at locations such as end, middle etc). These matrices were incorporated in VAWS.

Figures D.2-D.7 show the damage “heat maps” which displays the gust wind speeds at 10m height for the failure of claddings, battens, and for truss to wall connections, for two runs on a single house. The wind approach direction for these examples was taken as 135° (North West direction). The analysis was performed twice to show the difference in failures of each connection type due to the generation of random load action and strength data of each patch. Generally, the run two had more failures of connections than run one.

Similarly the vulnerability of number of houses located in a tropical town or a capital city can be obtained from VAWS for a specific or a random wind direction. The outputs from this research can improve these types of software to obtain more reliable vulnerability curves.

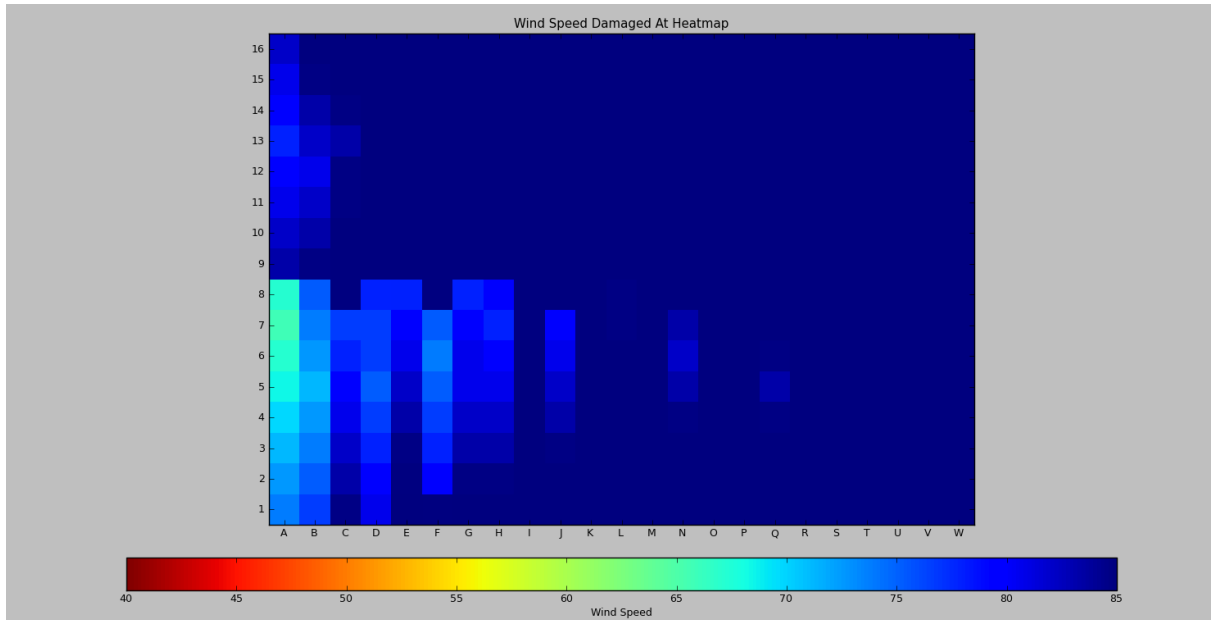


Figure D.2: Cladding failure with gust wind speed at 10m height – Run one

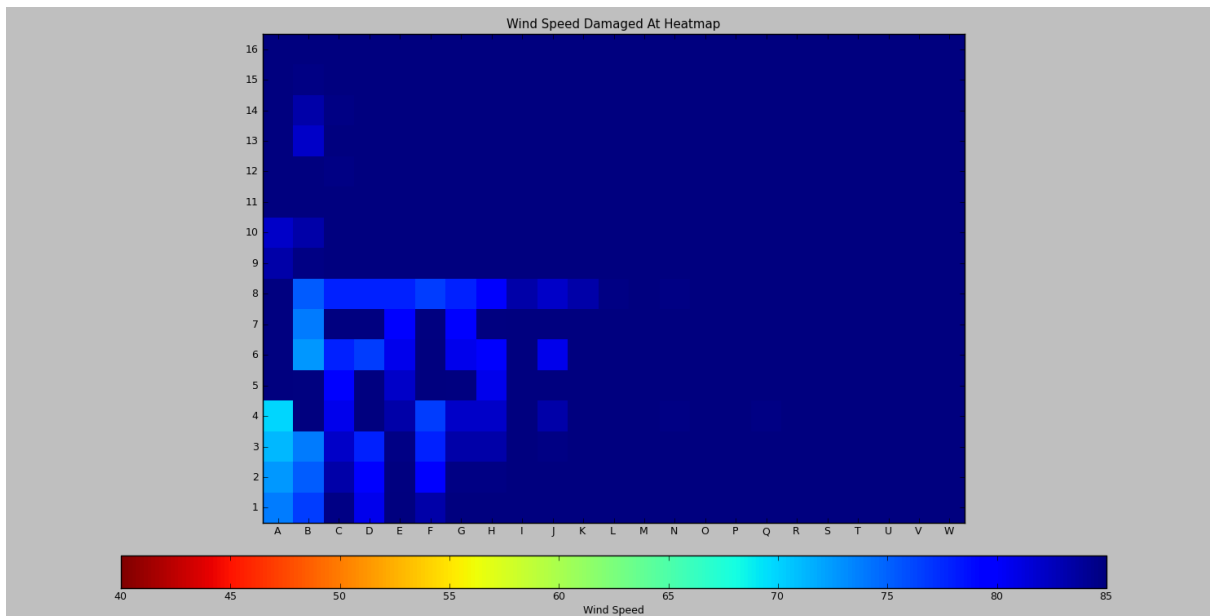


Figure D.3: Batten failure with gust wind speed at 10m height –Run one

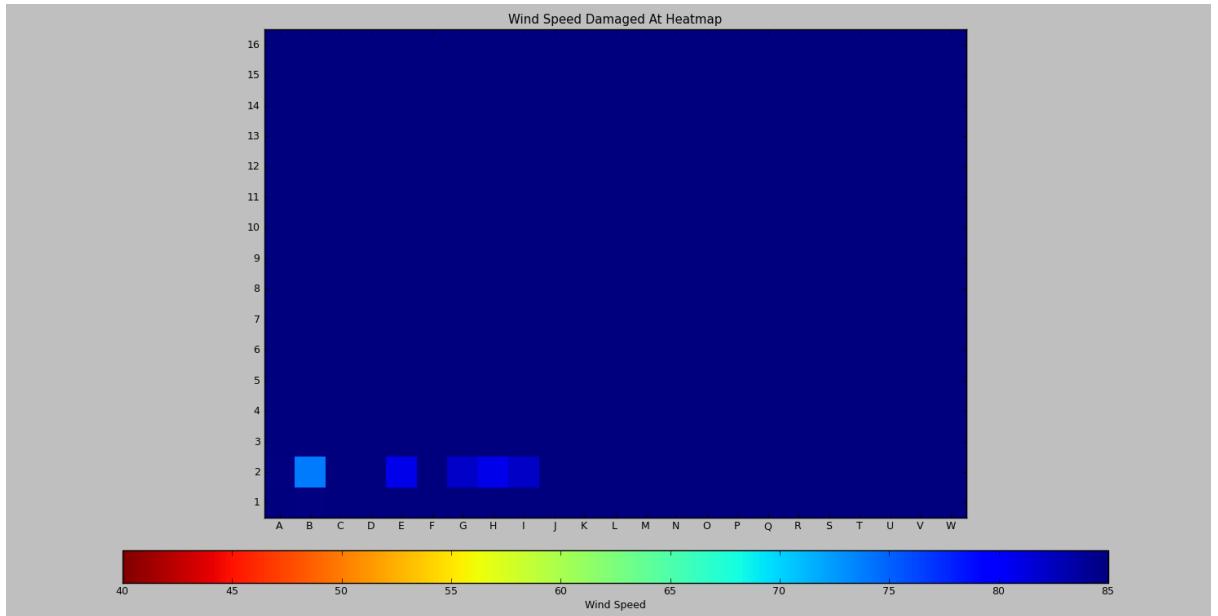


Figure D.4: Truss to wall connection failure with gust wind speed at 10m height -Run one

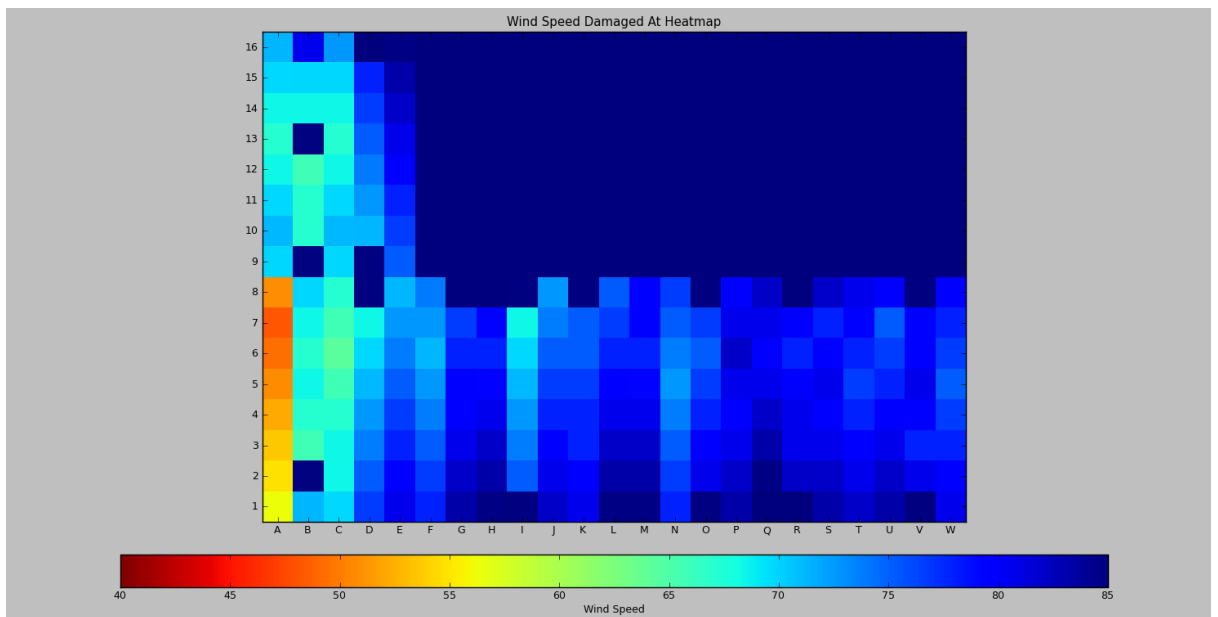


Figure D.5: Cladding failure with gust wind speed at 10m height - Run two

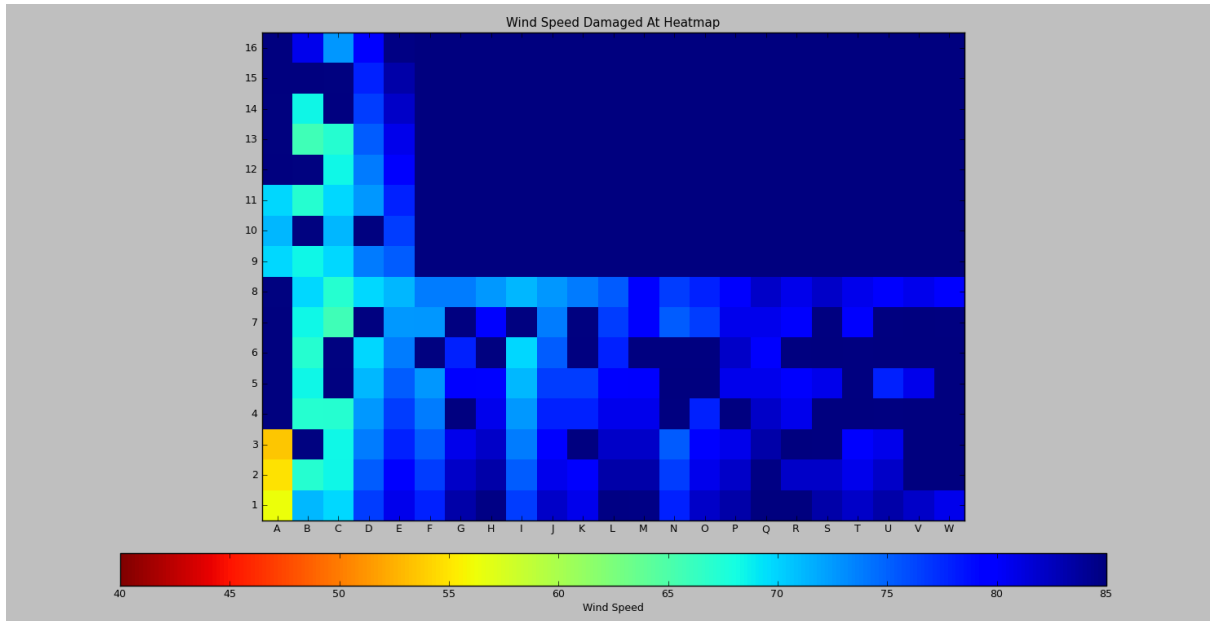


Figure D.6: Batten failure with gust wind speed at 10m height - Run two

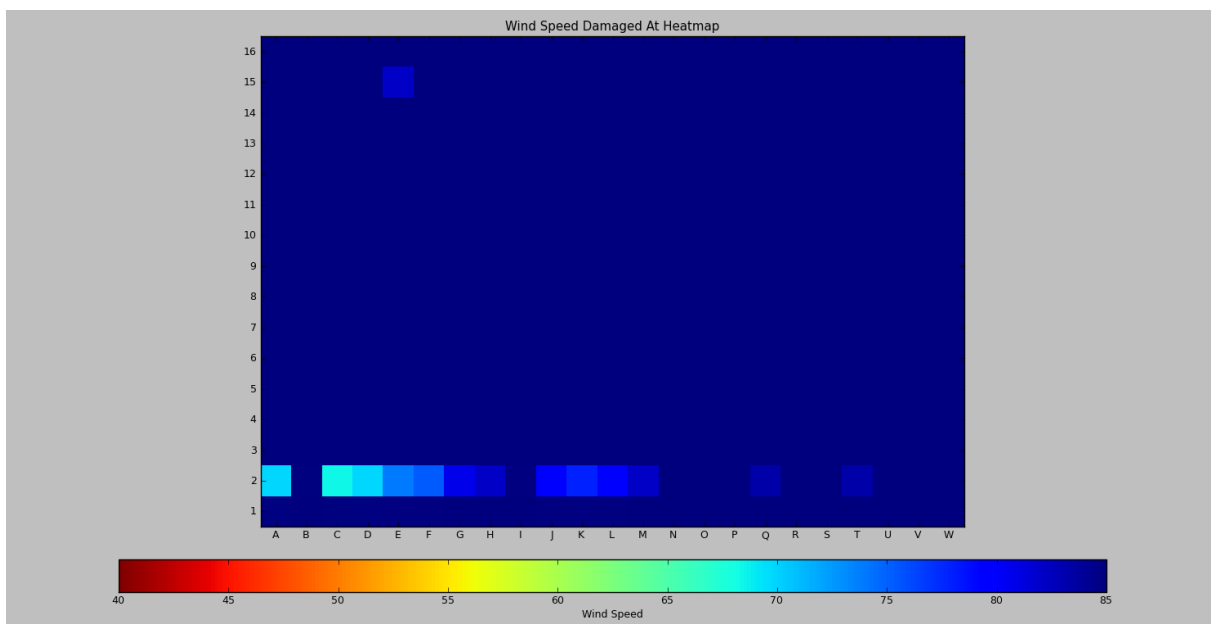


Figure D.7: Truss to wall connection failure with gust wind speed at 10m height - Run two